The interactions between pyrazinamide and urea derivatives and their role in the stabilization of the gamma form of pyrazinamide

Kangli Li

To cite this version:

Kangli Li. The interactions between pyrazinamide and urea derivatives and their role in the stabilization of the gamma form of pyrazinamide. Material chemistry. Normandie Université, 2021. English. NNT : 2021NORMR013 . tel-04198758

HAL Id: tel-04198758
https://theses.hal.science/tel-04198758v1

Submitted on 7 Sep 2023

THÈSE

Pour obtenir le diplôme de doctorat
label européen

Spécialité Chimie des matériaux

Préparée au sein de l'Université de Rouen Normandie

The interactions between pyrazinamide and urea derivatives and their role in the stabilization of the γ form of pyrazinamide

Présentée et soutenue par
Kangli LI

Thèse soutenue publiquement le 23 Mars 2021 devant le jury composé de		
M. Gérard COQUEREL	PR, Université de Rouen, France	Examinateur
M. Elias VLIEG	PR, Universiteit Nijmegen, Pays Bas	Rapporteur
Mme. Ermelinda EUSÉBIO	PR, Universidade de Coimbra, Portugal	Rapporteur
M. Gabin GBABODE	MCF, Université de Rouen, France	Examinateur
M. Ivo B. RIETVELD	MCF-HdR, Université de Rouen, France	Directeur de thèse
M. Dino AQUILANO	PR, Università degli Studi di Torino, Italy	Examinateur

Thèse dirigée par Dr. Ivo RIETVELD et Co-encadrée par le Dr. Gabin GBABODE au laboratoire Sciences et Méthodes Séparatives (EA 3233 SMS)

Acknowledgements

The past three years as a PhD student is an indelible mark in my life. People who helped me a lot are the brightest colors of this memory. I would like to express my sincerest appreciation to them.

First, I would like to extend my heartfelt gratitude to my supervisors, Dr. Ivo Rietveld, and Dr. Gabin Gbabode for their hard-working, meticulous guidance and constant encouragement. Thank you for sharing your profound knowledge with me. Thank you for trying your best to help me to overcome challenges in my research and my life. Thank you for your great enthusiasm shown for my research that encourages me not to give up. It is my great honor to be your student and work with you. The commendable traits you have shown as an excellent researcher that will inspire me to progress unceasingly and provide me with the motivation to explore the field of crystallization.

I am deeply grateful to Prof. Gérard Coquerel who founded the Laboratory "Sciences et Méthodes Séparatives" (SMS laboratory). Thank you for allowing me to study in the laboratory. I have benefited greatly from your interesting and wise ideas and suggestions.

I want to extend my sincere gratitude to the people who helped me a lot in my research. I am particularly grateful to Dr. Morgane Sanselme and Dr. Nicolas Couvrat for the kindness and help in my daily research, Dr. Béatrice Nicolaï for the single crystal X-ray diffraction measurements, Dr. Jean-Paul Itié for the support on the beamline Psiché, synchrotron Soleil (Gif sur Yvette), Marine Vergé-Depré and Dr. Benoît Robert from Sanofi for their help on the measurements of the vapor pressure, Muriel Sebban for the NMR measurements, Marie Vaccaro and Prof. Pascal Cardinael for the GC measurements, Aurélien Lemercier and Dr. Yohann Cartigny for the DVS measurements, Dr. Antoine Burel for the HPLC measurements, Dr. Bienvenu Atawa for the hyper-DSC measurements, Dr. Valérie Dupray for the Raman measurements, Dr, Simon Clevers for the SHG measurements, and Vincent Tognetti for the calculation on pyrazinamide dimers. I would like to thank Dr. Maria Barrio and Prof. Josep-Lluis Tamarit who gave me the opportunity to learn the use of high-pressure techniques in the Universitat Politècnica de Catalunya in Barcelona. I also would like to thank Dr. Yohann Cartigny and Dr. Samuel Jouen, who are members of my comité de suivi.

Next, I also sincerely acknowledge all the members of the SMS Laboratory. Thank you for

your great kindness and help during these three years. Working with you is one of the most memorable times in my life.

I gratefully acknowledge the Region Normandie for the financial support of my PhD project and the ERASMUS organization for a travel grant for three months for research in Barcelona. Your support gave me a precious opportunity to improve my research network, to enrich my scientific research experience and to accomplish a PhD degree.

Finally, I would like to thank my parents and my brother. You are always the strongest backers in my life. Thank you for your endless love and constant encouragement. I would like to thank all my family. Thank you for taking care of my parents and my brother, so that I can finish my PhD study without any worries. Special thanks to my cousin Chong Chu. You are always the first and even the only person to support all my decisions. Thank you for your infinite support and looking after me as a brother. Thank you to all my friends for your continued support and company.

Table of contents

List of Figures

List of Tables

General introduction

Polymorphism is a common phenomenon in pharmaceutical compounds; it has been confirmed to exist in the majority of small molecular pharmaceutical compounds.[1] Because many physicochemical properties vary with its crystal arrangement, a chemical compound may not exhibit the same activity as a pharmaceutical or an agrochemical depending on the polymorph. Therefore, polymorphism has attracted attention from researchers not only to avoid problems caused by the behavior of different polymorphs, but also to make use of them. One of the important challenges is the control over crystallization and persistence of polymorphs in production, storage, and during its use.

A previous study has shown that 1,3-dimethylurea appears to inhibit the phase transformation of the γ polymorph of pyrazinamide into a more stable form when obtained by spray drying.[2, 3] However, other tested urea derivatives, such as urea, *N*-methylurea, 1,1-diethylurea, and trimethylurea, did not appear to cause the same effect as 1,3-dimethylurea.[4] This result leaves us with a number of questions: Is 1,3-dimethylurea the only additive that can extend the persistence time of spray dried γ pyrazinamide? How does it work? The answers to these questions will not only help us to understand the effects of additives on the crystallization process and the final product but also provide new solutions for stabilizing metastable polymorphs.

Therefore, this thesis focusses on the polymorphism of pyrazinamide and the effect of 1,3-dimethylurea and of other additives with a structure similar to 1,3-dimethylurea. This objective has led to the exploration of the phase behavior of pyrazinamide, the interactions between pyrazinamide and additives, and the crystallization behavior in the spray drying process. Especially, the interactions between pyrazinamide and a number of urea derivatives have been studied in detail in solution as well as in the vapor phase.

Various crystallization methods have been applied to prepare the four known polymorphs of pyrazinamide. The thermal expansion and the compression of the four polymorphs have been analyzed and the relation between the observed behavior and the structures is discussed. This part is presented in chapter III. The phase behavior of the four polymorphs and the liquid phase has been investigated by differential scanning calorimetry and powder X-ray diffraction. The effects of the heating rate of the differential scanning calorimeter and of the sublimation on the phase transitions have been studied in detail. A pressure-temperature phase diagram involving forms α and γ, the liquid, and the vapor phase has been constructed using thermal analysis, specific volumes, and the vapor pressure. The stable domain for the γ form has been determined. This will be described in detail in chapter IV.

Chapters V and VI focus on the investigation into the interactions between pyrazinamide and the urea derivatives. The interactions in solution have been studied by proton nuclear magnetic resonance (NMR). The charge distributions and the electrostatic potential distributions have been calculated for pyrazinamide, the solvents, and the urea derivatives to reinforce the analysis of the NMR observations. The effect of the urea derivatives on the crystallization process of pyrazinamide in the vapor phase has been explored in the induction time, complete sublimation time of the γ form and the morphologies of the γ form crystals obtained in the absence and the presence of the urea derivatives.

In chapter VII, pyrazinamide crystallization during spray drying in the absence and the presence of the urea derivatives is discussed. In addition, the eutectic temperatures and the recrystallization temperatures of mixtures of pyrazinamide and the urea derivatives have been determined. Solubilities of pyrazinamide and the urea derivatives have been determined and ternary phase diagrams have been constructed to analyze the effect of the various urea related molecules on the crystallization behavior of pyrazinamide.

Chapter I: Generalities

I.1 The crystalline state

The states of matter can be solid, liquid, and gas. Among the condensed phases, what differentiates the solid from the liquid is the lack of three types of large-amplitude molecular motion: translation, rotation, and internal rotation or conformational motion.[5] Solids can be crystalline or amorphous, which can be differentiated by the presence or absence of long range order, respectively. Crystals exhibit three-dimensional long-range order as the molecules are arranged in a three-dimensional tri-periodic crystal lattice; however, disorder can exist in crystals compatible with the crystalline nature.[6, 7] Disorder can induce distortions or fluctuations in crystal lattices. Structural disorder may be either static or dynamic. Static disorder is temperature-independent, whereas dynamic disorder tends to increase with the temperature. The two types of disorder can be distinguished by temperature-dependent analysis using solid-state nuclear magnetic resonance (NMR) spectroscopy or single-crystal X-ray diffraction (XRD).[8]

Molecules, ions, atoms etc. can be found in different crystalline assemblies: polymorphs, solvates, hydrates, salts, co-crystals and so on. Figure I.1 exhibits several common crystalline assemblies. ‘Polymorph’ refers to the capacity of a single type of molecule (or other chemical entity) to exist in more than one crystal arrangement.[9, 10] A solvate is defined by the presence of solvent molecules in the crystal lattice of a given molecule. They can be divided into stoichiometric (including a fixed ratio between the solvent molecule and the host molecule) and non-stoichiometric solvates (with variable ratio between the solvent molecule and the host molecule).[10] A hydrate is a special case of solvate in which the solvent molecule is water, ubiquitous in many industrial environments. A salt can be in terms of a well-defined separation of charges due to the presence of metal ions, strong acids, or the pKa balance between different constituents in the crystal..[11, 12] G. Patrick Stahly has defined a cocrystal as: ‘co-crystals consist of two or more components that form a unique crystalline structure having unique properties’.[13] In this thesis, we placed an emphasis on crystalline solids, especially on their polymorphism.

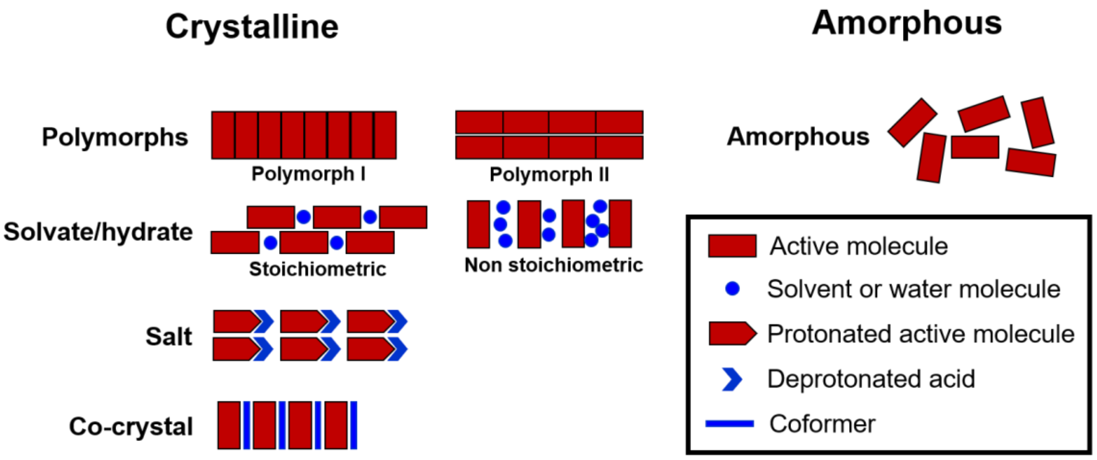

Figure I.1 Schematic depiction of several common types of solid forms

I.1.1 Polymorphism

Polymorphism is a common phenomenon in inorganic and organic systems. Different polymorphs of same chemical species exhibit different physicochemical properties, such as melting point, solubility, optical and electrical properties. For pharmaceuticals, it is important to understand their polymorphic behavior in order to choose the polymorph with the desired solubility, dissolution rate, and relative stability to achieve the appropriate level of bio-availability and drug stability.[14, 15]

Polymorphism can be classified into three categories based on the molecule and arrangement[16] (Figure I.2): 1) conformational polymorphism: differences in molecular conformation leading to different crystal structures, for example tolfenamic acid[17]; 2) packing polymorphism: the arrangement of rigid molecules, or of flexible molecules in the same conformation, differs, for instance the polymorphs of benzamide[18]; 3) synthon polymorphism: hydrogen bonding or supramolecular synthon may be differently positioned in crystal structures of the same chemical species, such as sulfathiazole[19, 20] and cocrystals of temozolomide[21]. These three categories can overlap.

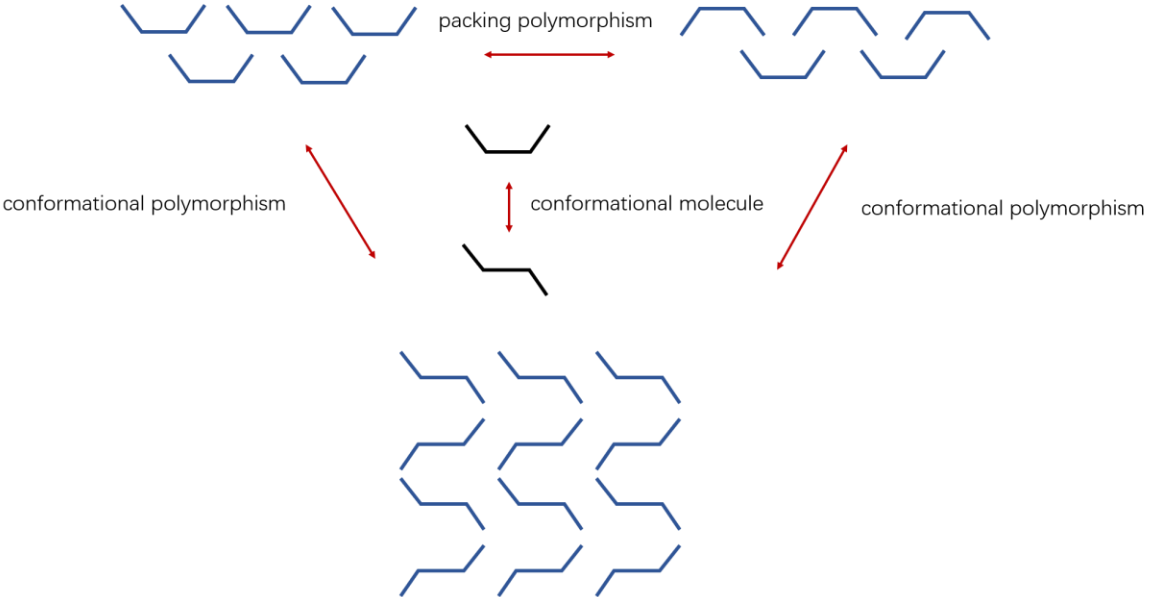

Figure I.2 Types of polymorphs

There are many characterization methods to investigate polymorphism and their transformations. X-ray diffraction (XRD) patterns are unique to specific crystalline arrangements and make XRD one of the most important techniques for identifying polymorphs. Single-crystal XRD is the most effective technique to determine crystal structures. Powder XRD can be used to quantify the relative composition of different polymorphs and in favorable conditions, solve their crystal structures if single crystals are hard to obtain. Differential scanning calorimetry (DSC) and thermal gravimetric analysis (TGA) can be used to measure thermal data to determine phase transformations. Infrared and Raman spectroscopy are other methods that can be used to distinguish polymorphs.[22]

I.1.2 Crystal morphology

The crystal morphology is defined by the set of crystallographic planes that describes the entire crystal surface, which is therefore inherently determined by the crystal structure.[23] Any factor that affects the molecular deposition rate will affect the crystal habit.[24] Those factors can be classified in two categories: internal and external. Internal factors include crystal defects for example, whereas external factors are related to experimental conditions and involve the solvent, the level of supersaturation, and impurities among others.[25, 26] Therefore, the same polymorph of a given compound may have different habits depending on the crystallization conditions. The crystal morphology and the crystal habit not only affect processes such as filtration, washing, and drying, but also product properties like bulk density and flowability.[27] A few models have been developed to predict the crystal morphology and habit from the crystal structure.

The Bravais-Friedel-Donnay-Harker (BFDH) model

Morphology prediction based on the crystal lattice geometry was firstly proposed by Bravais in 1866.[28] The basis of the relationship between morphology and internal structure was subsequently discussed by Friedel.[29] This theory was further developed by Donnay and Harker[30] resulting in the BFDH model. It can be summarized as 'taking into account submultiples of the interplanar spacing d_{hkl} due to space-group symmetry, the most important crystallographic forms will have the greatest interplanar spacings'.[31] Thus in the BFDH model, the crystal morphology is predicted using only the unit-cell parameters and the space group it belongs to.

The periodic bond chains (PBC) model

The periodic bond chains (PBC) model was developed by Hartman and Perdok.[32-34] In this model, it is assumed that crystal growth can be considered as the formation of bonds between the crystallizing molecules.[35] This theory applies if 1) crystal growth is controlled by the surface, 2) defects have no effect on the growth process, and 3) the growth process is carried out through the formation of relatively strong intermolecular interactions.

Attachment-energy (AE) model

The attachment-energy model is based on the PBC theory and was developed by Bennema and Hartman.[36] It takes into account the anisotropic energy in the unit cell.[37] The model assumes that the faces with higher attachment energies E_{att} should have a higher growth rate.

$$E_{att} = E_{latt} - E_{slice} \tag{I.1}$$

with E_{latt} the lattice energy and E_{slice} the energy of a growth slice of thickness d_{hkl}. R_{hkl}, the relative growth rate of the crystal face in vacuum is assumed to be proportional to E_{att}.

$$R_{hkl} \propto E_{att} \tag{I.2}$$

The AE model is usually used to predict the morphology of crystals obtained in the vapor phase.

I.1.3 Twinning

Twinning is an aggregation or intergrowth phenomenon of at least two crystals of the same molecular species joined together in a defined crystallographic orientation.[7, 25] Twins can be classified in different ways. 1) By morphology, including contact twins, sector twins, polysynthetic twins, penetration twins and so on. 2) By lattice domain overlap, including merohedral twins (twins with parallel axes) with full, three-dimensional lattice coincidence and nonmerohedral twins (twins with inclined axes) with two or one-dimensional lattice coincidence. 3) By their origin, including growth, transformation, mechanical, or deformation twins.[25]

Two formation mechanisms are hypothesized for twinning: either it appears during nucleation or during the growth process. Buerger proposed that twinning occurs during the first stage of spontaneous nucleation, before the nucleus reaches the critical size.[38] Penetration twins and sector twins point to twinning during nucleation. A number of models describe twinning during the crystal growth process. 1) A two-dimensional nucleus appears in twin position on a face of a macroscopic single crystal.[38] This type of twinning will be promoted by defects on the crystal face. 2) The twinning domains appear as 'inserts' and extend from the initiating defects into the direction of the growth of the face. These are merohedral twins.[39] 3) In melt or solution crystallization, small crystals may accidentally stick to each other with analogous faces $(hkl)_1$ and $(hkl)_2$ in twin position and then grow further as a twin.[40] 4) In some cases, the morphology of twinned crystals may be drastically modified compared to single crystals.[41, 42]

The twin boundary is the plane of contact between the faces of the two twin domains, and is also called twin interface, contact plane, composition plane, domain boundary or domain wall.[43] The twin boundary implies a reduction of the mutual surface energies. The occurrence of twinning and the shape and arrangement of a twinned crystal are governed by the twin interface, its structure, preferred orientation, and interfacial energy.[25, 43]

I.2 Crystallization methods

Crystallization is one of the oldest batch operations to obtain crystalline solids and which is widely applied in the pharmaceutical, chemical, and food industries for example.[44-46] Its widespread application is not only on the account of achieving both separation and purification in a single batch process, but also on the account of producing particles with well-defined qualities such as homogeneous particle size and level of purity. Interrelations between the crystallization process, the phenomena it invokes, its functions and the final product are presented in Figure I.3.[47] Kitamura published a paper about polymorph control in which various substances, crystallization methods, and processes have been investigated.[48] Lerond et al. studied the effect of the cooling profile in cooling crystallization on the filterability of the crystals demonstrating the influence of size and shape.[49] Lyophilization can produce high surface area powders with high dissolution rates.[50] Crystallization from solution is the most common method, including cooling crystallization, evaporation crystallization, antisolvent crystallization, reaction crystallization and so on. Some crystallization methods are solvent-free, such as melt crystallization and sublimation crystallization. There are other crystallization methods, like spray drying and freeze-drying. Cooling crystallization, evaporation crystallization, spray drying, and sublimation crystallization have been used in this study.

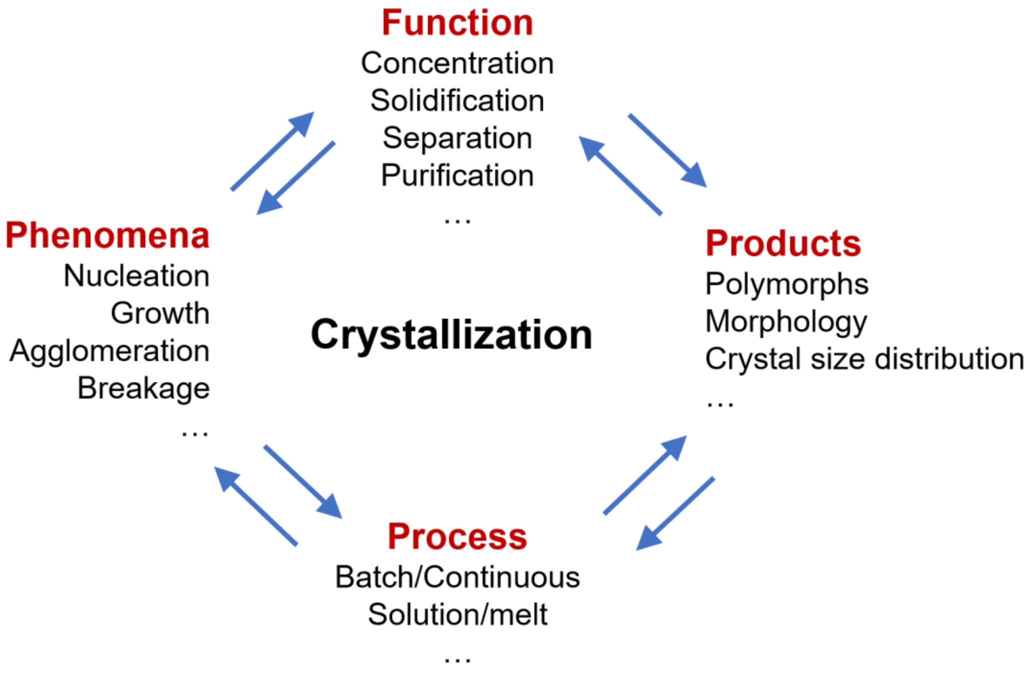

Figure I.3 Interrelations in crystallization

I.2.1 Crystallization from solution

Crystallization from solution includes different crystallization methods, and its thermodynamic driving force is supersaturation. The flows of material and energy and crystallization kinetics (nucleation and growth) determine the accessible degrees of supersaturation, which can be expressed as $\sigma = (c - c^*)/ c^*$. c is the real concentration. c^* is the saturation concentration, which is also known as the solubility. It is an important thermodynamic parameter in crystallization.

I.2.1.1 Solubility

Solubility is an important parameter in solvent screening. It is the main factor affecting product quality and yield. The difference in solubility between polymorphs can be used to study their relative stability. Solubility is defined as the equilibrium concentration of a solute in a solvent in the presence of its solid phase at a given temperature and a given pressure. It is the maximum stable amount of solute dissolved in a given quantity of solvent. Solubility is commonly expressed in terms of molar fraction:

$$x = \frac{n_{solute}}{n_{solute} + n_{solvent}} \tag{I.3}$$

Where, x is molar solubility and n the number of moles of the respective constituent. Solubility is determined with two experimental methods: thermodynamic and kinetic.[51] The two methods will be presented in section II.4.6.

I.2.1.2 Cooling crystallization

Cooling crystallization is generally applied for compounds whose solubility greatly increases with temperature.[52] Supersaturation is generated by cooling down the solution. Various operating conditions can affect the final crystals.

Important parameters are solubility and solvent. Solubility differs depending on the solvent. Hilfiker pointed out that the solubility used in cooling crystallization should be in the range of 10-100 mg mL^{-1}.[1] Too low or too high solubility is not conducive to yield good quality crystals. Khoshkhoo et al. investigated the effect of solvent on the polymorphs of sulphathiazole and it was concluded that some solvents selectively cause the crystallization of specific polymorphs, which was ascribed to kinetic effects.[53] The effect of the solvent on morphology was studied by Martino et al..[54] It was demonstrated that the polarity of a solvent may affect the solvent-solute interactions on certain crystal faces more than others resulting in different morphologies.

The cooling rate and the overall cooling profile are important operational factors that have a large influence on crystallization kinetics and thus on the final crystals. Cooling profiles can be linear or more sophisticated.[49] Mohameed et al. investigated the effect of cooling profiles on the crystallization kinetics and the mean final particle size of KCl and the natural cooling profile produces the smaller crystal size distribution than other cooling profiles used in the literature.[55] The cooling rate effect on polymorphs of pyrazinamide have been studied.[56] Metastable polymorphs are obtained at higher cooling rates, which can be explained by the Ostwald "Rule of Stages". This rule implies that the least stable polymorph should be crystallized first in the crystallization.[57]

Seeding is widely used in cooling crystallization. Polymorphism of seeds, seed loading and seed size affect the obtained polymorphs and the properties of the final crystals, such as the crystal size distribution.[58-60]

In addition to the factors mentioned above, others like stirring rate[61] and additives[62] can have an influence on the crystallization process and the final crystals.

I.2.1.3 Evaporation

Evaporation crystallization is suitable for substances whose solubility increases slightly, remains almost invariable, or even decreases with temperature.[52] The solute concentration increases and reaches supersaturation by evaporation. Solvent, evaporation temperature, evaporation rate and other parameters can affect the crystallization process and the product. Evaporation at ambient condition is a commonly used method to prepare single crystals and to screen for polymorphs.

I.2.2 Spray drying

Spray drying is defined as "the transformation of feed from a fluid state into a dried particulate form by spraying the feed into a hot drying medium."[63] The method was first mentioned in 1860 and the first patent about spray drying was registered in 1872 in the US.[64] Until World War II the spray drying technology continuously increased in process performance, efficiency, and safety. The demand of reducing the weight of food for transport strongly promoted the development of the technology. Milk powder was the first industrial spray-dried product.[65, 66] After a series of improvements, spray drying has become a widely used technology in fields of fertilizer, food, ceramics, detergent, and pharmaceutical processing.[67-71] The spray drying process involves four main stages: Atomization of the feed solution into a spray, spray-air contact, droplets drying and particle separation. Many parameters can be adjusted in spray drying to influence the properties of the final particles (see Table I.1).

Table I.1 Parameters and their influence during spray drying

Parameters	Influence	Ref.
Gas humidity	Higher humidity, moist particles can be obtained	[72]
Spray gas rate	Low flow rates of atomizing air increase mean particle size, enhances powder flowability	[73]
Feed concentration	Drying gas is dehumidified gas. The higher the feed concentration, the more rapid surface formation of particle, the larger the particle size and the higher the product yield	[72, 74]
The feed flow rate	The higher the flow rate the larger the droplet size	[75]
Inlet temperature	The higher the inlet temperature the lower the residual moisture	[75]
Aspirator speed	Lower aspirator speeds lead to lower residual moisture content and a lower degree of separation in the cyclone	[75]

I.2.3 Sublimation crystallization

Sublimation refers to transformation from the solid phase to the vapor phase: solid→vapor. For sublimation crystallization a condensation step is involved to grow the crystals; thus, the substance undergoes a solid → vapor → solid sequence of transformations. The principle of sublimation crystallization can be explained by the pressure-temperature phase diagram shown in Figure I.4. The three phases of a chemical compound are presented in their respective stability domains: solid, liquid, and vapor. These three phases are separated by the solid-vapor equilibrium curve (A-T), the solid-liquid equilibrium curve and the liquid-vapor equilibrium curve. The intersection of the three curves is the triple point T in the figure. In sublimation crystallization experiments, the solid is heated up to for example point B, which is below the triple point. Only solid and vapor will be present in the system. In some cases, solid may be heated up to point B' and the system will consist of liquid and vapor. Assuming that at point B, the vapor is not entirely in equilibrium with the solid, its vapor pressure will be lower. This lower pressure will be in equilibrium with the solid at a lower temperature. Thus within a temperature gradient, crystallization will take place once the vapor pressure finds its equilibrium temperature with the solid, as indicated by the dashed line B – D – E in Figure I.4.[76] Although sublimation crystallization is not as widely used as solution crystallization, it has a few advantages. Compared to cooling crystallization, the loss of material in sublimation is in principle negligible. The process is free from solvents and the final product is dry.[77] A major limitation of sublimation crystallization, however, is decomposition that may occur during sublimation.

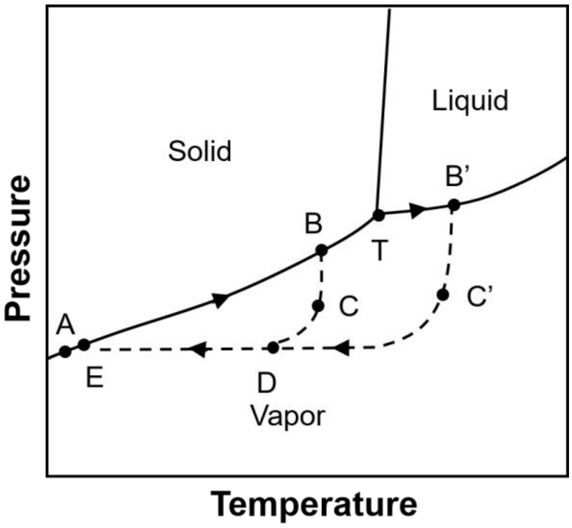

Figure I.4 Sublimation crystallization cycles under a temperature gradient

Sublimation crystallization equipment usually consists of a closed environment in the form of a tube with at one side a heating source to sublimate the raw material and at the other side a colder part for the condensation of the final crystals.[78] Gases or vacuum can be used to vary the sublimation and condensation conditions such as diffusion.[79] Commonly used sublimation crystallization equipment are a cold-finger[78], horizontal tubes attached to furnaces[80] and various in-house-constructed sublimators[79, 81]. Sublimation and condensation temperature[82], temperature gradient[83], vapor pressure[84], gaseous medium or additives[82] and the deposition surface or template[85] can affect the crystallization outcome. Shen et al. prepared different polymorphs of 5-methoxy-salicylaldhyde azine by sublimation crystallization at different temperatures.[86] Low temperature gradient sublimation in vacuo technique can be used to prepare high quality crystals.[81]

I.3 Phase transitions in the solid state

I.3.1 Direct and indirect solid-solid phase transition mechanisms

Solid-solid phase transitions, the transformation from one crystalline form into another, can be divided into direct and indirect transitions. The direct phase transition occurs spontaneously under the effect of temperature or pressure. Indirectly, the initial solid phase may transform into a different solid phase by the intervention of a third phase, such as solution-mediated or melt-induced transformations or as discussed just before transformations through the vapor phase.[10, 87, 88]

I.3.2 Mechanisms of solid-state phase transitions

Nucleation and growth have been used to explain certain solid-state phase transitions.[89] Two distinct mechanisms of this type can be discerned. In the first case, nucleation of the final phase appears at voids in the microstructure of the initial phase followed by crystal growth in a ‘molecule-by-molecule’ transformation. No particular orientational relationship needs to exist between the two phases. In the second case, nucleation appears at cracks with a specific orientational relationship with the second phase, such a mechanism is called ‘epitaxial’. Other mechanisms exists related to cooperativity, packing frustration, concerted movements, microstructure and mosaicity, modulated structures, zip-like mechanisms, anomalous thermal expansion, lattice strains, internal molecular motions, and mesoscopic effects, that have been proposed recently in relation to molecular motion in the mechanisms of solid-state phase transitions.[8]

I.3.3 Thermodynamics

Polymorphs of a given chemical compound may exhibit different properties and therefore their relative stability is of importance for industrial applications, such as in pharmacy. The polymorph with the lowest free energy is thermodynamically the most stable polymorph, while the other polymorphs with higher free energies may be metastable. The cause of the different free energies lies mainly in the interactions between the molecules, resulting in different internal energies and densities; in other words, if the molecular configuration or crystal configuration is not the same, the free energy must be different.

Polymorphs can exhibit enantiotropic or monotropic behavior. In a monotropic relationship, only one of the two polymorphs is stable, that is, the Gibbs free energy of one polymorph is always lower below its melting point than the free energy of the other polymorph. In an enantiotropic relationship, an intersection of the Gibbs free energy curves of the two polymorphs exists before the melting point of the two polymorphs. The temperature corresponding to the intersection is called the equilibrium temperature and the relative stability between the two polymorphs is inverted on either side of the equilibrium temperature.

I.3.3.1 Pressure-temperature phase diagram

Pressure-temperature (P-T) phase diagrams provide information on the relative stability between crystalline polymorphs as a function of the thermodynamic variables, characteristic of the Gibbs energy function, temperature and pressure. Such phase diagrams can be obtained by direct measurement, but due to experimental limitations, it is often easier to use the Clapeyron equation (eq. I.4) to construct or complete the phase diagram:

$$\frac{dp}{dT} = \frac{\Delta S}{\Delta V} = \frac{\Delta H}{T\Delta S} \tag{I.4}$$

in which, ΔS is the entropy change between the two phases, ΔH is the enthalpy change, ΔV represents the volume change, and T is the equilibrium temperature at which the enthalpy change has been obtained. Eq. I.4 provides the slope of a two-phase equilibrium as a function of the temperature and the pressure and phase diagrams obtained through extrapolation are called topological phase diagrams, because the positions of the equilibria will be qualitatively correct, but the uncertainty over their position may be larger than in the case of experimentally obtained equilibrium information.

I.3.3.2 Thermal expansion and compressibility

Thermal expansion of a solid is the result of an increase in the lattice vibrations with an increase in temperature. In 1929, Grüneisen proposed a simple theory for the thermal expansion of crystals with the expansion coefficient decreasing to zero if the temperature tends to absolute zero.[90] In general, the volumetric coefficient of thermal expansion α_V is used to express the volume change of a substance due to a temperature change[91] and it is expressed as:

$$\alpha_V = \frac{1}{V}\left(\frac{\partial V}{\partial T}\right)_p \tag{I.5}$$

where V is the volume and T is temperature.

In general, solids exhibit a positive thermal expansion, i.e. their volume increases upon heating. Some solids exhibit negative thermal expansion, although uniaxial negative thermal expansion is more common.[92]

Corresponding to the thermal expansion, the compressibility is used to express the relative volume change of a solid with a pressure change and the volumetric coefficient compressibility β_V can be expressed as:

$$\beta_V = -\frac{1}{V}\left(\frac{\partial V}{\partial p}\right)_T \qquad (I.6)$$

where p is pressure.

Like thermal expansion, the compressibility usually is positive, which means the volume decreases with the increase of pressure. However, the compressibility could be negative in some conditions.[93]

I.4 Effect of additives on crystallization and phase transition processes

Additives play an important role in crystallization processes, like nucleation and growth processes, and can lead to the change of polymorph, morphology and so on.[94] Additives can be divided into solid and dissolved additives. Solid additives can serve as a template or substrate to guide the crystallization process. Caridi et al.[95] investigated the crystallization of isonicotinamide in the presence of templates, for example synthetic zeolite ZSM-5, that exhibit porous and regular surface structures in the nanometer range. These heterogeneous templates enhance the nucleation rate. One of the templates consisting of TiO_2 also induced the nucleation of a metastable polymorph of isonicotinamide.[95] The crystallization mechanism induced by templates can be related to epitaxial growth.[96] Epitaxial growth occurs through a geometrical match of the crystallizing molecules and the substrate. Ledge-directed epitaxy was proposed by Ward and his colleagues and this mechanism can be described as crystal nucleation sites created by a substrate ledge with similar dimensions to a step plane of the nucleating crystal.[97, 98] Intermolecular interactions between solute and additives can play an important role in crystallization.[62, 99] The functional group on additives can strengthen interactions between additives and solutes and hence influence the nucleation process. In some cases, functional groups of the substrate may have an important effect on epitaxial growth.[100]

Dissolved additives can influence crystallization processes in different ways. They can control the crystallization process during nucleation and during growth. The influence of additives on nucleation can be studied through the changes of the metastable zone width in relation to the nucleation induction time in the presence of additives.[101] An additive can inhibit, delay, or enhance crystal nucleation.

Dissolved additives serving as an inhibitor in the nucleation process has been studied by many researchers. Peng and coworkers investigated the crystallization process of borax decahydrate in the presence of Cl^- and SO_4^{2-} ions.[102] The solubility increased in the presence of additives, the metastable zone was widened, and the induction period prolonged, thus slowing down the nucleation. In some research papers, the inhibition mechanism is explained by a solute removal mechanism. It can be presented as a complex set of molecular interactions that hinder the prenucleation aggregates from being formed.[103] Myerson and coworkers investigated the inhibition effect of a weakly hydrogen-bonding molecular additive on nucleation.[104] They proposed an inhibition mechanism in which the solute and the additives form intermolecular complexes, which hinder molecular aggregates to form and delay nucleation. Addadi et al.[105] compared the etch pits at preselected crystal faces in the absence and presence of inhibitors. They suggested that etching with additives can increase the surface area of crystals and this should influence the dissolution rate.[105]

There are many different ways in which additives can enhance nucleation. Han and co-workers investigated the influence of electrolytes on DL-alanine nucleation by measuring induction times.[106] They found that all electrolytes used in their research decreased the induction time. It means that the presence of electrolytes enhances nucleation of DL-alanine. They suggested that electrolytes may promote the formation of head-to-tail chains during prenucleation. These chains structurally match the crystalline packing of DL-alanine and act as crystal precursors, thus promoting DL-alanine nucleation. In another study, Han and co-workers studied the effect of inorganic acids and bases on nucleation of the polymorphs of glycine.[107] Nucleation rates of both α-glycine and γ-glycine accelerate in acidic and basic solutions and the acceleration for γ-glycine is larger. Their analysis suggests that glycine head-to-tail chains can form based on the glycine ions existing in acidic and basic solutions. These chains match γ-glycine crystalline packing, thus favoring γ-glycine nucleation over α-glycine nucleation. Such approaches can be applied to controlled crystallization of a specific polymorph.

Dalvi and Dave studied crystallization of four poorly water-soluble APIs in the presence of hydroxypropyl methyl cellulose (HPMC) while undergoing an ultrasound treatment.[108] The nucleation rate was estimated through population densities based on particle size distribution data. They thought that HPMC increases the viscosity of the solution and thus decreasing its diffusivity. In addition, HPMC could decrease the solid–liquid interface tension, which may act to reduce the energy barrier for nucleation. Hence, HPMC increases the nucleation rate of the APIs. Kim and coworkers explored the influence of amphiphilic additives on the nucleation process of hexahydro-1,3,5-trinitro-1,3,5-triazine (RDX) by analyzing induction time and by molecular simulation.[109] The molecular simulation supports the idea that the additives could interact with the surface of an RDX cluster, and thus decreases the interfacial energy.

Some papers have investigated both nucleation and crystal growth and the general conclusion that can be drawn is that nucleation inhibition is often more efficient than inhibition of crystal growth.[110, 111]

Besides influencing the nucleation and crystallization processes, additives have been reported to influence phase transitions, in particular the transition rate and the transition temperature. In some studies, additives can decrease the phase transition rate. Mukuta et al.[112] studied the solution-mediated phase transformation of one API in the presence of tailor-made impurities and the result indicated that the transition rate of metastable form to stable form decreased. They thought that the kinetic stabilization of the metastable form in the presence of additives was caused by the incorporation of the impurity into the stable form impeding its nucleation and growth. Kamali et al. investigated the influence of additives on the sublimation temperature and polymorph control.[113] In their study, temperature reduction and polymorph control were observed in the sublimation of carbamazepine in the presence of acetamide. Form III of carbamazepine sublimated at 120 °C leads to the crystallization of a mixture of forms I and III. In the presence of acetamide, pure form I could be obtained at 100 °C. The sublimation rate had increased as well. The authors proposed that the mechanism involves the formation of a more volatile hydrogen bonded adduct ‘carbamazepine-additive’. They also investigated the effect of polycrystalline powder templates on polymorph control.[85, 113] By using polycrystalline powder templates, the same polymorph as the template could be obtained for different polymorphs of carbamazepine, paracetamol, metaxalone, mefenamic for example.

I.5 Pyrazinamide

I.5.1 Introduction

Pyrazinamide (PZA, CAS: 98-96-4) was synthesized for the first time by Dalmer et al. in the 1930s.[114] However, it raised a lot of attention in the 1950s due to its remarkable anti-mycobacterium (tuberculosis) activity in mice.[115, 116] It was immediately used to treat tuberculous patients without further investigation and found to be effective.[117] It could shorten the treatment time of tuberculosis patients.[118] Presently, it is a first-line drug against tuberculosis.[119] Pyrazinamide has a formula of $C_5H_5N_3O$, and its molecular weight is 123.11 g mol^{-1}. Its molecular structure is shown in Figure I.5.

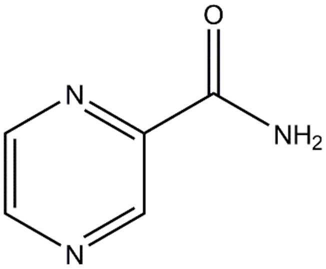

Figure I.5 Molecular structure of pyrazinamide

I.5.2 Polymorphs of pyrazinamide

I.5.2.1 Crystal structure of the four polymorphs of pyrazinamide

Pyrazinamide possesses at least four polymorphs, named α, β, γ, and δ. The crystallographic data of the four polymorphs found in the literature are presented in Table I.2. α, β and γ forms are monoclinic with space groups $P2_1/n$, $P2_1/c$, and Pc, respectively while δ form is triclinic with space group $P\bar{1}$.[120-132] Comparing the crystal packing of the four forms shown in Figure I.6, the γ form exhibits a different hydrogen-bond pattern than the other three polymorphs. In the γ form, intermolecular hydrogen bonds link the amide group and the top of the pyrazine ring forming linear molecular chains. However, the polymorphs α, β, and δ contain dimers with two N-H···O hydrogen bonds between the facing amide groups.

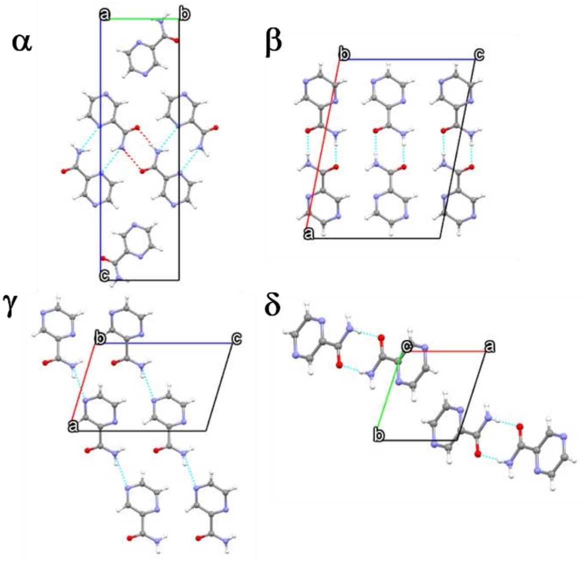

Figure I.6 Crystal packing of the four polymorphs of pyrazinamide

Table I.2 Crystallographic data of the four polymorphs of pyrazinamide in the literature

Polymorph	Space group	T / K	Unit cell parameters						V^a /Å^3	Specific volume^b /cm^3 g^{-1}	Ref.^{c}
			a	*b*	*c*	α	β	γ			
α	$P2_1/a$	RT^d	23.072	6.727	3.725	90	101.0	90	567.518	0.69403	PYRZIN [120]
	$P2_1/c$	RT^d	3.73(1)	6.84(3)	22.76(2)	90	101.1(5)	90	569.817	0.69684	PYRZIN04 [124]
	$P2_1/a$	RT^d	23.20(4)	6.77(1)	3.75(1)	90	101.2	90	577.773	0.70657	PYRZIN14 [131]
	$P2_1/n$	100	3.6147(4)	6.7384(8)	22.464(3)	90	92.499(2)	90	546.642	0.66850	PYRZIN15 [126]
	$P2_1/n$	180	3.6541(2)	6.7358(3)	22.537(2)	90	92.225(2)	90	554.291	0.67785	PYRZIN21 [127]
	$P2_1/n$	100	3.6173	6.7413	22.4625	90	92.395	90	547.276	0.66927	PYRZIN22 [130]
β	$P2_1/c$	RT^d	14.372(7)	3.711(3)	10.726(5)	90	101.92(5)	90	559.730	0.68450	PYRZIN01 [122]
	$P2_1/c$	90	14.3396(7)	3.6211(2)	10.6131(5)	90	101.0440(7)	90	540.881	0.66145	PYRZIN23 [132]
	$P2_1/c$	100	14.315(2)	3.6238(5)	10.6158(15)	90	101.119(2)	90	540.354	0.66081	PYRZIN18

											[129]
δ	$P\bar{1}$	RT[d]	5.728(2)	5.221(3)	9.945(6)	96.81(5)	97.27(4)	106.22(4)	279.557	0.68375	PYRZIN02 [123]
	$P\bar{1}$	100	5.1186(10)	5.7053(11)	9.857(2)	97.46(3)	98.17(3)	106.47(3)	268.818	0.65749	PYRZIN16 [126]
γ	*Pa*	RT[d]	10.84	3.75	7.2	90	106.9	90	280.040	0.68493	PYRZIN03 [121]
	Pa	RT[d]	10.72	3.73	7.185	90	106.73	90	275.136	0.67294	PYRZIN05 [125]
	Pc	293	7.1830(4)	3.7291(2)	10.7581(5)	90	106.767(2)	90	275.917	0.67485	PYRZIN17 [128]
	Pc (with disorder)[e]	100	7.1756(14)	3.6508(7)	10.663(2)	90	106.337(3)	90	268.057	0.65562	PYRZIN19 [129]
	Pc (without disorder)[f]	100	7.170(3)	3.6477(15)	10.648(4)	90	106.350(6)	90	267.226	0.65359	PYRZIN20 [129]

I.5.2.2 Preparation methods of the polymorphs

Preparation methods of the pyrazinamide polymorphs have been described in the literature. Solution crystallization is in particular a common method. The α form can be obtained by slow evaporation in water and a mixture of water and ethanol.[128] Cooling crystallization in aqueous and organic solution is another method to prepare α.[56, 96, 133] The δ form can be prepared by slow evaporation from certain organic solvents, including tetrahydrofuran (THF), nitromethane, methanol, acetone, acetic acid and dichloromethane.[128, 134] By controlling certain process parameters (solvent, cooling rate, seeds) in cooling crystallization, the δ form can be obtained in methanol, in 1,4-dioxane and in their mixtures.[56] Co-spray drying pyrazinamide and PVP in a mixture of water and acetone results in the δ form.[2, 4] The γ form can be prepared by solvent-free processes, in particular by sublimation and by direct transition at high temperature from other forms.[128, 134] Lyophilization in aqueous solution also results in the γ form.[128] Spray drying in water, ethanol, or acetone or a mixture of water and ethanol or water and acetone results in the γ form.[2, 4] In addition to the above-mentioned methods for the preparation of pure γ form, additives or templates can be added in solution to prepare the γ form. Urea and its derivatives and some other excipients approved by the FDA can be used as additive to prepare the γ form by spray drying.[2] Sulfonamide and purine templates can be used through hetero-nucleation of the γ form in aqueous solution.[62, 96] The β form has so far not been obtained as a pure polymorph powder either by evaporation or by cooling crystallization; It has always been obtained in a mixture with other polymorphs.[96, 128] However, single crystals have been obtained in some experiments.[122, 132, 134] The preparation methods for the four polymorphs of pyrazinamide are summarized in Table A.1 in Appendix A.

Cooling crystallization from solution specifically targeting the δ form has been published by Hermanto et al.[56]. Solubilities of α, γ, and δ in water and solubilities of α in four organic solvents and in one mixture of solvents have been determined. The results indicate that the solubility of pyrazinamide increases with increasing temperature and the solubility data in water from about 287 K to 316 K possess the following solubility ranking γ > δ > α. The solubility of α in various solvents has been obtained by Zhang et al.[135].

I.5.3 The phase relationships between the four polymorphs of pyrazinamide

The relative stability of the four pyrazinamide polymorphs has been investigated in a number of papers. Cherukuvada et al. reported on polymorph transition temperatures and enthalpies, relative stabilities and crystal structure data obtained at 100 K.[129] A schematic energy-temperature diagram has been established resulting in the following stability hierarchy at room temperature $\alpha > \delta > \gamma > \beta$ with α the thermodynamically stable polymorph.[129] Castro et al. reached similar conclusions with a stability hierarchy of $\delta > \alpha > \gamma$ at low temperature, which may or may not include room temperature.[128] Including pressure into the analysis, Tan et al. found crystallographic indications that γ transforms into β at a pressure of about 4 GPa at room temperature.[136] It implies that form β would be more stable than γ above 4 GPa. For α and δ, no transformations under pressure have been observed up to 13 GPa.[136] Smets et al. investigated the transformation mechanism of pyrazinamide and concluded that the transition from the γ form to the low temperature δ and α forms include a vapor-mediated recrystallization process, while the transition from the low temperature forms to the γ form during heating included nucleation and growth within the crystal.[3] γ is the stable form at high temperature in all references. Calorimetric data available in the literature on the different polymorphs have been compiled in Table I.3. The average melting temperature of form γ observed in the literature is 462(2) K[1] with very little variation in the data. The melting enthalpy exhibits a larger spread around the average value of 221(10) J g^{-1}, while the value of 177 J g^{-1} has been omitted as a clear outlier (Table I.3). The average solid-solid transition temperature observed for α-γ is 421(4) K with an enthalpy of 11(4) J g^{-1}. However, Castro et al. carried out thorough investigations on the phase behavior of pyrazinamide using differential scanning calorimetry (DSC) and thermal stage microscopy, supported by powder X-ray diffraction (PXRD) and infrared spectroscopy and they observed that the α-γ transition depends on the heating rate of the DSC.[128] This makes it rather doubtful that the average observed solid-solid transition temperature between α and γ is the equilibrium temperature. Pyrazinamide is prone to crystallize and the vitreous state is very difficult to reach. Borba et al. prepared the vitreous state by depositing vapor at 10 K and they observed recrystallisation into the δ phase at 260 K while heating,[137] which is the closest observation to a glass transition temperature reported in the literature, if one assumes that pyrazinamide crystallizes immediately once it reaches T_g on heating the glass.

---

[1] The number in parentheses is the uncertainty in the last digit of the value, i.e. 1.23(4) equals 1.23 ±0.04.

Table I.3 Calorimetric and crystallographic data of the different phase transitions of pyrazinamide in the literature[a]

Phase transition	T /K	ΔH /J g^{-1}	Heating rate /K min^{-1}	References
γ→L	461.4(5)	228(5)	10	[128]
	461.5(1)	228(3)	10	[138]
	461.8(2)	213(5)	5	[129]
	462.5(2)	220(5)	2	[139]
	462.25	221.6	10	[140]
	465.7(2)	220(5)	2	[141]
	463.15		10	[142]
	461.15	177	10	[143]
	461.4(5)	229(3)	5	[144]
	462.2(1)		10	[145]
	461.5(1)	217(24)	5	[2]
α→γ	418.15-419.15			[146]
	420.1(5)	13.2(7)	10	[128]
	428.25	10.6	5	[129]
	420.15	5	10	[143]
	420.4(5)	13.3(2)	5	[144]
	420.65	11.35	5	[2]
δ→γ	408(5)	17(2)	10	[128]
	404.35	13.5	5	[129]
δ→α	395(1)	$\Delta H > 0$[b]	10	[128]
β→γ	368.15	$\Delta H > 0$[b]	10	[128]
	372.55	6.3	5	[129]
pyrazinamide→vap		829(18)[c]		[147]
α→vap		915(13)[d]		[141]
α→vap		715(44)[e]		[148, 149]

[a] Values from the literature reported in °C or in J mol^{-1} are modified by adding 273.15 K or are divided by 123.11 g mol^{-1}, respectively; an average value is used in this table when multiple values have been reported in the same paper; values are rounded to the number of reported digits in the respective reference.

[b] Enthalpy values have not been mentioned in reference[128] but DSC curves in the figures indicate endothermic transitions with increasing temperature.

[c] Most likely form γ as the temperature of measurement is 421 K, however the enthalpy has been adjusted

by the authors to the value expected at 298.15 K.

[d] The temperature range is from 359.15 K to 383.15 K.

[e] The temperature range is from 353.15 K to 383.15 K.

A number of simulation studies involving pyrazinamide have been published. The most extensive is that of Wahlberg et al. demonstrating and quantifying disorder in the structure of the γ form[134] as mentioned before by Cherukuvada et al.[129]. Computational studies specifically targeting the β form of pyrazinamide have been published by Jarzembska et al.[132]. The α-γ phase transformation has been investigated by in situ Raman and density functional theory (DFT) leading to a transition temperature of 418.15-419.15 K.[146]

A few studies have been published on vapor pressure of pyrazinamide. Blokhina et al. provided the vapor pressure as a function of the temperature from 359.15 K to 383.15 K: $\ln(p\ /\mathrm{Pa}) = -13360(178)\ /T\ (/\mathrm{K}) + 38.3(5)$, which was verified to belong to the alpha phase.[141] Negoro et al. reported the vapor pressure of the α form as a function of temperature from 353.15 K to 383.15 K as well.[149] Ribeiro et al. obtained the vapor pressure of most likely the γ form, considering the measurement temperature, but the authors did not verify the polymorph under study.[147] The sublimation enthalpy values from the different vapor pressure measurements vary too much to draw any solid conclusions about the stability and the equilibrium temperature between the α and γ phases (Table I.3).

I.5.4 Pyrazinamide in cocrystals

Besides the polymorphs, a lot of crystallographic work has been carried out on mixtures of pyrazinamide with excipients or other APIs. Cocrystals containing pyrazinamide with carboxylic acids[142, 150-152], haloperfluorinated compounds[133], hydrochlorothiazide[153], pyrogallol[154] and diflunisal[155] have been described. Several polymorphs of cocrystals of pyrazinamide with succinic acid[142, 156], malonic acid[157] and theophylline[158] have been investigated. Different binary mixtures leading to either cocrystals or eutectic systems have been described by Rajbongshi et al.[159] A ternary cocrystal has been designed by using a "drug-bridge-drug" strategy involving pyrazinamide combined with another first-line antitubercular drug isoniazid using fumaric acid as the bridge.[160] Forty-six different co-crystal or solvate structures with pyrazinamide are reported in the Cambridge Structural Database (CSD), including some polymorphic cocrystals.

Pyrazinamide contains one hydrogen bond donor and three hydrogen bond acceptors and all hydrogen bond donors and acceptors are involved in hydrogen bonds in the co-crystals. The amide group of pyrazinamide and the two nitrogen atoms of the pyrazine ring form hydrogen bonds with coformers or pyrazinamide molecules. In all of co-crystal or solvate structures, only three coformers have amide groups, two of them form double N-H···O hydrogen bonds with pyrazinamide like pyrazinamide dimers.[161-163] Twenty-three structures contain only interactions between pyrazinamide and the coformers, whereas twenty-two structures show interactions between pyrazinamide molecules themselves. Among the twenty-two structures, nineteen exhibit dimers involving two pyrazinamide molecules with a double hydrogen bond linking the amide groups, as found in the crystal structures of polymorphs α, β, and δ (Figure I.7a). One crystal structure contains a dimer structure with mutual hydrogen bonds between the NH of the amide group and an N in the pyrazine ring (Figure I.7b).[164] Another structure possesses a linear chain of hydrogen bonds between the NH at the amide group and an N at the pyrazine ring, like in the γ form (Figure I.7c).[165] And finally, one crystal structure contains a linear hydrogen bond chain based on N-H···O contacts between the amide groups (Figure I.7d).[166]

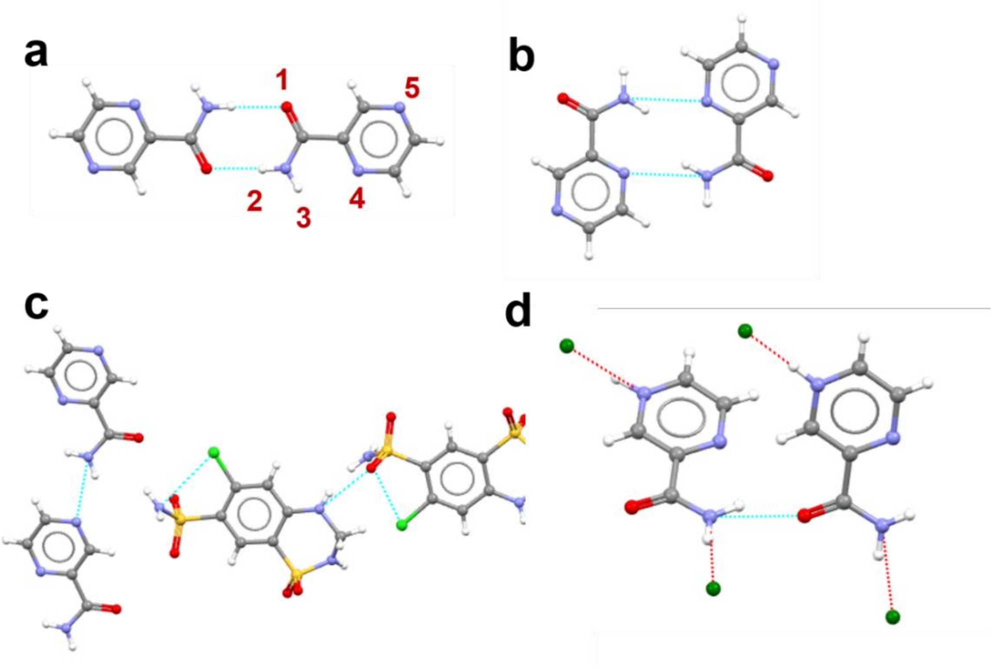

Figure I.7 Various hydrogen bonding assemblies in the cocrystals with pyrazinamide

I.6 Urea derivatives

Urea was isolated for the first time from urine by Rouelle in 1773 and it was the first organic compound that was synthesized from inorganic substances (ammonia and cyanic acid) by Wöhler in 1828.[167, 168] Although urea is a very simple and small molecule, it is a multifaceted functional group which exhibits a wide range of biological activities.[169] Therefore, urea and its derivatives are well-studied materials and they have been applied to many fields. In agriculture, urea is an important nitrogen fertilizer.[170] Because of its herbicidal activity, urea derivatives can be used as agricultural pesticides.[171, 172] In animal farming, urea is used as a nonprotein nitrogen compound in ruminant rations.[173-175] In manufacture, urea can be used as a raw material for preparing urea–formaldehyde resins.[176] Urea-plays an important role in the pharmaceutical industry, because of its biological and pharmacological activities, such as antiviral[177], antimicrobial[178], antimalarial[179] and anticancer activities[180] to mention a few.

In this thesis, acetamide, urea, *N*-methylurea, 1,1-dimethylurea (1,1-DMU), 1,3-dimethylurea (1,3-DMU), trimethylurea, 1,1-diethylurea (1,1-DEU), 1,3-diethylurea (1,3-DEU) and tetramethylurea are studied as additives to the crystallization process of pyrazinamide and they are collectively called urea derivatives in this work and their structures are presented in Figure I.8.

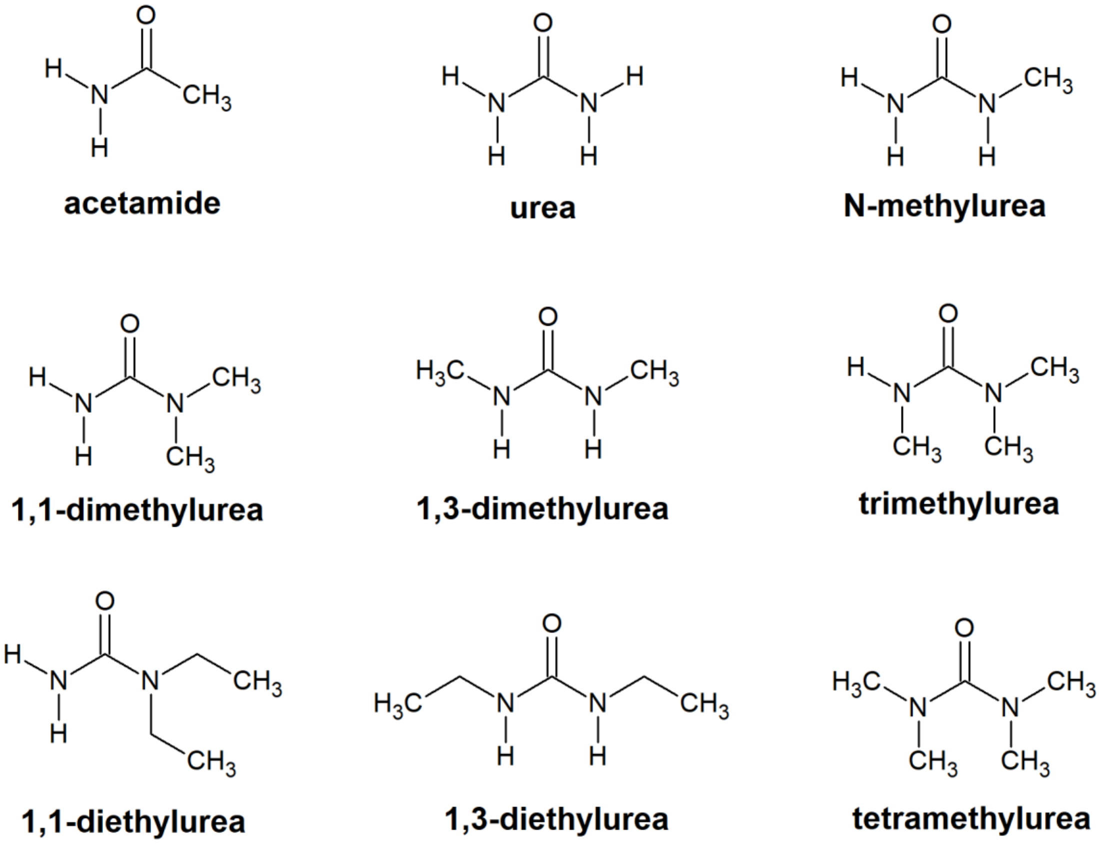

Figure I.8 Molecular structures of the urea derivatives

1.6.1 Acetamide

Acetamide (C_2H_5NO, 59.07 g mol^{-1} CAS: 60-35-5) can be used as raw material for medicine or as a solvent.[181] It has four known polymorphs. Form I is rhombohedral with space group *R*3*c*. It can be obtained by crystallization from organic solvents.[182] Form II is orthorhombic with space group *Pccn*. This polymorph is obtained by slow cooling of molten acetamide.[183] Form III is a monoclinic structure with space group $P2_1/n$. Single crystals have been obtained under pressure by Fabbiani et al.[184] Bridgeman proposed a pressure-temperature phase diagram of the four polymorphs of acetamide.[185] However, form IV has not been reported by any other researcher. Each molecule of acetamide possesses four hydrogen bonds and in forms II and III, two molecules form a dimer with the double O···H-N hydrogen bond (Figure I.9). Acetamide has been reported in many cocrystals and solvates; there are fifty-five different co-crystals or solvates listed in the CSD.

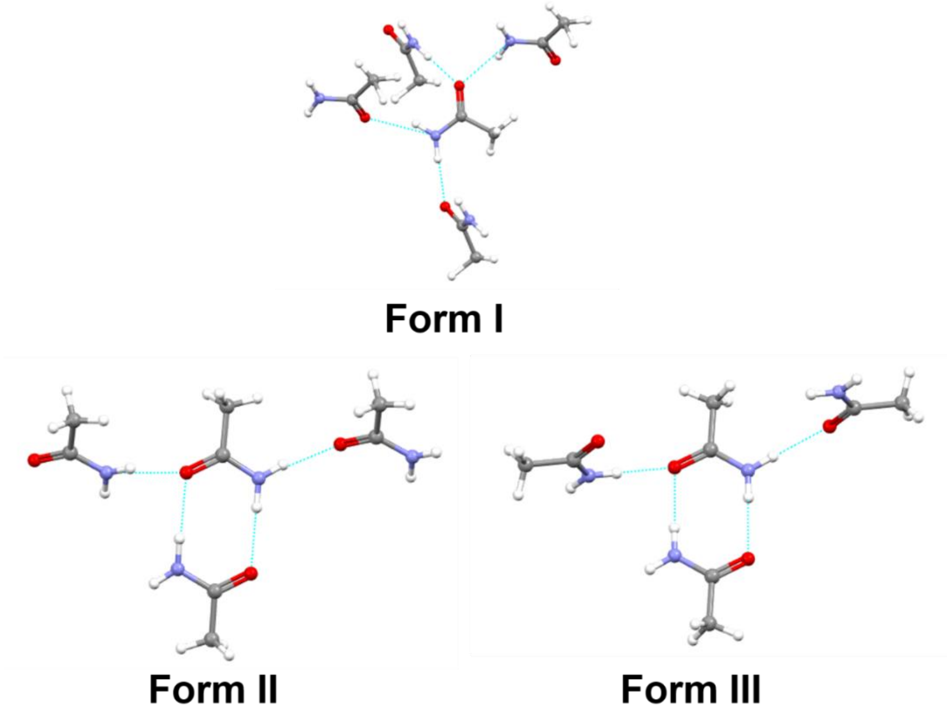

Form I

Form II

Form III

Figure I.9 Hydrogen bonds in different polymorphs of acetamide

I.6.2 Urea

Urea (CH_4N_2O, 60.06 g mol^{-1}, CAS: 57-13-6), a typical hydrogen-bonded molecular crystal, was one of the earliest organic compounds studied by X-ray diffraction.[186-189] At least four polymorphs have been observed, form I (tetragonal $P\bar{4}2_1m$)[190], form III (orthorhombic $P2_12_12_1$), form IV (which Bridgman named phase II[185], orthorhombic $P2_12_12$)[191] and form

V (orthorhombic *Pmcn*)[192, 193]. Rich polymorphic behavior is observed under pressure.[191] In forms I and IV, each urea molecule possesses eight hydrogen bonds and the oxygen in the carbonyl group interacts with the hydrogens in the amino groups, forming four O···H-N hydrogen bonds with three different molecules (Figure I.10). In phase III, each urea molecule forms six hydrogen bonds and the oxygen possesses three O···H-N hydrogen bonds with two different molecules (Figure I.10).

Because urea has four hydrogen bond donors and one acceptor, it is often used in crystal engineering studies. Anna Olejniczak et al. reported 477 cocrystals containing urea.[191] In a number of cocrystals, the urea molecules themselves did not share any hydrogen bonds. In most cocrystals in which interactions between urea molecules exist, urea exhibits a double hydrogen bond involving O···H-N forming a dimer with two urea molecules.

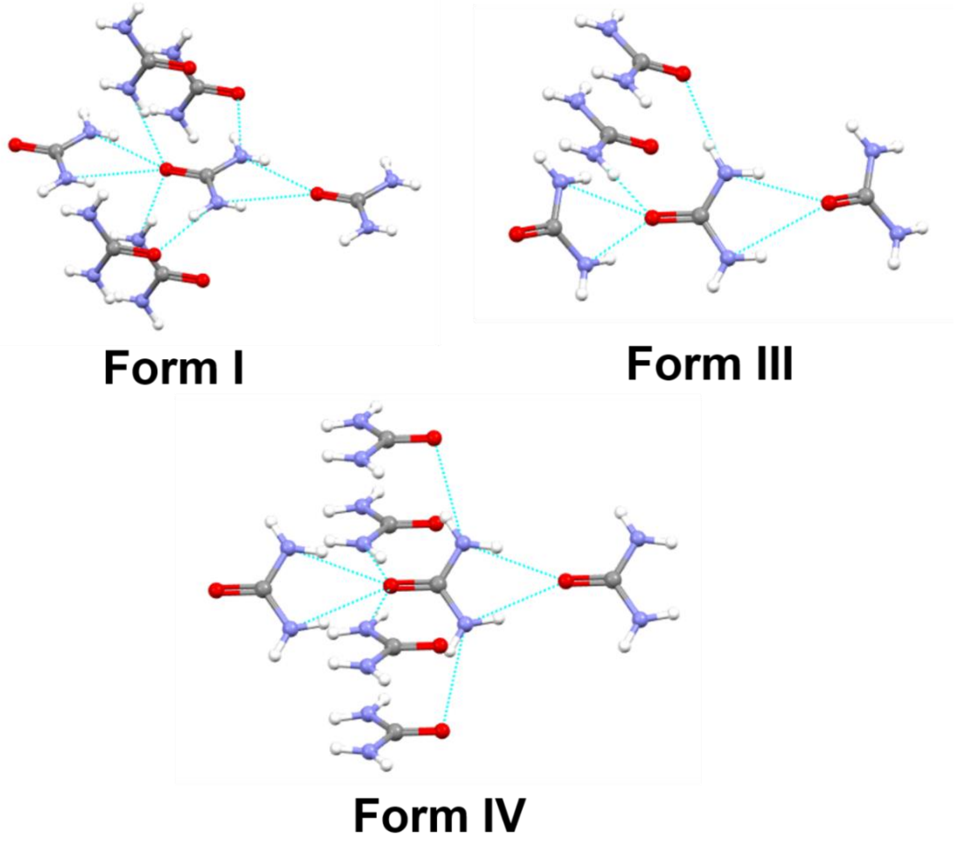

Form I

Form III

Form IV

Figure I.10 Hydrogen bonds in different polymorphs of urea

I.6.3 *N*-Methylurea

N-Methylurea ($C_2H_6N_2O$, 74.08 g mol^{-1} CAS: 598-50-5) is an ultraviolet nonlinear optical material.[194-197] It has three known polymorphs, forms I, II, and III.[198] Form I is the most stable polymorph. It has an orthorhombic structure with space group $P2_12_12_1$. The other two polymorphs are obtained by melt crystallization and their structures have been solved with powder X-ray diffraction. Both structures are monoclinic with space group $P2_1/c$. In forms I and II, as is shown in Figure I.11 each molecule possesses six O···H-N hydrogen bonds between the oxygen and the amino groups. In phase III, each molecule is linked by four O···H-N hydrogen bonds and molecules form a linear chain.

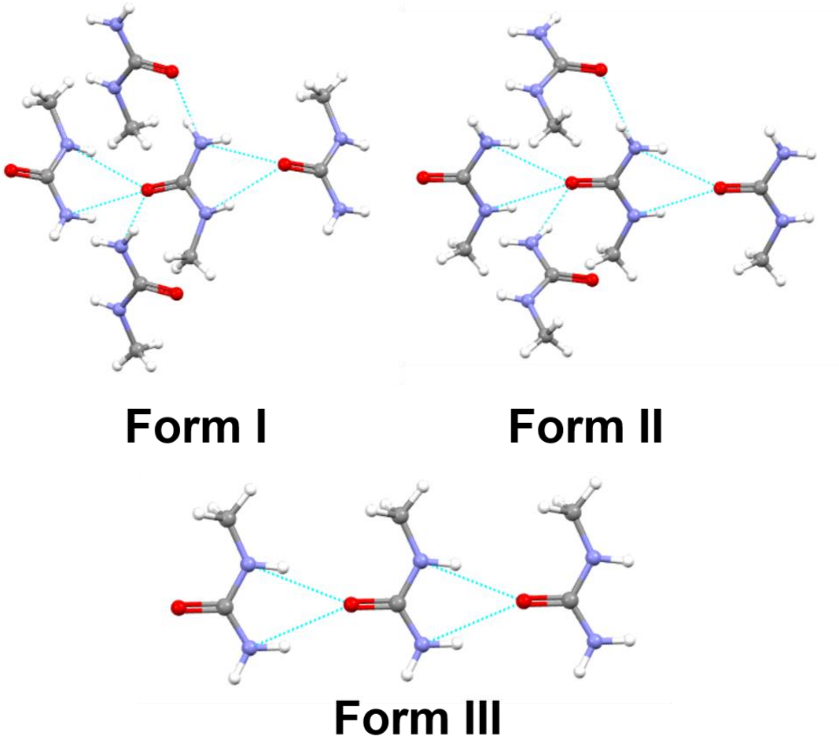

Figure I.11 Hydrogen bonds in different polymorphs of *N*-methylurea

Seven co-crystals, salts, or solvates with *N*-methylurea are reported in the CSD.[199-204] Only one coformer has an amide group.[201] Three co-crystals exhibit hydrogen bonding between the *N*-methylurea molecules. Two co-crystals exhibit a dimer with a double O···H-N hydrogen bond involving two methylamino groups of *N*-methylurea.[200] When *N*-methylurea forms dimers in a co-crystal, the conformation of *N*-methylurea changes (Figure I.12a). One crystal structure contains a linear hydrogen bond chain connecting *N*-methylurea molecules through the O···H-N hydrogen bond[199] (Figure I.12b).

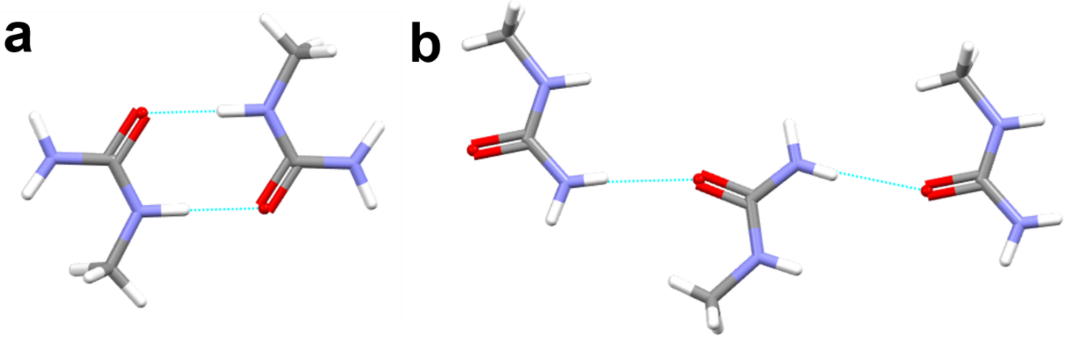

Figure I.12 Hydrogen bonds between *N*-methylurea molecules in co-crystals

I.6.4 1,1-Dimethylurea

For 1,1-dimethylurea ($C_3H_8N_2O$, 88.11 g mol^{-1} CAS: 598-94-7) only one crystal structure has been found, which has been solved in 1994 by Pathirana et al.[205] The structure is monoclinic with space group $P2_1/n$. In this crystal structure, each molecule possesses four N-H···O hydrogen bonds (Figure I.13). It has both dimers and linear chains in this crystal packing. There are some co-crystals reported in the CSD. In all of these co-crystal structures, 1,1-dimethylurea interacts with other compound molecules by forming N-H···O and O···H-O hydrogen bonds.[200, 206, 207] These compounds do not have amide groups.

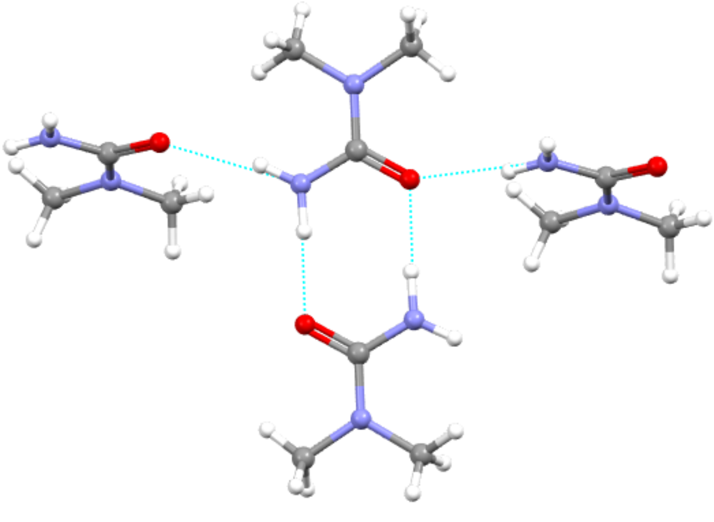

Figure I.13 Hydrogen bonds in 1,1-dimethylurea

I.6.5 1,3-Dimethylurea

1,3-Dimethylurea ($C_3H_8N_2O$, 88.11 g mol^{-1} CAS: 96-31-1) has two hydrogen bond donors and one hydrogen bond acceptor, however in contrast to 1,1-dimethylurea, the hydrogen bond donors are spread over two amino groups. 1,3-dimethylurea is used as an intermediate in the pharmaceutical industry.[208] The molecule has two polymorphs: form I (orthorhombic, space group *Fdd*2) and form II (orthorhombic, space group $P2_12_12$). Form I is more stable than form II at high temperature.[209] In both polymorphs, the oxygen atom interacts with two hydrogens on the two amino groups of another molecule and form a linear chain similar to *N*-methylurea form III (Figure I.14). A number of co-crystals have been found. In these cocrystals, 1,3-dimethylurea interacts with other compound molecules by forming hydrogen bonds.[207, 210-217] These compounds do not have amide groups. In most cases, the conformation of 1,3-dimethylurea is as presented in Figure I.15a, however in the cocrystal 1,3-dimethylurea – oxalic acid[207], the conformation of 1,3-dimethylurea is rotated, which appears to be uncommon, as presented in Figure I.15b.

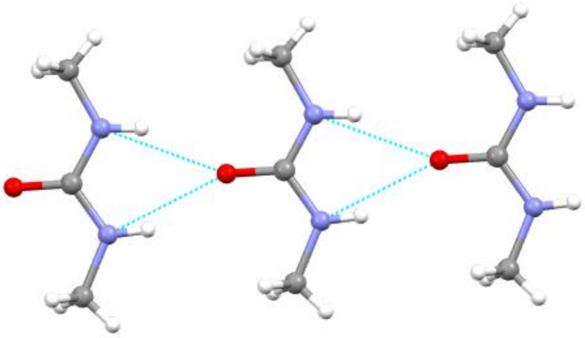

Figure I.14 Hydrogen bonds in the 1,3-dimethylurea structure

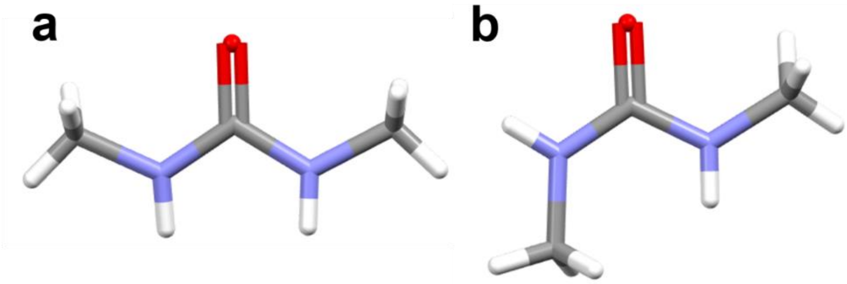

Figure I.15 (a) the common conformation of 1,3-dimethylurea and (b) a rarely observed conformation found in the 1,3-dimethylurea-oxalic acid cocrystal

I.6.6 Trimethylurea

The structure of trimethylurea ($C_4H_{10}N_2O$, 102.14 g mol^{-1} CAS: 632-14-4) was first reported in 2012.[218] It is orthorhombic with space group *Cmc*2_1. Each molecule possesses two O···H-N hydrogen bonds, forming chains with other molecules (Figure I.16). Four cocrystal structures have been reported in the CSD.[219-221] In these cocrystals, carbonyl oxygen of trimethylurea forms O···H-N hydrogen bond with other compounds.

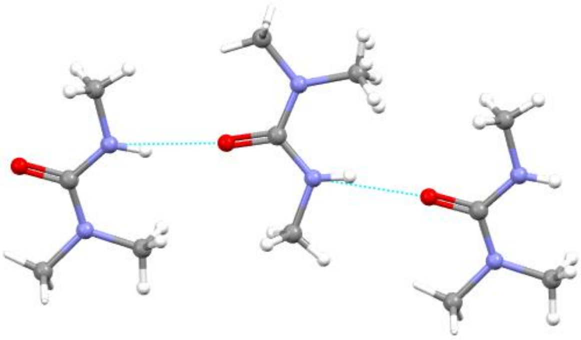

Figure I.16 Hydrogen bonds in trimethylurea

I.6.7 1,1-Diethylurea

1,1-Diethylurea ($C_5H_{12}N_2O$, 116.16 g mol^{-1} CAS: 634-95-7) is an unsymmetrically substituted urea, its structure has been reported in 2000 by Smith et al.[222] It is monoclinic with space group *C*2/*c*.[222] Each 1,1-diethylurea molecule forms two O···H-N hydrogen bonds with two different molecules (Figure I.17a). All co-crystals of 1,1-diethylurea so far consist of acidic coformers and the amide group of 1,1-diethylurea interact with the carboxylic acid group of coformers (Figure I.17b).[222, 223]

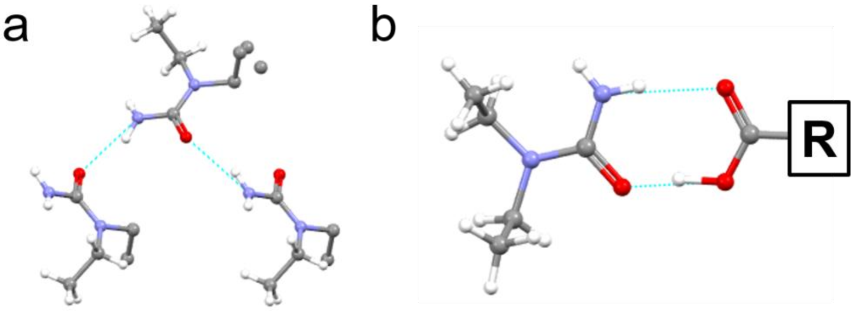

Figure I.17 Hydrogen bonds in 1,1-diethylurea and its cocrystals

I.6.8 1,3-Diethylurea

Structure data of 1,3-diethylurea ($C_5H_{12}N_2O$, 116.16 g mol^{-1} CAS: 623-76-7) have not been reported in the literature. It possesses two polymorphs which are mentioned in the literature.[224]

I.6.9 Tetramethylurea

A molecule of tetramethylurea ($C_5H_{12}N_2O$, 116.16 g mol^{-1} CAS: 632-22-4) exhibits twofold symmetry. Its crystal structure is monoclinic with space group *C*2/*c*.[225] Tetramethylurea is liquid at room temperature and can be used as a solvent. In cocrystals or solvates with tetramethylurea, the oxygen atom of tetramethylurea forms O···H-N or O···H-O hydrogen bonds.[226-233] It indicates that oxygen of tetramethylurea is a good hydrogen-bond acceptor.

Chapter II: Materials and methods

II.1 Introduction

Materials, experimental techniques and experimental methods applied in this work are presented in this chapter, which consists of four parts. In the first part, the materials used in this study will be introduced. In the second part, the analytical characterization techniques most used in this work will be presented and the principles of these techniques will be explained as well. The third part is devoted to the description of the experiments carried out and/or developed in this work. The calculation methods used in this thesis will be detailed in the last part.

II.2 Materials

II.2.1 Pyrazinamide

Pyrazinamide (purity ≥97.5%) was purchased from Sigma-Aldrich (France) and used without further purification. The crystal structure of commercial pyrazinamide has been verified by powder X-ray diffraction and is consistently found to be the α polymorph. The molecular structure is shown in Figure I.5.

II.2.2 Urea derivatives

Nine urea derivatives were used in this study without further purification. The purity and suppliers are listed in Table II.1 and their molecular structures are provided in Figure I.8.

Table II.1 Information on the urea derivatives

Urea derivatives	Chemical formula	Purity	Supplier
Acetamide	C_2H_5NO	≥99 %	Acros Organics
Urea	CH_4N_2O	≥99 %	Alfa Aesar
N-Methylurea	$C_2H_6N_2O$	≥97 %	Acros Organics
1,1-Dimethylurea (1,1-DMU)	$C_3H_8N_2O$	≥99 %	Sigma Aldrich
1,3-Dimethylurea (1,3-DMU)	$C_3H_8N_2O$	≥98 %	Merck KGaA
Trimethylurea	$C_4H_{10}N_2O$	-	Alfa Aesar
1,1-Diethylurea (1,1-DEU)	$C_5H_{12}N_2O$	≥97 %	Acros Organics
1,3-Diethylurea (1,3-DEU)	$C_5H_{12}N_2O$	≥97 %	Sigma Aldrich
Tetramethylurea	$C_5H_{12}N_2O$	≥99%	Alfa Aesar

II.2.3 Solvents

The solvents used in this work are acetone, chloroform, 1,4-dioxane, methanol, demineralized water and deuterated solvents used for NMR analysis. The solvent information is listed in Table II.2 and all solvents were used as received.

Table II.2 Purity and supplier list of the solvents

Solvents	Chemical formula	Purity	Supplier
Acetone	C_3H_6O	≥99.8 %	Fisher Chemical
Chloroform	$CHCl_3$	≥99.8 %	Fisher Chemical
1,4-dioxane	$C_4H_8O_2$	≥99.8 %	Sigma-Aldrich
Methanol	CH_4O	≥99.8 %	Fisher Chemical
Demineralized water	H_2O	-	Laboratory
Deuterated acetone	C_3D_6O	≥99.8 % D -	Acros Organics
Deuterated chloroform	$CDCl_3$	≥99.8 % D	VWR Chemicals
Deuterated dimethyl sulfoxide	C_2D_6SO	≥99.8 % D	VWR Chemicals
Deuterated water	D_2O	≥99.9% D	Sigma-Aldrich

II.3 Analytical characterization methods

The techniques that have been mostly used are X-ray diffraction (XRD), differential scanning calorimetry (DSC), differential thermal analysis (DTA), nuclear magnetic resonance (NMR) spectroscopy, infrared (IR) spectroscopy, microscopic analysis and gas chromatography (GC). Various types of XRD equipment were used for specific experimental purposes. Powder X-ray diffraction (PXRD) is mainly used for identifying the polymorphs of the investigated samples. IR was also used in certain cases for the same purpose in this work. Unit cell parameters of the four polymorphs of pyrazinamide as a function of the temperature and as a function of pressure were obtained based on the PXRD patterns measured by high-resolution powder XRD using either a laboratory source or synchrotron powder XRD diffraction. Single crystal XRD was used to investigate the crystal structure of the γ form. DSC was used for determining transition temperatures and enthalpies of the phase transitions of pyrazinamide. In addition, it was used to determine the eutectic points of mixtures of pyrazinamide and additives (50:50 w%) as well. The α-γ phase transition as a function of pressure was studied by DTA. Both polarized-light optical microscopy and scanning electron microscopy (SEM) were used to analyze the morphology of crystals obtained under different conditions. Polarized-light optical microscopy is a powerful technique to differentiate twinned crystals from single crystals. SEM is more suitable for observing the morphology of fine powder prepared by spray drying. GC was used to investigate the presence of additives in inclusions and as solid solutions in crystals of the γ form.

II.3.1 X-ray diffraction

X-rays were discovered in 1895 by Röntgen, a German physicist. Because the nature of the radiation was unknown at that time, they were called X-ray[234], although the name Röntgen radiation was and is still used too. In 1912, Max von Laue et al. discovered the phenomenon of X-ray diffraction by crystals and proved that X-rays are electromagnetic waves[235]. Currently, X-ray diffraction is a frequently used nondestructive technique for characterizing crystalline materials. This technique can provide detailed information about the crystal structure (qualitative and quantitative), physical properties such as crystallinity and crystal defects, and it can help in quantifying material composition or phase composition provided the crystal structure of the different solid phases is known.

A laboratory X-ray diffractometer is normally comprised of three basic components: an X-ray tube, a sample holder and an X-ray detector[236] [237]. X-rays are commonly generated by an X-ray tube composed of a cathode and an anode submitted to a high voltage (several tens of kilovolts typically). By filtering (metal filters or monochromators), monochromatic radiation is produced. Then the X-rays are collimated by optics and directed to the sample. When Bragg's law (eq. II.1) is satisfied, the X-rays of wavelength λ scattered by a specific family of reticular planes (hkl) interfere constructively with each other leading to diffraction patterns of those rays at specific angles. The X-ray detectors are photon counters and they register an intensity which is expressed in counts or counts per sec, that is, the number of X-ray photons counted.

Bragg's law is a relationship between the lattice spacing and the X-ray wavelength:

$$2d_{hkl}sin\theta_{hkl} = n\lambda \qquad \text{(II.1)}$$

where d_{hkl} represents the interplanar distance within the family of reticular planes (hkl), θ_{hkl} is the diffraction angle, n is the diffraction order, and λ is the wavelength of the incident X-rays.

II.3.1.1 Powder X-ray diffraction (PXRD)

Polymorph identification is an important part of this study. Polymorphs of a chemical substance are mainly identified by PXRD prior to subsequent analysis and characterization. PXRD patterns of the samples in this study were obtained by a D8 DISCOVER (Bruker) diffractometer with a Bragg-Brentano geometry. The instrument is equipped with a copper anode (Cu Kα radiation, λ = 1.5418 Å), and a Lynx Eye linear detector. Samples without grinding have been measured under ambient conditions with a scan step of 0.04° (2θ) in the angular range of 3-30° (2θ) and an intensity collection time of 4 s per step.

II.3.1.2 High-resolution powder X-ray diffraction as a function of the temperature

High-resolution PXRD was used to determine the unit cell parameters of the four polymorphs of pyrazinamide as a function of the temperature. Powdered specimens were placed in capillaries of 0.5 mm diameter. The measurements were carried out with a vertically mounted INEL CPS-120 diffractometer in Debye–Scherrer geometry and equipped with a cylindrical position sensitive detector (containing 4096 channels). Monochromatic Cu Kα_1 radiation (1.54056 Å) applying an asymmetrically focusing incident-beam curved germanium monochromator was used and diffraction intensities were registered simultaneously over a 2θ range from 3.0° to 111.878° with a step size of 0.029°. The temperature was controlled by a liquid nitrogen 700 series Cryostream Cooler (Oxford Cryosystems). The PXRD patterns were refined by FullProf software to refine the unit cell parameters and calculate the specific volumes [238].

II.3.1.3 Synchrotron powder X-ray diffraction

The unit cell parameters of four polymorphs of pyrazinamide as a function of the pressure at room temperature were obtained using PXRD data measured on the high-pressure diffraction beamline PSICHE at the synchrotron SOLEIL (Gif sur Yvette, France) using a focused monochromatic mode and a Ge solid state detector. High pressure was controlled by a membrane driven diamond anvil cell with an upper pressure limit of 2 GPa. Silicon oil was used as a pressure transmitting medium. NaCl was used as an internal reference to determine the pressure. The wavelength used for the experiments was 0.4859 Å. Pawley fits and Rietveld refinements were carried out using TOPAS-Academic V4.1 software to determine the lattice constants.

II.3.1.4 Single Crystal X-ray diffraction (SCXRD)

Single crystals of the γ form used for SCXRD were obtained by sublimation in the presence of 1,3-dimethylurea. These crystals are overall of better quality than crystals obtained by sublimation in the absence of additives. Diffraction measurements were carried out at different temperatures. A Bruker D8 Venture 4-circle diffractometer with a Photon II detector (Germany) was used with monochromatic Mo $K\alpha$ radiation (λ = 0.71073 Å) equipped with an Oxford cooling device (UK). Heating was carried out by placing the diffracting crystal inside an oven. The C, O and N atoms were located using direct methods with the program Apex 3 of Bruker.[239] The H atoms were localized by successive difference Fourier maps with SHELXL implemented in the WinGX software package.[240, 241]

II.3.2 Thermal Analysis

II.3.2.1 Differential Scanning Calorimetry (DSC)

The accurate definition of differential scanning calorimetry (DSC) is “the measurement of the change of the difference between the heat flow rate to the sample and to a reference while they are subjected to the same controlled temperature program”.[242] The name was given by Perkin - Elmer in 1963 to equipment that they had developed.[243] DSC is a very popular thermal analysis technique which can provide calorimetric properties of the sample. It can be used to achieve different goals, such as: characterization of a substance, construction and evaluation of phase diagrams, stability investigations and so on.[242]

Two basic types of differential scanning calorimeters (DSCs) exist: power compensation DSCs and heat flux DSCs. The schematic diagram of these two devices is provided in Figure II.1. Power compensation DSCs have two individual holders, each with its own heater and sensor. Both holders are kept at the same temperature. Temperature equilibrium is maintained by varying the required heat. This energy difference is displayed as a function of the program temperature and shown as a DSC curve. Compared to the power compensation DSCs, the heat flux DSCs possess only one chamber that includes sample and reference holders. Holders are separated by the thermoelectric disk which provides heat flows into both sample and reference. The difference of heat flows between the sample and the reference is determined based on the output of the two thermocouple junctions. Both types of DSCs display advantages: Power compensation DSCs benefit isothermal measurements. Their heating rate is faster, thus unwanted thermal phenomena can be more easily avoided. Heat flux DSCs result in flat and probably more reproducible baselines.[243, 244]

Calibration, DSC settings (purge gas, gas flow rate, heating rate), sample conditions (sample mass, sample structure (powder, granulates), sample purity, its thermal history and so on) can affect the accuracy of the analytical DSC results.[242] Therefore, in DSC measurements, all settings should be kept as similar as possible to obtain accurate, comparable experimental results.

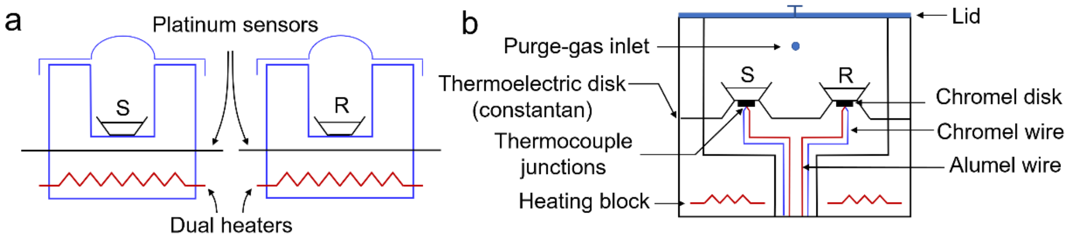

Figure II.1 Schematics of (a) the power compensation and (b) the heat flux differential scanning calorimeter

In this work, the thermal behavior of pyrazinamide was studied with two different calorimeters: a TA Q100 thermal analyzer and a DSC 214 from Netzsch. They are both heat flux DSCs.

The transition temperatures of pyrazinamide as a function of the heating rate were measured with the TA Q100 thermal analyzer. It was calibrated with indium and nitrogen gas was used to create an inert atmosphere around the sample. Different polymorphs of pyrazinamide were measured using heating rates from 0.05 K min^{-1} up to 200 K min^{-1} and DSC curves were treated using the TA universal analysis software.

The melting enthalpy of form γ as a function of the amount of material was investigated with the DSC 214 from Netzsch. Mercury, indium, tin, bismuth and zinc were used for calibration. Different quantities of material from 0.01 mg up to 15 mg were weighed in 45 µL aluminum pans and heated at 10 K min^{-1} under an inert atmosphere of nitrogen gas. Netzsch Proteus analysis software was used for data processing and DSC curve analysis.

II.3.2.2 High-Pressure Differential Thermal Analysis (HP-DTA)

Aside from differential scanning calorimeters (DSCs), there is another commercially available differential thermal instrument called differential thermal analyzers (DTA). Both techniques measure the difference between sample and reference, however, the difference between DSC and DTA is that DSC determines energy differences and DTA determines temperature differences (Figure II.2a).[244, 245] A DTA instrument usually consists of the following components: a furnace or a heater, a temperature programmer, sample and reference holders, a differential temperature detector, a controlled atmosphere, an amplifier, and a recorder.[245]

Transition temperatures as a function of pressure were measured using an in-house constructed high-pressure differential thermal analyzer similar to the design by Würflinger.[246] A schematic diagram of the HP-DTA instrument is presented in Figure II.2b. Therm240 oil from Lauda was used as the pressure-transmitting medium. Pyrazinamide was mixed with Galden perfluorinated liquid from Bioblock scientific to avoid the presence of air in the measurement pan, which may affect the thermodynamic equilibrium. DSC runs on the TA Q100 (see above) were carried out to verify that the perfluorinated liquid is inert in the presence of pyrazinamide. The HP-DTA has a temperature range of 298 to 473 K, a pressure range of 0 to 250 MPa and the heating rate was 2 K min^{-1}.

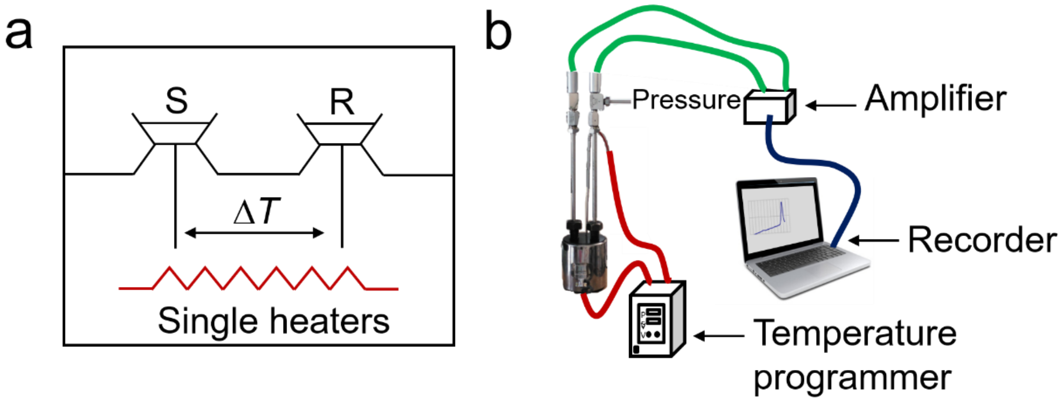

Figure II.2 Schematics of (a) a differential thermal analyzer measurement cell and (b) the high-pressure differential thermal analyzer used in this study

II.3.2.3 Thermogravimetric Analysis (TGA)

Sublimation of pyrazinamide was confirmed by thermogravimetric analysis (TGA). It was performed using a Netzsch STA 449 C instrument, simultaneously with DSC analysis. The sample was heated at a heating rate of 5 K min^{-1} under an inert atmosphere of helium gas. Mass loss was registered by the internal balances of the equipment and the results were analyzed using the Netzsch Proteus analysis software.

II.3.3 Nuclear magnetic resonance (NMR) spectroscopy

Nuclear magnetic resonance (NMR) spectroscopy was explored in 1945/1946 by two groups of physicists.[247, 248] Now, it is one of the most powerful analytical techniques for the elucidation and characterization of the molecular structure of chemical compounds and it is widely used in many fields, such as physics, chemistry and medicine.[249] ^{1}H and ^{13}C NMR spectroscopy are commonly used methods. In addition, ^{15}N, ^{19}F and ^{31}P NMR spectroscopy are complementary applied to complete molecular structure elucidation. Two-dimensional nuclear magnetic resonance (2D NMR) spectroscopy refers to NMR methods with two interrelated frequency sampling series.[250] 2D NMR spectroscopy can provide coupling effects between atoms and their spatial interactions, thus, the interatomic bonds and their configuration in space can be determined.[251] Correlated spectroscopy (COSY) and nuclear overhauser effect spectroscopy (NOESY) are commonly used 2D NMR techniques. COSY spectra can be used to identify atomic spins coupled to each other, and determine signals related to neighboring protons (usually up to four bonds).[252] It is the most widely used 2D

NMR spectroscopy method. The spectrogram of a NOESY experiment looks similar to that of a COSY experiment, but the cross peaks in a NOESY spectrogram are related to the cross relaxation of the spins.[253] NOESY spectroscopy is a powerful method to determine the spatial distance between two protons within a molecule for example, while the number of chemical bonds between those protons is irrelevant. Thus, NOESY is important for the identification of the stereochemistry of biomolecules such as proteins.[253, 254]

The chemical shift, indicated with the symbol δ, is the resonance frequency of a nucleus relative to a standard substance in the magnetic field.[249, 255] It is the abscissa of the NMR spectrum and its unit is ppm. Structure elucidation is based on the position, the number and the integration of the frequency peaks. Factors that can affect the chemical shift are: electron density, mesomerism and steric effects.[255]

In the current thesis, NMR spectra were used to study possible interactions including hydrogen bonds and other weak interactions between pyrazinamide and additives in solution. The ^{1}H NMR, ^{1}H–^{1}H COSY and ^{1}H–^{1}H NOESY were used to follow the chemical shifts of protons of the pyrazinamide molecule and the urea derivatives. The change in chemical shift as a function of the concentration was associated with the interactions between pyrazinamide and the derivatives. The spectra were recorded at room temperature on a 300 MHz Bruker Avance-300 spectrometer equipped with a 5mm BBO ATM Z axis gradient probe. The relaxation delay is 1 sec for ^{1}H NMR and 2 sec for ^{1}H–^{1}H COSY and ^{1}H–^{1}H NOESY. Pyrazinamide and/or additives were dissolved in deuterated solvents with different concentrations from 0.006 to 0.32 mmol mL^{-1}. NMR chemical shifts (δ) were calibrated on the residual proton resonance of $CDCl_3$ ($\delta = 7.26$ ppm), $(CD_3)_2SO$ ($\delta = 2.50$ ppm) or acetone ($\delta = 2.05$ ppm).

II.3.4 Infrared spectroscopy

Infrared (IR) spectroscopy is an analytical technique that can be applied to a large diversity of sample species, from solid to liquid to gas. It is based on the interactions of molecular vibrations with infrared light. Frequency, intensity and band shape can be used to characterize the IR vibrational peaks. These parameters reflect the vibrational energy, polarizability, and environments of interatomic bonds. The frequencies of molecular vibrations are related to the geometric arrangement of the atoms in the molecules and the strength of the bonds, for example. The regions from 800 and up reflect mainly molecular vibrations, whereas below 800 cm^{-1} the spectra contain mainly lattice vibrations. Thus, IR spectra display plenty of information about the molecular structure.[256, 257] The difficulty is often to extract the information that one is interested in.

In this thesis, IR was used as an alternative to PXRD to distinguish the polymorphs α and γ. IR spectra of α and γ are presented in Figure II.3 and they are consistent with the IR spectra reported in the literature.[128] The characteristic peaks marked by arrows were used to distinguish polymorphs α and γ. IR spectra were recorded in the 375-4000 cm^{-1} range at a 4 cm^{-1} resolution using the ALPHA FT-IR spectrometer from Bruker dedicated to the study of powder samples. Both sample and background measurements consist of 24 scans. The OPUS software was used for data processing.

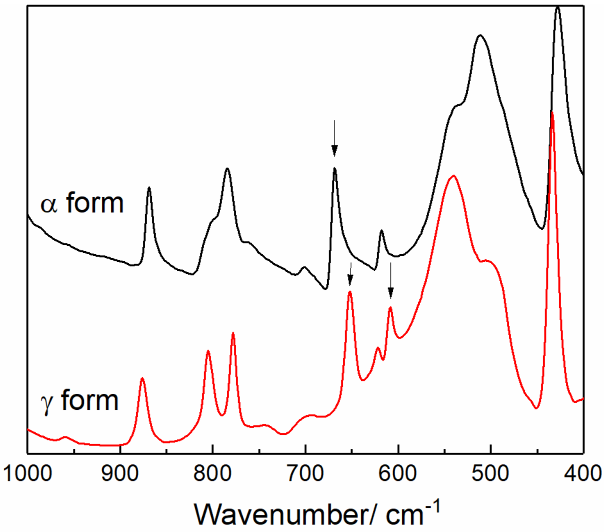

Figure II.3 The IR spectra of α and γ at room temperature

II.3.5 Microscopy analysis

II.3.5.1 Polarized-light optical microscopy

The Nikon Eclipse LV100 microscope with polarized light was used in this work for two main purposes. The first one is to differentiate twinned and single crystals. When the vibration directions and the extinction positions are not parallel in the domains of twinned crystals, they can be easily discerned as showing a different contrast on the microscope image.[258] The second one is to determine the morphology of the crystals. The details on the morphology analysis are described in section II.4.2.4 and section II.4.3.

II.3.5.2 Scanning electron microscopy (SEM)

Scanning electron microscopy (SEM) was employed to study the microscopic aspect of pyrazinamide powder obtained by spray drying using a JEOL JCM-5000 NeoScope instrument with an electron acceleration voltage of 10 or 15 kV. The powder sample was coated with gold in a NeoCoater MP-19020NCTR before the SEM measurements.

II.3.6 Gas chromatography (GC)

Gas chromatography-hydrogen flame ionization detector (GC-FID) was applied to analyze the presence of additives in γ crystals grown by co-sublimation with urea derivatives (see section II.4.2.4). GC 6890 Agilent with a flame ionization detector (FID) was used in this work. The inlet temperature was 523 K with a sample injection volume of 0.2 μL. A DB-35MS (30m × 0.25mm × 0.25μm) column was used with nitrogen as the carrier gas at a constant flow rate of 1.2 mL min^{-1} (average velocity 30 cm s^{-1}). A split ratio of 1:30 was used with a temperature ramp of 15 K min^{-1} from 353 K to 483 K (run time 8.66 min). The detector temperature was 573 K.

Single crystals with and without inclusions were selected by microscopy. Before preparing the sample for GC analysis, crystals were washed in saturated pyrazinamide solutions in acetone to dissolve additive left on the surface.

II.4 Experimental methods

II.4.1 Solution crystallization

II.4.1.1 Evaporation crystallization

Evaporation crystallization was used to prepare the β form of pyrazinamide. Excess commercial pyrazinamide was dissolved in chloroform, methanol or acetone. The saturated solutions were filtered with a 0.2 μm filter to remove any solid residue. The solutions were covered by a watch-glass and left to evaporate at room temperature. When the solvent had completely evaporated, a filter paper was used to dry the powder immediately. The polymorphic purity was determined by PXRD.

II.4.1.2 Cooling crystallization

Cooling crystallization in this study was applied to the preparation of the polymorphs β and δ. The detailed preparation method is as follows:

β form preparation method: Solutions of pyrazinamide ranging in concentration from 5.8 to 8.3 mg g^{-1} were prepared in chloroform. The solutions were heated up to 328 K and once clear allowed to cool down at different cooling rates (1 to 4.5 K min^{-1}) until crystallization using a Crystalline (Technobis, NL).

δ form preparation method: Clear saturated pyrazinamide solutions were obtained at 318 K in 1,4-dioxane by filtering the hot solution with a preheated filter. The solutions were cooled from 318 K to 288 K with a cooling rate of 1 K min^{-1}. The crystals were filtered and dried at room temperature.[56]

II.4.2 Sublimation

II.4.2.1 Sublimation with temperature gradients

A specifically manufactured sublimation setup (Cerhec, France) with a controlled temperature gradient was used in the sublimation experiments; the equipment is presented in Figure II.4. The temperature gradient is maintained by six independent heating elements indicated by Z1 to Z6. The Z6 heating element is used as the sublimation location. The glass tubes containing the sample inside the oven consists of an inner and an outer part. The inner part is the sectioned sublimating tube (Figure II.5) made up of sectioned glass tubes with on the right-hand side, section 0, the sample holder for sublimation. The outer tube, which is of a larger diameter and encloses the inner tube, can be connected to a vacuum pump to maintain a specifically chosen atmosphere (type of gas and pressure).

0.1 g of pyrazinamide powder was put into section 0. The sublimation temperature was set at 433 K (160 °C, Z6), the temperatures from Z5 to Z1 were 417 K (144 °C), 401 K (128 °C), 385 K (112 °C), 369 K (96 °C) and 353 K (80 °C). γ form crystals could be found in sections 0 to 3 (Z6 – Z3) and α form crystals could be obtained in the remaining sections. This method was mainly used to prepare α form single crystals.

Figure II.4 Sublimation equipment with temperature gradients

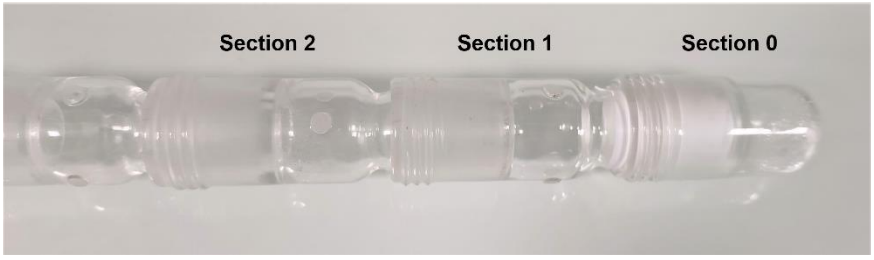

Figure II.5 Inner sectioned sublimating tubes

II.4.2.2 The α-γ transition temperature

A glass tube with 0.1 g of pyrazinamide was placed in the oven (Figure II.4) under atmospheric pressure. The six heating elements were set at the same temperature, and this temperature ranged from 353 K to 403 K (± 0.5 K). The polymorph of the sample was identified by PXRD. The time for sublimation experiments ranged from 2 days to 2 weeks depending on the sublimation temperature.

II.4.2.3 crystallization rate of the γ form

The effect of additives on the crystallization rate of the γ form during sublimation was studied in the following way. 30 mg of pyrazinamide and a small amount of additive were put into the set-up which is shown in Figure II.6. The set-up contains two vials of different size. Pyrazinamide powder was put in the larger vial and the additive was put in the smaller vial inside the larger one. This set-up avoids mixing before sublimation starts. Details on the different samples are provided in Table II.3. Samples were put in an oven whose temperature was set at 397 K (124 °C). After a time interval of 0.5 h or 1 h, the samples were analyzed by optical microscopy and IR. The results of three samples were averaged to determine the average nucleation rate of γ form in presence of different additives.

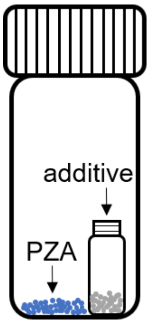

Figure II.6 Schematic setup for the sublimation experiments in the presence of additives

Table II.3 Experimental parameters for the crystallization rate investigation

No.	Mass of pyrazinamide /mg	Urea derivatives	Mas / mg
1	30	-	
2		Acetamide	10
3		Urea	30
4		*N*-methylurea	30
5		1,1-Dimethylurea	30
6		1,3-Dimethylurea	30
7		Trimethylurea	30
8		1,1-Diethylurea	30
9		1,3-Diethylurea	30
10		Tetramethylurea	15

II.4.2.4 γ form single crystals

Single crystals of the γ form were grown by sublimation using the same method as in section II.4.2.3. Details about the sublimation temperature and the duration varied with the additive and are indicated in Table II.4. Crystals were selected using optical microscopy.

Table II.4 Experimental parameters for pyrazinamide crystals obtained by sublimation

Mass of pyrazinamide /mg	Additive	Mass of additives /mg	Sublimation temperature /K	Time /h
30	-	-	397	96
	Acetamide	10	393	8
	Urea	30	397	24
	1,3-Dimethylurea	30	393	24
	1,3-Diethylurea	30	397	24
	Tetramethyl urea	15	397	24

II.4.3 Morphology determination of the γ form crystals

A polarized-light microscope was used to determine the morphology of the crystals obtained in II.4.2.4. For each sublimation condition (Table II.3), more than 100 crystals were analyzed. The length, width, and the diagonal of a number of faces as indicated in Figure II.7 by the dashed lines, have been measured and the face indexing of the most important faces has been indicated.

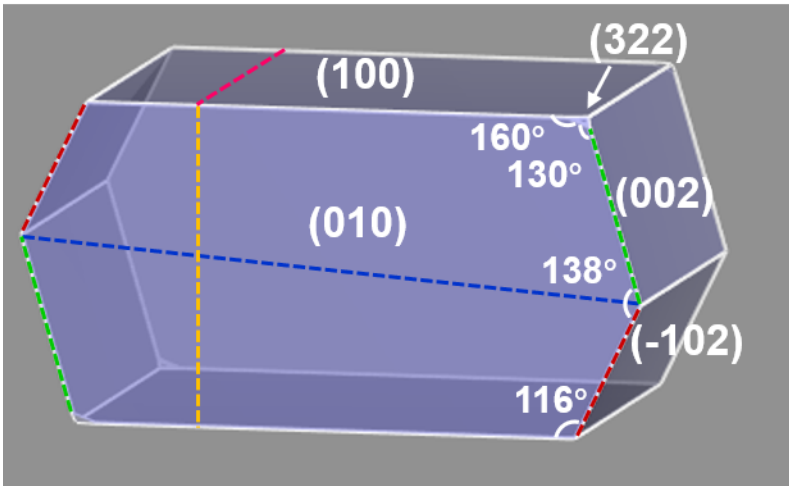

Figure II.7 Relevant distances within crystal faces of a γ form single crystal (the above represented crystal morphology has been calculated from the attachment energy theory –see below-) which are measured by optical microscopy

II.4.4 Spray drying

All of the spray drying experiments were carried out using the mini spray dryer B-290 from BUCHI and the equipment is shown in Figure II.8. The spray drying method has been presented in Chapter I. The concentration of pyrazinamide used in the feedstock was 5 mg mL^{-1} (solvent). For co-spray drying experiments in which the solution consists of a mixture of pyrazinamide and a urea derivative, the concentration of the additive is the same as that of pyrazinamide. The solvent used in all spray drying experiments was a (50:50 (v:v)) water-acetone mixture. The feedstock was filtered with a pore size of 0.20 µm before use. The feed flow rate was 6-8 mL min^{-1}, the removal pump rate 35 m^{3} h^{-1}, the nitrogen flow rate 473 L h^{-1} and the inlet temperature was set at 353 K (80 °C), 373 K (100 °C), 393 K (120 °C), 403 K (140 °C), and 413 K (150 °C). The powder obtained by spray drying was analyzed by PXRD and observed by SEM.

Figure II.8 BUCHI B-290 mini spray dryer used in this thesis

II.4.5 Pyrazinamide sublimation pressure measurements

Sublimation pressure measurements have been carried out in the Analytics Laboratory of Early Development of Sanofi R&D in Vitry sur Seine. The measurements were done isothermally in the temperature range of 293.15 K-383.15 K with a DVS Vacuum apparatus from Surface Measurements Systems, London, U.K., using a Knudsen cell whose orifice had a diameter of 440 micrometers and using benzoic acid as a standard.

II.4.6 Solubility measurements

Solubility was determined with two experimental methods: thermodynamic and kinetic.[51]

1) The thermodynamic or shake-flask method was proposed by Higuchi and Connors.[259] It is the most widely used method to measure solubility. The experimental procedure is as follows. In the first step an excess amount of solute is added to the solvent to prepare a suspension. In the second step, it is made sure that the suspension is in equilibrium, while the time for the equilibrium to establish is related to the dissolution rate. In the third step, the saturated solution is separated from the suspension in equilibrium. Filtration and centrifugation are two commonly used methods. In the last step, the mass or the concentration of the solute is determined.

(1) The solvent is evaporated from the saturated solution to obtain a solid. The solid mass divided by the solution mass before evaporation is the mass fraction solubility.

(2) Some analytical techniques such as UV, HPLC, or a refractometer can be used to determine the concentration of the solution using a standard curve or straight line obtained through solutions of known concentration.

The thermodynamic method is easy to execute, but some disadvantages exist. In particular, large quantities of compound are needed especially when they are highly soluble in the given solvent. Furthermore, in the case of compounds that decompose rapidly in solution or metastable polymorphs that rapidly transform into the stable polymorph, the suspension may not be in equilibrium and in that case the solubility is not reliable.

2) Kinetic methods are used to measure the so-called kinetic solubility. A given concentration of solution is prepared. Then solvent or solute is added little by little until equilibrium which means the solute no longer dissolves or that begin to precipitate and do not dissolve. Alternatively, a certain amount of suspension can be prepared that is then heated until the solution become clear.

II.4.6.1 α and γ form solubility

The solubility of polymorphs α and γ were measured by the kinetic method. The solubility in water has been measured in the temperature range of 283 K to 313 K. A vial with water, which had been weighed beforehand, was placed in a jacketed vessel, while the temperature was controlled by a thermostat bath (CF41 Julabo). A predetermined mass of pyrazinamide weighed with a balance with a precision of 0.1 mg was added step by step to the solution. When the suspension remains visible in the solution for more than one hour, the solution was considered to be saturated. The final weight of pyrazinamide divided by the total amount of water is taken as the solubility (m:m) at the set temperature.

II.4.6.2 Solubility of urea and its derivatives

The thermodynamic method was used for the solubility measurement of urea and its derivatives in water. An excess amount of material was introduced in a known quantity of water resulting in a suspension. The suspension was kept at constant temperature while stirring for more than 12 hours using a Crystal16 (Technobis, NL) to ensure solid-liquid equilibrium. The suspension was filtered with a preheated syringe and filter (0.20 μm). The concentration of the clear solution, i.e. the solubility of the urea derivatives, was measured by an RFM840 refractometer (Bellingham-Stanley Ltd., Kent, UK). The experimental steps for the determination of the concentration by refractometer are as follows:

1) Standard line: Standard solutions with different known concentrations of urea or a

derivative were prepared in water. The refractive index of pure water and the standard solutions were measured at 293 K. A straight line was obtained by fitting the refractive index against the concentration.

2) Solubility measurements: The saturated solution was weighed immediately after filtering. The solution was diluted to an appropriate concentration using a set weight of pure water after which the refractive index was measured. The solubility was determined with the standard line.

II.4.7 Ternary phase diagrams

Ternary phase diagrams of PZA-1,3-DMU-H_2O and PZA-1,3-DEU-H_2O were constructed using a kinetic method with the aid of a Crystal16 (Technobis, NL). Different proportions of pyrazinamide and 1,3-dimethylurea (or 1,3-diethylurea) were added into a set quantity of water resulting in suspensions of about 1 g in total at room temperature. The measurement temperature range was from room temperature to about 323 K. The heating rate was 0.1 K min^{-1} and the stirring rate was 600 rpm. The clear point detected by the Crystal16 was considered to be the saturation temperature of the mixture. The saturation concentration versus the measured temperature at a given composition of pyrazinamide and 1,3-dimethylurea (or 1,3-diethylurea) (pyrazinamide: additive 1:0, 1:1, 1:2, 1:3, 1:4, 1:6, 1:8, 1:10, 1:12, 1:50 and 0:1 (w%)) was fitted by a polynomial equation. The concentrations of pyrazinamide and the additive at the temperature of the ternary phase diagram were determined by interpolation.

II.5 Simulations and calculations

II.5.1 Morphology calculations

The γ form morphology was calculated using the Bravais-Friedel-Donnay-Harker or BFDH [28-30, 32] and the AE (attachment energy) methods[36] implemented in the morphology module package of Materials Studio (2019)[260] using the COMPASS II forcefield[261] and the recommended settings by Materials Studio at the ultra-fine computation level. The γ form crystal structure used for the calculations was published by Castro et al.[128] and obtained from the CSD (Cambridge Structural Database, refcode PYRZIN17).

II.5.2 Electrostatic potential calculations

The electron density and electrostatic potential (ESP) distribution were calculated using DFT/B3LYP with the B3LYP/6-31+G(d,p) basis setting in the Gaussian-09 software.[262] First the geometry of the molecular structure was optimized followed by the electron density and electrostatic potential calculations using the same computational settings. The results have been visualized and interpreted with Gauss View 6.[263]

Chapter III: Preparation and characterization of the four pyrazinamide polymorphs

III.1 Introduction

For pyrazinamide, four polymorphs have been reported in the literature, called α, β, γ, and δ. In this chapter, the stability of pyrazinamide at high temperature was studied by DSC and its sublimation was observed by TG-DSC. The four polymorphs used in this work were characterized by XRD and optical microscopy. PXRD as a function of the temperature and the pressure has been carried out and the unit cell parameters of the four polymorphs have been determined. Isobaric thermal expansion and isothermal compression have been determined based on the unit cell parameters.

III.2 Properties of pyrazinamide

III.2.1 Thermal stability of pyrazinamide

In order to investigate the thermal stability of pyrazinamide, a sample of commercial pyrazinamide underwent five subsequent heating-cooling cycles by DSC from 293 K to 493 K with a heating rate at 10 K min^{-1}. The result is provided in Figure III.1. Except for the melting peak that appeared in each heating cycle, a second transition peak could be observed only in the first heating cycle, which was ascribed to the α-γ transition. As shown in Figure III.1, the melting point and the enthalpy of fusion do not change significantly with each consecutive cycle. It indicates that there is no significant degradation taking place below 493 K.

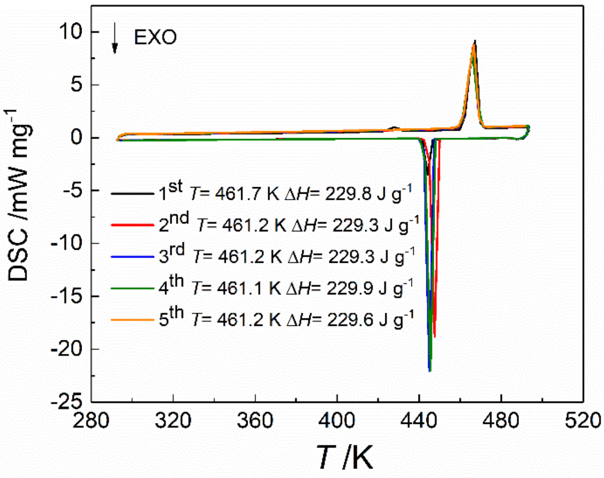

Figure III.1 Five subsequent DSC cycles of commercial pyrazinamide at a heating and cooling rate of 10 K min^{-1}

III.2.2 Sublimation

TG-DSC was used to observe the sublimation of pyrazinamide and the result is shown in Figure III.2. It shows that sublimation starts at about 400 K resulting in a significant weight loss. It can be concluded that sublimation is important in the pyrazinamide system. On the one hand, it will be possible to use sublimation in the study of pyrazinamide and on the other hand it may cause experimental error in the thermodynamic analysis, in particular for the melting enthalpy.[264]

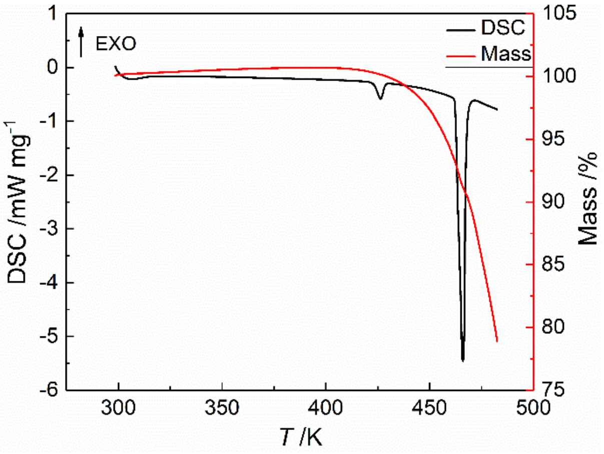

Figure III.2 TG-DSC curve of commercial pyrazinamide with a heating rate of 5 K min^{-1}

III.3 Identification and characterization of the four polymorphs of pyrazinamide

III.3.1 Polymorph crystallization

The polymorphs were prepared by different methods. Commercial pyrazinamide is mostly form α, and this was confirmed in our case by PXRD. The common method of preparing single crystals of form α is by slow evaporation such as in water, which yields needlelike crystals.[120, 126, 130] This crystallization method usually takes a considerable amount of time and sometimes the quality of the crystals is not good enough to obtain an exploitable diffraction pattern by SCXRD. In order to obtain single crystals of form α of good quality and of a larger size than by solution crystallization, the sublimation method with temperature gradients was used. Details of the experiments have been provided in section II.4.2.1. The result shows that pure γ form crystals appeared at high temperature (section 0 to section 2 of the glass tube, see II.4.2.1), and at lower temperature in glass-tube sections 5 and 6, pure α form crystals of good quality can be obtained. The characterization of single crystals of form α will be presented in the next chapter of the thesis.

Despite the fact that form β is not stable under ambient conditions, single crystals were obtained from solutions of alcohol at about 273 K[121, 122] or by slow evaporation in other organic solvents[129] and its crystal structure has been solved successfully in the literature. Until now, no mention of a reproducible method to prepare pure β form powder has been made in the literature, to the best of our knowledge.[128, 129] Solvent evaporation is one of the methods used to prepare β form powder in this work. Different solvents such as methanol, acetone and chloroform were used for slow evaporation at about 277 K or at room temperature. Although the evaporation process is difficult to control accurately, the structural purity of form β could still be improved by optimizing the method mentioned in section II.4.1.1. The improvement depends on the evaporation time of the used solvents. Due to their strong volatility, solvent-mediated transformation from β form to other forms is limited. Both increasing the evaporation area and drying the obtained powder immediately by filter paper rather than natural air drying may decrease transition of β into other forms. Nevertheless, a small amount of γ form often remains among the β form crystals. Cooling crystallization is an alternative method to prepare pure β form. Chloroform was chosen as the solvent based on the evaporation experiments. The cooling rate had a significant effect on the experimental results. Cooling at a rate of 1 K min^{-1} produces δ form. A faster cooling rate of 4.5 K min^{-1} produces β form, however, concomitant crystallization of γ occurs. The reproducibility of both methods to obtain pure β was not 100%, but in a number of samples other polymorphs could not be detected by PXRD.

The δ form was obtained by cooling crystallization in 1,4-dioxane with a cooling rate of 1 K min^{-1}, which had already been reported in the literature.[56]

The γ form was prepared by a number of different methods in this work. γ form powder used in PXRD and DSC measurements was produced by heating other polymorphs above the transition temperature. Spray drying is also a way to prepare γ form powder. In addition, γ form crystals were prepared by sublimation, for example under a temperature gradient. Sublimation under vacuum only resulted in a mixture of different pyrazinamide polymorphs, while under atmospheric pressure γ and α crystals were obtained, however, the quality of the single γ form crystals was not good enough for morphological characterization. While investigating the transition temperature between α and γ, it was found that the sublimation method presented in section II.4.2.4 provides good quality γ form crystals with suitable size and shape for subsequent crystal morphology analysis.

III.3.2 Characterization of the four polymorphs

III.3.2.1 PXRD results

All four polymorphs have been characterized by PXRD. The patterns are presented in Figure III.3. They are consistent with the patterns found in the literature for each polymorph[126, 129] and it can be concluded that the tested batches consist of pure polymorphs. The first, characteristic peak for each form α, β, γ, or δ is found at 7.9°, 12.6°, 12.8°, or 9.2° in 2θ, respectively.

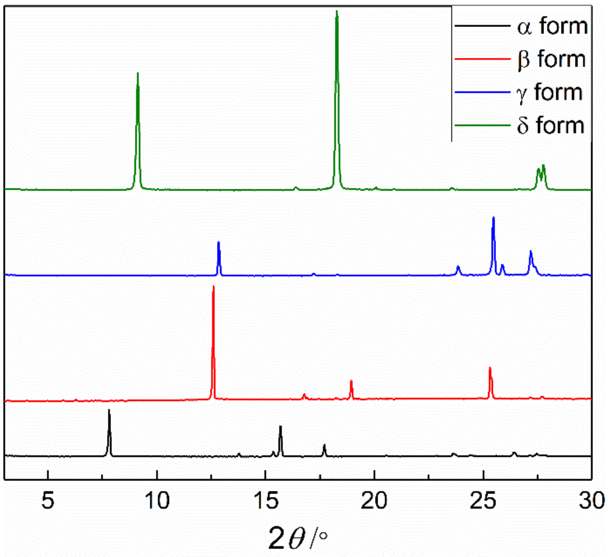

Figure III.3 PXRD patterns of the α, β, γ, and δ polymorphs prepared according to protocols detailed in section III.3.1

III.3.2.2 Characterization by microscopy

The crystals of the four polymorphs exhibit different shapes and sizes which also depend on the crystallization method used. The microscopy photographs are presented in Figure III.4. α form crystals obtained from water are needlelike (Figure III.4a), while those obtained by sublimation are rather blocky (Figure III.4b). The remarkable difference in the crystal habit of α obtained by different methods indicates that the solvent exerts a clear influence on its crystal habit. β-form crystals obtained by cooling crystallization and evaporation are rectangular plate crystals (Figure III.4c and 4d). γ crystals are blocky (Figure III.4e). δ-form crystals are parallelogram plate crystals (Figure III.4f). Sublimation is one of the main crystallization methods used in this study. Indeed, single crystals of both α and γ could be obtained in this way. The clear morphological differences shown in Figure III.4b and 4e reveal that α and γ crystals can be distinguished upon visual inspection by microscope.

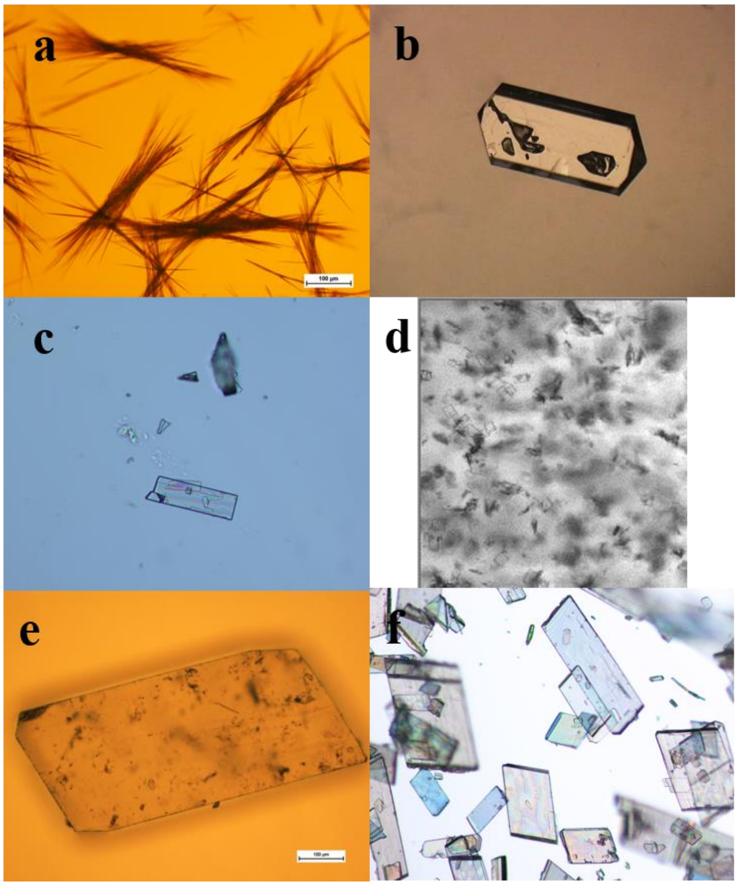

Figure III.4 Microscopy photographs of crystals of the four polymorphs of pyrazinamide: (a) α form obtained by solution crystallization in water, (b) α form obtained by sublimation, (c) β form prepared from evaporation of a methanol solution, (d) β form obtained by cooling crystallization, (e) γ form prepared by sublimation, (f) δ form obtained by cooling crystallization

III.3.3 Unit cell parameters as a function of the temperature of the polymorphs α, β, γ, and δ at atmospheric pressure

The PXRD patterns measured as a function of the temperature for the four polymorphs of pyrazinamide are provided in Figure III.5. Some peaks shift notably with the temperature. Unit cell parameters as a function of the temperature were determined from De Baille fits of the experimental data and the results are presented in Figure III.6 and Table A.1. For α, the *a* and *c* parameters increase with increasing temperature, whereas *b* decreases. For β and γ, all four unit-cell parameters increase with increasing temperature. For δ, *a*, *b*, and *c* increase with increasing temperature, while the angles *α*, *β*, and *γ* decrease with increasing temperature. The specific volumes of the four forms are presented in Figure III.7a. They all increase with increasing temperature. α possesses the largest specific volume and γ is the densest polymorph.

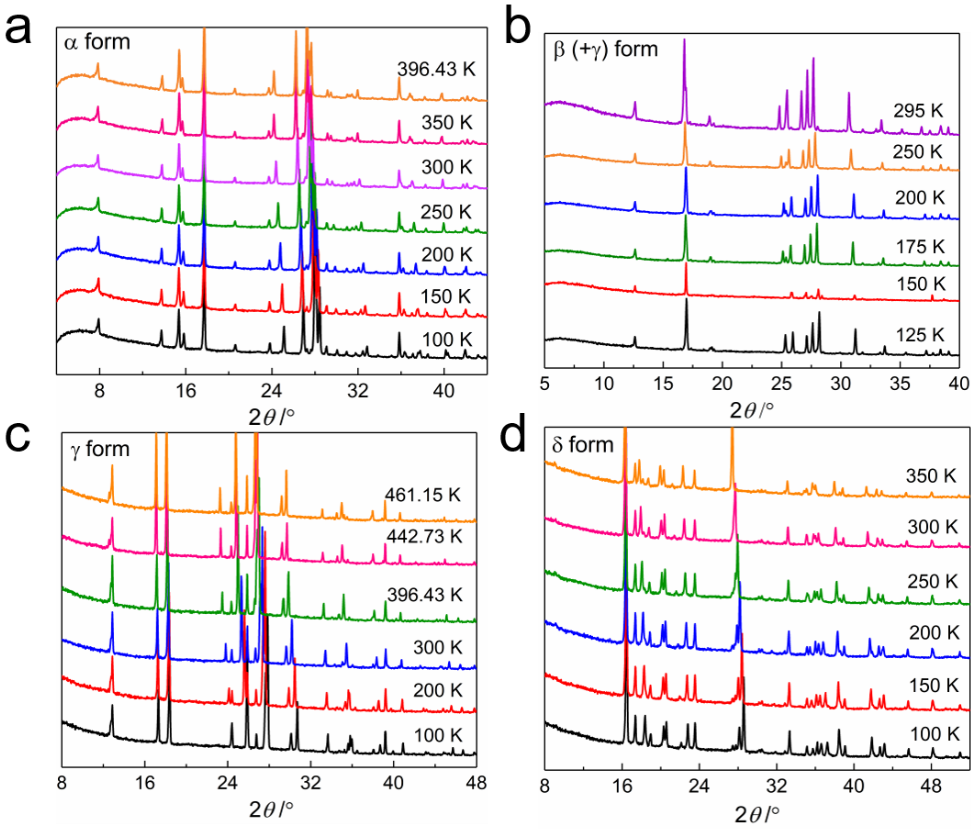

Figure III.5 Powder X-ray diffraction patterns (λ = 0.71073 Å) of the (a) α, (b) β, (c) γ and (d) δ forms of pyrazinamide as a function of the temperature

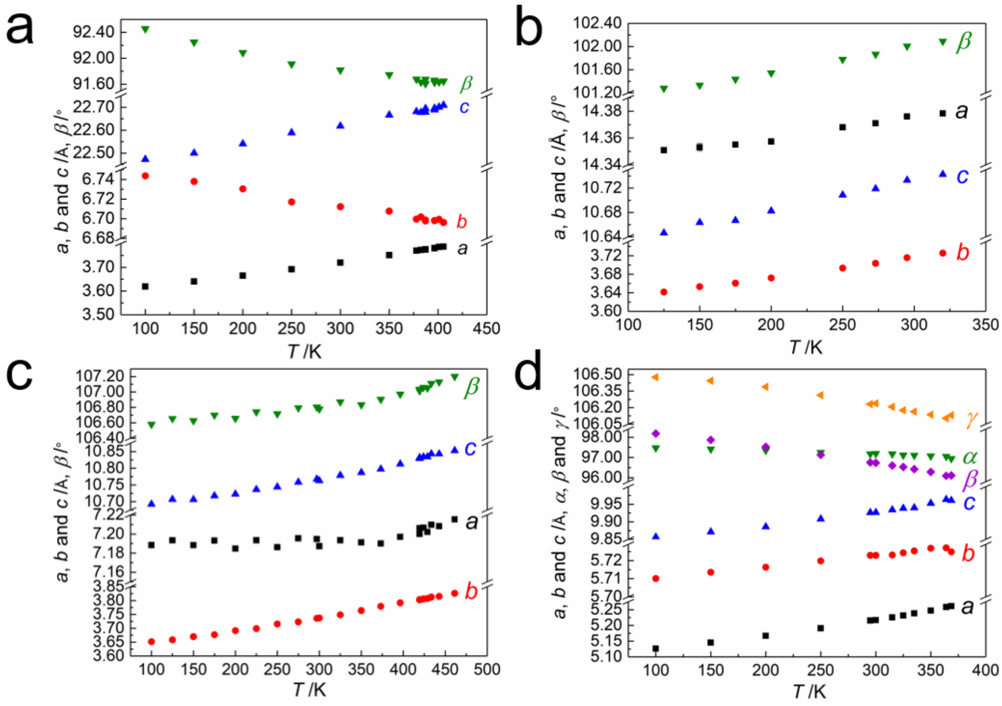

Figure III.6 The unit cell parameters of the pyrazinamide polymorphs (a) α, (b) β, (c) γ, and (d) δ as a function of the temperature

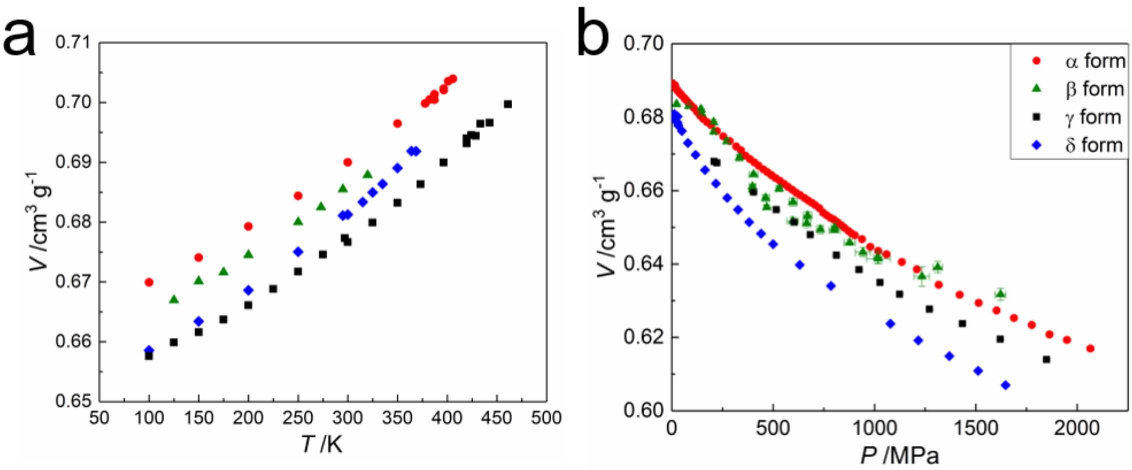

Figure III.7 The specific volumes of pyrazinamide forms α, β, γ, and δ as a function of the (a) temperature (at atmospheric pressure), (b) pressure (at room temperature). (●) form α, (▲) form β, (■) form γ and (◆) form δ

III.3.4 Unit cell parameters as a function of the pressure of the polymorphs α, β, γ, and δ at room temperature

The PXRD patterns as a function of the pressure of the four polymorphs of pyrazinamide were obtained at room temperature. They are shown in Figure III.8 and it can be seen that the diffraction peaks shift with pressure. The resulting unit cell parameters obtained with Pawley fits are presented in Figure III.9. Parameters *a*, *b*, and *c* of form α as a function of the pressure decrease with increasing pressure. For the forms β and γ, parameters *a*, *b*, *c* and *β* decrease with the increase of pressure. For form δ, parameters *a*, *b*, and *c* decrease with increasing pressure, while the angles *α* and *γ* are relatively unaffected. The angle *β*, however increases with increasing pressure. The specific volume of the four forms is presented in Figure III.7b. The specific volume decreases with increasing pressure. However, the δ form becomes the densest polymorph above 250 MPa.

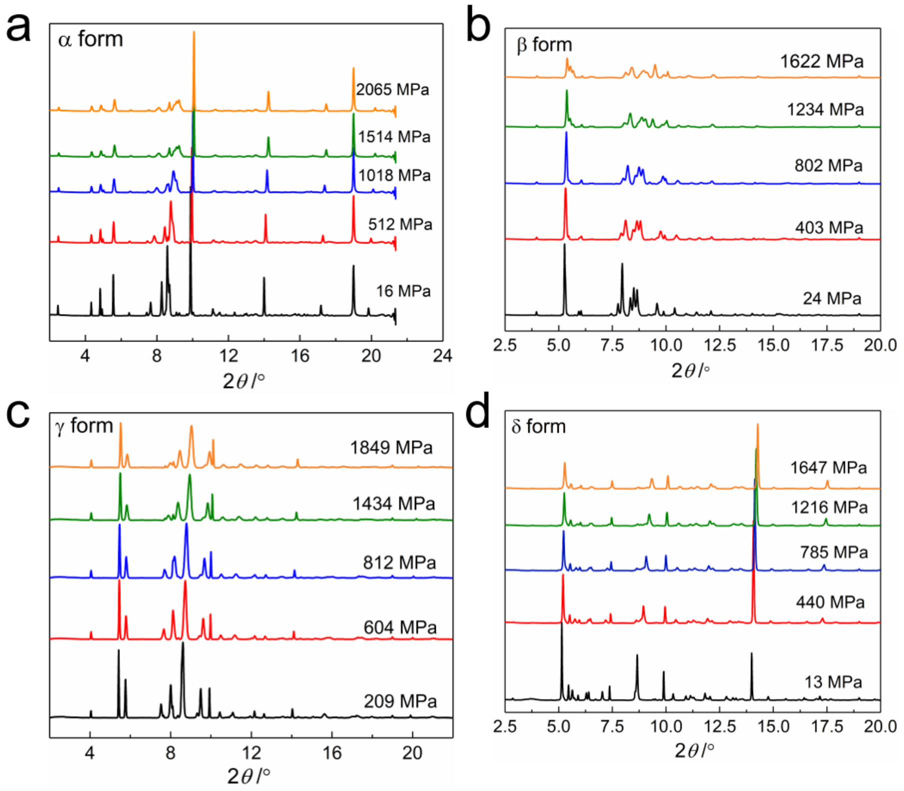

Figure III.8 Powder X-ray diffraction patterns (λ = 0.4859 Å) of the α, β, γ, and δ forms of pyrazinamide as a function of the pressure at 294 K

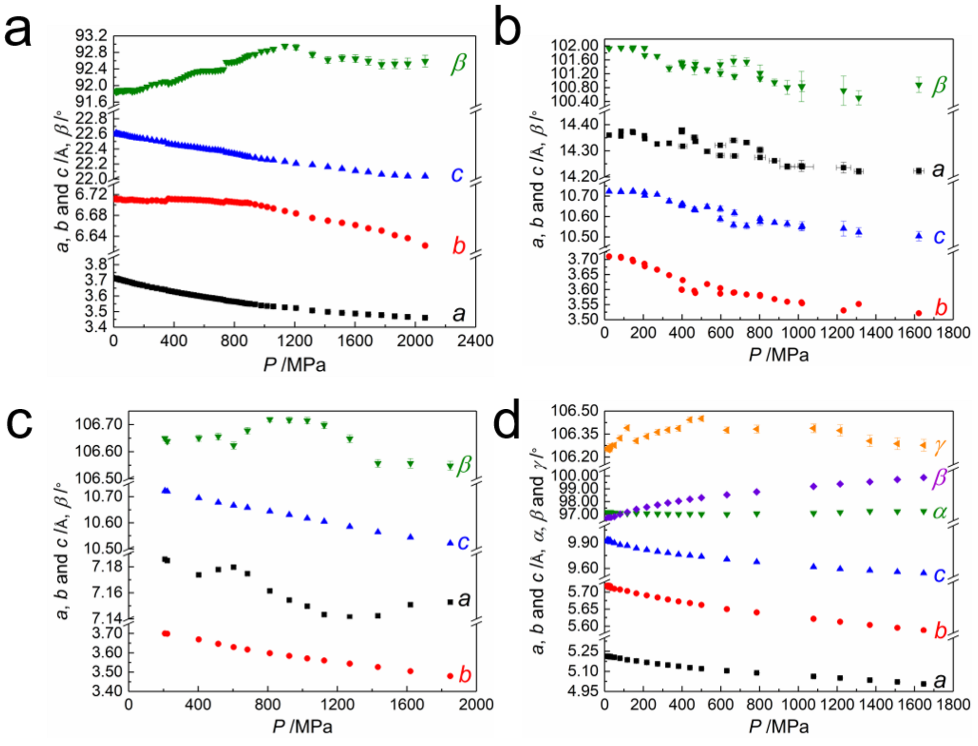

Figure III.9 Unit cell parameters of the pyrazinamide polymorphs (a) α, (b) β, (c) γ, and (d) δ as a function of the pressure at 294 K

III3.5 Thermal expansion and compressibility of polymorphs α, β, γ, and δ

III3.5.1 The thermal expansion and compressibility tensor

The isobaric thermal expansion tensor and the isothermal compressibility tensor of pyrazinamide polymorphs α, β, γ, and δ have been calculated with PASCal.[265] The input data for PASCal are temperature or pressure, volumes, and lattice parameters a, b, c, α, β, and γ. PASCal calculates the isobaric thermal expansion tensor or the isothermal compressibility tensor and presents it with its orthogonal coordinate system. The orthogonal axes are indicated with $\mathbf{E}_i$ and their orientations follow the convention of the Institute of Radio Engineers, in which $\mathbf{E}_1$ is parallel to the $\mathbf{a}*$ crystallographic axis, $\mathbf{E}_3$ is parallel to $\mathbf{c}$ and $\mathbf{E}_2$ is the vector product of $\mathbf{E}_1$ and $\mathbf{E}_3$. The transformation between crystallographic axes $\mathbf{C}_i$ to orthogonal axes $\mathbf{E}_i$ is represented by the square matrix $\mathbf{M}$:

$$\boldsymbol{M} \times \boldsymbol{C} = \boldsymbol{E} \tag{III.1}$$

The definition of strain $\boldsymbol{\varepsilon}$ is illustrated by eq. III.2 corresponding to both initial and final temperature or pressure conditions.

$$\boldsymbol{\varepsilon} = \frac{1}{2}(\boldsymbol{e} + \boldsymbol{e}^{\boldsymbol{T}}) \tag{III.2}$$

$$\boldsymbol{e} = \boldsymbol{M}_{final}^{-1} \times \boldsymbol{M}_{initial} - \boldsymbol{I} \tag{III.3}$$

The eigenvalues ε_i of the matrix $\boldsymbol{\varepsilon}$ are defined as the principal strain and the eigenvectors $\boldsymbol{e}_i$ represent the principal axes. The principal coefficients of the thermal expansion and compressibility are thermodynamically expressed as:

$$\boldsymbol{\alpha}_i = \left(\frac{\partial \varepsilon_i}{\partial T}\right)_p \tag{III.4}$$

$$\boldsymbol{K}_i = \left(\frac{\partial \varepsilon_i}{\partial p}\right)_T \tag{III.5}$$

To better appreciate the relationship between the tensor directions and the crystallographic axes, the normalized components of the principal tensor axes projected onto the crystallographic axes have been presented in the result.

III3.5.2 Thermal expansion and compressibility of polymorph α

The thermal expansion and compressibility of polymorph α are shown in Table III.1, and Figure III.10. Negative thermal expansion (NTE) is observed along $\boldsymbol{e}_{1,\mathrm{T}}$ (thermal expansion tensor) and the minimum compression direction is found parallel to $\boldsymbol{e}_{3,p}$ (compression tensor). Both are approximately parallel to the [010] crystallographic axis. The maximum thermal expansion direction is parallel to $\boldsymbol{e}_{3,T}$, which is approximately in the direction of the crystallographic axis [-100]. For the unit cell shown in Figure III.11, *a* varies significantly with both temperature and pressure. It indicates that the crystal deforms significantly along [-100]. The change in the *b* axis is the smallest; it exhibits negative thermal expansion when heated, while under pressure and up to 1000 MPa, this axis does not change in length.

Table III.1 Principal coefficients of the isobaric thermal expansion tensor, the isothermal compressibility tensor and the corresponding principal axes of form α of pyrazinamide

Thermal expansion tensor				
Principal axis, $e_{i,T}$	α_i (MK^{-1})	Component of $e_{i,T}$ along the crystallographic axes		
		a	*b*	*c*
1	-23.1(6)	0.0000	1.0000	0.0000
2	31 (2)	0.7588	0.0000	-0.6514
3	161(3)	-0.9993	0.0000	-0.0368
V	170(4)			

Compressibility tensor				
Principal axis, $e_{i,p}$	K_i (TPa^{-1})	Component of $e_{i,p}$ along the crystallographic axes		
		a	*b*	*c*
1	40.9(8)	-0.9994	0.0000	-0.0333
2	13.2(2)	0.7227	0.0000	-0.6911
3	2.7(2)	0.0000	1.0000	0.0000
V	55(2)			

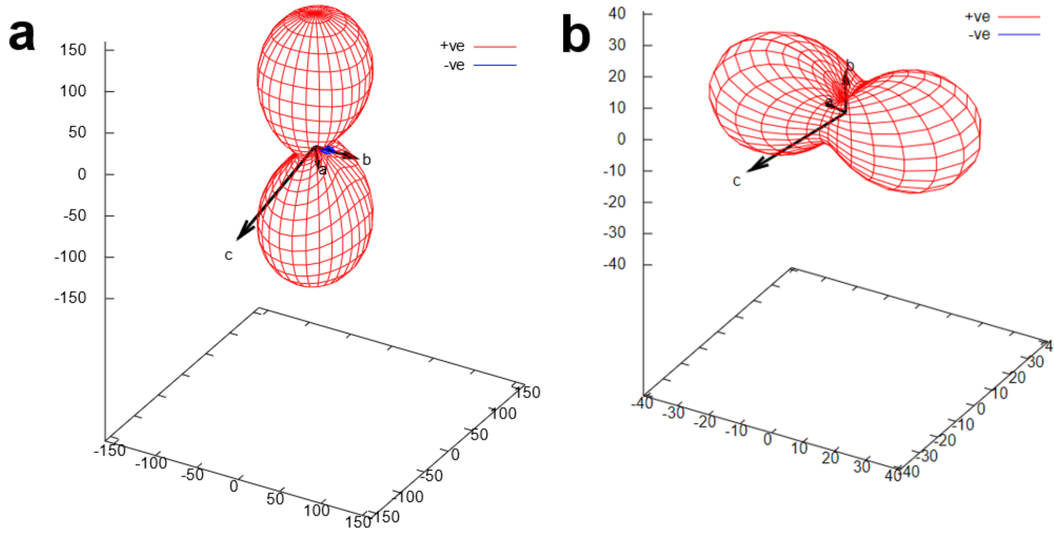

Figure III.10 The isobaric thermal expansion tensor (a) and isothermal compressibility tensor (b) of the α form. Positive thermal expansion is shown in red and negative thermal expansion is shown in blue. It can be observed that both types of behavior are very similar, when related to the unit cell parameters.

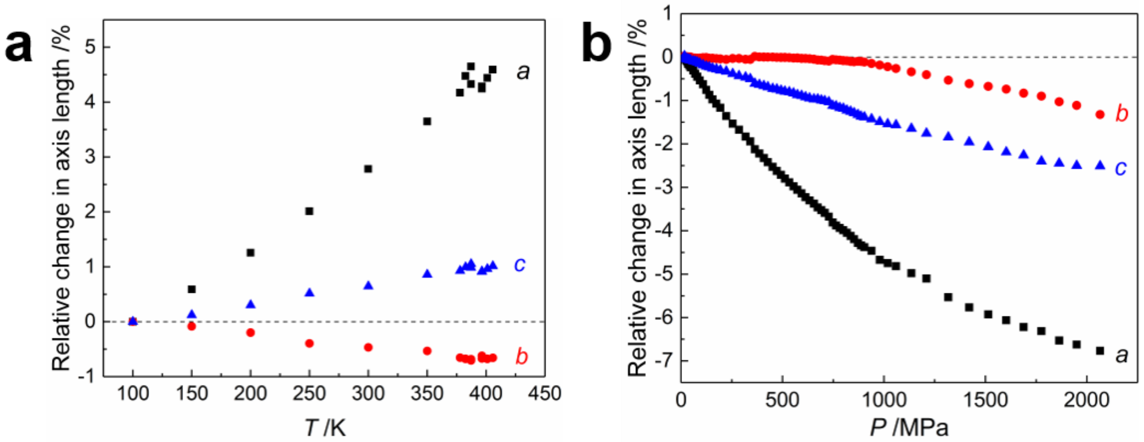

Figure III.11 Relative change in the axis lengths of form α as a function of (a) temperature and (b) pressure

Due to the interactions between the pyrazinamide molecules in form α an expansion in the direction of the red arrow (Figure III.12a) causes the structure to contract in the direction of the blue arrow. This can be explained as follows. Within the structure, four planes can be defined marked by yellow, pink, gray and light green, respectively. Molecules in the same plane interact with each other by N-H···N and N-H···O hydrogen bonds marked by blue dashed lines. The plane is interconnected with another plane with which it makes an angle of about 40° by C-H···N hydrogen bonds marked in magenta dashed lines. π-π interactions exist between the parallel planes. The softest direction in the crystal is marked by the red arrow in Figure III.12a; as mentioned above, there are no strong hydrogen bonds present between the molecular planes in this direction except for the C-H···N interactions. The 3D structure is simplified to a 2D schematic shown in Figure III.12c. With increasing temperature, the crystal expands along the softer directions, while due to the “trellis”-like constraints, the [010] direction exhibits a negative thermal expansion. Under pressure, the soft direction exhibits maximum compressibility, while the hard direction [010] exhibits very limited compressibility at room temperature below 1000 MPa as it is resisting compression due to the same trellis effect.

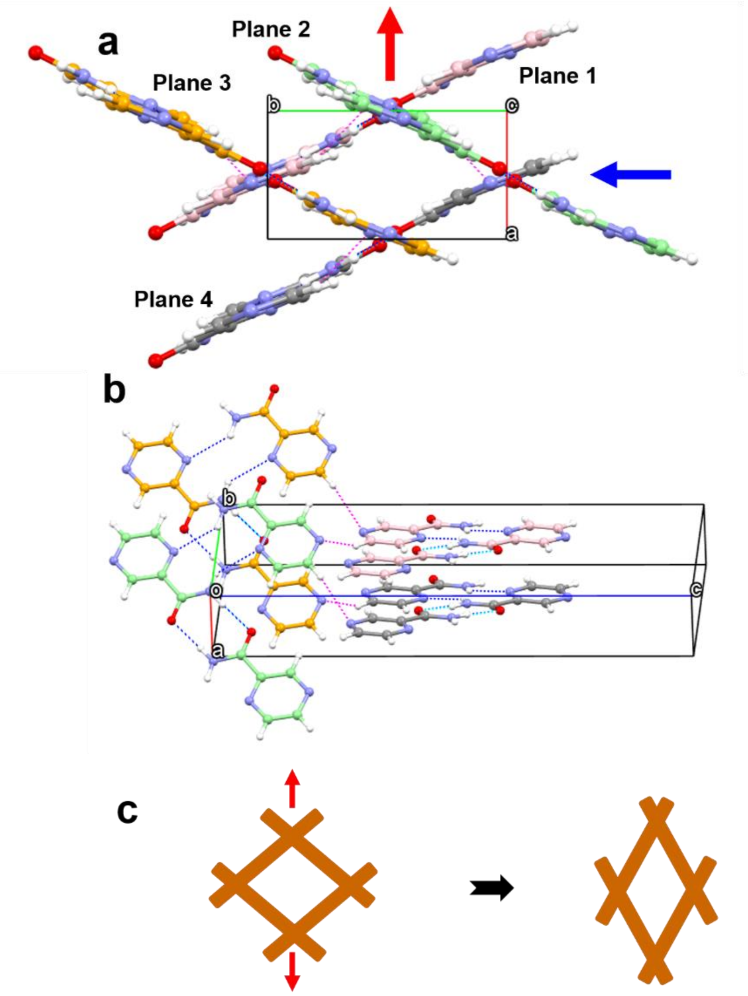

Figure III.12 (a) Projection of the crystal structure of form α on the (a, b) plane. The soft direction is marked by a red arrow and the hard (negative thermal expansion and minimum compression) direction is marked by a blue arrow, (b) short contacts in form α, (c) schematic to demonstrate the uniaxial negative thermal expansion in the system[2]

---

[2] The structure file is used PYRZIN15 in CSD.

III3.5.3 Thermal expansion and compressibility of polymorph β

The coefficients of the expansion and compression tensors of polymorph β are shown in Table III.2, and Figure III.13. Negative thermal expansion and compression are found in one direction which is approximately parallel to the [-10-1] crystallographic axis. The maximum thermal expansion is parallel to $\boldsymbol{e}_{3,\mathrm{T}}$ and the [0-10] crystallographic axis. The results shown in Figure III.14 indicate that the unit-cell changes are similar but opposite under temperature and pressure. The change of the *b* axis is bigger than that of the other two axes. The value of K_1 has a large error and it is close to the value of K_2. It means that the compressibility in the [0-10] and [-102] directions are very close (Figure III.13). Thus, the [0-10] direction can be considered the maximum compressibility direction. In fact, in directions [0-10] and [-102], the compressibility is relatively small, while in the third direction it is negative. So, overall, the β form appears to be rather resistant to pressure.

Table III.2 Principal coefficients of the isobaric thermal expansion tensor, the isothermal compressibility tensor and the corresponding principal axes of form β of pyrazinamide

Thermal expansion tensor

Principal axis, $e_{i,T}$	α_i (MK^{-1})	Component of $e_{i,T}$ along the crystallographic axes		
		a	*b*	*c*
1	-22.1(10)	-0.7464	0.0000	-0.6655
2	64(2)	-0.3690	0.0000	0.9294
3	119(2)	0.0000	-1.0000	0.0000
V	161(3)			

Compressibility tensor

Principal axis, $e_{i,p}$	K_i (TPa^{-1})	Component of $e_{i,p}$ along the crystallographic axes		
		a	*b*	*c*
1	13(8)	0.0000	-1.0000	0.0000
2	20(2)	-0.4839	0.0000	0.8751
3	-0.3(8)	-0.6727	0.0000	-0.7399
V	60(5)			

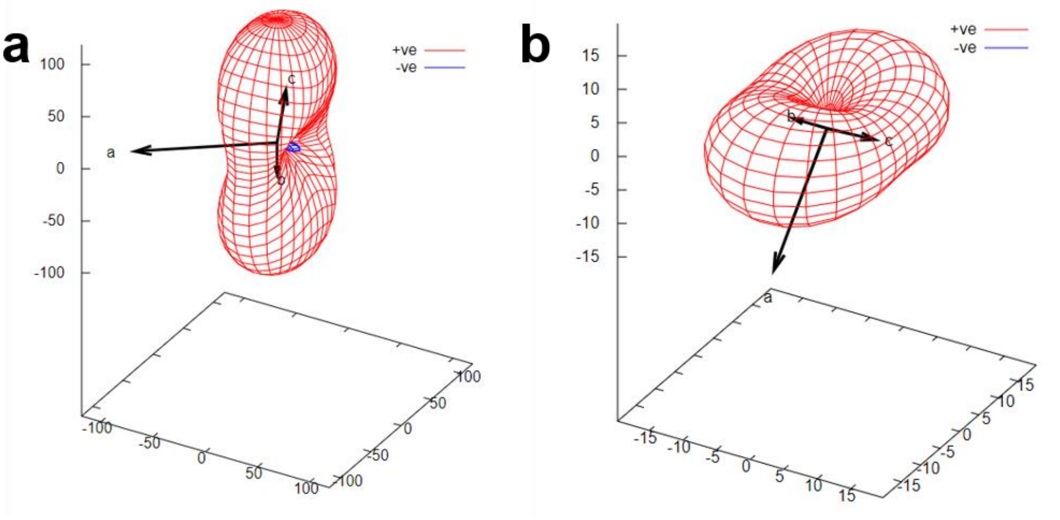

Figure III.13 The isobaric thermal expansion tensor (a) and isothermal compressibility tensor (b) of the β form. Positive thermal expansion is shown in red and negative thermal expansion is shown in blue.

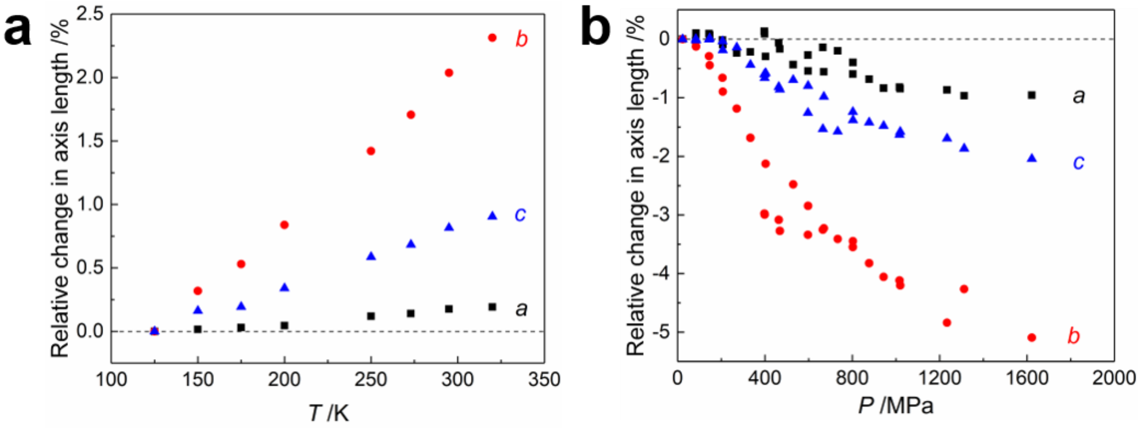

Figure III.14 Change in axis length of unit cell of β form as a function of (a) temperature and (b) pressure

The O-H···N hydrogen bonds, C-H···O, and C-H···N hydrogen bonds in form β create a tight network as shown in Figure III.15. Two planes can be distinguished with an angle between each other of 46°. These two planes interact through C-H···O and C-H···N hydrogen bonds marked with magenta dashed lines (Figure III.15a). The projection of the β form structure on the (a, b) plane shown in Figure III.15b is similar to the projection of the α form structure on the (a, b) plane. The thermal expansion of form β in the softest direction is smaller than the thermal expansion in form α. Like form α, the crystal expands along the [0-10] direction (that is, perpendicular to the molecular planes) when increasing the temperature, while the two interconnected planes form a trellis resulting in negative thermal expansion and compressibility along [-10-1].

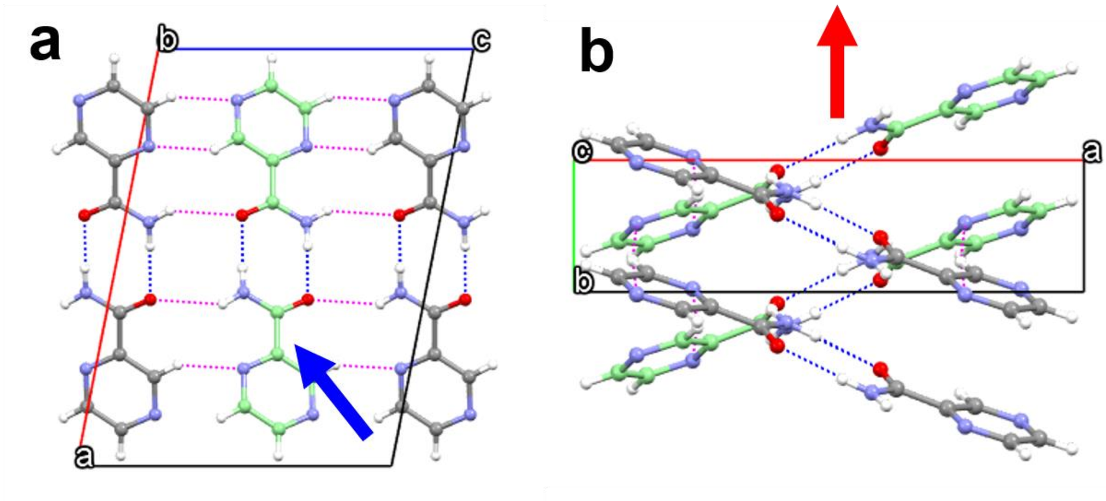

Figure III.15 Projection of the crystal structure of form β on (a) the *ac* plane, and (b) the *ab* plane. The blue arrow represents the negative thermal expansion and the negative compressibility of this structure, the red arrow indicates the maximum positive thermal expansion and the maximum compressibility[3]

III3.5.4 Thermal expansion and compressibility of polymorph γ

The thermal expansion and compressibility of polymorph γ are shown in Table III.3 and Figure III.16. Negative or zero thermal expansion was found along $\boldsymbol{e}_{1,T}$, which is approximately parallel to the [-100] direction. The minimum compression direction is almost parallel to the [-100] crystallographic axis as well. In the Figure III.17, it can be seen that the *a* axis changes little with temperature or pressure. The maximum thermal expansion and compression direction is parallel to the [0-10] crystallographic axis as can be seen in Figure III.17.

Compared to the other polymorphs, the molecular packing in form γ is different (Figure III.18). Molecules form linear chains through N-H···N hydrogen bonds. Other molecules are connected by C-H···O, C-H···N or N-H···O interactions. Figure III.18b shows that the structure projected on the *ab* plane is similar to that of form α on the same plane. The thermal expansion and compression exhibit a similar result as in the case of form α under temperature and pressure as well.

---

[3] The structure file used here is PYRZIN18 (CSD).

Table III.3 Principal coefficients of the isobaric thermal expansion tensor, the isothermal compressibility tensor and the corresponding principal axes of form γ of pyrazinamide

Thermal expansion tensor				
Principal axis, $e_{i,T}$	α_i (MK^{-1})	Component of $e_{i,T}$ along the crystallographic axes		
		a	*b*	*c*
1	-1.86(7)	-0.9593	0.0000	-0.2823
2	44(2)	-0.2507	0.0000	0.9681
3	137(3)	0.0000	-1.0000	0.0000
V	183(5)			
Compressibility tensor				
Principal axis, $e_{i,p}$	K_i (TPa^{-1})	Component of $e_{i,p}$ along the crystallographic axes		
		a	*b*	*c*
1	34.6(7)	0.0000	-1.0000	0.0000
2	11.3(2)	0.3839	0.0000	0.9234
3	3(2)	-1.0000	0.0000	-0.0058
V	51(3)			

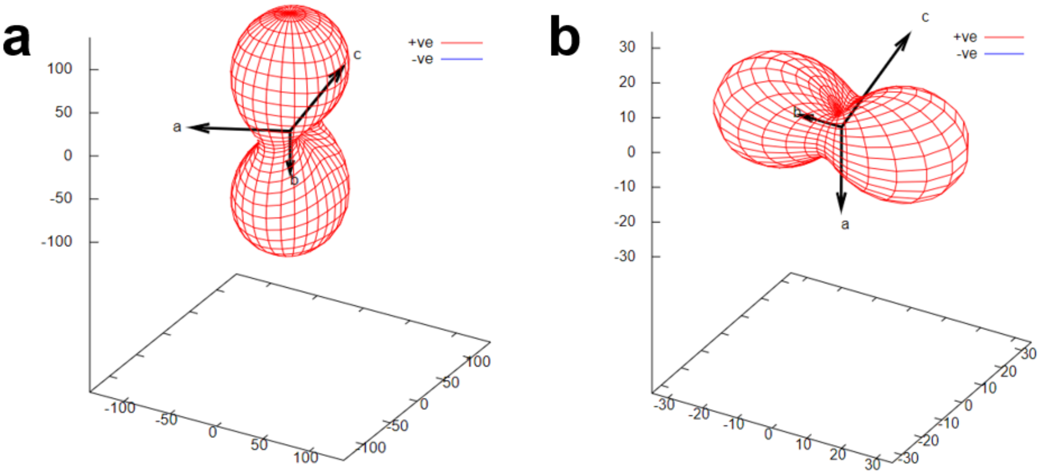

Figure III.16 The isobaric thermal expansion tensor (a) and isothermal compressibility tensor (b) of the γ form. Positive thermal expansion is shown in red and negative thermal expansion is shown in blue

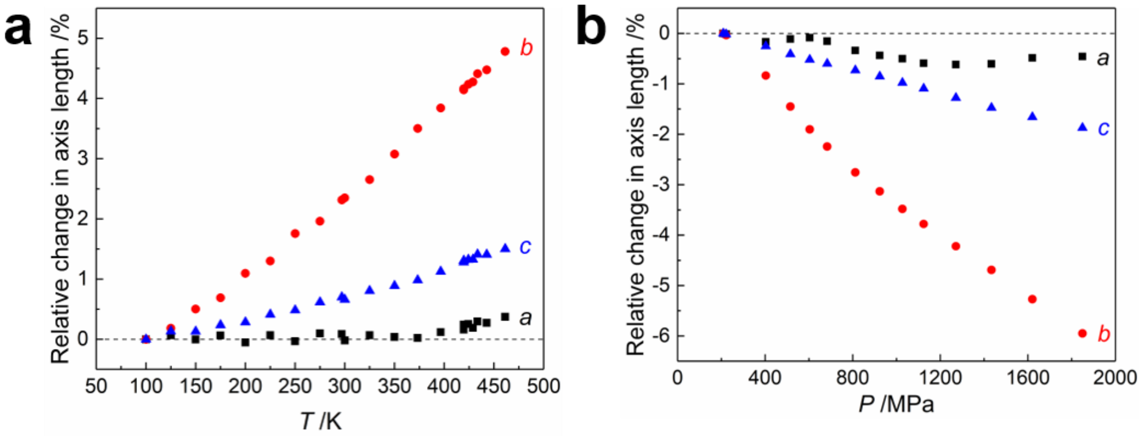

Figure III.17 Change in axis length of unit cell of γ form as a function of (a) temperature and (b) pressure

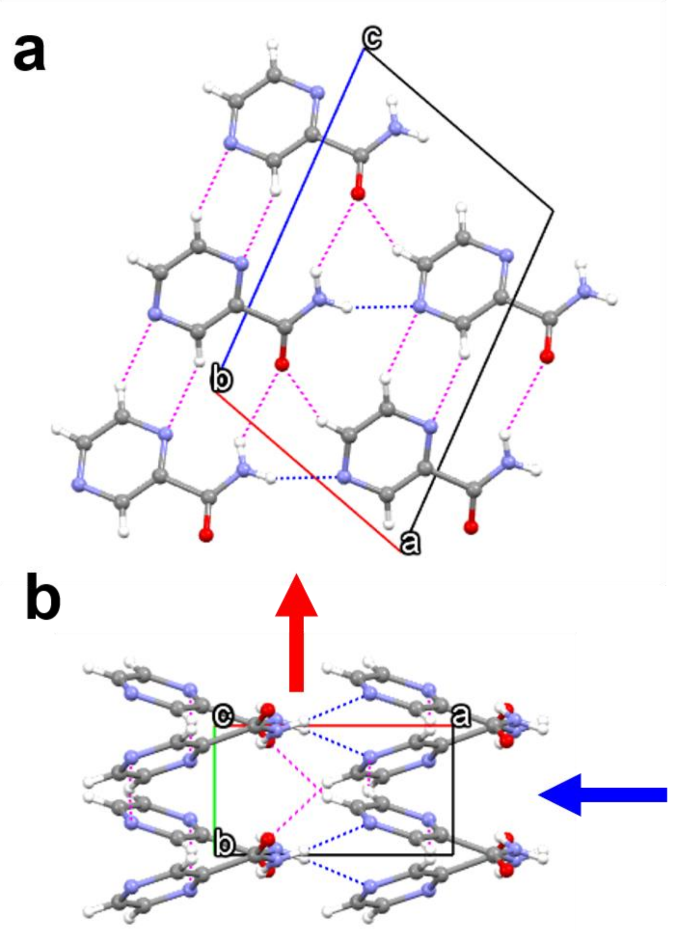

Figure III.18 Projection of the crystal structure of form γ (a) in the ac plane and (b) in the ab plane. The red arrow represents the maximum thermal expansion and compression of this structure, the blue arrow represents the negative thermal expansion and minimum compression[4]

---

[4] The structure file used here is PYRZIN17 (CSD).

III3.5.5 Thermal expansion and compressibility of polymorph δ

The thermal expansion and compressibility of polymorph δ are shown in Tables III.4 and Figure III.19. Negative thermal expansion was found along $\boldsymbol{e}_{1,T}$, which is approximately parallel to the direction of [11-1]. The maximum thermal expansion and compression direction is approximately parallel to the [311] direction. The compression in the direction of $e_{2,p}$ and $e_{3,p}$ are very similar. The changes in the *a*, *b* and *c* axes as a function of the temperature and pressure shown in Figure III.20 indicates that the *c* axis exhibits a better resistance to the temperature than to the pressure.

Table III.4 Principal coefficients of the isobaric thermal expansion tensor, the isothermal compressibility tensor and the corresponding principal axes of form δ of pyrazinamide

Thermal expansion tensor				
Principal axis, $e_{i,T}$	α_i (MK^{-1})	Component of $e_{i,T}$ along the crystallographic axes		
		a	*b*	*c*
1	-6.1(9)	0.5860	0.6391	-0.4981
2	17.1(7)	0.3459	-0.9099	-0.2290
3	178(6)	0.8848	0.3337	0.3252
V	192(7)			
Compressibility tensor				
Principal axis, $e_{i,p}$	K_i (TPa^{-1})	Component of $e_{i,p}$ along the crystallographic axes		
		a	*b*	*c*
1	82.0(8)	-0.8460	-0.2871	-0.4493
2	15(2)	-0.5175	-0.8242	0.2301
3	13.4(4)	0.6627	-0.6701	-0.3343
V	73(4)			

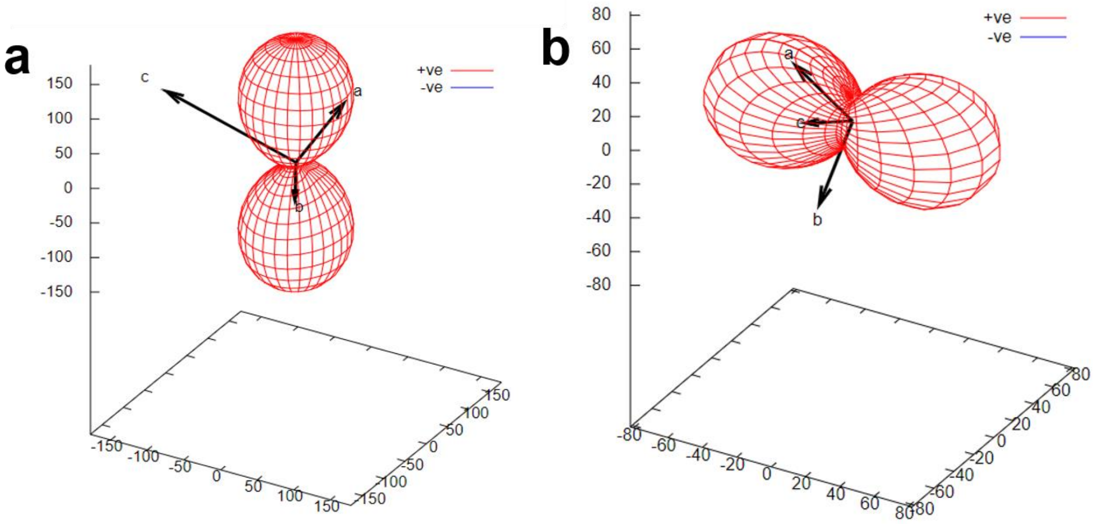

Figure III.19 The isobaric thermal expansion tensor (a) and isothermal compressibility tensor (b) of the δ form. Positive thermal expansion is shown in red and negative thermal expansion is shown in blue

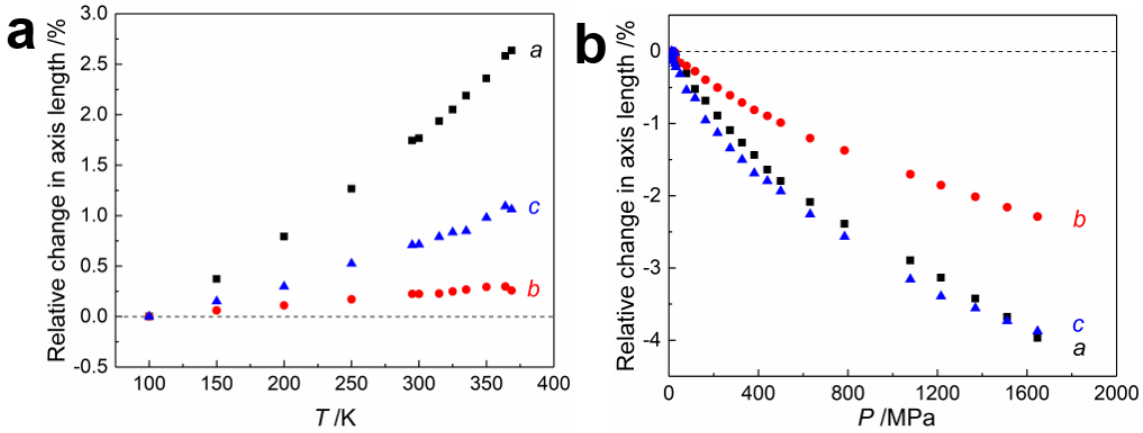

Figure III.20 Relative change in the unit-cell axes of form δ as a function of (a) temperature and (b) pressure

In form δ, pyrazinamide forms hydrogen bonded dimers, like in α and β. The dimers connect to each other through N-H···O and C-H···N hydrogen bonds. They form layered structures as shown in Figure III.21. The layer is approximately parallel to the *b* axis. The molecular arrangement and interactions in the same layer are shown in the Figure III.21a. Four pyrazine rings form an interaction square involving C-H···N interactions marked by magenta dashed lines. The maximum expansion and compression direction is along [311], which is almost perpendicular to the layer. In the direction of the negative thermal expansion the hydrogens on the two rings would be brought closer together. But all together, considering the electron density calculated later on, this unusual tetramer might be relatively strong. The rest of this direction is basically controlled by the twofold hydrogen dimer. Form δ exhibits the largest compression in comparison to the other polymorphs and it becomes the densest polymorph under pressure.

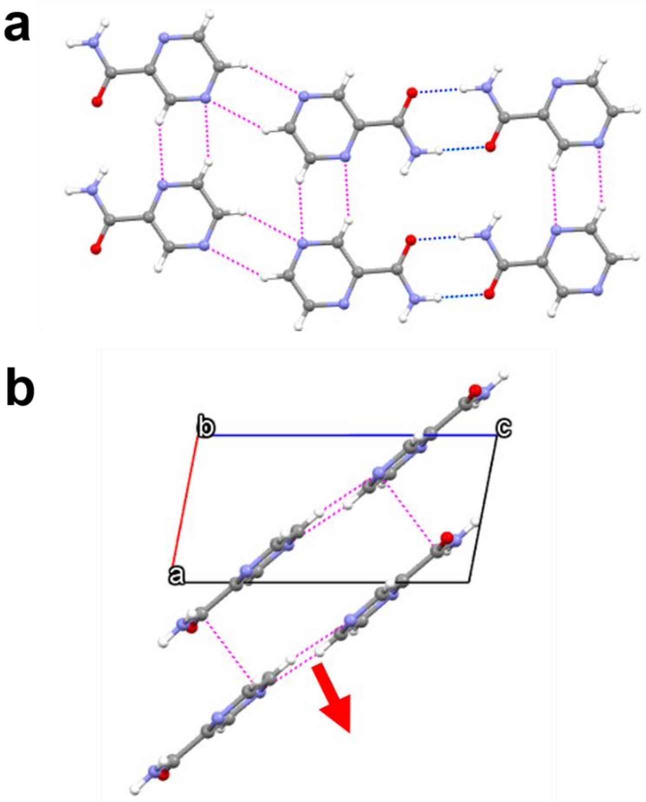

Figure III.21 (a) interactions between form δ molecules, (b) projection of the crystal structure of form δ in the *ac* plane. The red arrow represents the maximum thermal expansion[5]

III.4 Conclusion

In this chapter, chemical stability and the sublimation of pyrazinamide have been studied by thermal analysis. The results indicate that pyrazinamide is stable below 493 K. Sublimation of pyrazinamide is observed above 400 K. It provides the basis for the sublimation crystallization experiments in this chapter. Preparation methods of the α, β, γ, and δ polymorphs have been discussed. Preparing pure β form is still a challenge, but the trials with cooling crystallization in chloroform indicate that this could be a promising method to obtain pure β form. Thermal expansion and compression of α, β, γ, and δ polymorphs have been investigated using the unit cell parameters obtained by fitting the XRD patterns

---

[5] The structure file is used PYRZIN16 in CSD.

measured as a function of the temperature and the pressure. Uniaxial negative thermal expansion has been observed in all four polymorphs, although the values for γ and δ are close to 0. The hard and soft directions in the thermal expansion and the compression depend on the molecular interactions in the crystal structure. Form α, form β and form γ exhibit similar "trellis"-like constraints in the structure. The soft direction for the thermal expansion and the compression in form α coincides; it is parallel to the [-100] crystallographic axis. The hard direction for the thermal expansion and compression is parallel to the [010] crystallographic axis. In form β and form γ, the soft direction for the thermal expansion and compression is almost parallel to the [0-10] crystallographic axis. The hard direction for the thermal expansion and compression in form β is almost parallel to the [010] crystallographic axis and in form γ, it is almost parallel to the [-100] crystallographic axis. In form δ, the soft direction for the thermal expansion and compression is approximately parallel to the [311] crystallographic axis. The results reported in this chapter will support the study of the phase behavior of the polymorphs of pyrazinamide in the next chapter.

Chapter IV: The phase behavior of the four polymorphs α, β, γ, and δ

IV.1 Introduction

Physicochemical properties such as solubility and dissolution rate are different between polymorphs of the same molecule. Because metastable forms have a higher solubility, which is intrinsically connected with their lower stability, they are sometimes selected for the marketed drug product in the pharmaceutical industry. Therefore, having a full control over the stabilization of a metastable polymorph can be of significant pharmaceutical importance. A preliminary requirement for control is a solid understanding of the phase behavior of the drug molecule in question.

In this chapter, the phase relationships between the α, β, γ, and δ polymorphs of pyrazinamide are discussed. In particular, the phase relationship between the polymorphs α and γ has been extensively studied by DSC, PXRD, synchrotron PXRD and HP-DTA. The melting temperature and enthalpy of γ have been reviewed and those of α have been determined. In addition, a thorough study of the α-γ transition temperature and enthalpy has been carried out. The melting equilibrium of γ and the transition between α and γ have been measured by HP-DTA. The vapor pressure and the solubility of the α and γ forms have been obtained. All the data have been combined to construct a topological phase diagram demonstrating the stability hierarchy of the two polymorphs as a function of pressure and temperature. The phase relationships between β and the other polymorphs and between δ and the other polymorphs have been studied by DSC and PXRD and some preliminary conclusions have been drawn.

IV.2 The phase behavior between α and γ

IV.2.1 The melting equilibria of α and γ

IV.2.1.1 The melting of form γ

A typical DSC curve of commercial pyrazinamide (form α) can be found in Figure IV.1. At a scanning rate of 10 K min^{-1}, α transforms into γ at around 425 K followed by the melting peak of γ at around 462 K (Figure IV.1). To determine the enthalpy and the temperature of fusion of γ, measurements have been carried out at 10 K min^{-1} for 28 samples of different mass and the result is presented in Table C.1 in appendix C. During the measurements, it became clear that the enthalpy of fusion depends on the amount of material in the DSC capsule, similar to the cases of camphor[264] and adamantane[266]. Therefore, the enthalpy of fusion was plotted as a function of the "specific volume" of the sample as shown in Figure IV.2. The "specific volume" of the sample in a DSC experiment ($V_{\text{pan}}/m_{\text{sample}}$) is the volume of a sealed DSC pan (V_{pan}), which includes its dead volume not taken up by solid pyrazinamide, divided by the mass of the weighed-in sample (m_{sample}). In most cases, when the vapor pressure of the solid is low, no consistent variation in the melting enthalpy will be observed; however, for pyrazinamide, a clear decrease of the measured specific enthalpy of fusion is observed with increasing "specific volume" (i.e. with decreasing mass, see Figure IV.2). This sublimation can in fact be observed by DSC, as illustrated in Figure IV.1 illustrated by two DSC curves of samples with a large difference in mass. The bottom curve exhibits a regular melting peak observed for a sample with a weight of 5.88 mg, whereas the top DSC curve represents a sample of 0.01 mg. In the inset, an upward shift from the baseline can be observed as a result of sublimation. Only a small peak-like drop to the baseline is observed at 449 K below the recorded melting temperature indicating that the sample has completely sublimated before it could have melted. Obviously, this rise of the baseline is also present in the curves with clear melting peaks, but in that case this baseline effect is dwarfed by the melting peak.

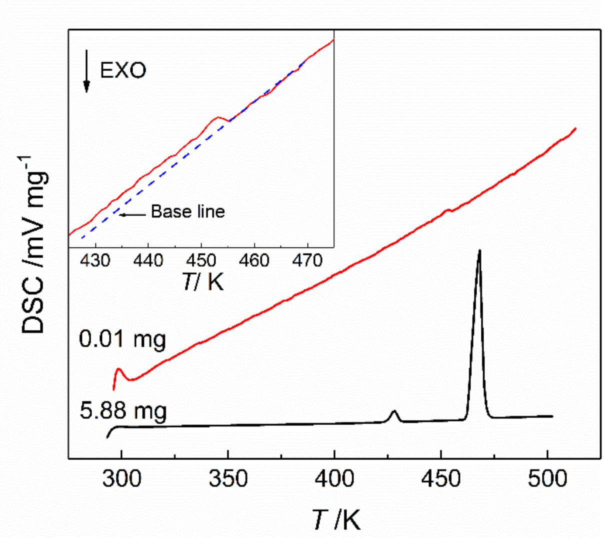

Figure IV.1 DSC curve (10 K min^{-1}) of commercial pyrazinamide form α transforming into γ at around 425 K, which melts at around 462 K (black line) and a DSC curve of a sample with a very large specific volume (V_{pan}/m_{PZA}) of which only the end of sublimation can be observed (449 K, red line). Inset: a close-up of the DSC curve of the 0.01 mg sample illustrating the end of sublimation before the melting point of γ is reached. The extension of the baseline is indicated by the blue dashed line

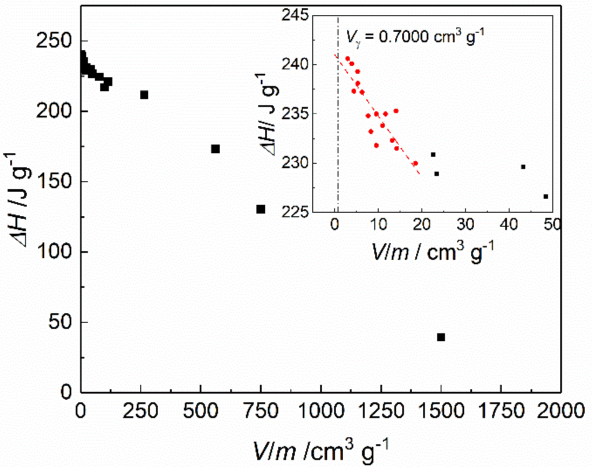

Figure IV.2 The enthalpy of fusion of form γ as a function of the specific volume available to pyrazinamide in the DSC capsule (see text). Inset: close-up on the evolution of the enthalpy of fusion at low specific volume; an upward curvature of the line can be observed

Taking the enthalpy data in Table C.1 in Appendix C and Figure IV.2, one can establish a linear relationship with the specific volume in the DSC pan: $\Delta_{\gamma\to L}H\,(V_{pan}/m_{sample}) = -0.130(3)\,V_{pan}/m_{sample} + 236.1(9)$ leading to an enthalpy of fusion for a fully filled pan in the order of

236 J g^{-1}. However, it can be seen in the inset of Figure IV.2 that at the lowest specific volumes (i.e. fully filled DSC capsules), the enthalpy of fusion tends to even higher values in the order of 240 J g^{-1}. In fact, in the inset of Figure IV.2 at its lower range, one can observe a slight upward curvature in the line. For this reason, only the points up to a specific volume of 20 cm^3 g^{-1} have been used for the extrapolation, leading to the expression for the melting enthalpy, $\Delta_{\gamma\rightarrow L}H$ (/J g^{-1}), as a function of the "specific volume", $V_{\mathrm{pan}}/m_{\mathrm{sample}}$ (/cm^3 g^{-1}):

$$\Delta_{\gamma\rightarrow L}H\,(V_{\mathrm{pan}}/m_{\mathrm{sample}}) = -0.623(10)\;V_{\mathrm{pan}}/m_{\mathrm{sample}} + 241.0(1.0) \qquad \text{(IV.1)}$$

Extrapolating this line to the specific volume of the γ form at its melting temperature (this translates to a capsule filled entirely with pyrazinamide without dead volume and is equal to 0.7003(31) cm^3 g^{-1} as reported in section IV.3.4) leads to an enthalpy of fusion of 240.6(1.0) J g^{-1}.

Considering the scatter over the enthalpy of fusion of form γ, the enthalpies and temperatures of fusion of three single crystals have been determined too; in particular because the surface to bulk ratio is much smaller than in the case of powder, it may diminish the effect of sublimation. The data can be found in Table VI.1; there is still a considerable scatter over the melting enthalpy data and it is not clear whether the relation between the weighed-in mass and the enthalpy (Table IV.1) is accidental or not, but the average of 240(5) J g^{-1} confirms the results obtained with capsules tightly filled with powder.

Table IV.1 The melting point and the enthalpy of fusion of single crystals of polymorphs α and γ measured by DSC [a]

Sample	α			γ		
	T_{fus} /K	ΔH /J g^{-1}	m /mg	T_{fus} /K	ΔH /J g^{-1}	m /mg
1	457.05	250.6	0.98	462.35	244	2.69
2	456.65	255.7	0.66	462.55	239.9	2.12
3				462.65	235.9	1.69
Average	457(1)	253(4)		462.5(5)	240(5)	

[a] heating rate is 100 K min^{-1} for α and γ.

The overall behavior of the melting enthalpy increasing with an increasing amount of pyrazinamide is clearly caused by the tendency of pyrazinamide to sublimate as is shown in Figure IV.2. It is not entirely clear why, at very high loads, the enthalpy appears to curve slightly upwards. How this curvature comes about with powder samples could possibly be explained by a combination of sublimation and disorder reported for the γ form.[129, 134] The melting temperature, which does not vary with sample mass, is much easier to determine. The average over 27 points is equal to 462.0(5) K (n = 27). This value is in accordance with the literature data.

IV.2.1.2 The melting of form α

The temperature and enthalpy of fusion of form α have been obtained using single crystals subjected to DSC measurements at 100 K min^{-1} (See Table VI.1). The high scanning rate was necessary to outrun the solid-solid transition from form α to form γ. The DSC has been specially calibrated for these measurements at 100 K min^{-1} with the four calibrants listed for the DSC 214 from Netzsch (See section II.3.2.1). The melting point has been found to be 457(1) K and the enthalpy of fusion equals 253(4) J g^{-1}. It was not possible to investigate the influence of sublimation on the melting properties of α, due to the inaccuracy of the DSC at 100 K min^{-1} and because changing to smaller crystals would cause them to turn into γ before melting. However, the high scanning speed and the fact that the sample was a single crystal, which decreases the surface to bulk ratio, may have limited the effect of sublimation considerably.

IV.2.2 The α-γ equilibrium temperature

The transition temperature of α to γ had been previously shown to depend on the heating rate of the DSC.[128] However, the value at infinitely low heating rate remains unknown. In the current study, once again different heating rates have been used to investigate the temperature of conversion of form α into γ and the results are presented in Figure IV.3 and the values can be found in Table C.2 in Appendix C. It is clear from Figure IV.3 that the transition temperature decreases with decreasing heating rate and there is no visible levelling off at very low heating rates even if the values observed are still lower than those reported by Castro et al.[128]. DSC appears not to be the most appropriate method to determine the transition temperature between forms α and γ due to this particular kinetic behavior of the transition. Therefore, each polymorph has been kept in an oven in separate experiments at a decreasing series of temperatures starting roughly at the lowest transition temperature observed by DSC. The results are presented in Table IV.2. It can be seen that at 392 K initial form α turns into form γ. Moreover, subjecting γ to a temperature of 391 K, a single crystal of form α is grown, while at 390 K, several α crystals can be observed. It can be concluded that the most likely equilibrium temperature between α and γ can be found between 391 and 392 K. Lacking any further precision, the average between these values will be rounded off to the nearest digit: $T_{\alpha\rightarrow\gamma}$ = 392(1) K.

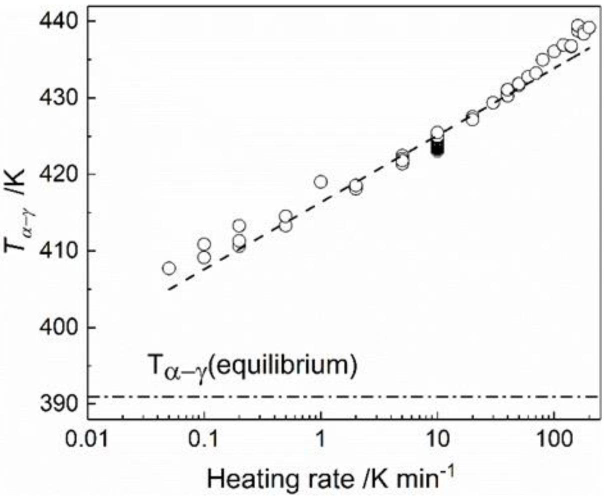

Figure IV.3 The temperature of the α to γ transition obtained by DSC at different heating rates (○). No conclusive equilibrium temperature can be obtained from this behavior. The dot-dashed line is the observed equilibrium temperature (Table IV.2)

Table IV.2 The stability of the polymorphs α and γ at constant temperature

T /K	Initial polymorph	Final polymorph	Comments
403	α	γ	
398	α	γ	
394	α	γ	
392	α	γ+α	γ is a single crystal
391	γ	γ+α	One single crystal of α
390	γ	γ+α	Few crystals of α
373	γ	α	
353	γ	α	

The enthalpy change associated to the α-γ transition has been determined at a scanning rate of 10 K min^{-1}. It did not depend on the sample mass as in the case of the melting point of γ, most likely because the lower temperature did not result in as much sublimation. Interestingly, the enthalpy difference between the two polymorphs remained constant even if the transition temperature ranged from 405 to 440 K (the result can be found in Table C.3 in Appendix C and Figure IV.4). The average over 83 samples of the α-γ transition enthalpy has been found to be $\Delta_{\alpha\rightarrow\gamma}H = 13.2(6)$ J g^{-1}.

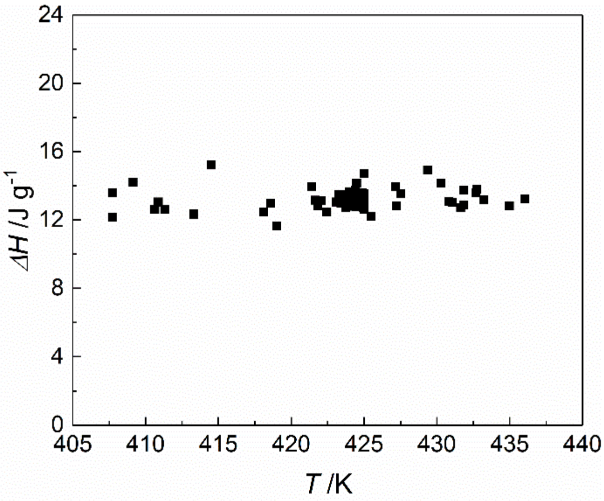

Figure IV.4 Transition enthalpy of α to γ form at different transition temperatures

The constant transition enthalpy between α and γ indicates that their difference in heat capacity does not change much with the temperature. For thermodynamic reasons, the sum of the enthalpies of the cycle α to γ to liquid to α must be equal to zero: $\Delta_{\alpha\rightarrow\gamma}H + \Delta_{\gamma\rightarrow L}H - \Delta_{\alpha\rightarrow L}H = 13.2 + 240 - 253 = 0.2 \cong 0$. The fact that this sum indeed equals zero indicates that the enthalpy differences between phases α, γ, and the liquid appear to be consistent. One may therefore conclude that most likely the enthalpy difference between α and γ is temperature independent between their equilibrium temperature and the melting point of pyrazinamide. The transition enthalpy is equal to the values reported in the literature.[128, 267] However, the transition temperature between the two solids at 392 K appears to be at least 20 degrees lower, than previously reported in the literature[128].

IV.2.3 The α-γ transition and the fusion of γ under pressure

High-pressure differential thermal analysis curves containing the peaks for the α to γ transition and the fusion of γ are shown in Figure IV.5a. The observed transitions have been plotted as a function of the pressure and the temperature and are presented in Figure IV.5b. The values can be found in Appendix C (fusion of γ: Table C.3 and the α-γ transition: Table C.4). The solid-solid transition was difficult to measure and only a few points could be obtained. In both cases the data have been fitted to a straight line in the form of the pressure P(/MPa) as a function of the temperature T(/K):

$$\gamma\rightarrow\mathrm{L}: P = 3.5(3)\ T - 1623(100) \tag{IV.2}$$

$$\alpha\rightarrow\gamma: P = -3.6(7)\ T + 1510(283) \tag{IV.3}$$

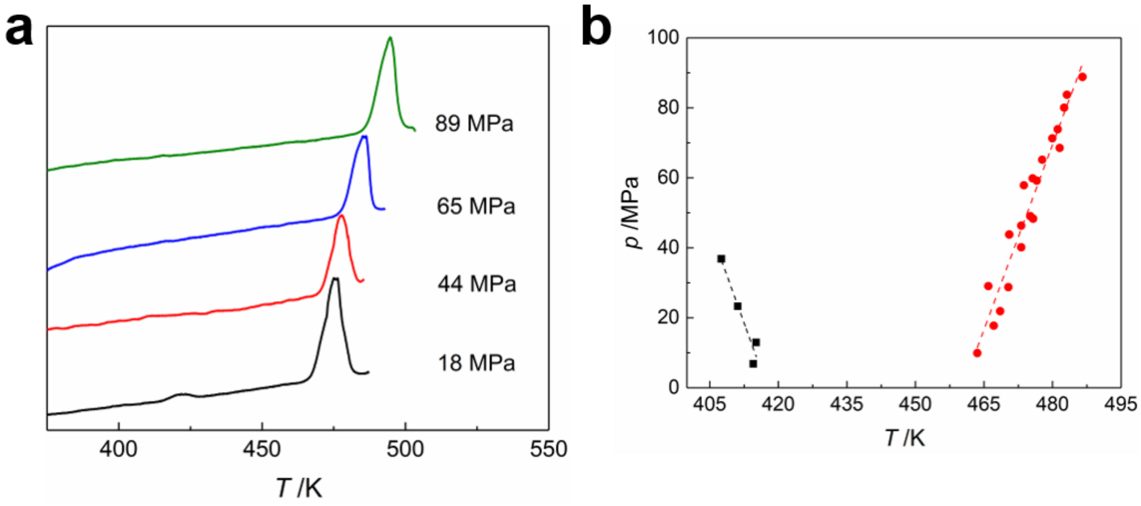

Figure IV.5 (a) High-pressure differential thermal analysis curves and (b) the transition pressure of α to γ (■) and the melting pressure of γ (●) as a function of the temperature

IV.2.4 The temperature dependence of the specific volume

The specific volumes of forms α and γ as a function of the temperature have been obtained by high-resolution PXRD. The resulting specific volumes are presented in Tables A.1 and A.3 in Appendix A and Figure IV.6. The data has been fitted to the following expressions of the specific volume V_i (/cm^3 g^{-1}) as a function of the temperature T (/K):

$$V_\alpha = 0.6624(7) + 6.8(6) \times 10^{-5}\ T + 8.44\ (1.06) \times 10^{-8}\ T^2 \tag{IV.4}$$

$$V_\gamma = 0.6520(7) + 4.8(5) \times 10^{-5}\ T + 1.22(9) \times 10^{-7}\ T^2 \tag{IV.5}$$

Comparing the specific volume of forms α and γ measured in this work and the literature (see Figure IV.6), it can be seen that the specific volume of form α is larger than that of form γ in the entire measured temperature range: $V_\alpha > V_\gamma$. In other words, the density of α is lower than that of form γ: $d_\alpha < d_\gamma$. Interestingly, the difference in specific volume hardly changes from 100 K up to 400 K: $\Delta_{\alpha\rightarrow\gamma}V(T) = -0.01242(23) - 1.1(9) \times 10^{-6}\ T$ and the average difference in volume between α and γ is $\Delta_{\alpha\rightarrow\gamma}V = -0.0127(4)$ cm^3 g^{-1} with an error of less than 2.5% (see also Figure IV.6). Although the literature data appears to be somewhat scattered in Figure IV.6, the γ form is clearly denser than α.

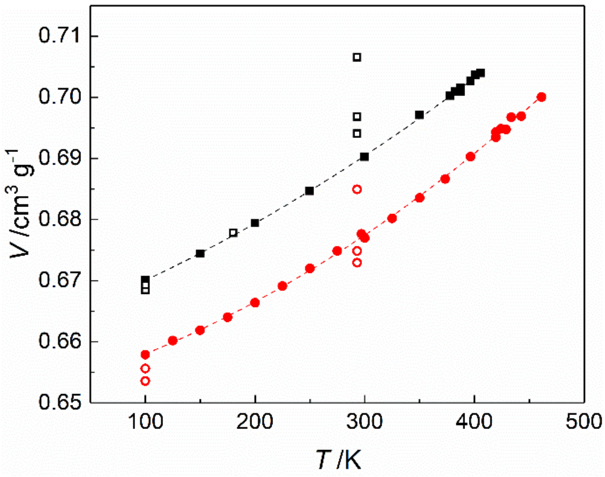

Figure IV.6 The specific volume of pyrazinamide form α and form γ at different temperatures. (■) α this work, (●) γ this work, (□) α from the literature[120, 124, 126, 127, 130, 131], (○) γ from the literature[121, 125, 128, 129]

IV.2.5 The vapor pressure of α and γ

A few papers contain data on the vapor pressure of the α form[141, 148, 149], however, data obtained by different methods are difficult to compare. Thus, the vapor pressure of α and γ as a function of the temperature is measured in this work using the method described in section II.4.5 and the result is shown in Table C.5 in Appendix C. Using the Clausius–Clapeyron equation ($\ln p = -\Delta_{S\rightarrow Vap}H/RT + B$, $\Delta_{S\rightarrow Vap}H$ is the enthalpy of sublimation, B is a constant), the vapor pressure P(/Pa) can be expressed as a function of the temperature T(/K):

$$\alpha\rightarrow\text{Vap: } \ln p = -94945(1024) / RT + 32.3(4) \quad (R^2 = 0.9991) \tag{IV.6}$$

$$\gamma\rightarrow\text{Vap: } \ln p = -92192(2024) / RT + 31.5(7) \quad (R^2 = 0.9986) \tag{IV.7}$$

with the numerator being the enthalpy of sublimation in J mol^{-1} and R the gas constant, 8.3145 J K^{-1} mol^{-1}. The sublimation enthalpies from eqs. IV.6 and IV.7 reflect the differences in enthalpy between the respective polymorph and the vapor phase. It implies that the difference between these two enthalpies must be similar to the transition enthalpy between the two solid phases: $\Delta_{\alpha\rightarrow\gamma}H = \Delta_{\alpha\rightarrow Vap}H - \Delta_{\gamma\rightarrow Vap}H = 94945 - 92192 = 2.75(2.27)$ kJ mol^{-1} or 22(19) J g^{-1}. Obviously, the error over the large enthalpy values is considerable, which is reflected in the large error over the transition enthalpy of 22 J g^{-1}; however, the value is equal within error with that of the DSC even if the vapor pressure is simply not precise enough to determine an accurate enthalpy difference. In comparison with the literature values in Table I.5 in Chapter I, the enthalpies of vaporization found here, 771 J g^{-1} for α and 749 J g^{-1} for γ, are similar; however, the spread in the values in Table I.5 is large and it seems essential that data for different polymorphs are obtained with a single apparatus for reliable comparison.

The intersection between the two lines described by eqs. IV.6 and IV.7, where the vapor pressure of the two polymorphs is equal, should coincide with the equilibrium temperature of α-γ transition. It is found at about 398 K, which is somewhat higher than 392 K, the result obtained in Table IV.2.

IV.2.6 The solubility of α and γ

The solubilities in water of the α and γ polymorphs measured at different temperatures and those found in the literature[56, 135] are provided in Table C.6 (Appendix C) and Figure IV.7. The solubility of γ is higher than the solubility of α in the investigated temperature domain. The solubility of α measured in this work is similar to the data measured in the literature, but the solubility of γ is lower than the data in the literature. This may be explained by the metastability of γ, which may cause a larger error over the result. The solubility data can be fitted using the van't Hoff equation:

$$ln x_i = -\frac{\Delta_{d(i)}H}{RT} + \frac{\Delta_{d(i)}S}{R} \qquad \text{(IV.8)}$$

where x_i is the mole fraction solubility of form i (/mmol mol^{-1}), $\Delta_{d(i)}H$ (/J mol^{-1}) and $\Delta_{d(i)}S$ (/J mol^{-1} K^{-1}) represent the dissolution enthalpy and entropy of form i in water, respectively. T is the temperature (/K), and R is the gas constant.

$$\alpha: ln\, x = -28917(643) / RT + 12.5(3) \qquad (R^2 = 0.9985) \qquad \text{(IV.9)}$$

$$\gamma: ln\, x = -26714(1034) / RT + 11.7(5) \qquad (R^2 = 0.9955) \qquad \text{(IV.10)}$$

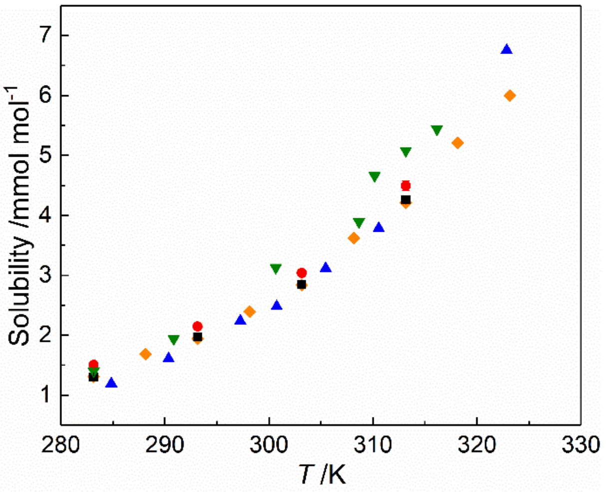

Figure IV.7 The solubility of polymorphs α and γ at different temperatures in water. (■) α (this work), (●) γ (this work), (▲) α obtained by Hermanto et al., (◆) α obtained by Zhang et al. (▼) γ obtained by Hermanto et al.. The error bars for the data obtained in this work are smaller than the symbols

Like the enthalpy of sublimation, the transition enthalpy can be calculated: $\Delta_{\alpha\rightarrow\gamma}H = \Delta_{d(\alpha)}H - \Delta_{d(\gamma)}H = 28.917 - 26.714 = 2.21(1.3)$ kJ mol^{-1} or 18 (10) J g^{-1}. Errors are again large due to the comparison between two large values; however, the overall difference in enthalpy between the two polymorphs is not far from the value of 13.2 J g^{-1} obtained by DSC. The equilibrium transition temperature between α and γ in the presence of water can be calculated using eqs. IV.9 and IV.10, the intersection of these two lines being the transition temperature. It is found at 330(4) K. This temperature is lower than that obtained through the oven and the vapor pressure experiments. This could be due to the difficulties in interpreting the solubility data due to metastability of the γ form. Nonetheless, it could also be due to the interaction between the solvent and the solute, which may affect the chemical potentials of the polymorphs as described by the Gibbs-Duhem equation.

IV.2.7 The pressure-temperature phase diagram involving α, γ, and the liquid

Using the data presented above, a pressure-temperature phase diagram can be constructed describing the behavior of the three condensed phases that have been investigated. Eq. IV.2 describes the pressure-temperature behavior of the melting equilibrium of γ. Considering that this transition is observed in the direction of a solid-liquid transformation and thus no significant kinetic barrier exists for the transition, there is little doubt that the obtained equation reflects the equilibrium behavior within error.

The same cannot be said about the α-γ transition, as is very clear from Figure IV.3, where the transition temperature decreases as the heating rate decreases. This implies that $p(T)_{\alpha\to\gamma}$, should be shifted to lower temperatures assuming that the slope will stay the same. In fact, the slope of the α-γ equilibrium can be verified with the Clapeyron equation, using the calorimetric and volumetric data discussed above: $T_{\alpha\to\gamma}$ = 392(1) K, $\Delta_{\alpha\to\gamma}H$ = 13.2(6) J g^{-1}, and with $\Delta_{\alpha\to\gamma}v$ (392 K) = −0.0124 (38) cm^3g^{-1}, as v_α (392 K) = 0.7021(29) $cm^3g^{-1}$and v_γ (392 K) = 0.6897(25) cm^3g^{-1}. This leads to a slope of −2.7(9) MPa K^{-1}. Even if the values of the slopes (−3.6(7) MPa K^{-1} in eq. IV.3) overlap within error, it is most likely that the slope of the α-γ equilibrium is closer to −2.7 MPa K^{-1}, because the transition points obtained by HP-DTA may suffer an overestimation in temperature as observed in the regular DSC measurements for this solid-solid transition. Thus, the pressure (p /MPa) of the α-γ equilibrium can be expressed as a function of the temperature (T /K) in the following adjusted way:

$$\alpha\to\gamma\text{: } p = -2.7(9)\, T + 1064(327) \qquad \text{(IV.11)}$$

In which the line is shifted to pass through 392 K at 0 MPa (representing the vapor pressure of pyrazinamide in megapascal).

Taking the intersection of eqs. IV.2 and IV.11, one finds the triple point where the phases α, γ, and the liquid are in equilibrium, leading to 431 K and −105 MPa. Using this triple point in turn with the melting temperature of form α, 457 K at 0 MPa, the relation of the pressure (p /MPa) for the melting equilibrium of form α as a function of temperature (T /K) can be obtained:

$$\alpha\to\text{L: } p = 4.0\, T - 1823 \qquad \text{(IV.12)}$$

It can be seen that this melting equilibrium is the steepest in the phase diagram as expected for the three diverging equilibria, α-γ, α-L, and γ-L, with increasing pressure.

For statistical reasons, it is of interest to study the change in the specific volume of the melting solid. In particular for cases for which it is not possible to have experimental access to the slope of the melting equilibrium using statistical data, an estimate of the slope can be obtained and a topological phase diagram can be constructed through thermodynamic reasoning.

In the case of pyrazinamide, the slope of the melting of the γ phase has been found to be 3.5(3) MPa K^{-1} based on the HP-DTA data. Taking the melting enthalpy of 240(5) J g^{-1} obtained above, the melting temperature of 462.0(5) K and the specific volume of the γ form at the melting temperature, V_γ (462.0 K) = 0.7003(31) cm^3 g^{-1}, one obtains through the Clapeyron equation the volume change on melting, $\Delta_{\gamma\to L}V$ = 0.1473(92) cm^3 g^{-1}, and the specific volume of the liquid at the melting point: V_L (462.0 K) = 0.8476(97) cm^{3}g^{-1}.

For the melting of form α, information on the thermal expansion of the liquid can be used. From the results in this paper and from those of Borba et al., it can be concluded that the glass transition temperature can be found around at 260 K.[268] Because at the glass transition, the liquid turns into a glass, by approximation its density can be set equal to that of the least dense polymorph of pyrazinamide, which is form α. At 260 K, form α will have a specific volume of V_α (260 K) = 0.6858 cm^3 g^{-1}. With the specific volume of the liquid at the melting point of the γ form, the specific volume of the liquid (V_L /cm^{3}g^{-1}) as a function of the temperature (T /K) can be described by a straight line (see Figure IV.8):

$$V_L = 0.47756 + 8.0101 \times 10^{-4} T \qquad \text{(IV.13)}$$

Using the known data on the melting of the α form, $T_{\alpha\to L}$ = 457(1) K, $\Delta_{\alpha\to L}H$ = 253(4) J·g^{-1}, V_α ($T_{\alpha\to L}$) = 0.7112(35) cm^3 g^{-1} and V_L ($T_{\alpha\to L}$) = 0.8435(3) cm^3 g^{-1} a change in the volume on the melting of α can be determined $\Delta_{\alpha\to L}V$ = 0.1323(36) cm^3 g^{-1}. This leads to a slope for the melting equilibrium of 4.2(2) MPa K^{-1}. Comparing this to the slope in eq. 14 of 4.0 MPa K^{-1}, which has been obtained by extrapolation of the γ-L equilibrium and the α-γ equilibrium, demonstrates the strength of the topological method and the redundancy in the data due to the thermodynamic requirements they need to fulfill.

The ratio of the volume of the liquid by that of the melting solid form is V_L/V_γ = 1.21 for γ and V_L/V_α = 1.19 for α. These values are large in comparison with most small organic molecules and only form III of piracetam with a ratio of 1.18 comes anywhere near these values.[269] Goodman et al.[270] found an average expansion on melting of about 12% for small organic molecules based on 21 compounds. Based on different distributions of small pharmaceutical molecules, similar expansions with an average in the order of 11% have been recorded.[271, 272] The reason for the large difference in the specific volume between the solid state and the liquid state must lie in the flatness of the molecule, which makes efficient stacking possible in the solid, but which is obviously lost in the liquid state. The density of the γ form is indeed rather high for an organic substance with 1.43 g cm^{-3} at its melting point and 1.48 g cm^{-3} at room temperature.

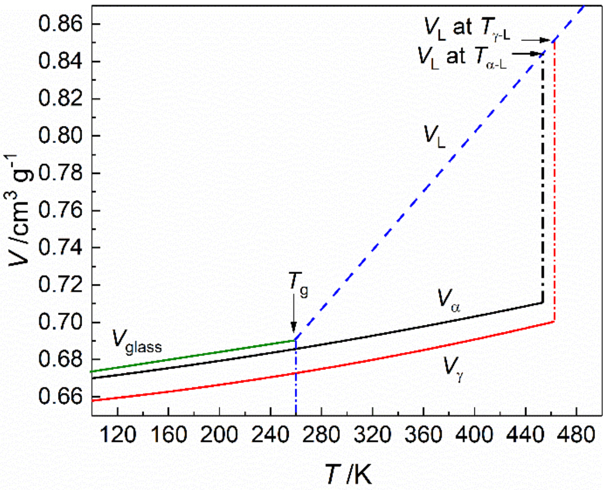

Figure IV.8 Schematic representation of the thermal expansion of the liquid in relation to the thermal expansion of the solids

The resulting topological pressure-temperature phase diagram of α-γ-L-V is presented in Figure IV.9. This phase diagram is constructed based on eqs. IV.2, IV.11, and IV.12 for the condensed phases and eqs. IV.6 and IV.7 for the vapor phases. The final liquid-vapor (L-V) equilibrium curve can be calculated as follows. The enthalpy of vaporization is $\Delta_{L\rightarrow V}H = \Delta_{\gamma\rightarrow V}H - \Delta_{\gamma\rightarrow L}H$; $\Delta_{\gamma\rightarrow V}H$ can be obtained from eq. IV.14 and amounts to 749(17) J g^{-1} and $\Delta_{\gamma\rightarrow L}H$ is 240(5) J g^{-1}, so that $\Delta_{L\rightarrow V}H$ is 509(17) J g^{-1}. Eqs. IV.2 and IV.7 can be used to calculate the triple point of γ-L-V through which the L-V equilibrium curve must pass leading to the expression (with p in Pa and T in K):

$$\text{L}\rightarrow\text{V: } \ln p = -7535 / \text{T} + 23.8 \qquad \text{(IV.14).}$$

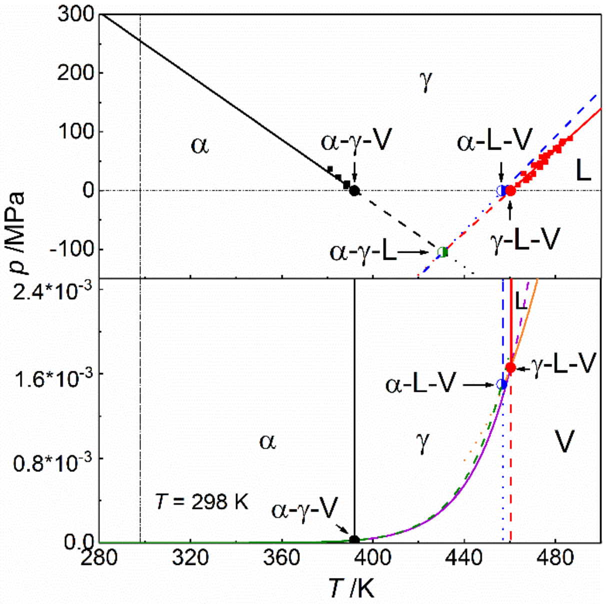

Figure IV.9 The two-panel pressure-temperature phase diagram of the α and γ polymorphs, the liquid, L, and the vapor phase, V. High pressure panel (Top): Two-phase equilibria: black (line + points (■)): α-γ, blue line: α-L, red (line + points (🟥)): γ-L. (◑) is metastable triple point α-γ-L, (●) is stable triple point α-γ-V, (◑) is metastable triple point α-L-V and (●) is stable triple point γ-L-V. Low pressure panel (below): Zoom on the vapor phase with orange line: L-V equilibrium, purple line: γ-V equilibrium and green line α-V equilibrium. Solid lines: stable equilibria, dashed lines: metastable equilibria, dotted lines: super-metastable equilibria. Solid circle: stable triple point, semi-solid circle: metastable triple point

IV.3 Phase relationships between form δ and the other polymorphs

DSC measurements of form δ samples with different heating rates have been carried out and the result is provided in Figure IV.10 (see also Table D.1 in Appendix D). It can be seen in the figure that the transition of δ to γ depends on the heating rate. When the heating rate is higher than 2 K min^{-1}, δ transforms into γ, because no other transition other than melting is observed. The observed transition temperature increases with increasing heating rate. For a heating rate lower than 2 K min^{-1}, δ transforms into α instead as two consecutive peaks are observed (see Figure IV.10b). Considering the difficulty in determining the equilibrium temperature between α and γ, it is likely that the observed transition temperatures related to δ are also not the equilibrium temperatures, which are expected to be lower than the observed ones. Nonetheless, it is clear from the data that at 385 K, δ is less stable than α and at 400 K, δ must be less stable than γ. The mean enthalpy of the δ-γ transition at 10 K min^{-1} was found to be $\Delta_{\delta\rightarrow\gamma}H = 17.1(7)$ J g^{-1}. The mean enthalpy of the δ-α transition ($\Delta_{\delta\rightarrow\alpha}H$) is 5.7(5) J g^{-1}.

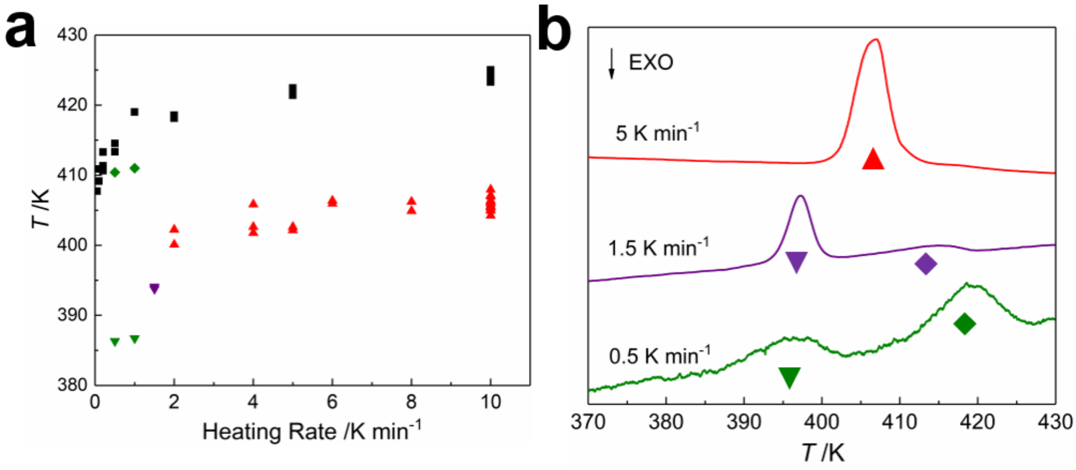

Figure IV.10 (a) Observed transition temperatures for δ to α and δ to γ as a function of the heating rate and (b) DSC curves at different heating rates. (■) α -γ transition(for comparison from Figure IV.3), (▲) δ -γ transition, (▼+◆) combined δ-α and δ -γ transitions, (▼) δ -α transition followed by a separate α -γ transition (◆)

IV.4 Phase relationships between form β and the other polymorphs

Time-resolved PXRD of form β was measured. Some PXRD patterns are presented in Figure IV.11. The data demonstrate that β starts to transform into δ at about 340 K. A typical DSC curve of form β is shown in Figure IV.12. Two endothermic peaks appear before the melting transition of form γ. Based on the transition behavior of β observed in the PXRD measurements, it is inferred that the two observed endothermic peaks are a transition peak of β to δ ($T_{\beta\rightarrow\delta} = 368$ K, $\Delta_{\beta\rightarrow\delta}H = 7.8$ J g^{-1}) followed by the transition of δ to γ, which may pass through α too considering the observations above for δ (observed $T_{\delta\rightarrow\alpha \text{ or } \gamma} = 393$ K, ΔH for this peak is 7.2 J g^{-1} which is much lower than 17.1(7) J g^{-1} obtained in section IV.3 above for δ→γ, but this is probably due to the lack of a well-defined baseline). The enthalpy of the transition of β to α can be obtained by other enthalpies: $\Delta_{\beta\rightarrow\alpha}H = \Delta_{\beta\rightarrow\delta}H + \Delta_{\delta\rightarrow\alpha}H = 7.8 +$

5.7 = 13.5 J g^{-1}. These observations imply that β is possibly stable at very low temperatures, because it turns into the other forms with an endothermic transition. It can be concluded that β is less stable than δ at 340 K.

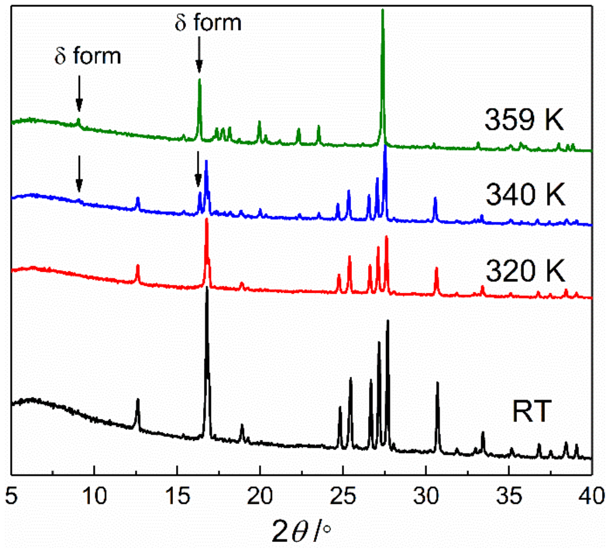

Figure IV.11 Powder x-ray diffraction (PXRD) patterns of form β at different temperatures

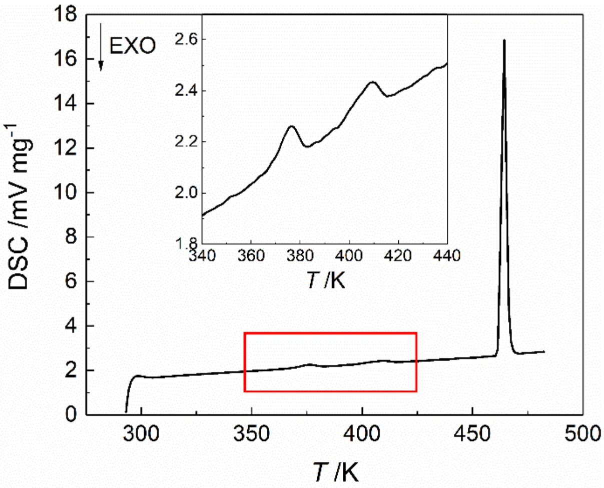

Figure IV.12 DSC curve of form β (heating rate 10 K min^{-1})

IV.5 Conclusion

This chapter gives a clear demonstration of the fact that it can be very hard to obtain equilibrium data for molecular systems. Pyrazinamide demonstrates two important problems: a high sublimation pressure at high temperatures and extremely slow solid-solid phase transformations between almost all solid forms.

The high vapor pressure of pyrazinamide at elevated temperatures affects the melting enthalpy. Only single crystals and fully packed DSC capsules appear to approach the ideal melting enthalpy. Finding the proper transition temperature between two solid phases, if it occurs, at even lower temperatures when decreasing the scanning rate of the DSC is not an easy endeavor.[273, 274] In the present case, only keeping samples in an oven for weeks appears to have provided the temperature of the solid-solid equilibrium between forms α and γ. Whether this approach will deliver any equilibrium temperature in relation to the other solid forms is not clear yet. The vapor pressure data confirmed the equilibrium temperature; the solubility data, however, resulted in an estimate that is 60 K lower. Nonetheless, extrapolation and the uncertainties over the vapor pressure and solubility data give rise to a rather large error margin for the equilibrium temperature. The pressure-temperature phase diagram presented in this thesis only contains information in relation to the phases α and γ, the two most studied phases of pyrazinamide. Transformation behaviors of β and δ have been investigated by PXRD and DSC. Based on the experimental results at about 340 K the stability ranking of the polymorphs is likely to be α > δ > β, while γ is less stable than α, but its relation towards δ and β is not known at this temperature. Above 393 K, the stability ranking is γ > α > δ > β.

Chapter V: Investigation into the intermolecular interactions between pyrazinamide and urea derivatives by nuclear magnetic resonance spectroscopy and electrostatic potential calculations

V.1 Introduction

Control over polymorphism and morphology is important in the pharmaceutical industry to obtain crystals with the desired properties. The pharmaceutical dosage form is a combination of an API together with a number of excipients. One of the functions of the excipients is to stabilize the API such as reducing the degradation rate of the API or stabilizing the chosen polymorph of the API. As the effects of excipients are related to their interactions with the API, understanding these interactions is key to explaining the effects.

In this chapter, we explore the interaction between pyrazinamide and a number of urea derivatives including 1,3-dimethylurea in solution by nuclear magnetic resonance (NMR). The deuterated solvents DMSO, chloroform, and acetone have been selected for the experiments. Pure pyrazinamide, urea derivatives, and mixtures of pyrazinamide and urea derivatives have been analyzed by ^{1}H-NMR at different concentrations and the resulting changes of the chemical shifts have been linked to interactions between pyrazinamide and the urea derivatives and also with the solvents. In addition, the charge distribution and the electrostatic potential (ESP) distributions have been calculated for pyrazinamide, solvents and the urea derivatives. They have been used to interpret the observed interactions in the NMR experiments.

V.2 Solvent selection

For solution NMR, the solvent[275], the sample concentration[276], and the temperature[277] among other factors have an influence on the chemical shift. The solvent effect on the chemical shift is attributed to the solute-solvent interactions.[278] Buckingham et al.[279] classified the solvent effects in four types of interaction: hydrogen bonding, the anisotropy of the solvent molecules, the polar effect and the van der Waals effect. Moreover, the concentration dependence of the chemical shifts can be ascribed to aggregation phenomena and the self-association of the solute molecules.[280, 281] Thus, interactions between solvent and solute molecules and between the solute molecules themselves affect their chemical shift and the change in chemical shift can therefore be used to evaluate intra- and inter- molecular interactions occurring through noncovalent bonding.[282]

A suitable solvent for the investigation of interactions between pyrazinamide and urea derivatives should possess the following characteristics:

1) The hydrogen atoms of the amide group of pyrazinamide are very mobile and their excitation will be lost on exchange with solvent protons. Therefore, the solvent should limit any hydrogen exchange.

2) pyrazinamide and the urea derivatives need to be soluble in the solvent, so that the concentration dependence between pyrazinamide and the urea derivatives can be explored.

Three deuterated solvents have been chosen for this study: DMSO (DMSO-d_6 hereafter), chloroform ($CDCl_3$ hereafter) and acetone (acetone-d_6 hereafter). The results are presented below.

V.3 ^{1}H-NMR measurements of pyrazinamide in solution

V.3.1 In DMSO-d_6

The experimental ^{1}H NMR spectrum of pyrazinamide in DMSO-d_6 has been reported by Cox et al. and Chis et al.[283] Chis et al. measured the ^{1}H-^{1}H COSY NMR spectrum of pyrazinamide in DMSO-d_6 and they published a calculated proton NMR spectrum of pyrazinamide.[283] With the experimental and simulation results, the authors concluded that[283]:

1) The conformation presented in Figure V.1(a) is the only one existing in solution at room temperature.

2) In solution, pyrazinamide molecules tend to form the dimer that also exists in the solid forms α, β, and δ (Figure V.3a).

^{1}H NMR spectra of different concentrations of pyrazinamide in DMSO-d_6 have been obtained and the chemical shifts are provided in Figure V.2 and Table V.1. The chemical shifts do not change within the solubility range and the data is consistent with the result reported in the literature[283]. DMSO-d_6 is a hydrogen bond acceptor, and it has been reported, using NMR measurements, that it interacts with water and alcohols.[284-286] The amide group of pyrazinamide contains both a hydrogen-bond acceptor, the carbonyl oxygen, and a donor, the amine group. In solution, the sp^2 oxygens of DMSO-d_6 and pyrazinamide will compete as a hydrogen-bond acceptor for an amine group of a second pyrazinamide molecule. The most likely hydrogen-bond conformations are presented in Figure V.3. In Table V.1, it can be seen that the concentration dependence of the chemical shifts of pyrazinamide in DMSO-d_6 is insignificant indicating that self-association of the solute is weak. In fact, the enormous quantity of DMSO-d_6 molecules present as solvent reduces the chances to a very high extent that pyrazinamide molecules will interact with each other. Therefore, the interaction shown in Figure V.3c is expected to be by far the major one in solution, contrary to the conclusion in the literature[283].

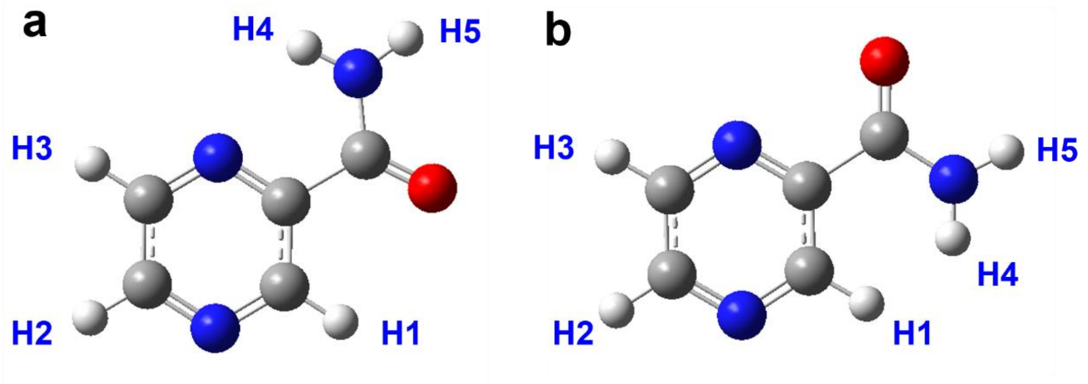

Figure V.1 Molecular structure and hydrogen numbering schemes of the two pyrazinamide conformations

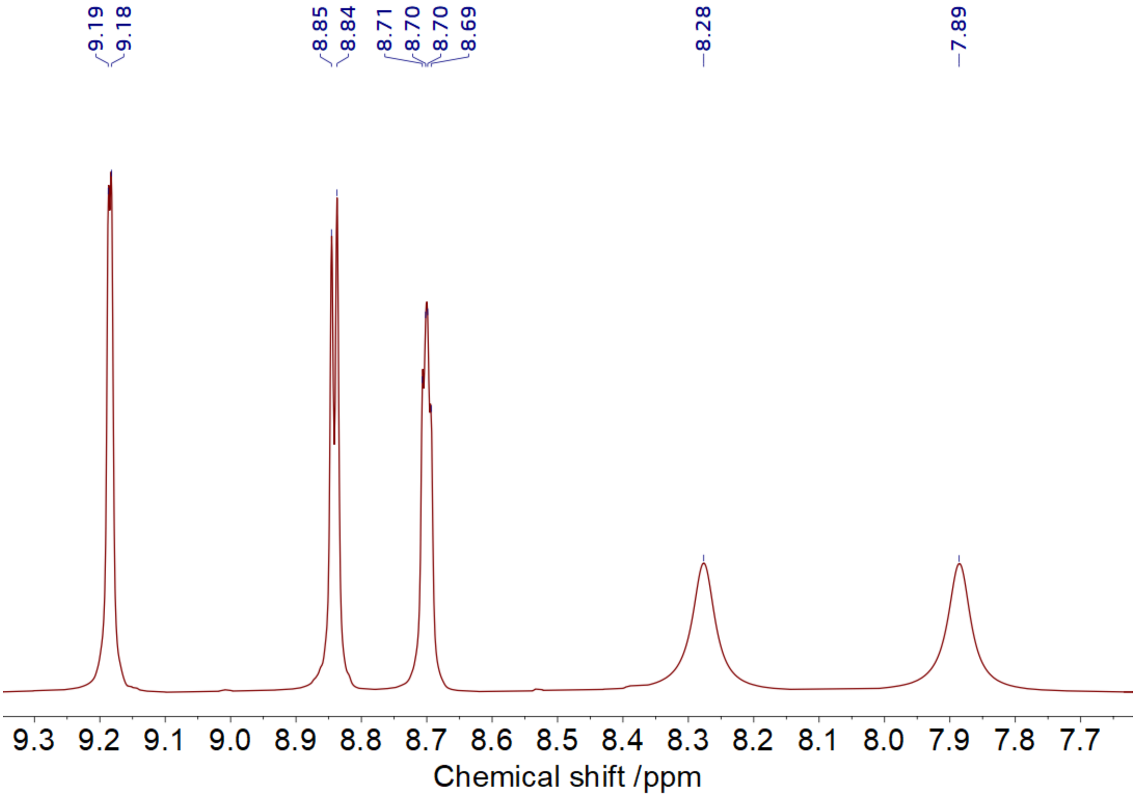

Figure V.2 ^{1}**H NMR spectrum of pyrazinamide in DMSO-d$_6$ (0.677 mol L^{-1})**

Table V.1 Chemical shifts of hydrogen atoms of pyrazinamide in DMSO-d$_6$

Ref.	Concentration		Chemical shift/ ppm				
			H1	H2	H3	H4	H5
[283]	-	-	9.20	8.72	8.85	7.90	8.30
[287]	5	mol%	9.253	8.756	8.896	7.900	8.280
This work	Saturated		9.19,9.18	8.69,8.69,8.69,8.68	8.84,8.83	7.89	8.28
	0.677	mol L^{-1}	9.19,9.18	8.71,8.70,8.70,8.69	8.85,8.84	7.89	8.28
	0.135		9.19,9.18	8.72,8.72,8.71,8.71	8.86,8.85	7.88	8.28
	0.068		9.19,9.18	8.72,8.72,8.72,8.71	8.86,8.85	7.87	8.27
	0.034		9.19,9.18	8.73,8.72,8.72,8.71	8.86,8.85	7.87	8.27

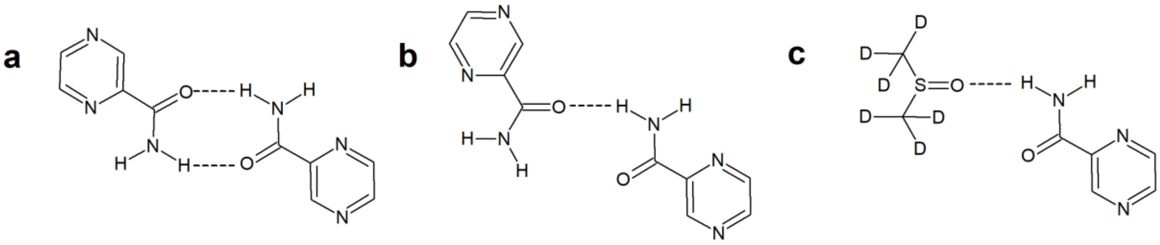

Figure V.3 Schematic representations of (a), (b) pyrazinamide dimers and (c) a DMSO-d$_6$ – pyrazinamide dimer

V.3.2 In $CDCl_3$

The results of the NMR measurements of pyrazinamide in DMSO-d_6 indicate that the solvent-solute interaction overwhelms all other interactions, as no effect of a change in pyrazinamide concentration is observed in the chemical shift. Thus, DMSO does not lend itself as a useful solvent for the study of the interaction between pyrazinamide and the urea derivatives. Therefore $CDCl_3$, another common solvent used in NMR, was chosen for this study.

The chemical shifts of the pyrazinamide protons at different concentration in $CDCl_3$ have been determined and they are shown in Table V.2 and Figure V.4. Compared to the chemical shifts in DMSO-d_6 at a concentration of 0.034 mol L^{-1}, the chemical shifts in $CDCl_3$ at the same concentration exhibit a large difference. This large chemical shift difference between the solvents $CDCl_3$ and DMSO-d_6 has been reported by Raymond et al.[275] The chemical shift of each pyrazinamide proton in $CDCl_3$ needs to be determined for the analysis of the interaction between the pyrazinamide molecules. Next to ^{1}H NMR, ^{1}H–^{1}H COSY and ^{1}H–^{1}H NOESY have been used to determine the chemical shift positions.

The ^{1}H–^{1}H COSY spectrum is shown in Figure V.5. The proton with a chemical shift at about 8.56 ppm shows couplings with the other two protons at about 8.78 ppm and 9.43 ppm, respectively. The intensity of the off-diagonal peaks in the red box shown in Figure V.5 is stronger than that of the peaks in the blue box. Thus, the off-diagonal peaks in the red box should be the coupling between H2 and H3 (atom numbering shown in Figure V.1a), which are only one C-C bond away, and the weaker off-diagonal peaks relate to the coupling between H2 and H1, which are two C-C bonds away. This result was also reported in the literature.[283] Thus, in $CDCl_3$ the chemical shift of H1 is 9.43, the chemical shift of H2 is 8.56 and the chemical shift of H3 is 8.78 (at a concentration of 0.041 mol L^{-1}). These chemical shifts are comparable to those obtained in DMSO-d_6. However, the chemical shifts of H4 and H5 cannot be distinguished by ^{1}H–^{1}H COSY NMR, because they belong to the same nitrogen atom. As shown in Figure V.1a, the spatial distance between H4 and H3 may be within the NOESY NMR experimental range and the same could be stated for H1 and H4 for the conformation in Figure V.1b. However, experimental results only showed off-diagonal peaks between H4 and H5 from the same amide group (Figure V.6), which did not lead to a clear indication of the chemical shift of H4; however, it does confirm that the conformation in Figure V.1.b does not occur in solution, otherwise a clear interaction between H4 and H1 would have been observed.

It is clear that only one chemical shift at around 5-6 ppm changes significantly, which therefore must be a proton that is affected by the pyrazinamide concentration through a possible exchange or interaction with other pyrazinamide molecules. This can only be the free H5 proton in the amide group (Figure V.1a), as mentioned in the literature.[283] Therefore, the chemical shift of H4 must be 7.65 and the chemical shift of H5 is 5.86 at a concentration of 0.041 mol L^{-1}. The large difference in chemical shift of H5 between DMSO-d_6 and $CDCl_3$ can be explained by the interaction between H5 and the oxygen of DMSO-d_6. The interaction will cause a decrease in electron density on the proton, which will cause the atom to change to low field, then increasing its chemical shift. H4 on the other hand must be strongly interacting with the nitrogen on the pyrazine ring (through intramolecular hydrogen bonding), because it is not affected at all by concentration changes in pyrazinamide.

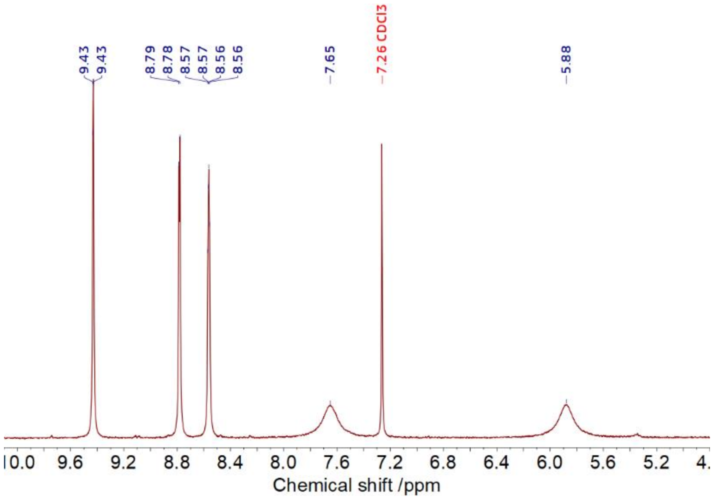

Figure V.4 ^{1}H NMR spectrum of pyrazinamide in $CDCl_3$ (0.041 mol L^{-1})

Table V.2 Chemical shifts of pyrazinamide hydrogen atoms in $CDCl_3$ at different concentrations

Concentration /mol L^{-1}	Chemical shift /ppm				
	H1	H2	H3	H4	H5
saturated	9.42,9.42	8.57,8.56,8.56,8.55	8.78,8.77	7.65	5.93
0.041	9.43,9.43	8.57,8.57,8.56, 8.56	8.79,8.78	7.65	5.88
0.034	9.43,9.42	8.57,8.56,8.56,8.55	8.78,8.78	7.65	5.86
0.027	9.43,9.42	8.57,8.56,8.56,8.56	8.79,8.78	7.64	5.78
0.014	9.43,9.42	8.57,8.56,8.56,8.56	8.79,8.78	7.64	5.70

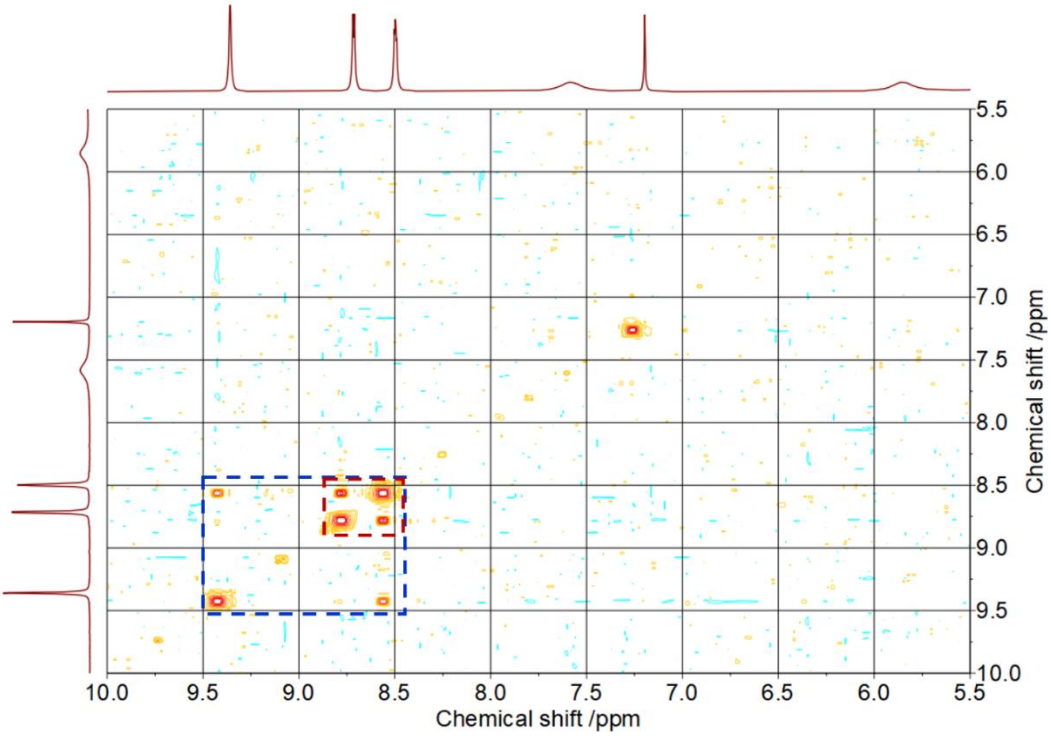

Figure V.5 ^{1}H–^{1}H COSY NMR spectrum of pyrazinamide in CDCl$_3$ (0.041 mol L^{-1})

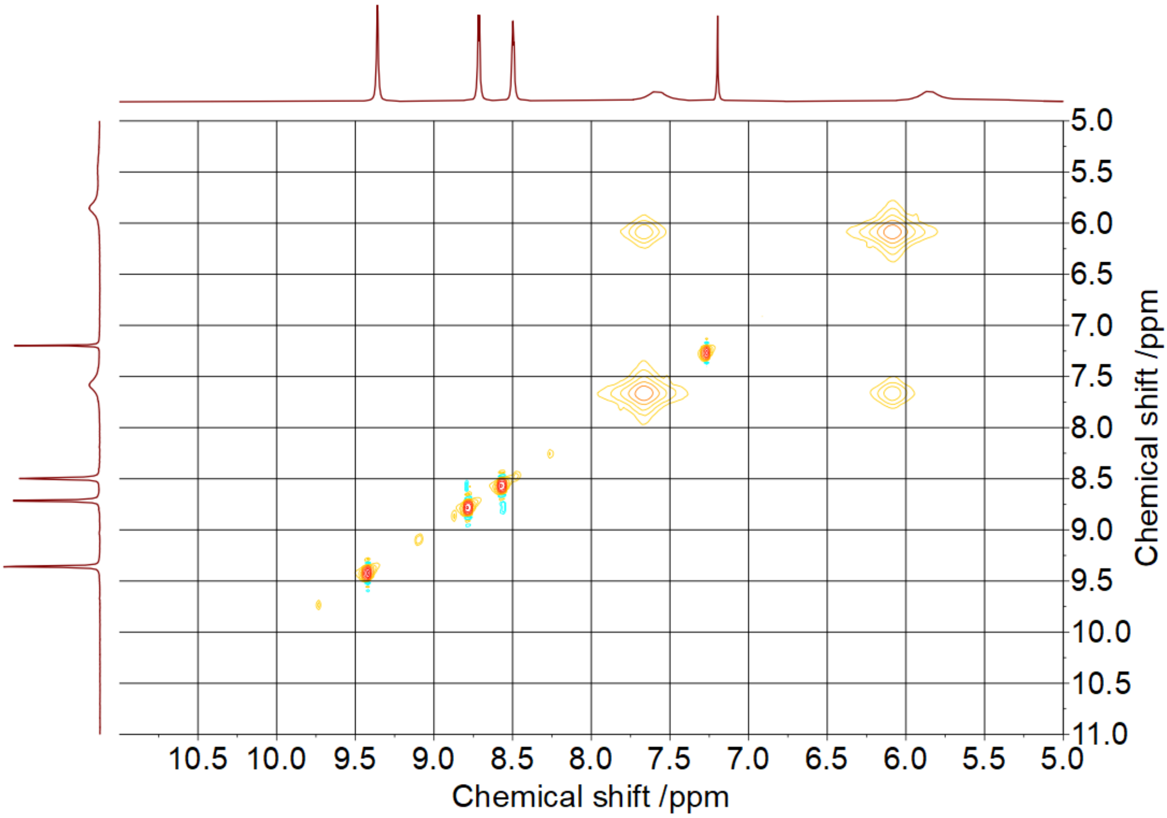

Figure V.6 ^{1}H–^{1}H NOESY NMR spectrum of pyrazinamide in CDCl$_3$ (0.041 mol L^{-1})

V.3.3 In acetone-d_6

An ^{1}H NMR spectrum of pyrazinamide in acetone-d_6 is provided in Figure V.7 and the chemical shifts are listed in Table V.3. The values for H1 to H4 in acetone-d_6 are very close to those in DMSO-d_6. It can be inferred that the interactions between of pyrazinamide and solvent molecules in DMSO-d_6 and in acetone-d_6 are very similar. The only difference is that the sulfur atom in DMSO-d_6 is substituted by a carbon atom in acetone. The large difference in chemical shift for H5 is most likely due to the interactions between pyrazinamide and acetone molecules as acetone, like DMSO, possesses an oxygen atom which can interact with H5 (Figure V.8). The charge distribution over the atoms of DMSO and acetone is presented in Figure V.9. It demonstrates that the oxygen of DMSO has more negative charge causing a stronger deshielding effect than acetone under the same conditions. A stronger deshielding effect gives rise to a larger chemical shift of H5 in DMSO. Thus, the interactions between pyrazinamide and DMSO appear to be stronger than the interactions between pyrazinamide and acetone.

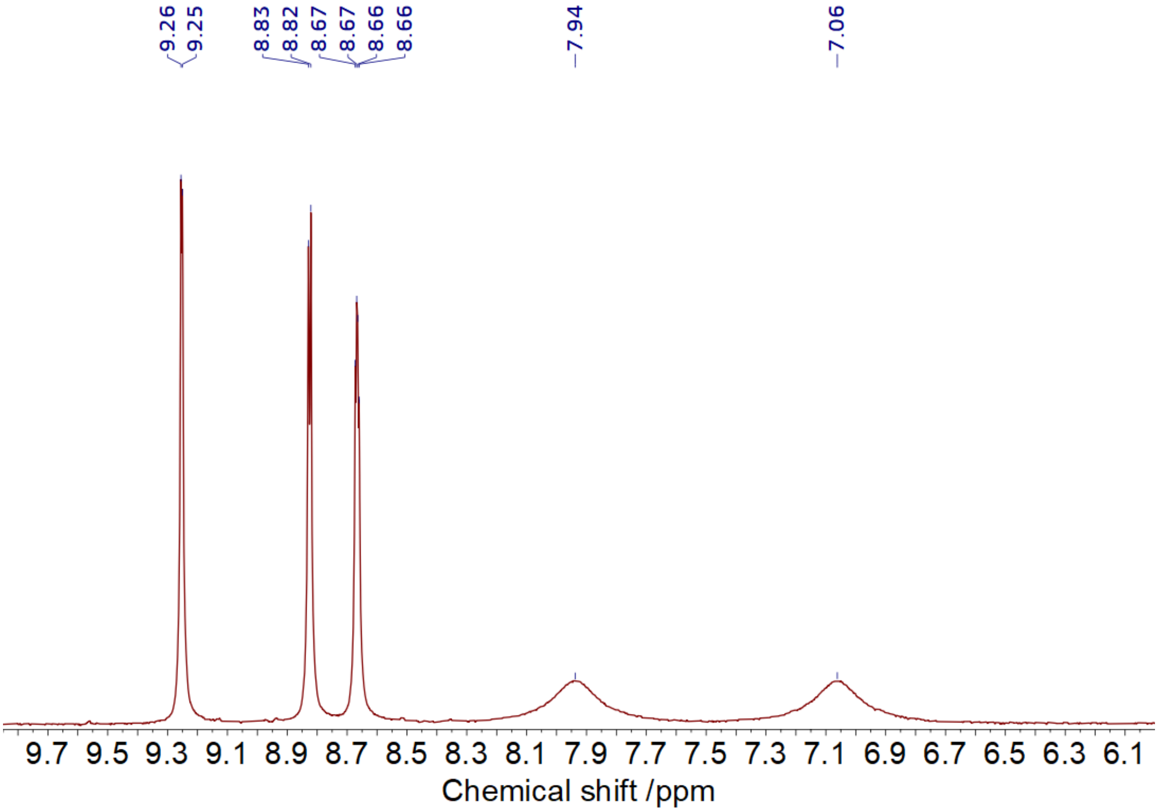

Figure V.7 ^{1}H NMR spectrum of pyrazinamide in acetone-d_6 (0.067 mol L^{-1})

Table V.3 Chemical shift of pyrazinamide hydrogen atoms in acetone-d_6

Concentration /mol L^{-1}	Chemical shift /ppm				
	H1	H2	H3	H4	H5
0.067	9.26,9.25	8.67,8.67,8.66,8.66	8.83,8.82	7.94	7.06
0.009	9.25,9.25	8.67,8.67,8.66,8.66	8.83,8.82	7.94	7.03

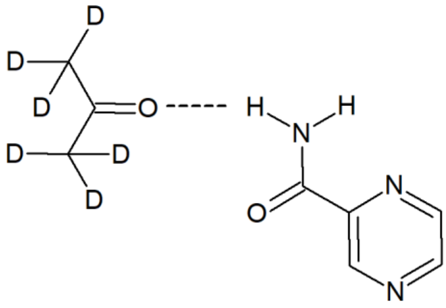

Figure V.8 Schematic representation of a pyrazinamide-acetone dimer in acetone-d_6 solution

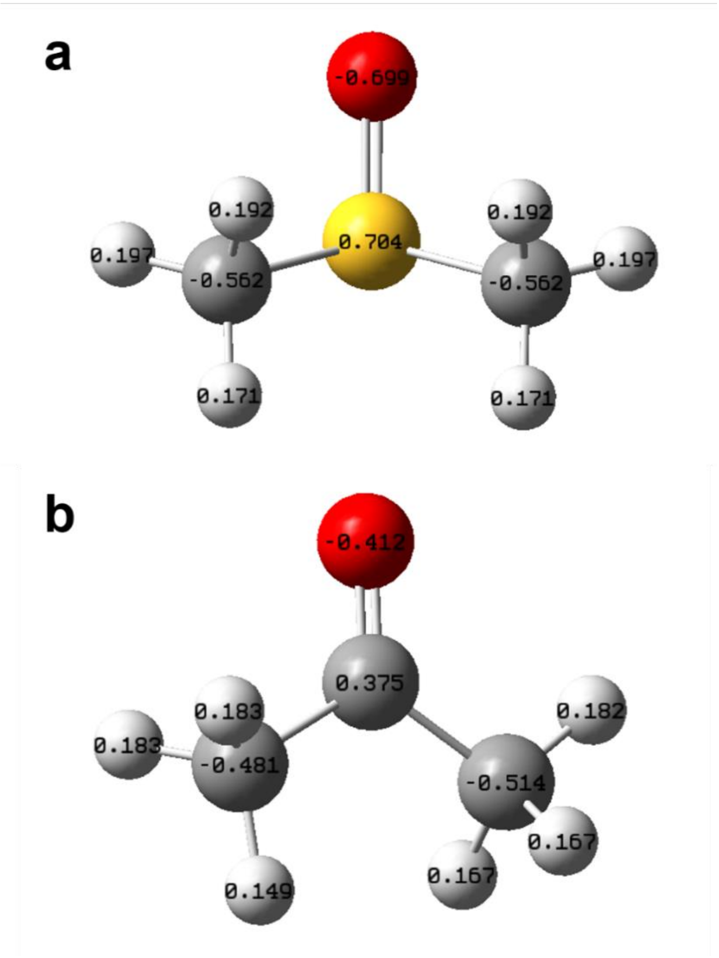

Figure V.9 Atomic charge distribution of (a) DMSO and (b) acetone

V.4 ^{1}H-NMR of urea derivatives in different concentrations

Different concentrations of tetramethylurea, acetamide, and 1,3-dimethylurea in $CDCl_3$, 1,3-dimethylurea in DMSO-d_6 and urea in acetone (due to its low solubility in $CDCl_3$) have been investigated to analyze the interactions between pyrazinamide and the respective urea derivatives.

V.4.1 Tetramethylurea in $CDCl_3$

The NMR results of tetramethylurea are presented in Figure V.10 and Table V.4. The difference of tetramethylurea compared to the other urea derivatives studied in this work is that all of hydrogen atoms in the amide groups are replaced by methyl groups, thus, only one peak belonging to the methyl groups can be observed in the NMR spectrogram at about 2.80 ppm. It can be used for comparison with the protons in the methyl groups of the other urea derivatives. For about a tenfold increase in concentration, the chemical shift can be seen to decrease with 0.04 ppm.

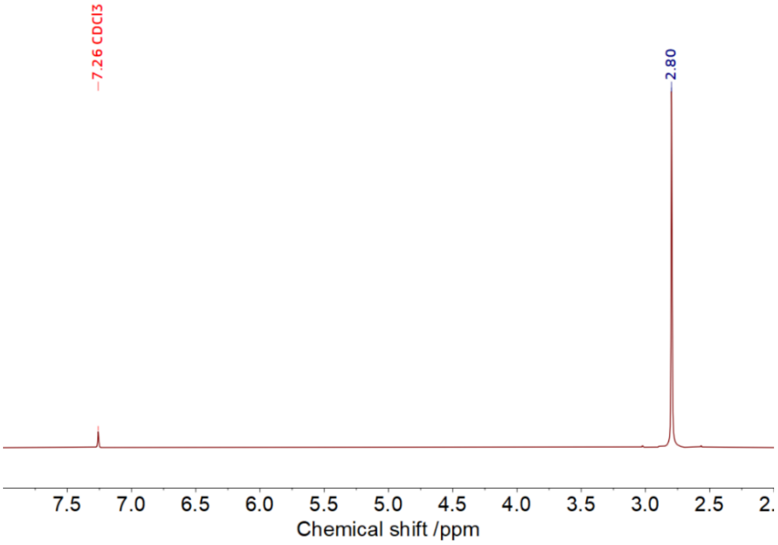

Figure V.10 ^{1}H NMR spectrum of tetramethylurea in $CDCl_3$ (0.041 mol L^{-1})

Table V.4 Chemical shift of tetramethyl urea in $CDCl_3$

Concentration /mol L^{-1}	Chemical shift /ppm
	CH_3
0.325	2.76
0.041	2.80

V.4.2 Acetamide in $CDCl_3$

^{1}H NMR data on acetamide at different concentrations in $CDCl_3$ were measured. The ^{1}H NMR spectrum is presented in Figure V.11 and the chemical shifts are listed in Table V.5. It appears that the chemical shift of the NH2 group of acetamide increases with increasing concentration at low concentration. Moreover, a single wide peak corresponding to these protons is observed while it splits into two peaks at high concentration. It indicates that acetamide molecules self-associate with increasing concentration. As reported in the literature, it is likely that acetamide is mainly forming dimers through two symmetrical hydrogen bonds between the amide groups as shown in Figure V.12.[288] The chemical shift of the methyl group is smaller than for tetramethylurea, which is probably due to the fact that the methyl group of acetamide is not directly bound to a nitrogen atom, but to the carbon of the carbonyl.

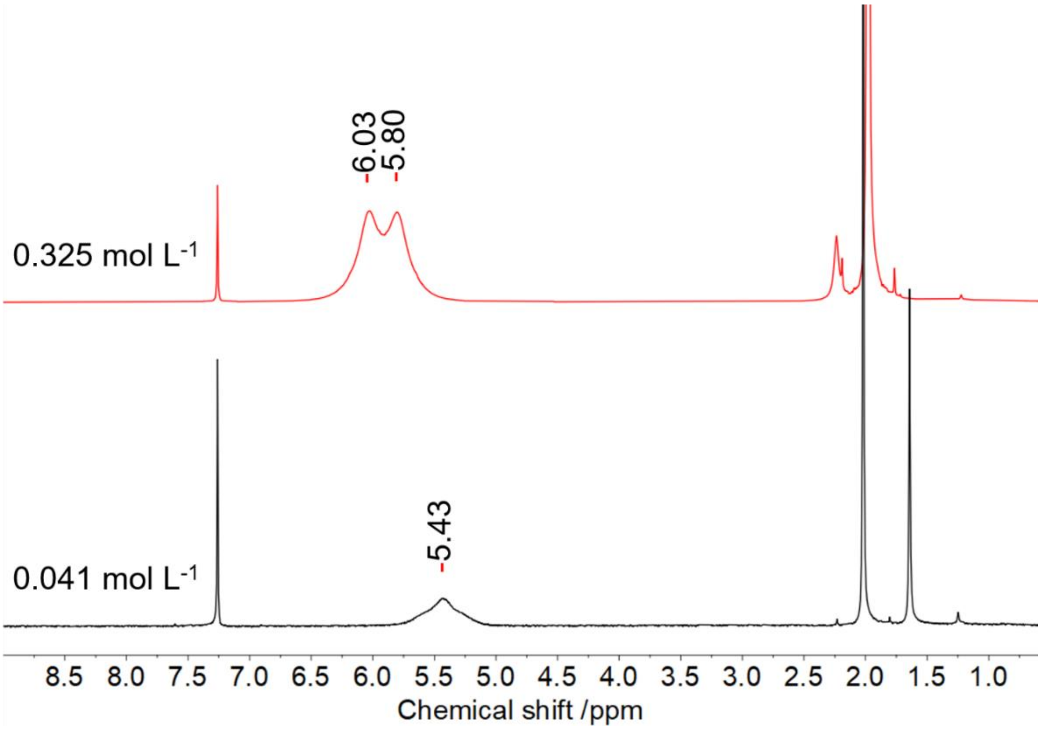

Figure V.11 ^{1}H NMR spectrum of acetamide in $CDCl_3$

Table V.5 Chemical shift of acetamide hydrogen atoms in $CDCl_3$

Concentration /mol L^{-1}	Chemical shift /ppm	
	CH_3	NH_2
0.325	1.98	5.80,6.03
0.041	2.02	5.43
0.006	2.02	5.31

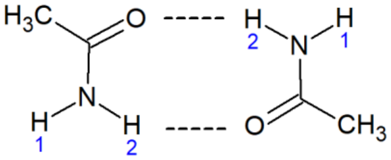

Figure V.12 Schematic representation of an acetamide dimer in $CDCl_3$ solution

V.4.3 1,3-Dimethylurea in $CDCl_3$ and in DMSO-d_6

1,3-Dimethylurea in $CDCl_3$ has been studied by ^1H NMR and the results are presented in Figure V.13 and Table V.6. The chemical shift of the methyl group of 1,3-dimethylurea is really close to that of tetramethylurea. A significant concentration dependence of the chemical shift of the N-H protons of 1,3-dimethylurea in $CDCl_3$ is observed, which has been reported previously by Karl et al.[289] In the literature, the chemical shift at high concentration is reported to be 5.75 ppm.[289] 1,3-Dimethylurea samples in DMSO-d_6 have been studied with two different concentrations. The ^1H NMR spectrum is shown in Figure V.14 and the chemical shifts are listed in Table V.7. The chemical shifts of 1,3-dimethylurea do not change significantly with concentration. The chemical shift of the NH proton in DMSO-d_6 is found to be 5.74 ppm. In the literature, if 1,3-dimethylurea is dissolved in solvents that act as good hydrogen-bond acceptors such as DMF and DMSO, the chemical shift was reported to be rather close at a value of about 5.8 ppm.[289] This result indicates that the interactions between the 1,3-dimethylurea molecules themselves and between 1,3-dimethylurea and hydrogen-bond accepting solvent molecules are basically the same. They are related to the N-H proton of 1,3-dimethylurea and the sp^2 oxygen on 1,3-dimethylurea, DMF, or DMSO. The atomic charge distribution of 1,3-dimethylurea is shown in Figure V.15. The negative charge on the oxygen of 1,3-dimethylurea is less than that of DMSO and it is the same for other urea derivatives (shown in Figure E.1 in appendix E) Thus, it can be expected that DMSO will strongly compete with 1,3-dimethylurea in interacting with pyrazinamide molecules. It will likely drown out any effect of intermolecular interaction between the two solute molecules.

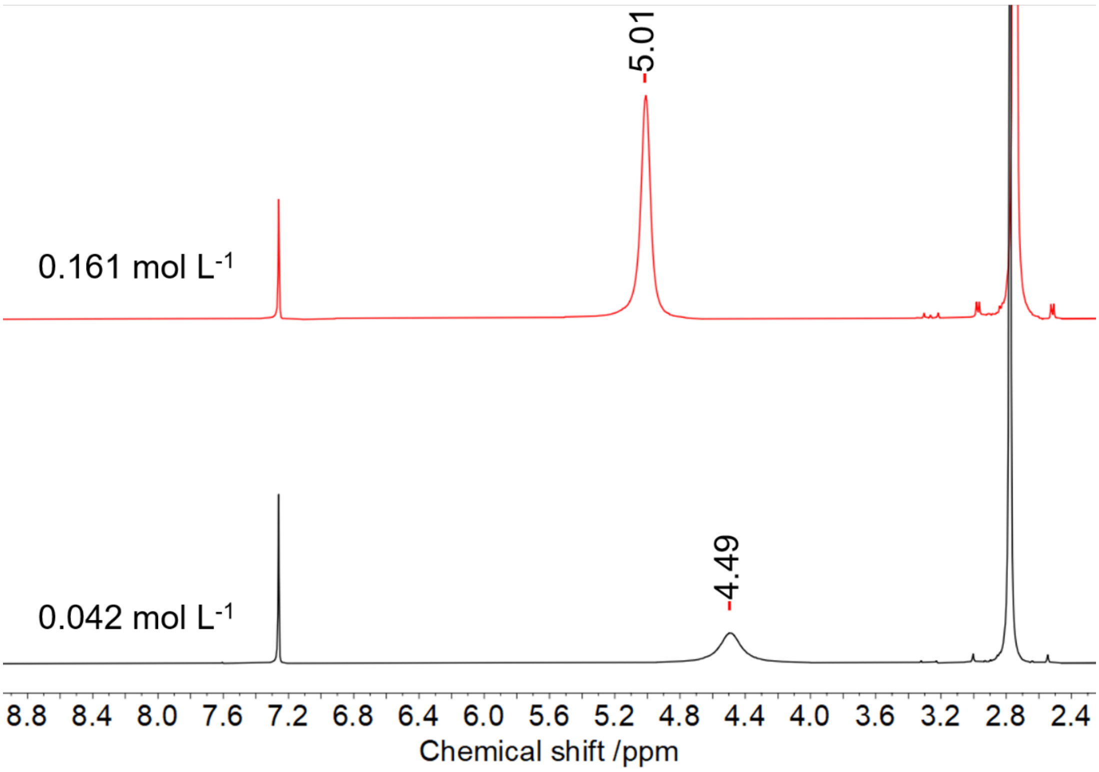

Figure V.13 ^{1}H NMR spectrum of 1,3-dimethylurea in $CDCl_3$

Table V.6 Chemical shift of 1,3-dimethylurea hydrogen atoms in $CDCl_3$

Concentration /mol L^{-1}	Chemical shift /ppm	
	CH_3	NH
0.330	2.73, 2.72	5.36
0.161	2.76,2.74	5.01
0.081	2.78,2.77	4.70
0.081	2.77,2.76	4.73
0.081	2.77,2.76	4.73
0.042	2.79	4.42
0.042	2.78	4.49
0.042	2.78	4.49
0.021	2.79	4.26
0.021	2.79	4.28
0.021	2.79	4.29

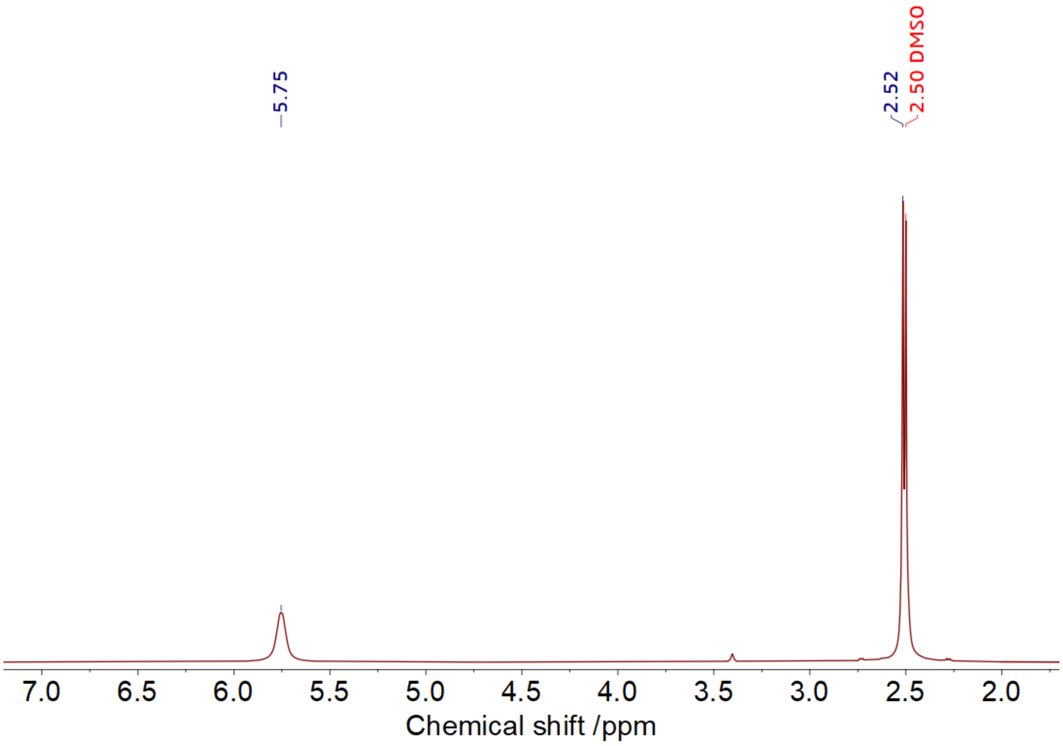

Figure V.14 ^{1}H NMR spectrum of 1,3-dimethylurea in DMSO-d$_6$

Table V.7 Chemical shift of 1,3-dimethylurea hydrogen atoms in DMSO-d$_6$

Concentration /mol L^{-1}	Chemical shift /ppm	
	CH$_3$	NH
1.084	2.52	5.75
0.135	2.52	5.73

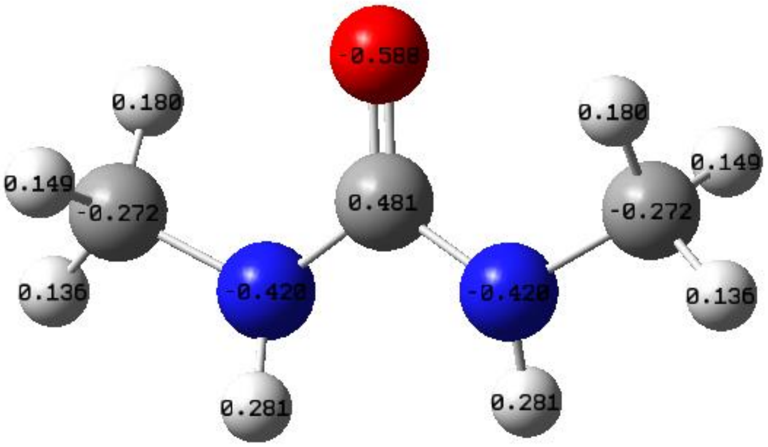

Figure V.15 Atomic charge distribution for 1,3-dimethylurea

V.4.4 Urea in acetone-d$_6$

Urea is not soluble in chloroform; therefore, acetone was used for the NMR studies of urea. Two different concentrations of urea were studied and the results are presented in Table V.8. As is shown in Table V.8, the chemical shift of the protons of the amine group displays a small difference for the two concentrations: a threefold increase in concentration changes the chemical shift of +0.05 ppm, which can indicate an increase in deshielding due to increased interaction. Nevertheless, due to the low solubility of urea in acetone-d$_6$, the interactions between urea and acetone and between urea molecules themselves are difficult to study. In addition, similar behavior with the oxygen of acetone as observed for DMSO will play a role in the limited change of the chemical shift with concentration.

Table V.8 Chemical shift of urea hydrogen atoms in acetone-d$_6$

Concentration /mol L^{-1}	Chemical shift /ppm
	NH$_2$
0.036	5.19
0.013	5.14

V.5 ^{1}H-NMR of pyrazinamide and urea derivatives mixtures

V.5.1 Pyrazinamide and tetramethylurea in CDCl$_3$

The chemical shifts of pyrazinamide in mixtures with tetramethylurea are presented in Table V.9. The chemical shift of H5 increases with the concentration of tetramethylurea, while the chemical shifts of the other hydrogens do not change. Thus, in the presence of tetramethylurea in solution, H5 of pyrazinamide interacts with the oxygen of the carbonyl group of tetramethylurea like in acetone and DMSO.

Table V.9 NMR results of pyrazinamide mixture with tetramethylurea in $CDCl_3$ (concentration of pyrazinamide is 0.041 mol L^{-1})

P:T (mol:mol)	Chemical shift /ppm					
	Pyrazinamide (P)					Tetramethylurea (T)
	H1	H2	H3	H4	**H5**	CH_3
1:8	9.38,9.37	8.53,8.52,8.52	8.73,8.74	7.64	6.14	2.76
1:1	9.42	8.56,8.56,8.55	8.78,8.78	7.65	5.95	2.79
1:0	9.43,9.43	8.57,8.57,8.56, 8.56	8.79,8.78	7.65	5.88	-
0:1	-	-	-	-	-	2.80

V.5.2 Pyrazinamide and acetamide in $CDCl_3$

The chemical shifts of pyrazinamide mixtures with acetamide are presented in Table V.10. In the presence of acetamide, the chemical shift of H5 increases with the increase in acetamide concentration. The chemical shift of NH_2 of acetamide increases with the increase of the concentration of pyrazinamide as well.

Table V.10 NMR results of mixtures of pyrazinamide and acetamide in $CDCl_3$

P:A (mol:mol)	Chemical shift /ppm						
	Pyrazinamide (P)					Acetamide (A)	
	H1	H2	H3	H4	**H5**	**NH_2**	CH_3
concentration of pyrazinamide constant at 0.041 mol L^{-1}							
1:8	9.36,9.37	8.55, 8.54, 8.54, 8.54	8.75, 8.74	7.65	6.75	5.82,6.09	1.98
1:1	9.42,9.41	8.57, 8.56, 8.56, 8.55	8.78, 8.77	7.65	6.04	5.54	2.02
1:0	9.43,9.43	8.57, 8.57, 8.56, 8.56	8.79,8.78	7.65	5.88	-	-
concentration of acetamide constant at 0.006 mol L^{-1}							
7:1	9.42, 9.42	8.57, 8.56, 8.56, 8.55	8.78, 8.77	7.64	5.92	5.57	2.03
1:1	9.43, 9.42	8.57, 8.56, 8.56, 8.55	8.78, 8.78	7.61	5.68	5.44	2.03
0:1	-	-	-	-	-	5.31	2.02

V.5.3 Pyrazinamide and 1,3-dimethylurea in $CDCl_3$

Mixtures of pyrazinamide and 1,3-dimethylurea in $CDCl_3$ have been investigated by ^1H NMR. The results are shown in Table V.11. The changes are comparable to the changes in the mixture of pyrazinamide and acetamide. The chemical shift of H5 of pyrazinamide increases with the increase in concentration of 1,3-dimethylurea and the chemical shift of the NH groups of 1,3-dimethylurea increases with the increase of the concentration of pyrazinamide.

Table V.11 NMR results of mixture of pyrazinamide-1,3-dimethylurea in $CDCl_3$

P:D	Chemical shift /ppm						
	Pyrazinamide (P)					1,3-Dimethylurea (D)	
	H1	H2	H3	H4	**H5**	**NH**	CH_3
	concentration of pyrazinamide constant at 0.041 mol L^{-1}						
1:8	9.38,9.37	8.55,8.55,8.54	8.76,8.75	7.67	6.41	5.35	2.73,2.72
1:4	9.40,9.39	8.56,8.56,8.55,8.55	8.77,8.76	7.66	6.25	5.00	2.76,2.74
1:2	9.41,9.41	8.57,8.56,8.56,8.55	8.78,8.77	7.66	6.15	4.74	2.77,2.76
1:2	9.41,9.40	8.56,8.56	8.77,8.76	7.66	6.15	4.74	2.76
1:2	9.41,9.40	8.56,8.56,8.55	8.77,8.76	7.66	6.15	4.75	2.76
1:1	9.43,9.42	8.56,8.56,8.55	8.78,8.77	7.66	6.05	4.55	2.78
1:1	9.42,9.41	8.56,8.56,8.56,8.55	8.78,8.77	7.65	6.04	4.49	2.78
1:1	9.42,9.41	8.56,8.56,8.56,8.55	8.78,8.77	7.65	6.04	4.49	2.78
1:0.5	9.43,9.42	8.57,8.56,8.55	8.78,8.77	7.65	5.93	4.36	2.79
1:0.5	9.42,9.42	8.57,8356,8.56,8.55	8.78,8.77	7.65	5.98	4.39	2.78
1:0	9.43,9.43	8.57, 8.57, 8.56, 8.56	8.79,8.78	7.65	5.88	-	-
	concentration of 1,3-dimethylurea constant at 0.008 mol L^{-1}						
5:1	9.42,9.42	8.56, 8.56, 8.56, 8.55	8.78,8.77	7.65	5.92	4.34	2.79
1:1	9.43,9.42	8.57, 8.56, 8.55	8.78,8.78	7.63	5.72	4.26	2.79
0:1	-	-	-	-	-	4.24	2.79

V.5.4 Pyrazinamide and urea in acetone-d_6

^1H NMR spectra have been measured for pyrazinamide-urea mixtures in acetone-d_6 at different compositions. The results are shown in Table V.12. Because the oxygen of acetone interferes, there is no large change of the chemical shift neither in pyrazinamide nor in urea, but a small change can anyway be observed for H5 suggesting a likely interaction between pyrazinamide and urea.

Table V.12 NMR results of pyrazinamide-urea in acetone-d_6 (concentration of pyrazinamide is 0.009 mol L^{-1}(1:1))

P: U (mol:mol)	Chemical shift /ppm					
	Pyrazinamide (P)					Urea (U)
	H1	H2	H3	H4	H5	NH_2
1:4	9.25,9.25	8.67,8.67,8.66,8.66	8.83,8.82	7.92	7.17	5.19
6:1	9.25,9.25	8.67,8.67,8.66,8.66	8.83,8.82	7.94	7.09	5.16
1:1	9.25,9.25	8.67,8.67,8.66,8.66	8.83,8.82	7.94	7.07	5.12
1:0	9.25,9.25	8.67,8.67,8.66,8.66	8.83,8.82	7.94	7.03	-

V.6 Interaction between pyrazinamide and urea derivatives

The results presented above demonstrate that urea-type molecules interact in solution with the H5 proton of pyrazinamide and that pyrazinamide interacts with the protons on the nitrogen atoms in the urea derivatives. In order to analyze these interactions further, the molecular electrostatic potentials (ESP) have been calculated. The molecules with a color-coded electrostatic potential are presented in Figure V.16, while the ESPs of other urea derivatives including *N*-methylurea, 1,1-dimethylurea, 1,1-diethylurea, 1,3-diethylurea and trimethylurea are presented in Figure E.2 of Appendix E. The calculated ESP of pyrazinamide presented in Figure V.16 demonstrates that the highest electron density is found around the oxygen of the amide group; the same can be seen for the carbonyl oxygens of the urea derivatives. Locations with high electron density are attracted to regions with low electron density. The lowest electron density in pyrazinamide can be found at the hydrogens of the amide group. The same is true for the amine moieties in acetamide, urea, and 1,3-dimethylurea, whereas in tetramethylurea, the methyl groups are lowest in electron density, although not as low as the aforementioned amine groups. The carbonyl oxygen of tetramethylurea, like the other urea derivatives, interacts with H5 of pyrazinamide, and this could be verified by the NMR result. The interactions between pyrazinamide-acetamide and pyrazinamide-urea may involve dimers with a double hydrogen bond, because of the proximity of high and low electron density in either molecule. For 1,3-dimethylurea, the amine group of pyrazinamide with the lowest electron density region will most likely interact with the carbonyl oxygen of 1,3-dimethylurea as is consistent with the NMR result. Just as the carbonyl oxygen of pyrazinamide interacts with the NH of 1,3-dimethylurea.

The chemical shift of H5 in the presence of different concentrations of acetamide, 1,3-dimethylurea and tetramethylurea is plotted in Figure V.17. The result indicates that acetamide has the strongest effect on the chemical shift of H5, while tetramethylurea shows the weakest effect. The main interactions in these mixtures are similar, the urea derivatives compete with other pyrazinamide molecules to form pyrazinamide-additive complexes. So, the change in chemical shift of H5 can be considered as a reflection of the strength of the interaction between pyrazinamide and the additive. The stronger the interaction the larger the change in the chemical shift of H5. Therefore, the order of the interaction strength is pyrazinamide-acetamide > pyrazinamide-1,3-dimethylurea > pyrazinamide-tetramethylurea. This order is also clearly repeated by the protons on the nitrogen of the urea derivatives with in particular acetamide showing a clear effect on the chemical shift of its amine protons, whereas the effect on 1,3-dimethylurea is already much weaker. The strong shift of H5 in the presence of acetamide may therefore point in the direction of the formation of double bounded dimers that form on the fly due to the flexibility of acetamide and the proximity of the necessary hydrogen bond donors and acceptors. The main pyrazinamide-urea derivative dimers that may exist in the solution are presented in Figure V.18.

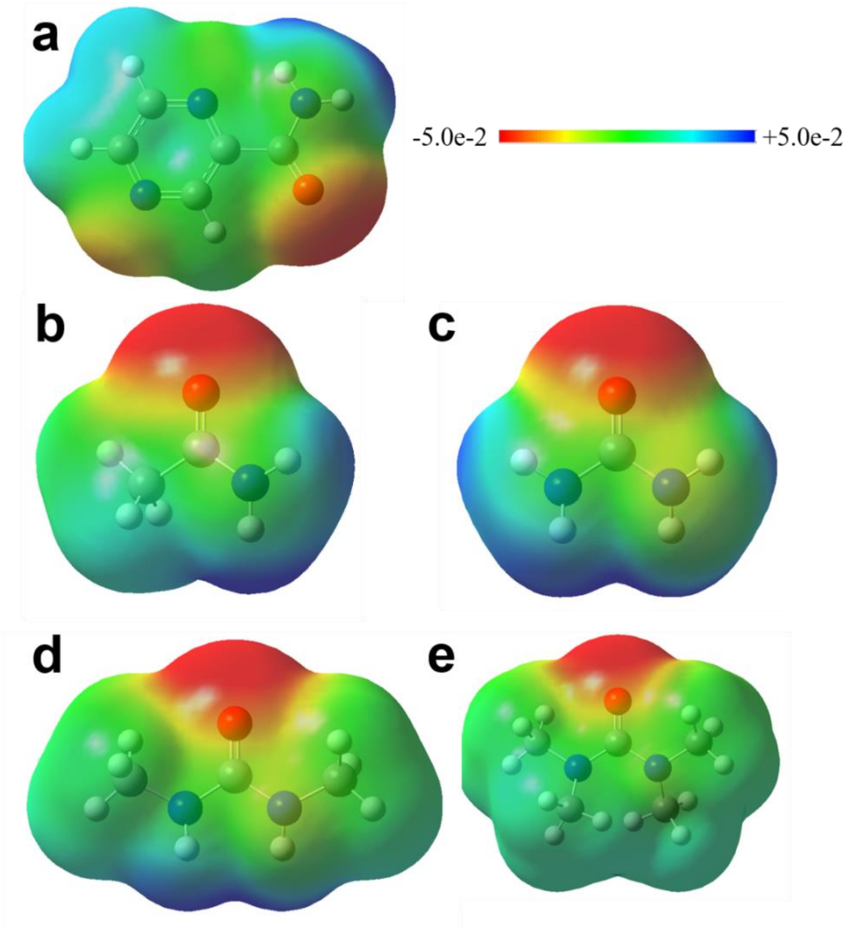

Figure V.16 Electrostatic potential distribution maps of (a) pyrazinamide, (b) acetamide, (c) urea, (d) 1,3-dimethylurea, and (e) tetramethylurea

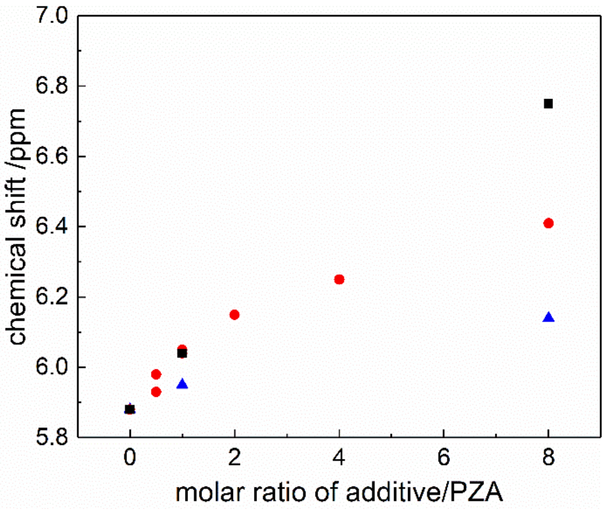

Figure V.17 The chemical shift of H5 of pyrazinamide in $CDCl_3$ solvent with urea derivatives (■) acetamide, (●) 1,3-dimethylurea, (▲) tetramethylurea

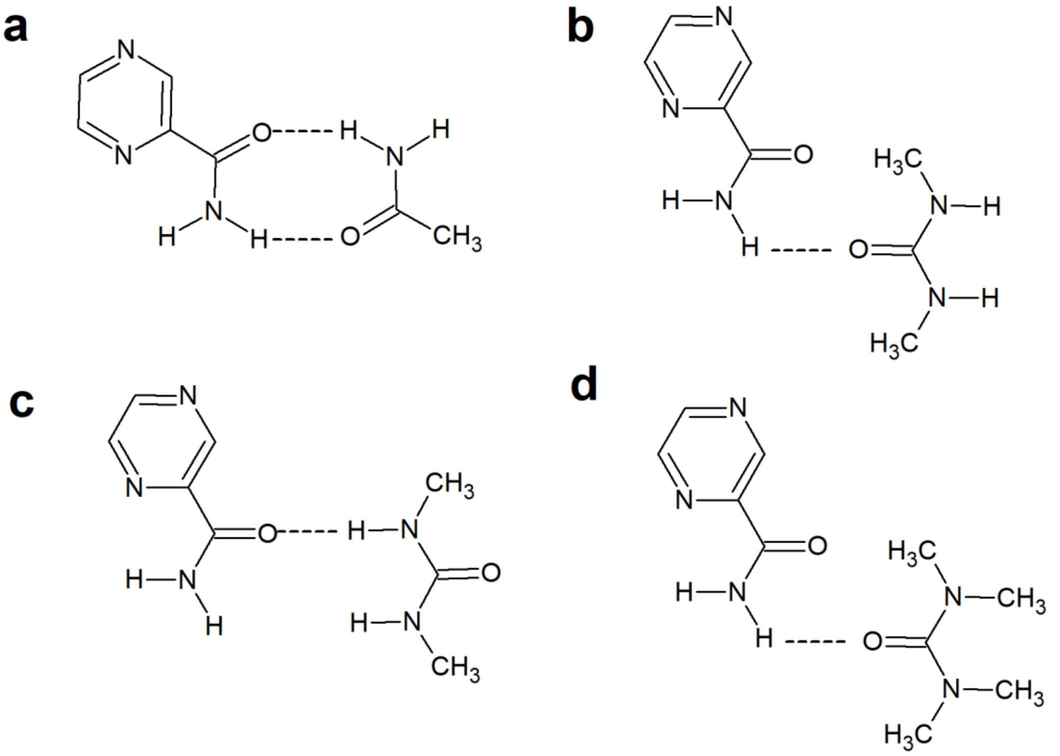

Figure V.18 The main pyrazinamide-urea derivative dimers that may exist in the solution (a) acetamide, (b) and (c) 1,3-dimethylurea, (d) tetramethylurea

V.8 Conclusion

The interactions between pyrazinamide and a number of urea derivatives have been investigated with the support of NMR, charge distributions and ESP maps. The results from ^1H-^1H COSY and ^1H NMR at different pyrazinamide concentrations confirmed the positions of the ^1H chemical shifts for pyrazinamide in $CDCl_3$. Two off-diagonal peaks in the COSY spectrum reflect the couplings between the three protons on the pyrazine ring. Only one proton changes with the concentration, which must be H5 on the pyrazinamide molecule and which indicates that only H5 is prone to exchange. Chemical shifts listed for H1 to H5 are 9.43, 8.57-8.56, 8.79-8.78, 7.65 and 5.86 respectively at a concentration of 0.041 mol L^{-1}. The chemical shift of H5, the free proton in the amide group, changes to low field when urea derivatives are added to the solution. Combining NMR results with the ESP maps, it is clear that the amide protons with the lowest electron density on pyrazinamide interact with the carbonyl oxygen with the highest electron density on the urea derivatives. This conclusion can also be confirmed by the experimental result obtained in DMSO-d_6 and acetone-d_6. The corresponding chemical shifts of all protons of pyrazinamide in DMSO-d_6 and acetone-d_6 showed no concentration dependence within the experimental concentration range. This indicates that the interactions between pyrazinamide and these solvent molecules are ubiquitous. Both solvents have electronegative double bonded oxygens and are similar in structure to tetramethylurea. The H5 proton of pyrazinamide interacts with the oxygen of DMSO-d_6 or acetone-d_6 and its chemical shift is much higher than in $CDCl_3$.

Moreover, the chemical shifts of the nitrogen protons of acetamide and 1,3-dimethylurea increase with the addition of pyrazinamide. It indicates that those protons interact with the carbonyl group of pyrazinamide as well, in particular acetamide interacts strongly. Based on the changes in chemical shift of pyrazinamide in the presence of the different urea derivatives in $CDCl_3$, the order of the interaction strengths is: pyrazinamide-acetamide > pyrazinamide-1,3-dimethylurea > pyrazinamide-tetramethylurea. The result of urea is less clear, because it could not be studied in the same solvent.

The work in this chapter clearly demonstrates the interactions between pyrazinamide and the urea derivatives in solution and also with the solvent molecules themselves. This result can be used to interpret the crystallization behavior of pyrazinamide in the next chapters.

Chapter VI: The effect of urea derivatives on the crystallization of pyrazinamide from the vapor phase

VI.1 Introduction

Smets et al.[3] studied the effect of 1,3-dimethylurea on spray-dried pyrazinamide samples in more detail and high-energy ball milling of form γ crystals obtained by sublimation. They think that 1,3-dimethylurea may reduce the vapor pressure of pyrazinamide and then reduce the transition rate, thus, it could stabilize the surface of form γ. Alternatively, DMU could prevent nucleation of low temperature forms of PZA. This chapter focuses on the interactions between pyrazinamide and several urea derivatives which are used as additives in the vapor phase. Because investigating molecular interactions in the vapor phase is difficult, they are inferred by analyzing the macroscopic experimental results, while keeping in mind the results obtained in the previous chapter on interactions in solution studied by NMR. Two aspects of the effects of the urea derivatives on the crystallization of the γ form of pyrazinamide are looked at in particular. The first aspect involves the influence of the urea derivatives on the nucleation rate of the γ form by determining the 'induction time' (defined here as the time interval between the start of the sublimation experiment and the first observation of γ form crystals) in the presence of a urea derivative (a total of 9 molecules were considered, see below). The second aspect involves the effect of urea derivatives on the morphology of γ form crystals. The crystal morphologies of more than five hundred crystals have been studied by careful inspection. They were prepared with and without urea derivatives. The nine urea derivatives used as additives were acetamide, urea, *N*-methylurea, 1,1-dimethylurea, 1,3-dimethylurea, trimethylurea, 1,1-diethylurea, 1,3-diethylurea and tetramethylurea. Disorder and twinning are frequently observed phenomena in the γ form.[129, 134] The nature of the disorder will be discussed in this chapter. Twinned crystals are often observed in sublimation experiments. The relationship between disorder and twinning will be discussed at the end of the chapter.

VI.2 Characterization of the urea derivatives

VI.2.1 Powder X-ray diffraction

Except tetramethylurea, which is liquid at room temperature, all the other urea derivatives have been characterized by PXRD. The PXRD patterns are presented in Figure VI.1. Using the PXRD patterns in the CCDC, the crystal structures of the urea derivatives have been identified, except for 1,3-diethylurea, which was identified through a publication.[224] The information is presented in Table VI.1. The differences in the PXRD pattern of trimethylurea between this work and the literature are caused by a difference in measurement temperature. Preferential orientation occurred in some cases and caused differences in relative peak intensities between the experimental and reference PXRD patterns.

Table VI.1 Polymorphs of commercial urea derivatives used in this work

Compound	Polymorph	Space group	Ref.
Acetamide	Rhombohedral	$R3c$	[290]
Urea	I	$P\bar{4}2_1m$	[291]
N-Methylurea	I	$P2_12_12_1$	[292]
1,1-Dimethylurea	-	$P2_1/n$	[293]
1,3-Dimethylurea	I	$Fdd2$	[209]
Trimethylurea	-	$Cmc2_1$	[218]
1,1-Diethylurea	-	$C2/c$	[223]
1,3-Diethylurea	α	-	[224]

VI.2.2 Thermal analysis

DSC curves obtained at a heating rate of 10 K min^{-1} are provided in Figure F.1 in Appendix F. As shown in Table VI.2, the melting point difference between the experimental data obtained in this work and the literature data[294] is within 5%.

Table VI.2 Melting points of the urea derivatives measured in this work and in the literature

Name	Melting point /K	
	This work	literature[294]
Acetamide	353.6	354(1)
Urea	406.9	406.5(9)
N-Methylurea	371.4	375(3)
1,1-Dimethylurea	455.0	454.6(9)
1,3-Dimethylurea	376.9	379(3)
Trimethylurea	337.4	344.4
1,1-Diethylurea	336.6	342.3
1,3-Diethylurea	375.2	383.4
Tetramethylurea	267.4	271(2)

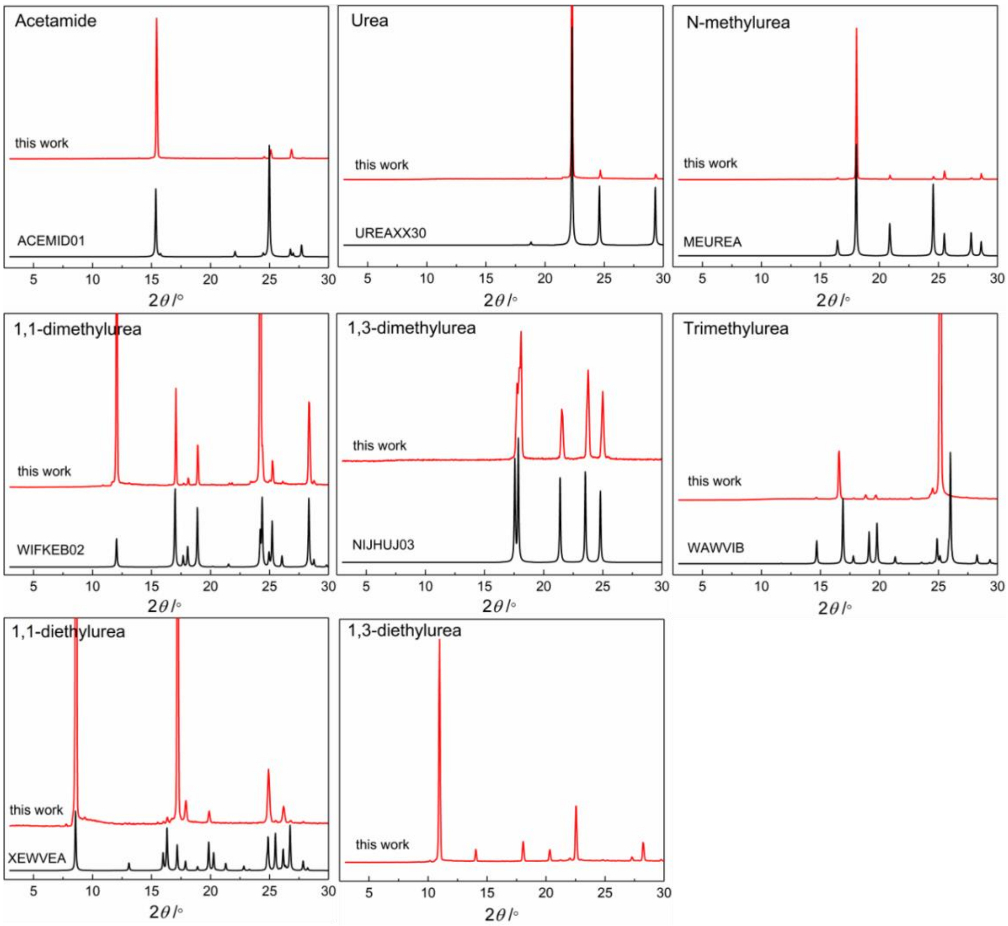

Figure VI.1 Powder X-ray diffraction patterns of the crystalline urea derivatives used in this work and in the literature

VI.2.3 Vapor pressures in the literature

The investigation of the influence of the urea derivatives on the crystallization process by sublimation was carried out at 397 ±1 K. Before the experiments, the necessary quantity per additive was estimated using the vapor pressure data from the literature to make sure that the respective additive saturated the vapor phase. As is shown in Figure VI.3, except urea and 1,1-dimethylurea, the additives are liquid at the experimental temperature. However, the vapor pressure at the experimental temperature of 1,3-dimethylurea, trimethylurea, 1,1-diethylurea and 1,3-diethylurea are estimated by using the vapor pressure of the solid. The pressure-temperature equations of the additives were fitted to the data reported in the literature and the results are listed in Table VI.3. (For trimethylurea, the literature did not provide vapor pressure data, therefore the equation used in this work was directly taken from the literature). The used vapor pressure data are listed in Appendix G.

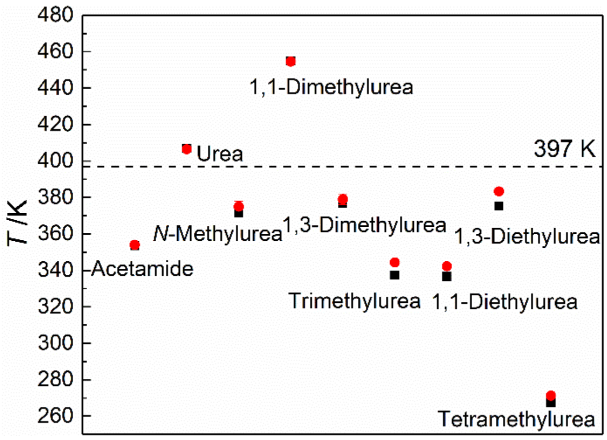

Figure VI.2 Melting points of the urea derivatives measured in this work (■) and in the literature (●) in relation to the sublimation temperature of 397 K (dashed line)

Table VI.3 Vapor pressure from the literature and minimum sublimation amount for the urea derivatives

Compound	$\log p = A - B/T$ (p /Pa, T /K)			p_V (397 K) /Pa	Mass[a] /mg	Ref.
	A	B	Temperature range			
Acetamide (liquid)	11.89(1)	3313(4)	324.07-364.47	3490	7.4	[295]
Urea (solid)	13.0(1)	4717(392)	353.15-403.15	13	0.005	[296]
N-Methylurea (liquid)	12.9(2)	4332(47)	377.2-410.3	95	0.04	[297]
1,1-Dimethylurea (solid)	14.3(2)	4765(52)	346.3-398.3	181	0.1	[298]
1,3-Dimethylurea (solid)	13.4(2)	4396(48)	317.14-377.61	179	0.1	[299]
Trimethylurea (solid)	14.7(2)	4683(64)	345-375	802	0.5	[300]
1,1-Diethylurea (solid)	15.7(2)	4975(48)	305.11-347.10	1393	1.0	[299]
1,3-Diethylurea (solid)	14.9(4)	5015(118)	323.42-384.73	165	0.1	[299]
Tetramethylurea (liquid)	10.0(2)	2249(47)	318.92-450.70	21714	14.6	[301]

[a] Minimum mass necessary to saturate the sublimation volume at 397 K with the urea derivatives calculated with the listed equation. The mass is calculated by $m=M\cdot p\cdot V/R/T$, M is the molar mass of the urea derivatives, p is the saturated vapor pressure at 397 K, V is the vial volume 20 mL, R is the ideal gas constant, T is the sublimation temperature: 397±1 K.

VI.3 The effect of the urea derivatives on the crystallization process of pyrazinamide

In solution crystallization, the solute in the clear solution does generally not crystallize immediately when supersaturation occurs. This lag period is called the induction time. In sublimation experiments, the induction time is counted from the moment the sample is put at its sublimation temperature until the first crystals appear. Two processes occur during the induction time. First, a critical nucleus needs to form and second it needs to grow into a crystal with a size that is detectable. A second time interval can be defined as the ‘complete sublimation time’, which is the time it takes for the original sample to have sublimated entirely and thus no sample is left on the sublimation location.

The ‘induction time’ and the ‘complete sublimation time’ were measured as described in section II.4.2.3. The results are presented in Table VI.4 and they clearly indicate that the urea derivatives can significantly shorten the ‘induction time’ and the complete sublimation time of the sublimation experiments. Their presence accelerates either the nucleation rate or the growth rate or both. Nonetheless, differences in the effect of the urea derivatives can be observed. The induction time in the presence of acetamide, 1,1-dimethylurea and 1,3-dimethylurea is the shortest with crystals detected within one hour. Even though the induction time in the presence of 1,1-diethylurea, 1,3-diethylurea, and tetramethylurea is longer, it still only takes a third of the induction time measured in the absence of any additives. The ‘complete sublimation times’ are listed in Table VI.4 as well. For experiments in the presence of acetamide, *N*-methylurea, 1,1-dimethylurea, and 1,3-dimethylurea, α transformed completely into γ within a day, which is tenfold faster than in the absence of additives. For trimethylurea, 1,3-diethylurea, and tetramethylurea, the ‘complete sublimation time’ was more than one day. A more precise time cannot be obtained, because of decomposition of some of the urea derivatives. Compared to crystallization without additives, their presence significantly accelerates the crystallization of form γ. However, the crystallization rates vary considerably for the different additives.

The presence of the urea derivatives significantly decreases the induction time. Comparing the vapor pressures at 397 K (Table VI.3) and the induction time, the urea derivatives appear to fall into three groups (Figure VI.3): One group containing at least one available nitrogen bound proton and for the rest only methyl groups to which acetamide, urea, *N*-methylurea, 1,1-dimethylurea, 1,3-dimethylurea, and trimethylurea belong, one group with at least one available nitrogen proton combined with ethyl groups and the last group consisting of only tetramethylurea with no available nitrogen protons at all. For the first group, the induction time clearly decreases with increasing vapor pressure, so it can be concluded that acetamide is more effective than urea simply because of its higher vapor pressure. It implies that methyl groups as long as a N-H group is present do not play an important role in the interaction between pyrazinamide and the urea derivatives. Furthermore, it seems that the number of methyl groups affect the vapor pressure for the methylated urea derivatives (acetamide and diethylurea excluded): urea < methylurea < dimethylurea < trimethylurea < tetramethylurea. The overall favorable effect of both 1,3-dimethylurea and 1,1-dimethylurea on the induction time is noteworthy even if not entirely understood, but it can very well be part of the scatter in the data.

Table VI.4 Induction time and complete sublimation time of γ in the presence of urea derivatives

Pyrazinamide /mg	Urea derivatives	Mass of urea derivatives /mg	Induction time /h	Complete sublimation time /h
30	-	-	7.5	252(17)
	Acetamide	10	1	< 24
	Urea	30	2	108(17)
	N-Methylurea	30	1.5	< 24
	1,1-Dimethylurea	30	1	< 24
	1,3-Dimethylurea	30	1	< 24
	Trimethylurea	30	1.25	>24
	1,1-Diethylurea	30	2.25	36(17)
	1,3-Diethylurea	30	2.5	>24
	Tetramethylurea	15	2.5	>48

The induction times in the presence of 1,1-diethylurea or 1,3-diethylurea are longer, but the slope in Figure VI.3 is similar to that of the methylated molecules, i.e. overall higher vapor pressure within this group favors smaller induction times. The overall higher induction times compared to the methylated molecules might be due to an element of steric hindrance of the ethyl groups. Tetramethylurea has the highest vapor pressure by far, but the induction time is relatively long. Clearly the available amine proton is important in the interaction of the urea derivatives with pyrazinamide in addition to the electron-rich carbonyl oxygen.

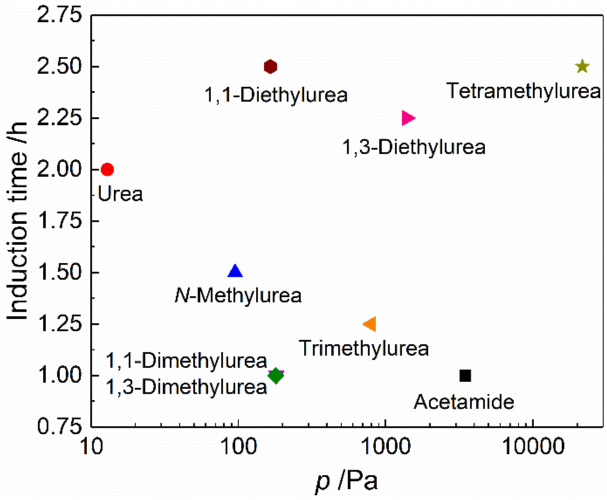

Figure VI.3 Induction time of form γ as a function of the vapor pressure of the available urea derivative

VI.4 The effect of urea derivatives on the morphology of the γ form

VI.4.1 Characterization of single and twinned crystals

VI.4.1.1 Characterization by polarized-light microscopy

γ form crystals obtained by sublimation in the absence and presence of additives have been analyzed with polarized-light microscopy. Both single and twinned crystals have been observed in all experiments. Micrographs of these crystals are presented in Figure VI.4. As the twinned domains interact differently with polarized light, single crystals and twinned crystals can be distinguished and separated. The morphological changes resulting from the presence of additives are discussed in detail in the following sections.

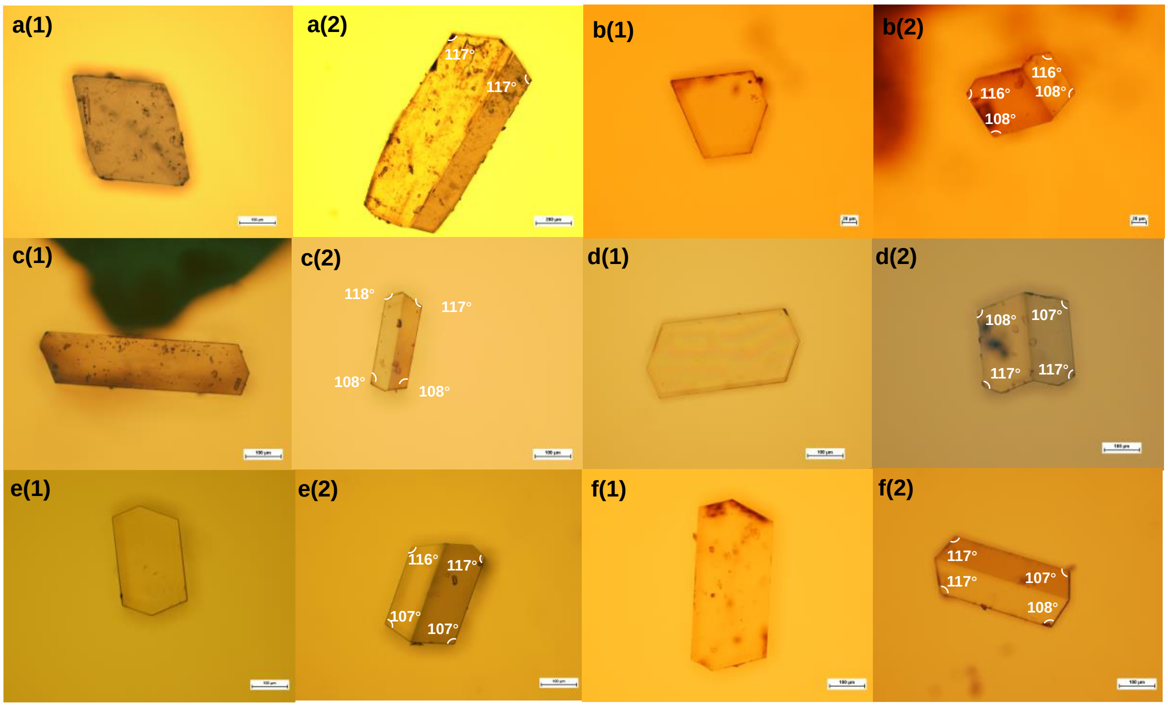

Figure VI.4 Micrographs of γ form (1) single and (2) twinned crystals (a) in the absence of additives or in the presence of (b) acetamide, (c) urea, (d) 1,3-dimethylurea, (e) 1,3-diethylurea, or (f) tetramethylurea

VI.4.1.2 Inclusions in crystals

Inclusions have been observed in crystals obtained in the presence of the urea derivatives (Figure VI.5). Gas chromatography (GC) was used to determine if the inclusions contained the urea derivatives and the results are shown in Figure VI.6 and Figure VI.7. The retention times of pyrazinamide, 1,3-dimethylurea and tetramethylurea are 6.9 min, 5.2 and 3.8 min, respectively. Crystals with inclusions were washed with a saturated pyrazinamide solution in acetone to remove the urea derivatives that might be attached to the surface of the crystals. Only the peak of pyrazinamide at 6.9 min was detected in all measurements. Clearly the concentration of additives is too low to be detected by GC making it unlikely that large amounts of additives were present in the inclusions or as solid solution in the crystal.

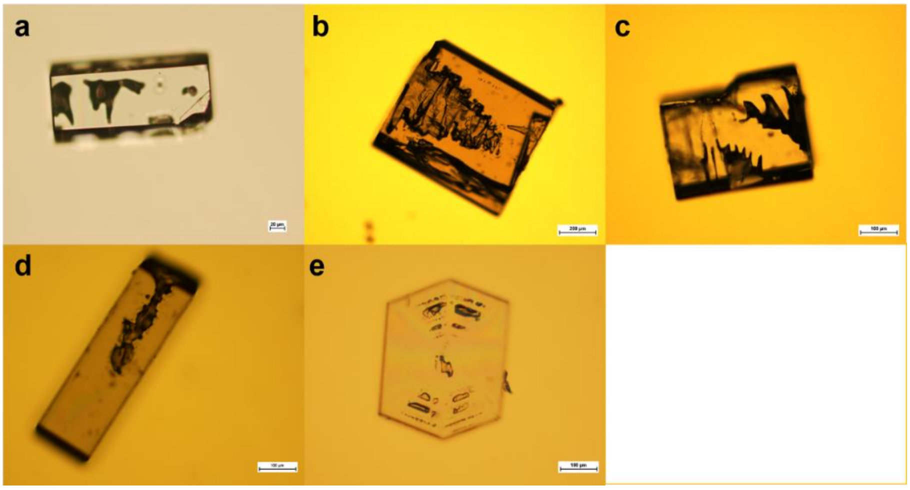

Figure VI.5 Crystals with inclusions obtained in the presence of (a) acetamide, (b) urea, (c) 1,3-dimethylurea, (d) 1,3-diethylurea and (e) tetramethylurea

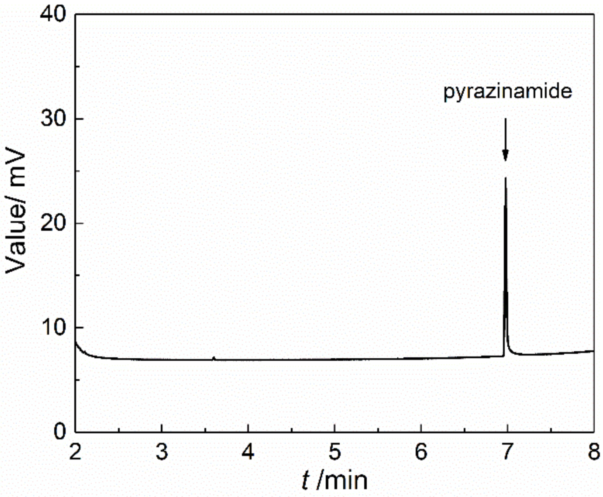

Figure VI.6 Gas chromatography result of crystals with inclusions obtained in the presence of 1,3-dimethylurea

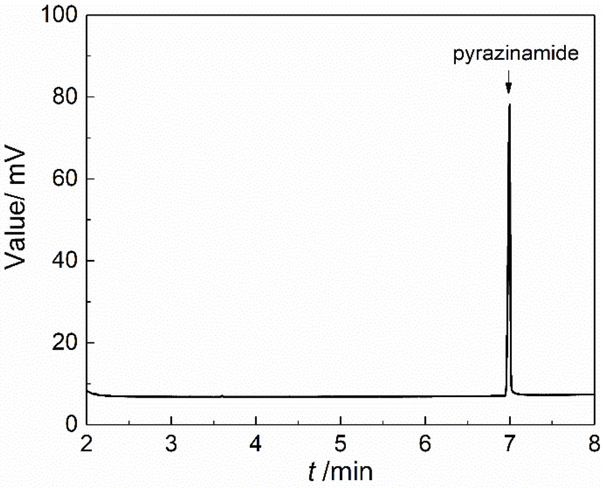

Figure VI.7 Gas chromatography result of crystals with inclusions obtained in the presence of tetramethylurea

VI.4.1.3 Precession plots by single crystal X-ray diffraction

Precession plots of a single and a twinned crystal are presented in Figure VI.8. Directions [0kl] and [h0l] do not exhibit any clear indication of twinning; however, the [hk0] precession plot contains the tell-tale splitting of diffraction spots indicative of closely aligned twins.

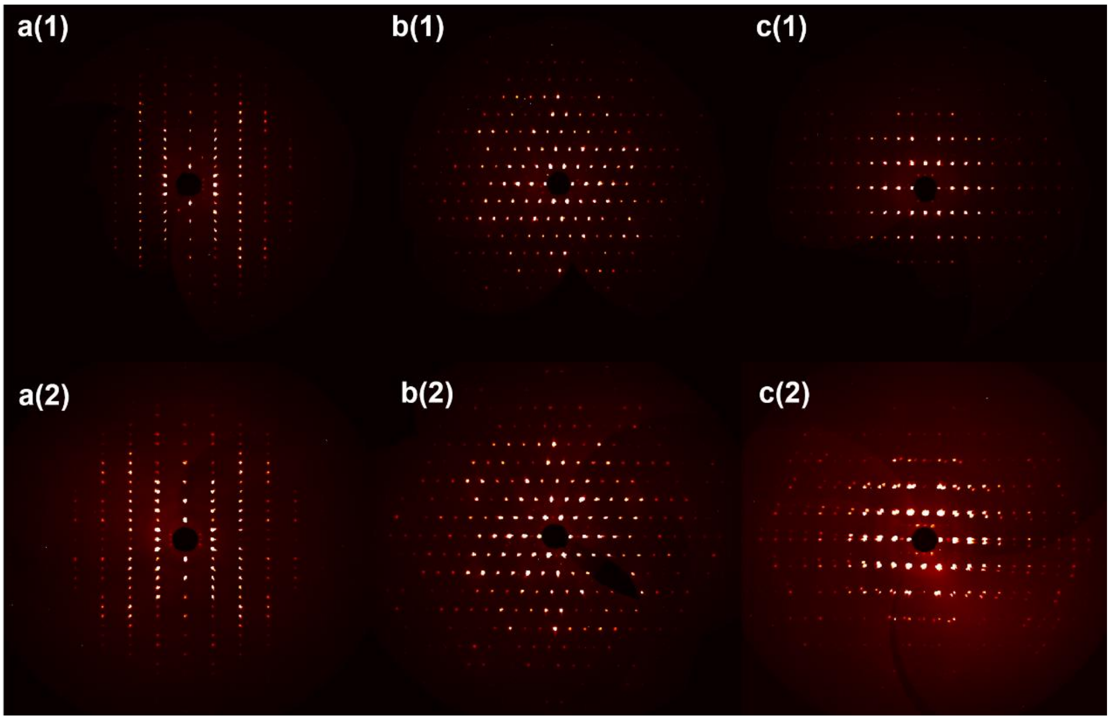

Figure VI.8 Precession plots of directions (a) [0kl], (b) [h0l], and (c) [hk0] of (1) single and (2) twinned γ form crystals

VI.4.2 The calculated γ form morphology

The morphology calculated with the Bravais-Friedel-Donnay-Harker (BFDH) model and the attachment energy (AE) model are presented in Figures VI.9a and b, respectively. Both crystal morphologies are similar but a few differences can be noticed. One of the distinct differences between the calculated morphologies obtained with the BFDH (Figure VI.9a) and AE (Figure VI.9b) models is the aspect ratio of the faces. Another difference is the (111), (1-11), (-11-1) and (-1-1-1) faces and (322), (3-22), (-32-2) and (-3-2-2) faces, which are respectively present and absent in the crystal morphology calculated with the BFDH model and respectively absent and present in the morphology calculated with the AE model. This results in a difference in the angles between the faces (100), (111) / (322) and (002). Compared to the experimental morphology (Figure VI.9c), the morphology calculated with the AE model matches the experimental morphology better. Thus, the result of the AE model is used as the reference morphology in the following. Two angles with the values of 160° and 130° found in the calculated morphology (Figure VI.9b) are similar but not completely equal to the experimental values of 165° and 125°. It is therefore not clear whether face (322) is observed experimentally or whether it is another face with a similar orientation.

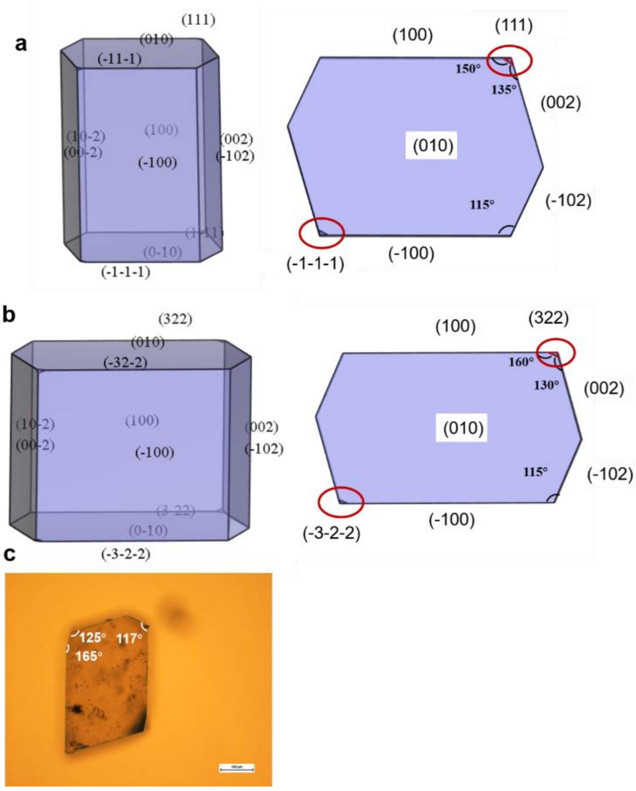

Figure VI.9 The γ form morphology (a) calculated with the BFDH model, (b) calculated with the AE model, and (c) obtained from sublimation in the absence of urea derivatives

VI.4.3 The morphology of γ form single crystals

VI.4.3.1 The morphology in the absence of urea derivatives

Microscopy photographs of γ form single crystals obtained in the absence of any additives are presented in Figure VI.10. Although the crystals in Figure VI.10 have been obtained under the same conditions, for several crystals a number of faces is absent. The photographs in Figure VI.10a, c, d, e, and f have been taken along the [010] axis of different crystals. Figure VI.10b contains a photograph of face (100) or (-100) of the same crystal as in Figure VI.10a. In the photographs from VI.10a to e, the crystals exhibit less and less faces. In Figure VI.10c, one of the (322), (3-22), (-32-2) or (-3-2-

2) faces has disappeared and a new included angle (the angle between face (100) and (002)) of about 108° (=123°+165°-180°see Figure VI.10a) replaces the included angles of 123° and 165°. In Figure VI.10e, the {-102} faces have disappeared and a new included angle (the angle between faces (-100) and (002)) has been formed with a value of 75° (=117°+138°-180° (see Figure VI.10a)). A less well-defined crystal can be observed in Figure VI.10f, whose morphology seems to be twinned even if by polarized light microscopy no twinning could be detected.

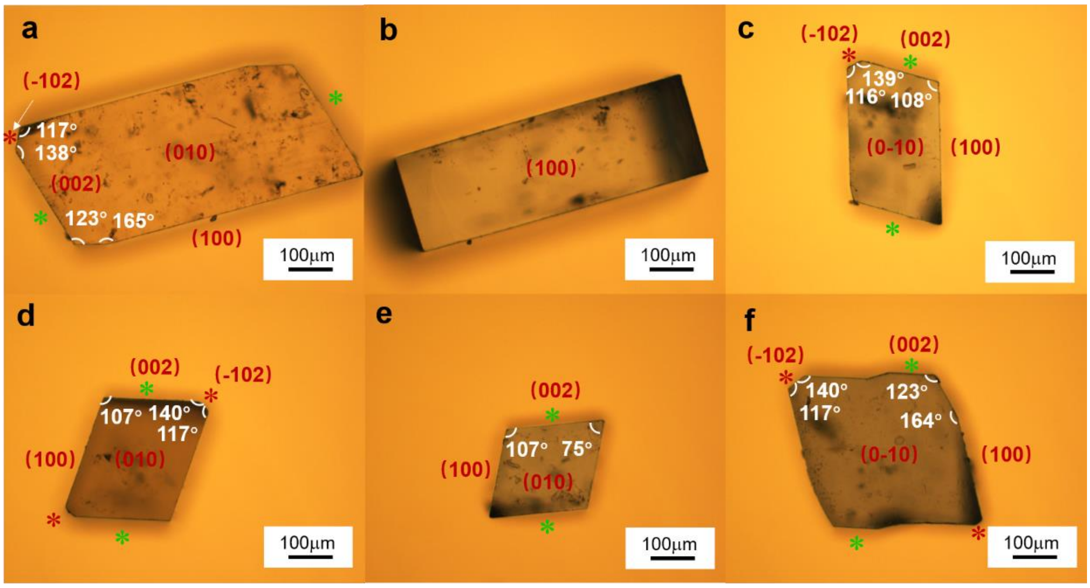

Figure VI.10 Microscopy photographs of different γ form crystals prepared by sublimation without any urea derivatives on (a, c, d, e, f) the {010} face and (b) the (100) face of the crystal shown in (a). Faces marked by * are either face (002) or (00-2) and faces marked by * are either face (-102) or (10-2)

VI.4.3.2 The morphology in the presence of the urea derivatives

Microscopy photographs of single crystals of the γ form in the presence of acetamide, urea, 1,3-dimethylurea, 1,3-diethylurea and tetramethylurea are presented in Figure VI.11b-f. For crystals in the presence of additives, the same angles can be observed as for the crystals obtained without additives (Figure VI.11a). There are two distinguishing features of the morphology obtained in the presence of most urea derivatives:

1) the size of the (10-2) and /or (-102) faces is larger than those obtained without additives and one of these faces tends to be even larger than faces (002) and (00-2) for some of these crystals.

2) the aspect ratio of the (100) and (-100) face is generally smaller than those grown without additives.

More details about the morphology in the presence of additives is discussed in the next section.

VI.4.3.3 Crystal morphology statistical analysis

In order to analyze the growth of the individual crystal faces, statistical information on their sizes has been obtained by microscopy. More than five hundred crystals in total for all the conditions have been selected. The conditions are: 1) absence of additives, presence of 2) acetamide, 3) urea, 4) 1,3-dimethylurea, 5) 1,3-diethylurea and 6) tetramethylurea (see Table VI.6). Various lengths have been measured for each of these crystals: the {010} diagonal (blue dashed line in Figure VI.12), the {010} width (yellow dashed line), the width of {100} (pink dashed line), the lengths of (002) and (00-2) (green dashed lines) and (-102) and (10-2) (red dashed lines) lines. The length obtained for the {010} diagonal divided by its width can be regarded as the aspect ratio of {010}. This ratio is used to compare the growth rates of the (-102) and (002) faces ({010} diagonal) on the one hand and the (100) and (-100) faces ({010} width) on the other hand. Because the lengths of the (100) and (-100) faces are usually different, the length of the {010} diagonal is used to represent the lengths of the {100} faces. The {010} length divided by the width of face (100) can be regarded as the aspect ratio of {100}. Furthermore, the ratio of the {010} width and the {100} width is a measure of their relative growth rates. The smaller the “width-thickness” ratio, the higher the relative growth rate of face {010} and vice versa.

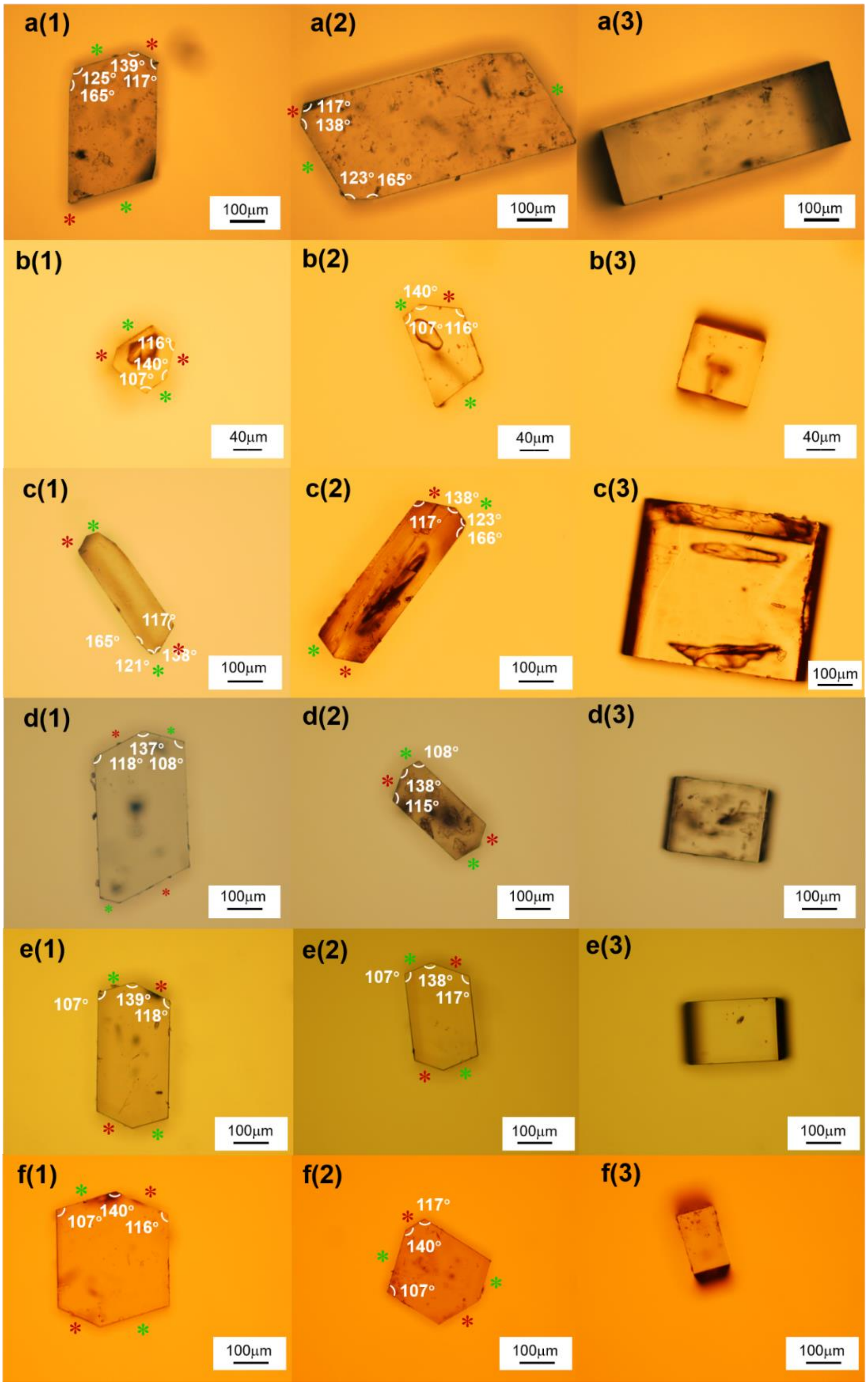

Figure VI.11 The morphology of γ form crystals obtained (a) in the absence of urea derivatives or in the presence of (b) acetamide, (c) urea, (d) 1,3-dimethylurea, (e) 1,3-diethylurea, or (f) tetramethylurea. (1) and (2) different crystals photographed on the {010} face and (3) on the {100} face of the same crystal as in (2). Faces marked by * are face (002) and face (00-2) and faces marked by * are face (-102) and face (10-2)

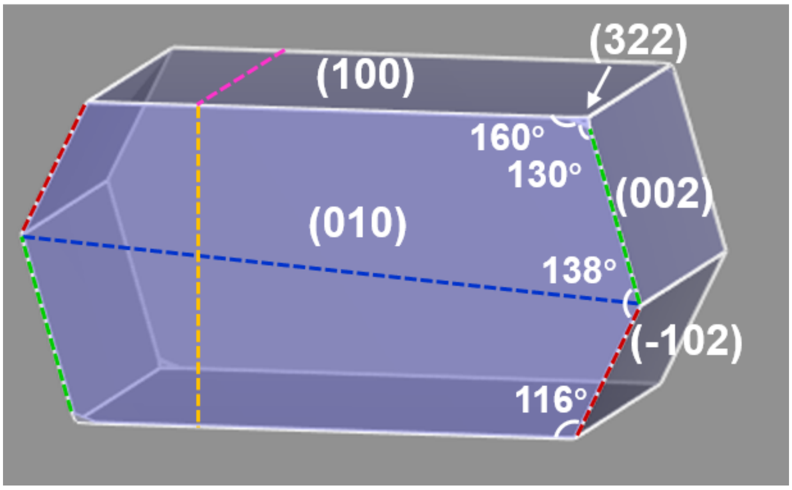

Figure VI.12 Measured lengths of the γ form crystal

From the calculated morphology presented in Figure VI.9b and the microscopy photographs (Figure VI.10), it can be observed that the lengths of adjacent faces (002) and (-102) (and (00-2) and (10-2)) are different. A length ratio will be defined as the length of (-102) divided by the length of (002), which will be called "adjacent-faces ratio". Two of these can be defined, one for each side of the crystal. This ratio is used to compare the relative size of face (-102) and face (002). As can be observed in Figure VI.9b, "reciprocal faces" (that is, with opposite hkl indexes) in the calculated morphology appear to have the same size. However reciprocal faces in the experimental setting clearly possess different sizes (which is of course allowed for the non-centrosymmetric *Pc* space group of form γ). For example, in Figure VI.10, at least two pairs of reciprocal faces, such as faces (002) and (00-2), faces (-102) and (10-2) demonstrated an obvious difference in surface size, which implies that these reciprocal faces have been subjected to different growth rates. If it is possible to infer the effect of the urea derivatives on those faces, it may be possible to specifically define the reciprocal crystal faces. The "reciprocal-faces ratio" will be defined as the length of the smaller reciprocal face divided by the larger reciprocal face and this ratio will therefore always be smaller than or equal to 1. Two reciprocal-faces ratios are used in this work for (002) and for (-102). In the following, the aspect ratio ({010} diagonal/width), width-thickness ratio ((010) width/ (100) width), the two adjacent-faces ratios ((-102) length/ (002) length and (10-2) length/ (00-2) length) and reciprocal-faces ratio for faces (002) and (00-2) and faces (-102) and (10-2) are used to analyze the relative growth rates of various crystal faces. All ratios used in this statistical study are summarized in Table VI.5.

Table VI.5 Ratios of the γ crystal dimensions used to interpret relative growth rates of the crystal faces

Name	Formula
aspect ratio of face {010}	{010} diagonal/ {010} width
aspect ratio of face (100)	{010} diagonal/ (100) width
width-thickness ratio	(010) width/ (100) width
adjacent-faces ratios	(-102) length/ (002) length or vice versa (10-2) length/ (00-2) length or vice versa
reciprocal-faces ratio	length of the smaller reciprocal face divided by the larger reciprocal face for faces (002), (00-2) and faces (-102) and (10-2)

The mean of the aspect ratio of face {010} is presented in Table VI.6 and histograms of the distributions of the {010} aspect ratio are shown in Figure VI.13. It is clear from the histograms that urea has the most significant impact on the aspect ratio; its histogram has a very broad distribution with a mean value of 3.5 (Table VI.6). This effect is also observed to a lesser extent for crystals grown in the presence of 1,3-dimethylurea. For the other urea derivatives, the aspect ratios have not changed as much. However, for the derivatives with a high vapor pressure the maximum of the histogram tends to aspect ratios closer to 1, which could be ascribed to a high overall growth rate. An increased aspect ratio indicates that the crystals tend to grow much faster along the diagonal direction, the (002), (00-2), (10-2) and (-102) faces, then widthwise (along the [100] direction) and they tend therefore to be needle shaped.

The mean of the aspect ratio of face (100) is shown in Table VI.6. The result indicates that the acetamide and urea lead to a significant reduction of this aspect ratio in comparison to the crystals obtained without additives. Histograms of the distribution are shown in Figure VI.14. The histograms exhibit two clear changes: 1) the mode of the aspect ratio of all urea derivatives is smaller than the mode of the aspect ratio in the absence of additives; 2) the histogram for the crystals obtained in the absence of additives has a broad distribution with a mean value of 3.5 (Table VI.6).

Table VI.6 The mean values of the aspect ratio and the width-thickness ratio of form γ single crystals as a function of the urea derivatives

Urea derivatives	Number of crystals	(010) Aspect ratio	(100) Aspect ratio	Width-thickness (010)/(100) ratio
-	101	1.8(3)	3.5(16)	1.9(9)
Acetamide	100	1.7(6)	1.4(8)	0.9(5)
Urea	101	3.5(12)	1.5(6)	0.5(2)
1,3-Dimethylurea	106	2.4(9)	2.4(11)	1.1(6)
Tetramethylurea	100	1.5(4)	2.9(13)	2.1(10)
1,3-Diethylurea	10	1.9(6)	2.2(5)	1.4(6)

The mean values and histograms of the width-thickness ratios are presented in Table VI.6 and in Figure VI.15. Urea causes the most distinct impact on the crystals. The mean width-thickness ratio in the presence of urea decreases to 0.5 compared to a value of 1.9 for crystals grown in the absence of any additives. The distributions for acetamide and 1,3-dimethylurea are narrower than the distribution without additives and their modes have shifted to lower values. It indicates that the growth rate perpendicular to face (010), along [010], increases compared to that in the [100] direction. For tetramethylurea, the distribution is broader than that without additives and its mode has shifted to higher values, which is also reflected in its mean value.

The distributions in the Figures VI.13-15 reflect the effects of the urea derivatives on crystal morphology of pyrazinamide in three directions: 1) [010], 2) [100], and 3) more or less perpendicular to 1 and 2 the diagonal of {010}, which is related to the growth in the [002] and [-102] directions. The results in absence of additives reveal that the growth rate in direction [010] is smaller than the growth rate in direction [100], while the growth rate in the direction of the {010} diagonal is the largest.

In the case of acetamide, the aspect ratio of (010) does not change, but the aspect ratio of (100) and the width-thickness ratio are much smaller than the result in the absence of additives. It indicates that the growth rate in the [010] direction is larger than in the other two directions.

In the case of tetramethylurea, the changes of these ratios are smaller than the changes caused by other urea derivatives. The decrease of the (010) aspect ratio and the increase of the width-thickness ratio indicates that the growth rate in the [100] direction is larger than the growth rate in the [010] direction. For urea and 1,3-dimethylurea, the tendency is the same but the effect of 1,3-dimethylurea is weaker. The significant increase of the (010) aspect ratio and the decrease of the width-thickness ratio indicate that both growth rates in the direction of the {010} diagonal and in the [010] direction are larger than the growth rate in the [100] direction. The (100) aspect ratio implies that the growth rate in the direction of the {010} diagonal is larger than the direction of the [010].

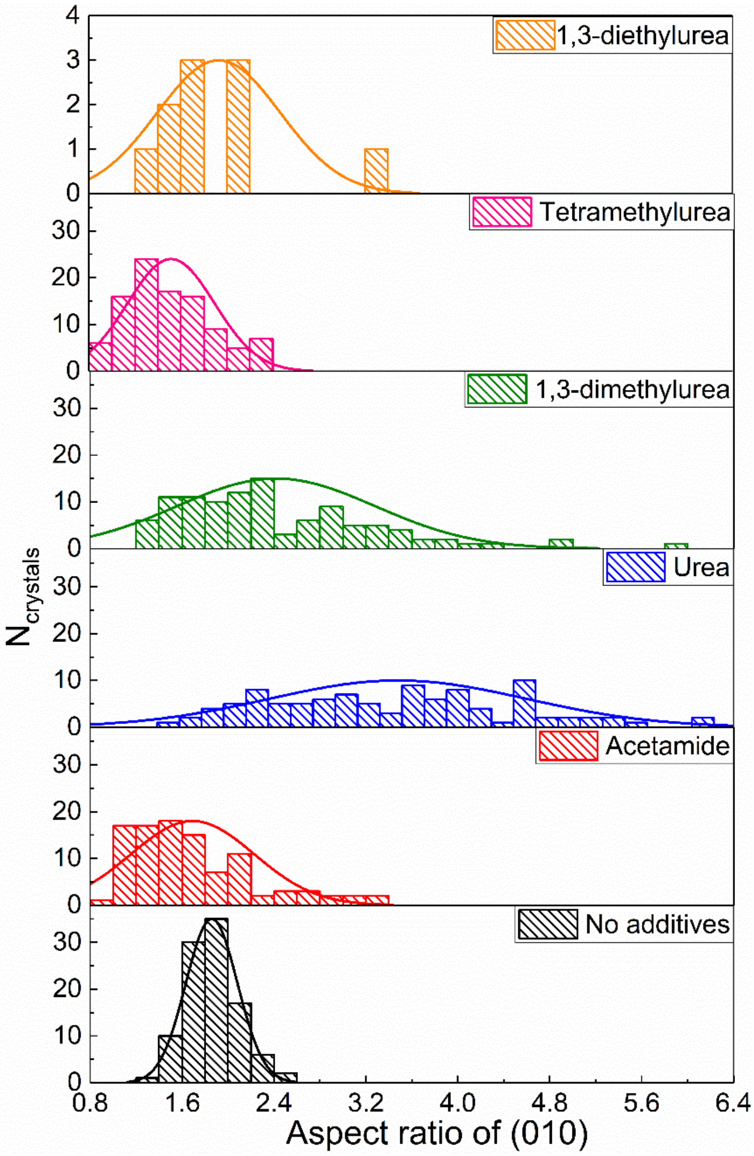

Figure VI.13 Histograms of the (010) aspect ratio distributions with different urea derivatives

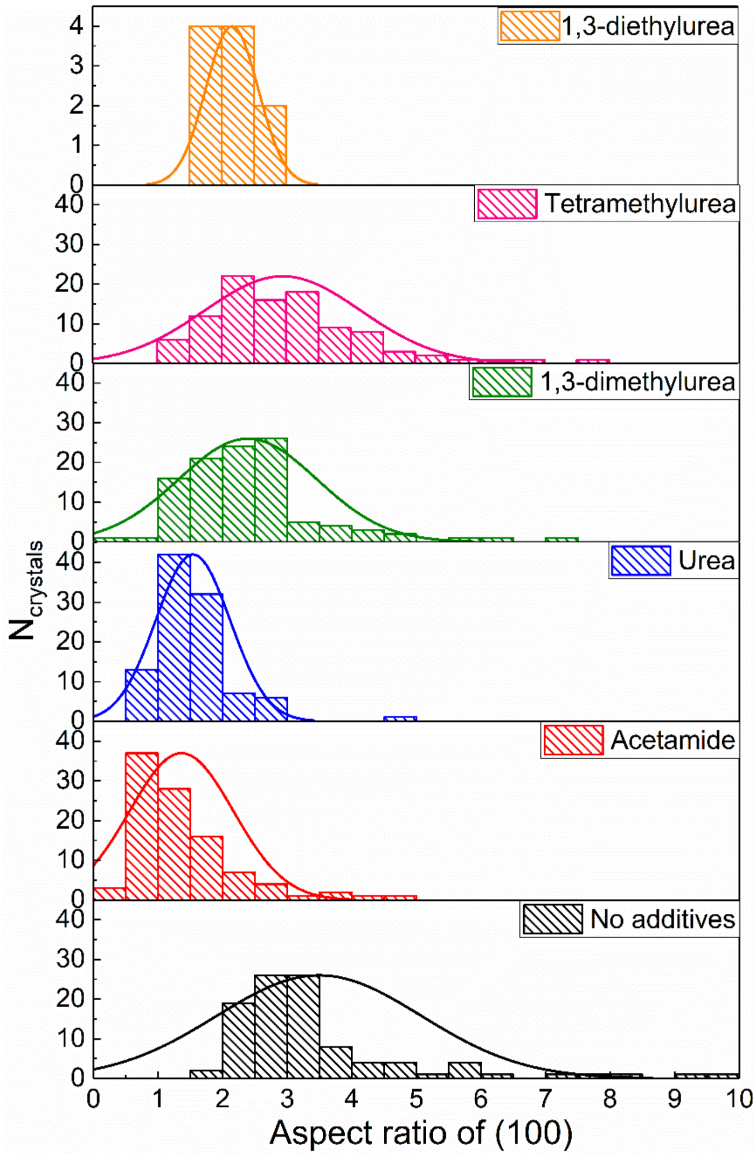

Figure VI.14 Histograms of the (100) aspect ratio distributions with different urea derivatives

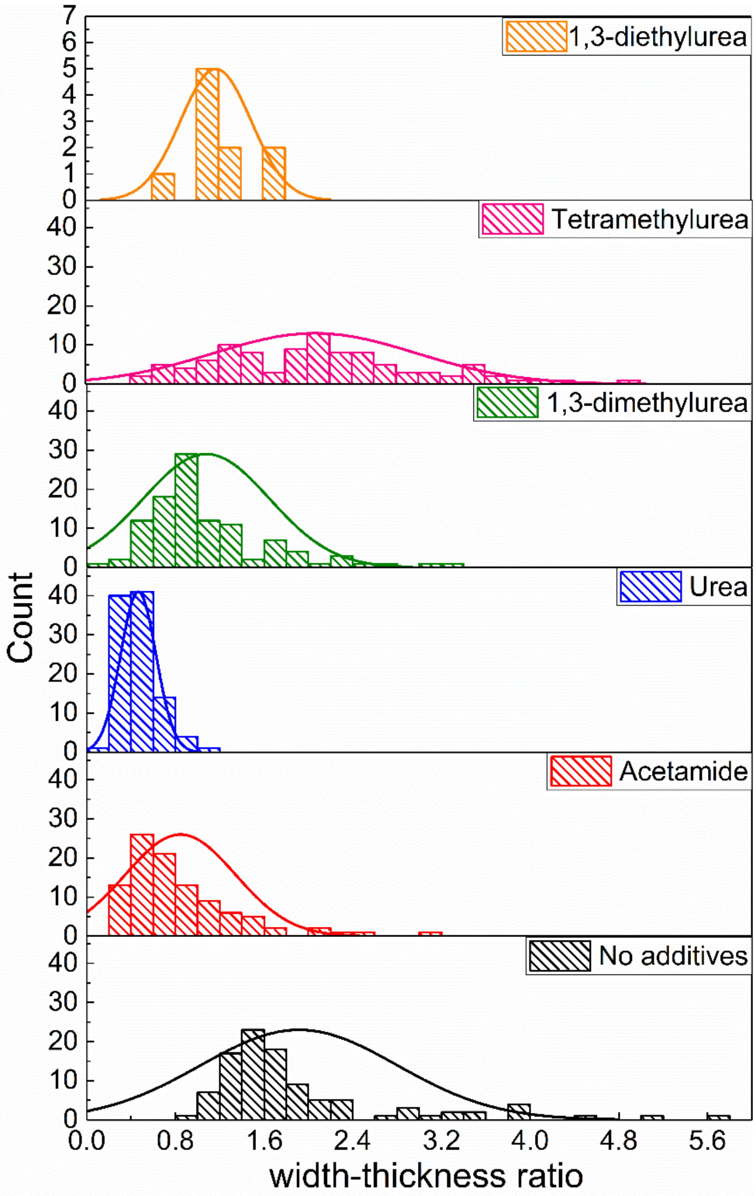

Figure VI.15 Histograms of the width (010) - thickness (100) ratio distributions for different urea derivatives

Two adjacent faces ratios (L(-102)/L(002) and L(10-2)/L(00-2) with L = length) have been defined. These two ratios are used to compare the size of face (-102) against that of face (002); however, with the present definition the ratio ranges from zero to infinity. In order to obtain a more balanced distribution, the ratio (-102)/ (002) is changed to the ratio (002)/ (-102), once the former becomes larger than 1, so that the determined ratio is always comprised between 0 and 1. In this way, there are only three cases possible:

1) both L(-102) / L (002) and L(10-2) / L (00-2) are ≤ 1,

2) both L(002) / L (10-2) and L(00-2) / L(-102) are <1,

3) one L(-102) / L(002) (or L(10-2) / L(00-2)) is ≤1 and one L(002) / L (10-2) (or

L(00-2) / L(-102)) is <1.

The result is presented in Table VI.7 and the histograms of the adjacent faces ratio distributions are presented in Figure VI.16. All crystals obtained in the absence of additives had a ratio L(-102)/L(002) is ≤ 1. It means that the size of face (-102) or (10-2) is consistently smaller than that of face (002) or (00-2) without additives, which in turn implies that the relative growth rate of the faces (002) or (00-2) is slower than that of the faces (-102) or (10-2). For crystals obtained in the presence of the urea derivatives, at least one of the two adjacent faces ratios becomes larger than 1. It means that the size of the (-102) or (10-2) face becomes larger than its respective adjacent face (002) and (00-2) implying that the relative growth rate of the former decreases and/or of the latter increases.

Table VI.7 The number of crystals, N, with three distinctive adjacent-faces ratio distributions for γ form single crystals: both L(-1 0 2)/L(0 0 2) ≤ 1, one of L(-1 0 2)/L(0 0 2) ≤ 1, and both L(0 0 2)/L(-1 0 2) <1

Urea derivatives	N	Both L(-1 0 2)/L(0 0 2) ≤ 1	One of each	Both L(0 0 2)/L(-1 0 2) <1
-	101	101	0	0
Acetamide	100	18	82	0
Urea	101	15	40	46
1,3-Dimethylurea	106	27	40	39
Tetramethylurea	100	48	51	1
1,3-Diethylurea	10	0	8	2

Histograms of the adjacent-faces ratios are presented in Figure VI.16. The result of the adjacent-faces ratios indicates that additives have a clear effect on the (002), (00-2), (-102), and (10-2) faces. In fact, the presence of the additives creates in a general way a more balanced crystal with relatively speaking smaller (002) and (00-2) faces and larger (-102) and (10-2) faces.

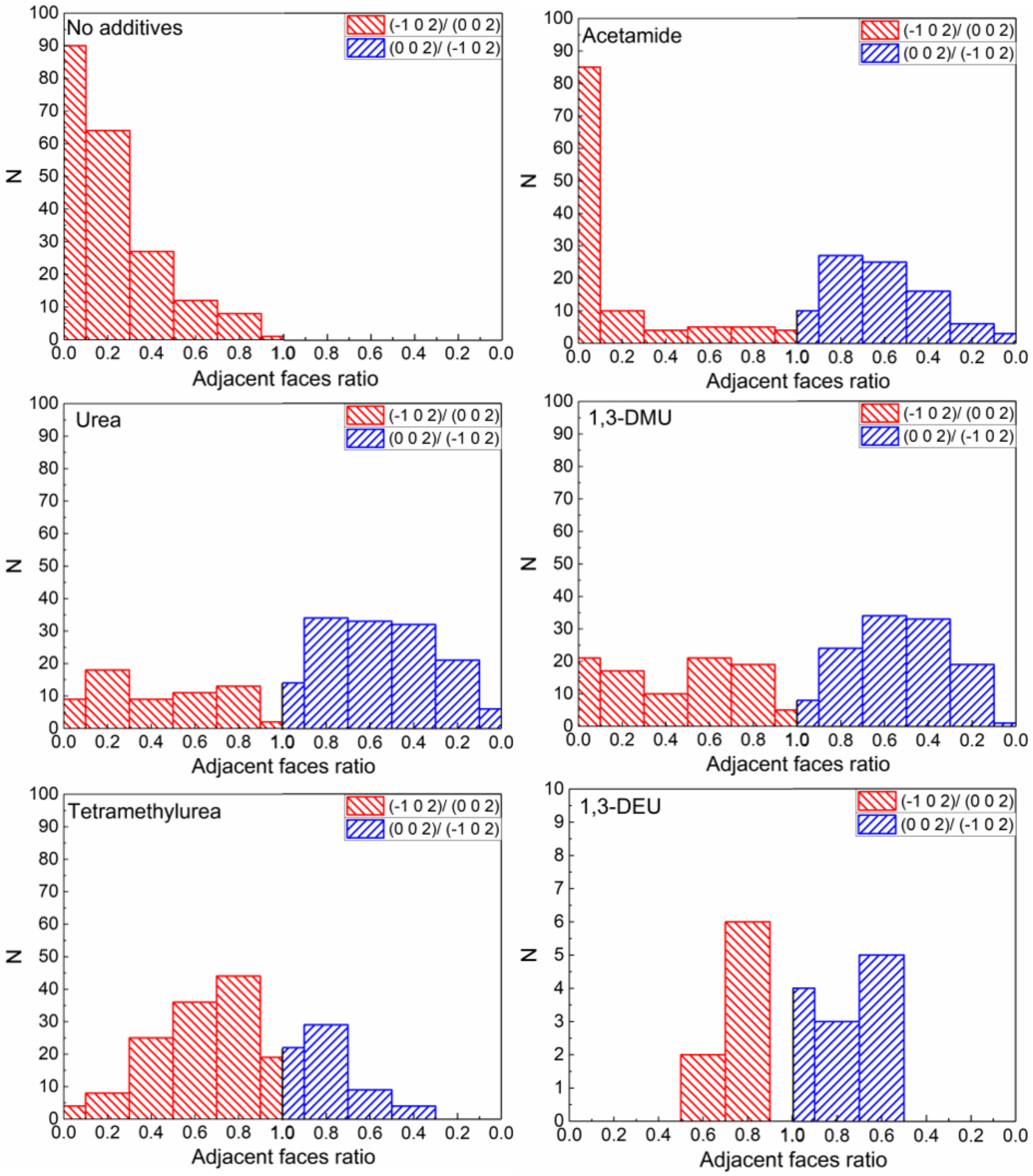

Figure VI.16 Histograms of the adjacent-faces ratios

In order to understand the effect of the additives on the (002), (00-2), (10-2) and (-102) faces in more detail, the two reciprocal-faces ratios of (002) and (-102), respectively, have been analyzed. This ratio is calculated by dividing the shorter length by the longer length. Hence, the reciprocal-faces ratio is always equal or less than 1. In the case that both reciprocal faces are 0, the ratio is set to 1. The closer the ratio is to 1, the more comparable is their growth rate. The mean values for the two reciprocal-faces ratios are shown in Figure VI.17. For crystals obtained in the absence of additives, the mean of the reciprocal-faces ratio distribution for (002) is larger than 0.8 thus indicating that the growth rates of the faces (002) and (00-2) are comparable. The mean of the reciprocal-faces ratio histogram for (-102) is less than 0.4, thus, the growth rates between faces (-102) and (10-2) show distinct differences. With additives, the distribution of the reciprocal-faces ratios changes. Figures VI.18 and VI.19 present the distributions of the reciprocal-faces ratios for (002) and (-102) faces, respectively. In the case of acetamide, a more pronounced trend than the other additives towards a decrease of the modes of both reciprocal-faces ratio distributions is exhibited. Thus, the difference in growth rate between the reciprocal faces (002) and (00-2) becomes larger than without additives. Similarly, the difference in growth rate between reciprocal faces (-102) and (10-2) increases with acetamide.

In the case of most other additives (urea, 1,3-dimethylurea, tetramethylurea and 1,3-diethylurea), the mode of the reciprocal-faces ratio distribution of (-102) increases in comparison to no additive. However, the distributions become flat with only tetramethylurea showing a clearer tendency towards a maximum around 0.8. So overall, the presence of these additives decreases the difference in relative growth rate between the faces (-102) and (10-2). Considering Figure VI.17, acetamide shows a strong 'destabilizing' effect on both reciprocal-faces ratios (002) and (-102), while other additives have a more obvious 'stabilizing' effect on the ratio between (-102) and (10-2).

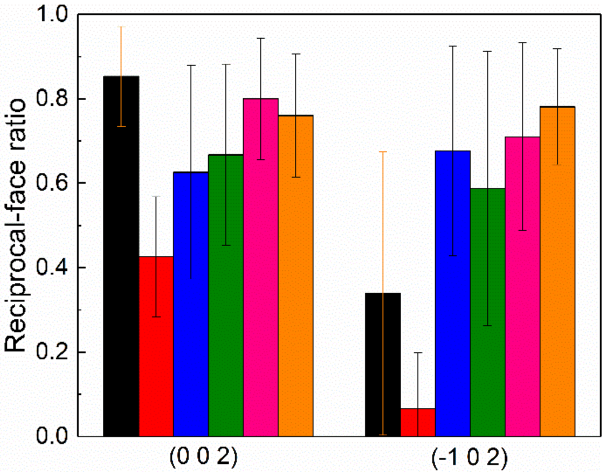

Figure VI.17 The mean of the reciprocal-faces ratios of pyrazinamide with different additives; black: no additives, red: acetamide, blue: urea, olive: 1,3-dimethylurea, pink: tetramethylurea, orange: 1,3-diethylurea

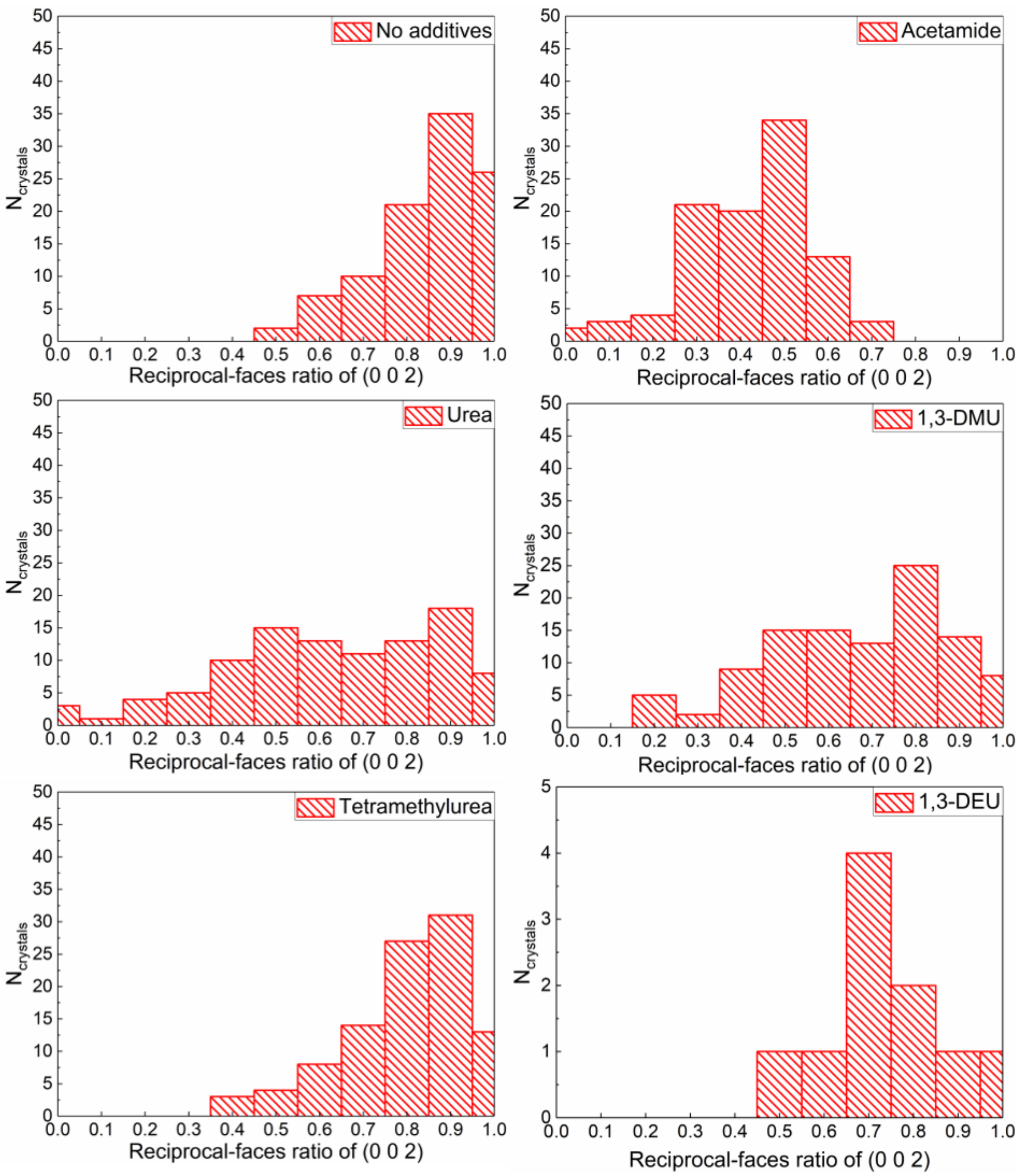

Figure VI.18 Histograms of the reciprocal-faces ratios of (002) for different urea derivatives

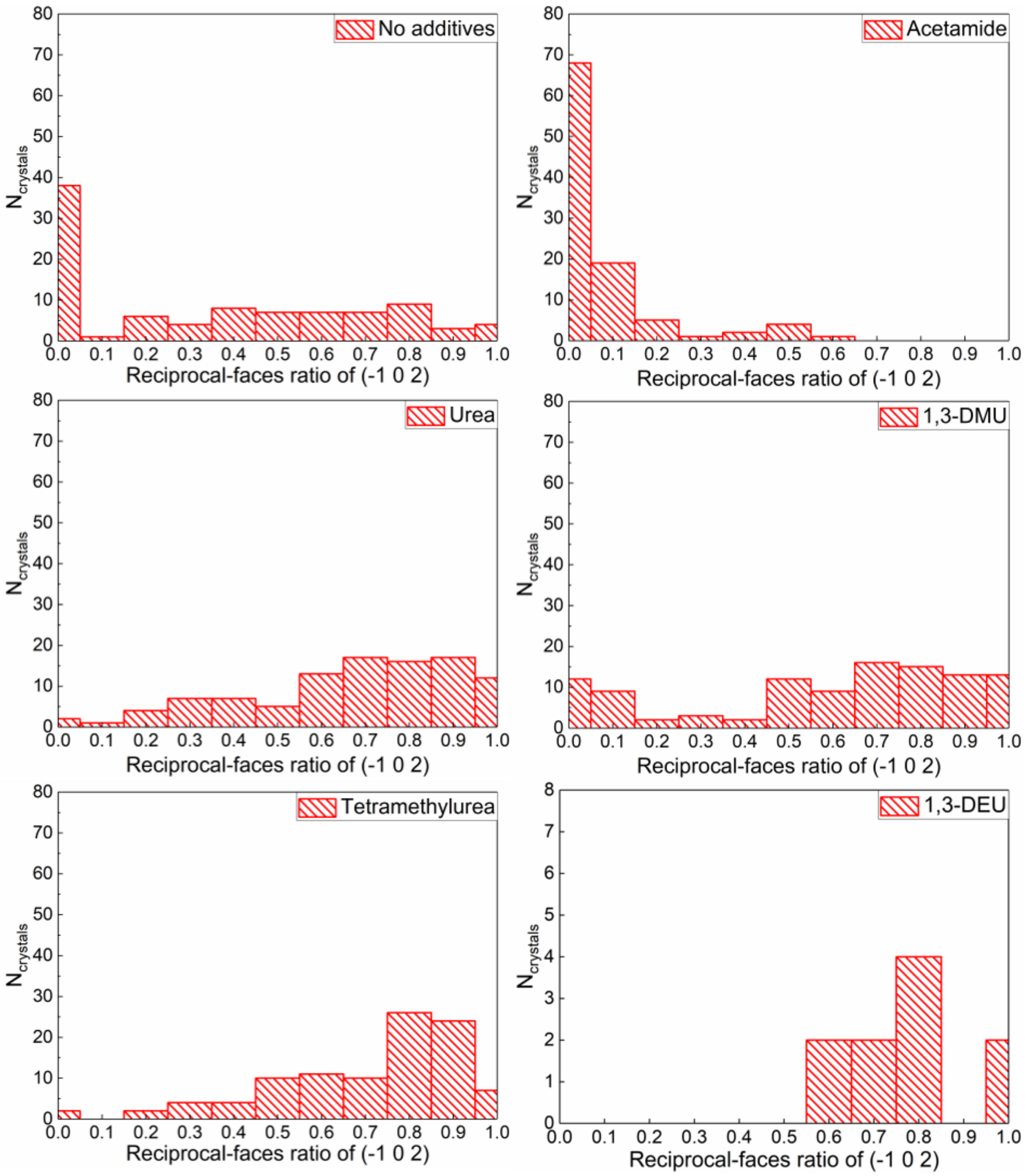

Figure VI.19 Histograms of the reciprocal-faces ratios of (-102) for different urea derivatives

VI.4.4 The mechanism of the effect of the urea derivatives on the γ crystal morphology

The configuration of the pyrazinamide molecules in the γ form at the relevant crystal faces (e. g. those observed in the experimental crystal morphology of pyrazinamide) is presented in Figure VI.20. The pyrazine ring is exposed at the faces (-100), (00-2) and (-102), the carboxyl group at the faces (10-2) and (100), and the amine group at the faces (002) and (100), and the entire molecule at the faces (010) and (0-10). In the γ form structure, one hydrogen bond connecting the amide group and the nitrogen on the pyrazine ring farthest from the amide forms linear chains. Thus, faces (-100) and (00-2) contain a hydrogen bond acceptor and faces (100) and (002) a hydrogen bond donor that are important in the γ form.

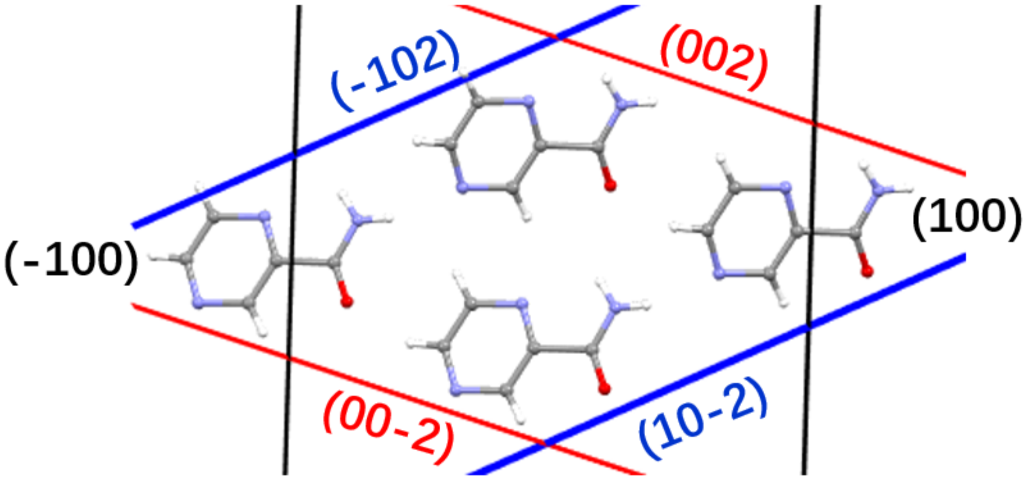

Figure VI.20 Packing of the γ form in relation to some key crystal faces. The top face in this representation is (0-10)

It can be seen in the ESP maps of pyrazinamide and the additives in Figures V. 17 and Figure E.2 in Appendix E, that the oxygen atom in the amide of pyrazinamide and in the carbonyl of the urea derivatives possesses a high electron density, whereas the hydrogens of the amide and amine groups possess a low electron density; thus, interactions are likely to occur between these moieties. Both the oxygen and the furthest nitrogen atom in the pyrazine ring are good hydrogen bond acceptors as can be judged from the ESP map in Figure V.17 (the closer nitrogen is involved in an internal hydrogen bond interaction and possesses therefore considerably less electrostatic potential).

For crystals obtained in the absence of additives, the growth rate of the faces (10-2) and (-102) is relatively higher than the growth rate of the faces (00-2) and (002). As mentioned above, oxygen, the highest electron density region is exposed on face (10-2). Fast growth of this surface will diminish the surface tension. Therefore, face (10-2) is most often smaller than face (00-2). For face (-102), molecules attaching on it diminish the exposure of the oxygen on the pyrazinamide. So, it is energetically favorable to reduce the size of these two surfaces. Oxygen and the high electron density nitrogen atom in the pyrazine ring are exposed on the faces (100) and (-100), respectively. Thus, these two faces growth faster than face (010) and (0-10).

The sublimation crystallization process is accelerated in the presence of the urea derivatives. In addition, the crystal shape is clearly affected by their presence. Both observations indicate that the urea derivatives must be interacting with pyrazinamide during sublimation crystallization. From the previous chapter, it can be recalled that the NMR result shows that:

1) pyrazinamide molecules interact with each other and these interactions increase with the concentration,

2) interactions exist between pyrazinamide molecules and the urea derivatives.

It can therefore be expected that in the vapor phase pyrazinamide molecules interact with each other too. Nonetheless, the equilibrium concentrations of single pyrazinamide molecules, pyrazinamide dimers, and interspecies dimers will be affected by their interaction energies and the temperature (Boltzmann), thus at the sublimation temperature less dimers are expected than at room temperature. Borba et al.[137] calculated the energy of the pyrazinamide dimer in the gas phase and it was found to be $E = 46.6\ \text{kJ mol}^{-1}$ for a double hydrogen bond of N-H···O. Using the Boltzmann distribution based on this energy, the proportion of dimer again monomer in the gas phase can be calculated at 393 K resulting in a presence of about 98.6% dimer. This can be expressed in an equation in which single pyrazinamide molecules are in dynamic equilibrium with dimers:

$$\text{PZA} + \text{PZA} \rightleftharpoons \text{PZA-PZA} \tag{VI.1}$$

If the urea derivatives are added to the vapor phase, a second equilibrium will come into play, that between a pyrazinamide dimer and the urea derivative (AD) (eq VI.2):

$$\text{PZA-PZA} + \text{AD} \rightleftharpoons \text{PZA} + \text{PZA-AD} \tag{VI.2}$$

The two equations suggest that adding the urea derivatives to the sublimation medium will increase the number of pyrazinamide molecules that can be brought into the vapor phase above the number that would exist in the gas phase based on its own sublimation pressure alone as long as a sublimation source is present; this may help increase the crystallization rate.

Investigating first the effect of tetramethylurea will facilitate the interaction analysis, because it eliminates the hydrogen bond donors on the additive and hence, only the interactions between the carbonyl oxygen on tetramethylurea and the hydrogens of the pyrazinamide amide group will need to be considered for the most likely interaction between the two species. Summarizing the data from section VI.4.3.3, the {010} aspect ratio in the presence of tetramethylurea points to little relative change for the {010}, (100) and (-100) faces. The reciprocal-faces distribution for (002) and (00-2) does not show a significant change either. The reciprocal-faces ratio distribution of (-102) demonstrate that the difference in growth rate between the faces (-102) and (10-2) narrows dramatically. In particular either the (-102) face or the (10-2) face exhibits a significant relative slowdown in growth rate in comparison to sublimation-deposition of pure pyrazinamide, which is confirmed too by the shift in the adjacent-faces ratio distribution (Figure VI.16). Tetramethylurea may interact with pyrazinamide either in the vapor phase or on the crystal surface. For single tetramethylurea molecules, the carbonyl oxygen may interact with the low electron density regions on the crystal surface in particular faces (-102), (002), (-100) and (100). Because the amide hydrogens represent the lowest electron density, tetramethylurea most likely interacts with the (002) and (100) faces. In the vapor phase, possible tetramethylurea-pyrazinamide dimers appear to promote pyrazinamide sublimation as described in the previous section and increase the crystallization rate. If the interaction between pyrazinamide and tetramethylurea is limited to the amide hydrogens of pyrazinamide, such dimers will have different effects on different faces. The pyrazinamide oxygen is still available in the pyrazinamide-tetramethylurea dimer, which is different from the pyrazinamide dimers. This available oxygen will compete with the oxygen exposed on face (10-2). Thus, the relative growth rate on face (10-2) would slow down compared to other faces and the relative growth rate on the direction of [100] comparatively increases as experimentally observed. As all urea derivatives have a carbonyl oxygen, the growth rate of face (10-2) would exhibit a relative growth decrease in their presence.

Urea itself has a stronger effect, affecting in particular the (100) face except face (10-2). Because the (100) aspect ratio and the width-thickness ratio in the presence of urea is smaller than that in absence of urea derivatives, which means that the growth rate on [100] direction is relatively slowed down. Andreas et. al found that urea vapor is in the monomolecular form at atmospheric pressure.[296] Pyrazinamide may interact with urea and pyrazinamide-urea dimers may form in the vapor phase in the presence of urea.

While urea is involved in a dimer with pyrazinamide, the second amine group may be available for interaction with other molecules in the vapor or on the crystal surface. It may therefore compete with pyrazinamide in its interaction with the oxygen exposed on the (100) face relatively slowing down growth on this face. This would result in the {010} aspect ratio becoming smaller compared to crystals obtained in the absence of additives.

The changes in the crystal habit in the presence of 1,3-dimethylurea are similar to those in the presence of urea. Pyrazinamide molecules may interact with the oxygen atom of 1,3-dimethylurea, similar to the interaction between pyrazinamide and tetramethylurea; however, this would leave the amine groups on 1,3-dimethylurea available for other interactions. In the case of pyrazinamide interacting with one of the NH groups, the other NH group of 1,3-dimethylurea may compete with the amine group of pyrazinamide and thus affect the growth of face (100).

Acetamide shows the strongest effect. The aspect ratios and width-thickness ratio show that the growth rate in the [010] direction is larger than in other two directions. The results in Figure VI.17, VI.18, and VI.19 show that the growth rate differences between faces (002) and (00-2) and faces (-102) and (10-2) become larger in the presence of acetamide. The microscopy pictures shown in Figure VI.11, the results shown in Table VI.6 and Figure VI.16 indicate that one of face between face (10-2) and face (-102), and only of face between face (002) and face (00-2) are relatively slowed down in the presence of acetamide. In chapter V it was concluded that acetamide interacts with pyrazinamide in solution. It implies that pyrazinamide-acetamide dimers and acetamide-acetamide dimers may appear if acetamide is added to the vapor phase. Acetamide possesses an amide group like the pyrazinamide molecule, which may compete with pyrazinamide in the interaction with all crystal faces, especially faces (002), (100), and (10-2) where the lowest and highest electron density regions are exposed. Moreover, pyrazinamide-acetamide dimer formation is suggested in the literature for similar molecules[85, 113] and it was concluded that the presence of acetamide accelerated the sublimation crystallization.[85, 113] but relatively slowed down both face (10-2) and face (002).

VI.4.5 The morphology of twinned crystals

Shapes of twinned crystals obtained in the absence of the urea derivatives are shown in Figure VI.21. Compared to the single crystals discussed above, the shapes of the domains of the twinned crystals are different. (-102) or (10-2) faces are larger than their neighbors (002) or (00-2) in some of the twin domains, such as in Figure VI.21a and c.

This has not been observed for the single crystals. Another difference is a change in certain angles in the twin domains, which are close to 90°, like the crystals in Figure VI.21b and c. Some of the twinned crystals exhibit more than two twin domains and many crystals lack a clear interface, as can be observed in Figure VI.21d, e and f. Photographs of twinned crystals grown from sublimation in the presence of the urea derivatives have been presented in Figure VI.4. These crystals usually contain only two domains and possess a clear twinning boundary. No changes in the angles are observed, in contrast to the twinned crystals presented in Figure VI.21.

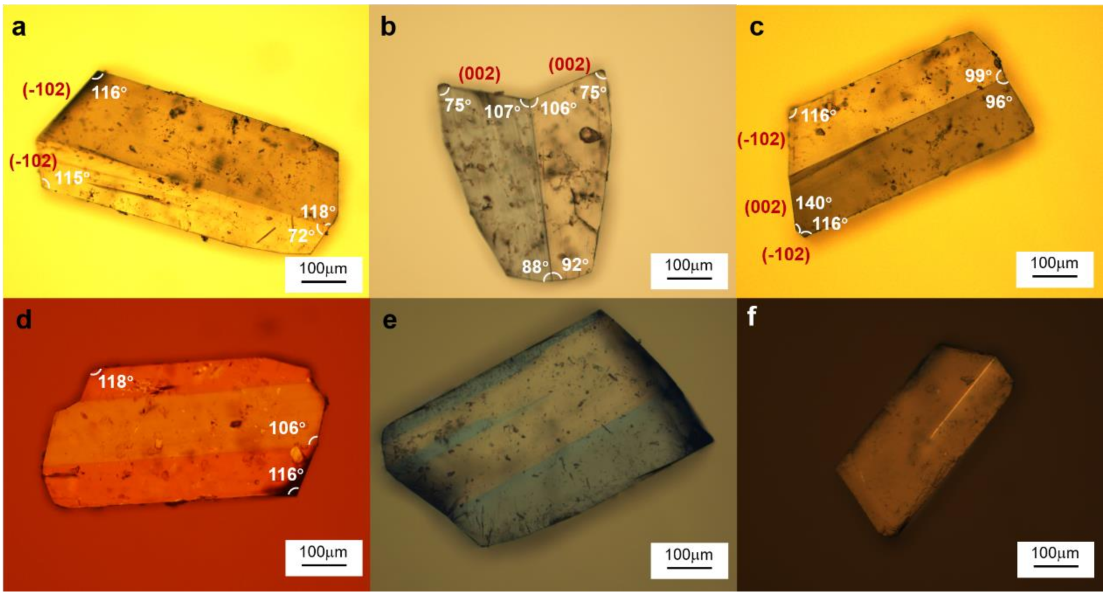

Figure VI.21 Microscopy photographs of twinned γ form crystals obtained by sublimation without the urea derivatives

VI.4.6 The nature of the disorder in crystals of the γ form

Disorder in the γ form manifests itself through two orientations of the pyrazinamide molecule on its Z' = 1 site in the unit cell (Figure VI.22).[129, 134] The unit-cell parameters of a single crystal as a function of the temperature have been listed in Table A.5. The occupancy factor of the two orientations as a function of the temperature is provided in Table VI.8. The mean orientational occupancy was consistently found to be 0.79(1) over the entire temperature range from 110 to 450 K.

Cherukuvada et al. prepared single crystals of the γ form in solution at room temperature, and SC-XRD was carried out at 100 K. The disorder site occupancy was found to be 13%.[129] Wahlberg et al. prepared a single crystal of the γ form by transforming a single crystal of the α polymorph at around 420 K and crystallographic data were collected at 122 K. The disorder site occupancy was found to be about 20%.[134] In the current experiments, crystals have been obtained by sublimation at around 390 K. The disorder site occupancy was found to be 21%. Hence, the site occupancy may be related to the crystallization method or the temperature during crystallization, but it is clear that an overall tendency for disorder exists in the γ form. Moreover, the disorder site occupancy appears to be independent of the temperature once the crystal has been formed, i.e., static disorder, as can be concluded from the data provided in Table VI.8.

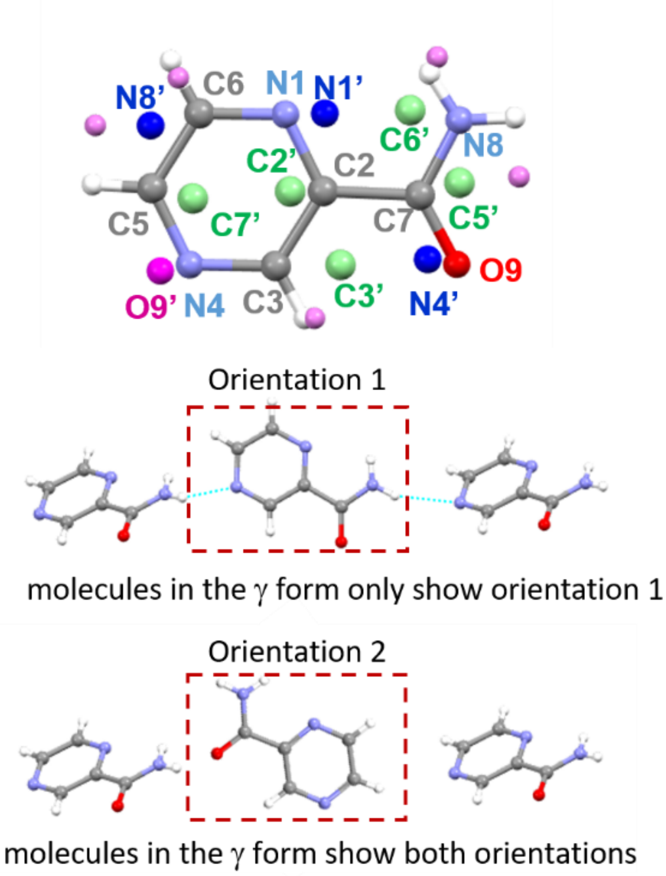

Figure VI.22 Disorder in form γ: two existing molecular orientations (around 79% of occurrence for orientation 1 and around 21% for orientation 2)

Table VI.8 Disorder in form γ: molecular occupancy factor as a function of the temperature

T/ K	Orientation occupancy (orientation 1, orientation 2)
110(1)	0.771(7), 0.229(7)
150(1)	0.795(3), 0.205(3)
200(1)	0.794(3), 0.206(3)
250(1)	0.790(3), 0.210(3)
293(2)	0.786(3), 0.214(3)
294(1)	0.793(3), 0.207(3)
294(1)	0.799(5), 0.201(5)
308(1)	0.791(4), 0.209(4)
320(1)	0.797(2), 0.203(2)
343(2)	0.789(3), 0.211(3)
355(1)	0.792(3), 0.792(3)
375(1)	0.791(3), 0.209(3)
395(1)	0.786(3), 0.214(3)
400(2)	0.790(3), 0.210(3)
415(1)	0.793(3), 0.207(3)
435(1)	0.787(3), 0.213(3)
450(1)	0.790(4), 0.210(4)

VI.4.7 The twinning interface

Through the angles between the crystal faces, the ideal twinning morphology has been determined (Figure VI.23a). Typical experimental twinning morphologies are shown in Figure VI.23b and c and Figure VI.4. The twinning morphology in the absence of urea derivatives demonstrates that the growth process changes in the case of twinning. The first change is the face marked by green star, which becomes large and even larger than its adjacent face making an angle of 107° with the twinning interface. This also happens in the presence of the urea derivatives. In addition, a distinct difference is that the angle between the two faces marked by red line seems to become almost straight. However, the morphology of twinned crystals in the presence of tetramethylurea does not show such a change and the angles remain the same as those in the ideal morphology (Figure VI.23a).

Based on the angles in the twinned crystals, and the possible arrangement of pyrazinamide molecules at the twinning interface (e.g., head-tail, head-head or tail-tail configurations) three twinning configurations can be proposed as shown in Figure VI.24. Face (10-2) is marked in red. As remarked above, the growth rate of the faces in twinned crystals is different from that of single crystals; the two domains grow symmetrically with the interface as a mirror plane. This observation excludes twinning scenario 1 (Figure VI.24).

Pyrazinamide crystals are polar and the (10-2) face contains the amide oxygens. In scenario 3, the growth along the twinning interface reduces the size of the (10-2) face leaving the oxygen atoms less exposed and the same occurs for the amine groups on the (002) faces at the other side of the twinning interface. As a result, the overall dipole of the twinned crystal is reduced with respect to a single crystal and the highly electronegative oxygen and electropositive amide hydrogens have been removed from the surface. The twinning interface is therefore most likely (100) on which amide group exposed for both domains. The proposed twinning configuration can be observed in Figure VI.24c. Although in this presentation the oxygens appear juxtaposed, on the twinning plane, these groups are actually angled and can shift along the twinning plane in order to form hydrogen bonds with the amide hydrogens, making scenario 3 even more likely.

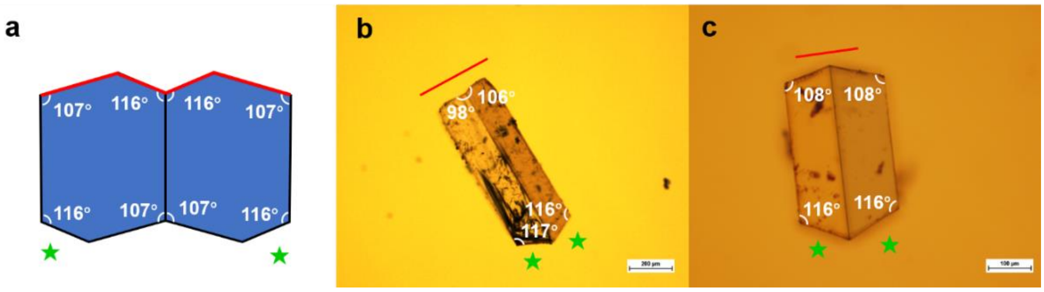

Figure VI.23 Typical twinning morphology: (a) ideal, (b) in the absence of additives, (c) in the presence of tetramethylurea

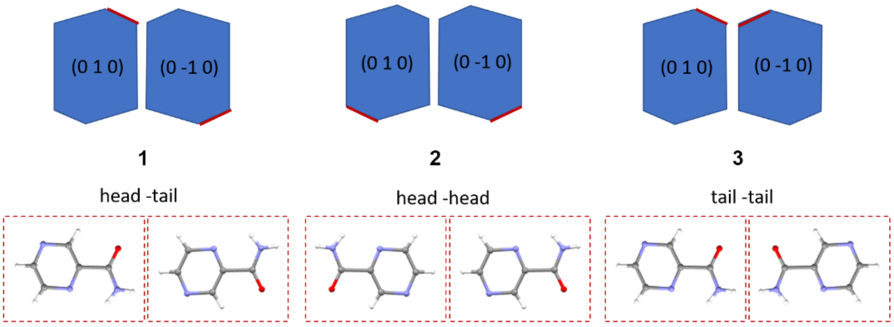

Figure VI.24 The three possible twinning configurations based on the observed angles (surface (10-2) is marked in red) and the packing arrangement of two pyrazinamide molecules at the twinning interface

VI.5 Relationship between disorder and twinning

As has been concluded just above, twinning is in part a means for the crystal to compensate its overall dipole moment. In addition, the interface is reinforced by a network of strong hydrogen bonds between the amide groups. It would appear logical to see the disorder in the same light as a means to decrease the overall dipole of the γ crystal, while the disordered molecules are kept in place by strong interactions.

As is shown in Figure VI.21d, e and f, in the absence of the urea derivatives, twinned crystals contain often more than two domains with some twinned crystals even looking like a jigsaw puzzle. The presence of urea derivatives does not eliminate twinning but optimizes them. Most of the crystals obtained in the presence of the urea derivatives have a clear interface and only contain two domains (Figure VI.4) Hence, the urea derivatives cannot prevent twinning and it should therefore be related to the molecular structure and the inherent interaction between pyrazinamide molecules[302] as mentioned at the beginning of this section.

In the energy calculations by Wahlberg et al.[134], the disordered form was modeled as a separate crystal structure, which would basically be similar to a form of twinning. Nonetheless, the calculations by these authors are the best estimate for the energy of the disordered system. Three different models were constructed by the authors: model A consisted of molecules in the ideal ordered orientation with an occupation of 0.8 in the real crystal, model B consists of 100% of the molecules in the disordered orientation and model C was the combination of A and B reflecting the observed disorder. Their result showed that the energy of model A was the lowest one, the energy of model B was 12 kJ mol^{-1} higher than model A and the energy of model C was 3 kJ mol^{-1} higher than model A. Adding entropy to this value, would bring the Gibbs energy difference between model C and A down to 3 - 1.65 = 1.35 kJ mol^{-1}. Considering that there may be a reasonable margin in the actual lattice energies calculated for the “pure” form and the disordered form, it can very well be that with the entropy, the disordered form might be the more stable one, possibly even just due to the entropic contribution.

For crystals without disorder, a pyrazinamide molecule possesses twelve short contacts (Figure VI.25b and Table VI.9, the data is obtained from the single γ crystal measured at 294 K for disorder occupancy), which are effectively six short contacts per molecule.

The strongest interaction is the N-H···N hydrogen bond with an H···N distance of 2.305 Å (3 and 8 in Figure 25b). For the molecule with orientation 2, the short contacts are shown in Figure VI.25c and Table VI.9. Some of these contacts are even shorter than those in the ordered crystal: O···H-N with 2.051 Å (2’ in Figure VI.25c), N-H···O with 2.147 Å (1’ in Figure VI.25c) and C-H···O with 2.283 Å (9’ in Figure VI.25c). Thus, it can be seen that disorder gives rise to relatively strong interactions between the amide groups, which is the main motif in the other three polymorphs of pyrazinamide, while partially compensating the crystal wide dipole moment. The physical reason behind this is that the disorder diminishes the polar aspect of the crystal, because the dipole of the disordered molecules has turned. Thus, disorder and twinning appear to have the same cause in the γ form of pyrazinamide.

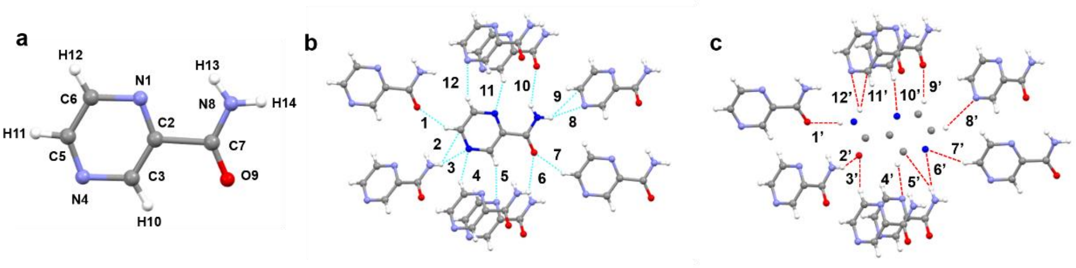

Figure VI.25 Short contacts between the pyrazinamide molecules in the γ form: (a) molecular structure of pyrazinamide, (b) short contacts in the γ form with molecule of orientation 1, (c) short contacts in the γ form with molecule of orientation 2

Table VI.9 Short contacts in the γ form with molecule of orientation 1and orientation 2

Orientation 1			Orientation 2		
Label	Short contacts	Distance/Å	Label	Short contacts	Distance/Å
1	C(5)-H(11)···O	2.476	1’	N(8)-H(14) ···O	2.147
2	C(5) ···H-N	2.848	2’	O(9) ···H-N	2.051
3	N(4) ···H-N	2.305	3’	O(9) ···H-C	2.339
4	N(4) ···H-C	2.541	4’	C(3)-H(10)-N	2.613
5	C(3)-H(10) ···N	2.598	5’	C(3) ···H-N	2.972
6	O(9) ···H-N	2.548	6’	N(4) ···H-N	2.612
7	O(9) ···H-C	2.476	7’	N(4) ···H-C	2.925
8	N(8)-H(14) ···N	2.305	8’	C(5)-H(11) ···N	2.729
9	N(8)-H(14) ···C	2.848	9’	C(6)-H(12) ···O	2.283
10	N(8)-H(13) ···O	2.548	10’	N(1) ···H-C	2.566
11	N(1) ···H-C	2.598	11’	N(8)-H(13) ···C	3.237
12	C(6)-H(12) ···N	2.541	12’	N(8)-H(13) ···N	2.798

VI.6 Conclusion

In this chapter, the effects of urea derivatives on the crystallization process in sublimation and on the γ form morphology have been discussed. The twinning interface, the nature of the disorder and the relationship between twinning and disorder have been discussed too.

1) By measuring "induction time" and sublimation time, it is found that urea derivatives dramatically accelerate the crystallization of the γ form of pyrazinamide. Combined with the results presented in the last chapter, it can be inferred that the pyrazinamide molecule interacts with the urea derivatives and tends to form PZA-UD dimers in the vapor phase next to PZA-PZA dimers. Adding the urea derivatives creates therefore a new dynamic equilibrium and as a result more pyrazinamide molecules will be present in the gas phase accelerating the crystallization process.

2) The morphologies of the γ form crystals have been studied by experimental and computational methods. The effect of the urea derivatives (acetamide, urea, 1,3-dimethylurea, 1,3-diethylurea and tetramethylurea) on the morphology has been statistically investigated. The aspect ratio, the width-thickness ratio, the adjacent-faces ratio and the reciprocal-faces ratio have been determined and have been used to compare the changes in crystal morphology in the absence and in the presence of the urea derivatives. Dimerization between pyrazinamide and urea derivatives in the vapor phase must be the main cause of the increase in the relative growth rate of different surfaces. For tetramethylurea, its oxygen interacts with the hydrogen of the amide group of pyrazinamide, thus it limits the interaction between the pyrazinamide amine and the oxygen exposed on face (10-2) and relatively slows down the growth rate of this face. The main influence of urea and of 1,3-dimethylurea on crystal habit is similar. After forming dimers with pyrazinamide, the free amine group on urea, 1,3-dimethylurea, or 1,3-diethylurea, may interact with the crystal surface and relatively slow the growth for the (100) face for example. Acetamide mainly affects the faces with exposed amide groups such as faces (002), (100), and (10-2), which may be due to its capability to form strong double hydrogen bonds with pyrazinamide and that in combination with a high vapor pressure.

3) The SC-XRD measurements as a function of the temperature demonstrate that the disorder site occupancy is independent of the temperature, which suggests that the disorder is static. The twinning interface is most likely face (100). The orientation and

interactions of ‘disordered’ molecules and those of the molecules on the twin boundary are similar, while both effects somewhat counteract the crystal wide dipole moment. Thus, disorder and twinning are inherent to the γ form and disorder may give rise to twinning during crystallization.

Chapter VII: The effect of urea derivatives on the γ form of pyrazinamide obtained through spray drying

VII.1 Introduction

From the foregoing chapters, it has become clear that the interactions between pyrazinamide and 1,3-dimethylurea are similar to those of other urea derivatives in solution and in the vapor phase. It implies that the interactions of 1,3-dimethylurea as such are not the only factors that explain the persistence of form γ at room temperature for spray dried samples in the presence of 1,3-dimethylurea. The way how form γ crystalizes in the presence of additives may play a role in its persistence. Thus, in this chapter the spray drying process is analyzed. The effects of the spray drying inlet temperature and of co-spray drying of pyrazinamide with various urea derivatives on the persistence of form γ is studied. Based on parameters obtained from the experiments, the temperature profile during the spray drying process is evaluated. Mixtures of pyrazinamide with urea derivatives have been investigated by DSC and the solubilities of those urea derivatives in water have been determined too. Finally, ternary phase diagrams have been drawn to study the drying and solidification process in spray drying. The chapter will be concluded with an evaluation of which factors are important for the stabilization of the γ form.

VII.2 Spray drying experiments

VII.2.1 Effect of the inlet temperature

The effect of the spray dryer's inlet temperature on the resulting pyrazinamide polymorph has been studied. Spray drying experiments were carried out with different inlet temperatures: 353 K (80 °C), 373 K (100 °C), 393 K (120 °C), 413 K (140 °C), and 423 K (150 °C). All other parameters including concentration, solvents, feed rate, gas flow, and vacuum pump rate were kept constant to allow comparison between the experiments; the details have been described in section II.4.4. The PXRD patterns of the obtained powder samples are provided in Figure VII.1. Pyrazinamide sprayed with inlet temperatures of 353 K, 373 K, and 393 K, results in pure γ form. At 413 K and 423 K, a peak related to the α form appears in the PXRD pattern. Baaklini et al. also found that samples sprayed at 423 K exhibited mixtures of polymorphs; however, in their case, the mixture contained γ and δ.[4] They suggested that fast evaporation of the solvent at 423 K causes the appearance of δ.

The γ form samples obtained by spray drying at different inlet temperatures were stored at room temperature in closed vials and frequently observed by PXRD to monitor their stability. The result is presented in Figure VII.2. The sample prepared at 353 K retained the γ form for more than one month. In the samples prepared at 373 K and 393 K other polymorphs appeared within three weeks. It appears therefore that the persistence of samples prepared at higher inlet temperatures are worse than those prepared at 353 K. SEM micrographs of the powder samples of the γ form obtained at the different temperatures are presented in Figure VII.3. The sample at 353 K was observed after 18 days of storage; the other samples were observed on the second day after preparation. The product obtained with an inlet temperature of 353 K consists of well-defined crystals; however, in the product produced with an inlet temperature of 373 K, many spherical crystalline agglomerates are present. The spherical agglomerates contain many small crystals, which possibly are of poor crystallinity. The large specific surface area of these crystallites in addition to possible defects may accelerate the transition from γ into α, which is the more stable phase at room temperature.[303] Because δ is also more stable than the γ form at room temperature,[128, 129] this polymorph is likely to appear too on drying and aging of the γ form samples.

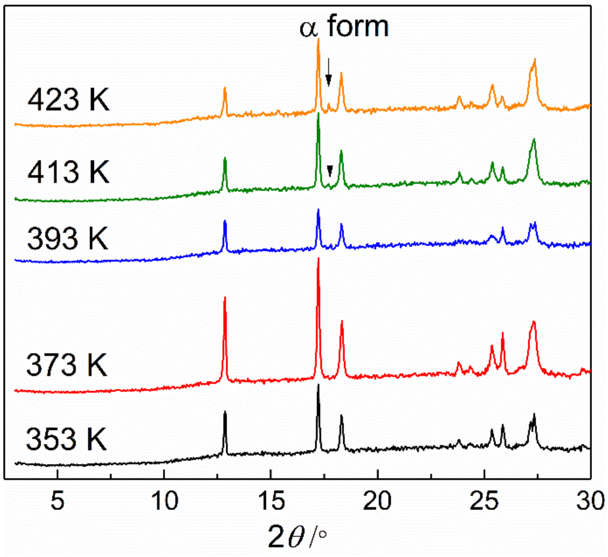

Figure VII.1 Powder X-ray diffraction patterns of pyrazinamide samples obtained by spray drying at inlet temperatures from 353 K (black) up to 423 K (orange) measured directly after the spray drying

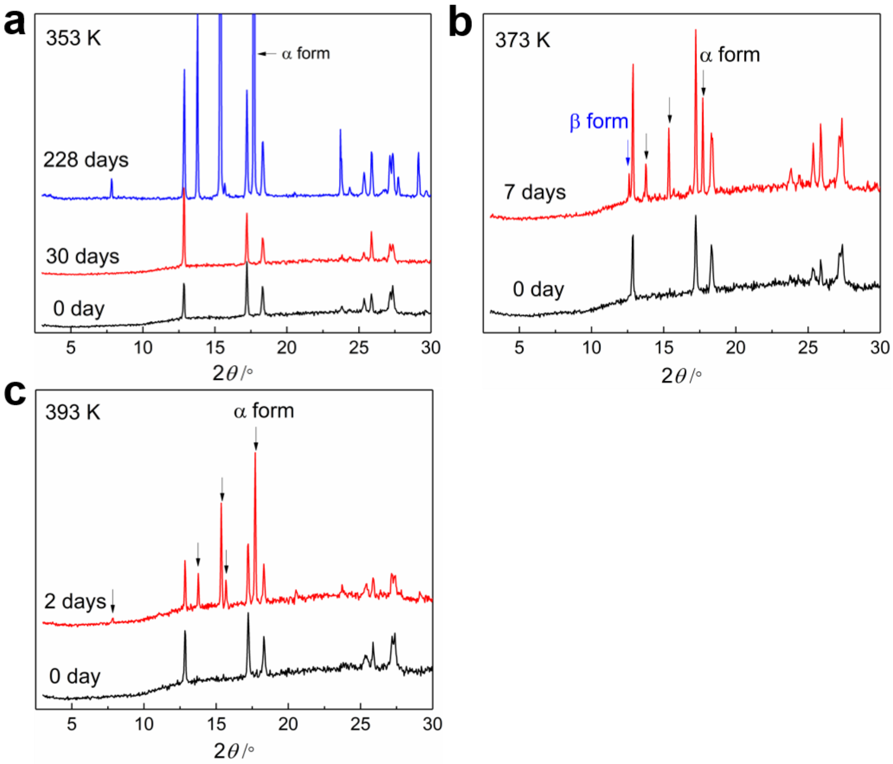

Figure VII.2 Powder X-ray diffraction patterns of pyrazinamide samples obtained by spray drying at the inlet temperature of (a) 353 K, (b) 373 K and (c) 393 K measured after different storage time intervals[6]

---

[6] Because of the confinement due to the COVID 19 pandemic and a long additional time that the PXRD equipment was out of order, a more precise time of transition could not be determined

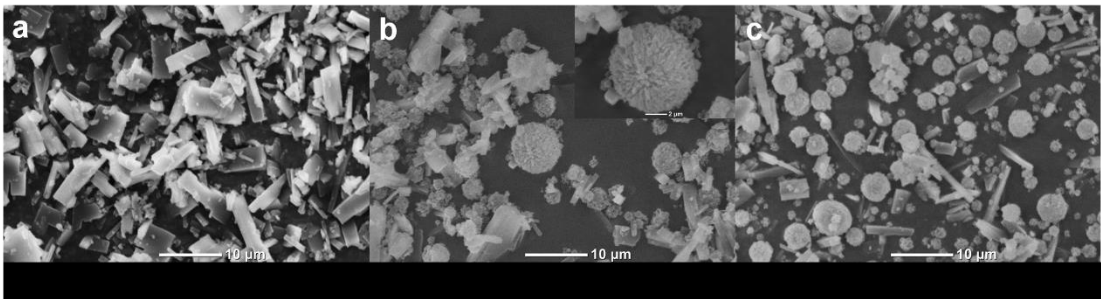

Figure VII.3 SEM micrographs of the γ form obtained by spray drying at different inlet temperatures: (a) 353 K, (b) 373 K, and (c) 393 K

VII.2.2 Co-spray drying of pyrazinamide with urea derivatives

Urea, *N*-methylurea, 1,1-dimethylurea, 1,3-dimethylurea, trimethylurea, 1,1-diethylurea, 1,3-diethylurea, and tetramethylurea were used as additives in co-spray drying experiments with an inlet temperature of 373 K. In addition, co-spray drying of pyrazinamide with 1,3-dimethylurea and 1,3-diethylurea was carried out at 353 K too.

VII.2.2.1 Urea

The product obtained by co-spray drying pyrazinamide in the presence of urea was analyzed by PXRD. It was found to be a mixture of γ and polymorph I of urea. Samples were monitored every one or two days and the α form appeared after 10 to 14 days depending on the sample (Figure VII.4). This is consistent with previous findings.[4]

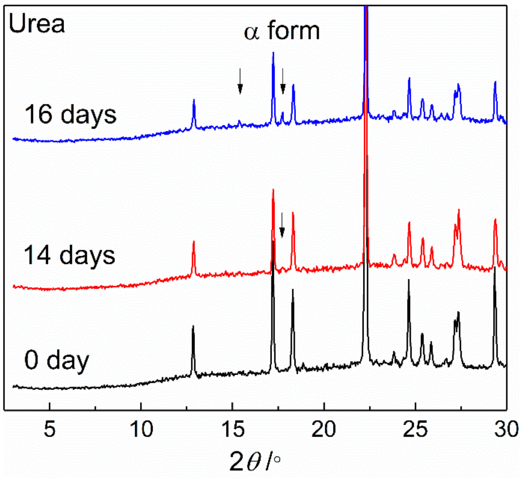

Figure VII.4 Powder X-ray diffraction patterns of the γ form obtained by spray drying in the presence of urea measured directly after spray drying and after 14 and 16 days

VII.2.2.2 *N*-Methylurea

Spray drying a pyrazinamide and *N*-methylurea mixture resulted in the γ form with a mixture of two *N*-methylurea polymorphs which were form I and form II (determined by Baaklini)[4]. This result has been reported previously as well by Baaklini.[4] During storage, form II of *N*-methylurea and form γ transformed into more stable polymorphs at room temperature, as is shown in Figure VII.5. For pyrazinamide, form α appeared after 5 days up to 1 month depending on the sample.

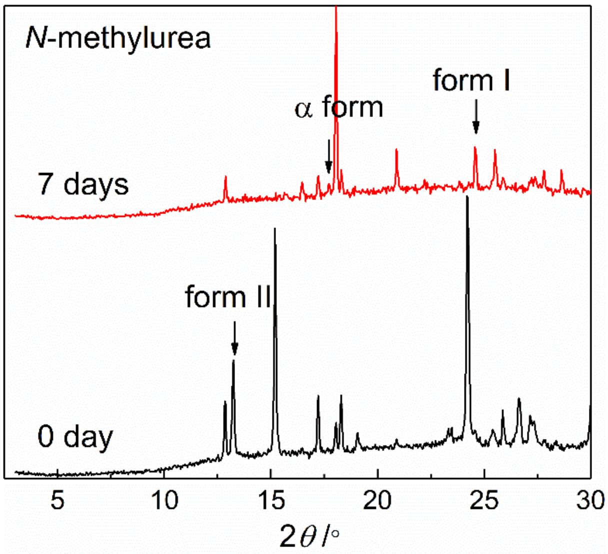

Figure VII.5 Powder X-ray diffraction patterns of the γ form obtained by spray drying in the presence of *N*-methylurea measured directly after spray drying and after 7 days

VII.2.2.3 1,1-Dimethylurea

Powder obtained by spray drying pyrazinamide with 1,1-dimethylurea in an acetone-water solution was a mixture of the γ form and the commercial polymorph of 1,1-dimethylurea (named form I here). Pyrazinamide form δ was detected in the PXRD patterns within 3 days to 1 week depending on the sample (Figure VII.6).

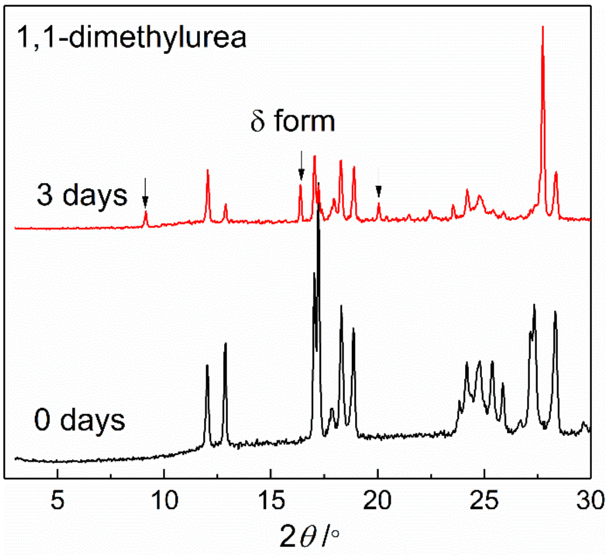

Figure VII.6 Powder X-ray diffraction patterns of the γ form obtained by spray drying in the presence of 1,1-dimethylurea measured directly after spray drying and after 3 days

VII.2.2.4 1,3-Dimethylurea

Co-spray drying experiments of pyrazinamide with 1,3-dimethylurea were carried out with inlet temperatures of 353 K and of 373 K. The resulting samples were mixtures of polymorph γ and form I of 1,3-dimethylurea; both are stable at high temperature. The PXRD patterns are provided in Figure VII.7. The PXRD pattern of the sample prepared at 373 K exhibits a small peak belonging to α after nine months. The samples prepared at 353 K have not changed for more than 7 months at the moment of observation. SEM micrographs of these samples are provided in Figure VII.8. There are no spherical particles in the mixture of pyrazinamide and 1,3-dimethylurea as observed in the pure pyrazinamide samples. Spray dried samples of pure 1,3-dimethylurea were obtained under the same spray drying conditions. The PXRD pattern presented in Figure VII.9a demonstrates that 1,3-dimethylurea consists of form I, but part must be amorphous. A SEM micrograph of a spray dried 1,3-dimethylurea sample can be seen in Figure VII.9b. The crystals of 1,3-dimethylurea have an irregular shape as if it were still liquid; however, in the mixture of pyrazinamide and 1,3-dimethylurea samples, all crystals are well defined with regular shapes.

Gas chromatography experiments carried out for the current study (section VI.4.1.2) demonstrate that no trace of 1,3-dimethylurea can be found in the pyrazinamide crystals. The Raman mapping of the mixture shown in Figure VII.10a (from Baaklini)[4] indicates that pyrazinamide and 1,3-dimethylurea form a heterogeneously dispersed ("eutectic") mixture of particles. Figure VII.10b (from Baaklini)[2, 4] contains a Raman spectrum of a pyrazinamide particle, which shows the presence of small amounts of 1,3-dimethylurea (Form I). Taking into account the findings in this thesis and the binary phase diagram of pyrazinamide and 1,3-dimethylurea constructed by Baaklini lacking any trace of solid solution[4], it can be stated that this system most likely does not form solid solutions in any significant quantity.

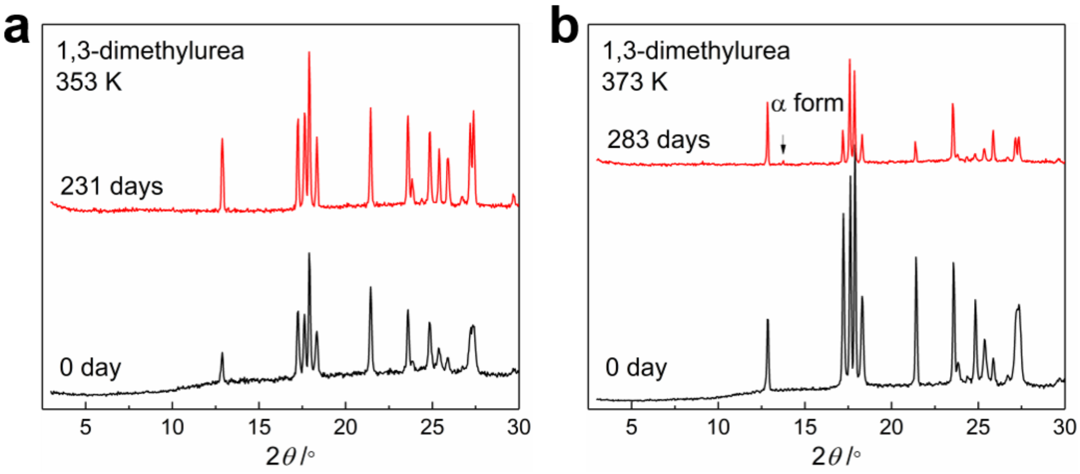

Figure VII.7 Powder X-ray diffraction patterns of the γ form obtained by spray drying in the presence of 1,3-dimethylurea at an inlet temperature of (a) 353 K and (b) 373 K measured after different storage times

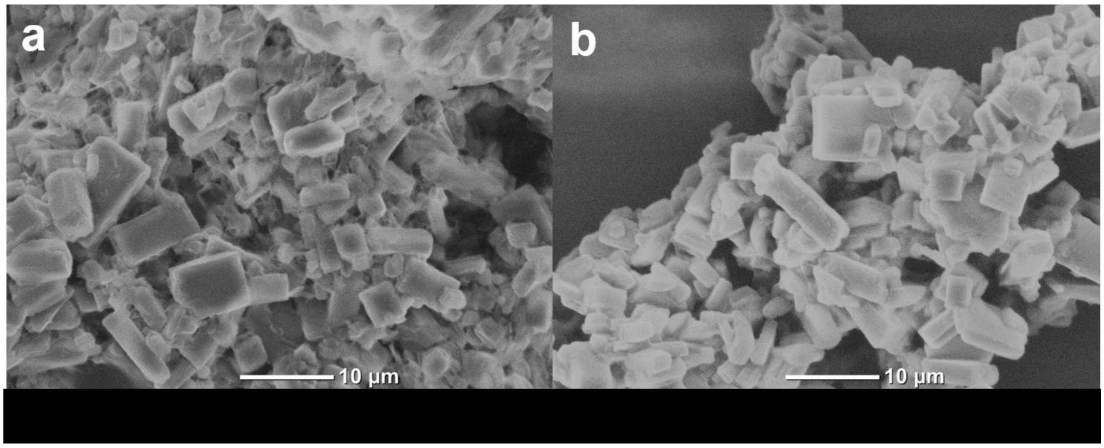

Figure VII.8 SEM micrographs of γ pyrazinamide obtained by spray drying in the presence of 1,3-dimethylurea at inlet temperature (a) 353 K and (b) 373 K

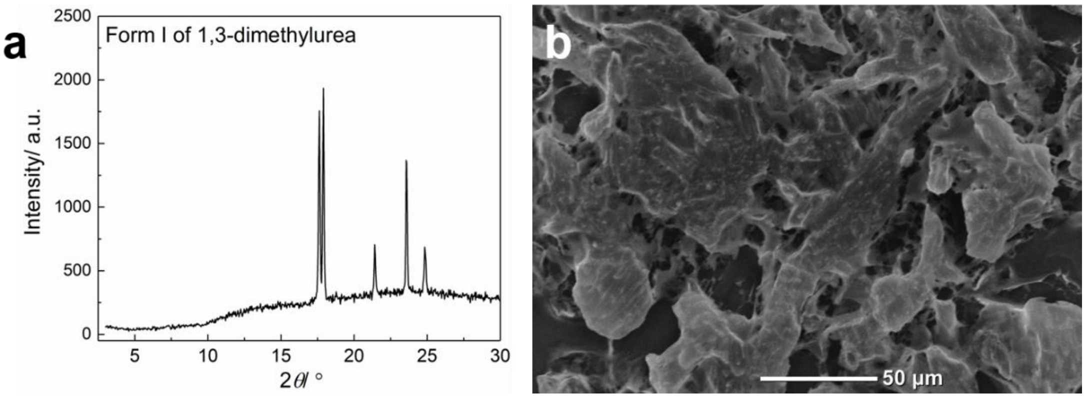

Figure VII.9 Powder X-ray diffraction pattern and SEM micrograph of 1,3-dimethylurea obtained by spray drying at an inlet temperature of 373 K

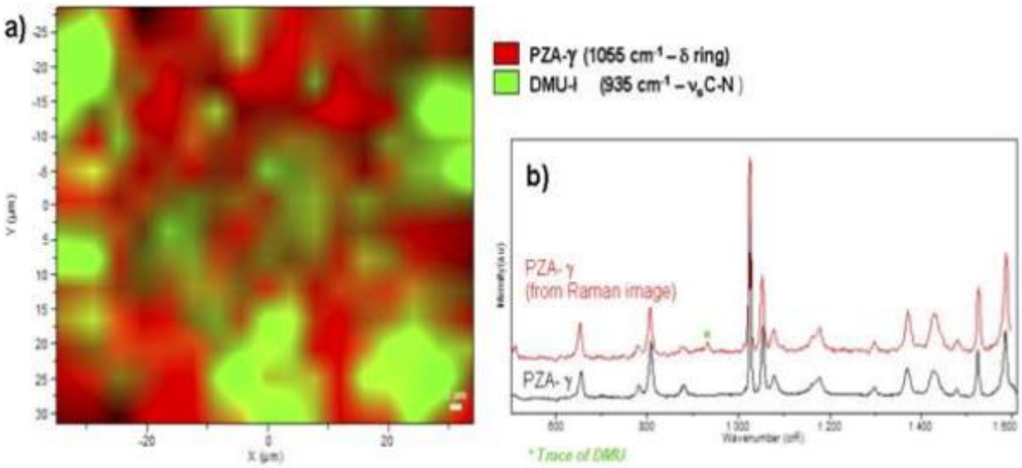

Figure VII.10 (a) Raman mapping of co-spray dried pyrazinamide in the presence of 1,3-dimethylurea, (b) comparison between the reference spectrum of pyrazinamide γ and the spectrum of pyrazinamide extracted from the Raman image[7]

VII.2.2.5 Trimethylurea

The concentration of pyrazinamide and trimethylurea solution used in co-spray drying experiments was 5 mg mL^{-1} solvent as for the other solutions. The mass fraction of pyrazinamide and trimethylurea in the initial solution is the same, however, after spray drying only a few small peaks of trimethylurea can be observed and these peaks disappear during storage. The persistence time of γ form in these samples varies greatly. In part of the samples form δ appeared after about two weeks; however, some samples

---

[7] Reprinted from International journal of pharmaceutics, 479, Baaklini, G, Dupray, V, Coquerel, G, Inhibition of the spontaneous polymorphic transition of pyrazinamide γ form at room temperature by co-spray drying with 1, 3-dimethylurea, page 167, Copyright (2015), with permission from Elsevier.

remained in form γ for more than 50 days. One of the samples remained unchanged at room temperature for more than eight months (Figure VII.11). The SEM micrograph in Figure VII.12 shows that the shape of the crystals is regular and no agglomerated spherical crystals can be observed. This morphology is similar to the crystals obtained in the presence of 1,3-dimethylurea. In contrast, Baaklini[4] found that γ obtained in the presence of trimethylurea starts to convert into other polymorphs after 10 days to one month. Considering the current findings, it seems likely that sample stability is related to the crystallization conditions during the spray drying process.

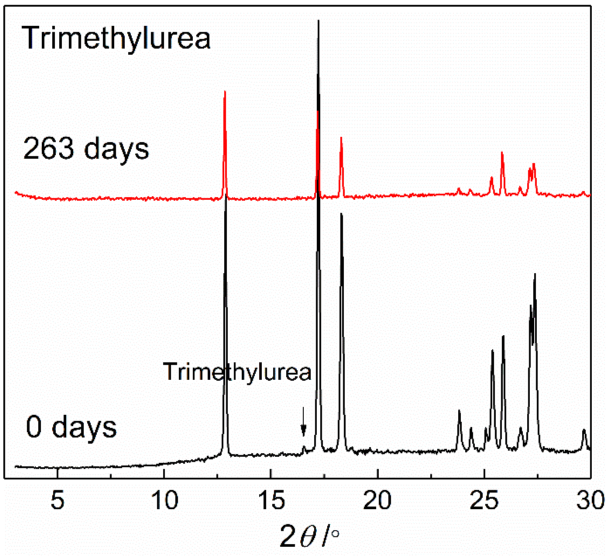

Figure VII.11 Powder X-ray diffraction patterns of the γ form obtained by spray drying in the presence of trimethylurea directly after spray drying and after 263 days

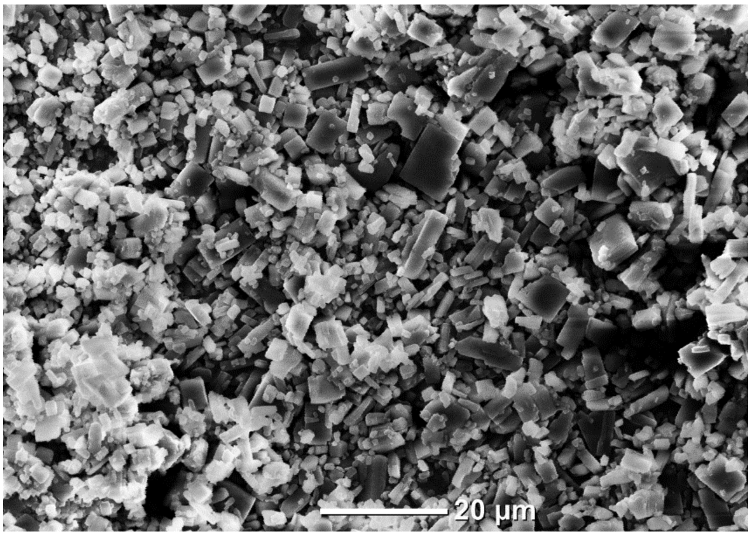

Figure VII.12 SEM micrograph of form γ obtained by spray drying in the presence of trimethylurea at 373 K (after 48 days)

VII.2.2.6 1,1-Diethylurea

Co-spray dried mixtures of pyrazinamide and 1,1-diethylurea were analyzed by PXRD. They were found to be mixtures of γ pyrazinamide and the commercial form of 1,1-diethylurea with a space group of *C*2/*c*. The α form of pyrazinamide was detected after about two weeks of storage. (Figure VII.13).

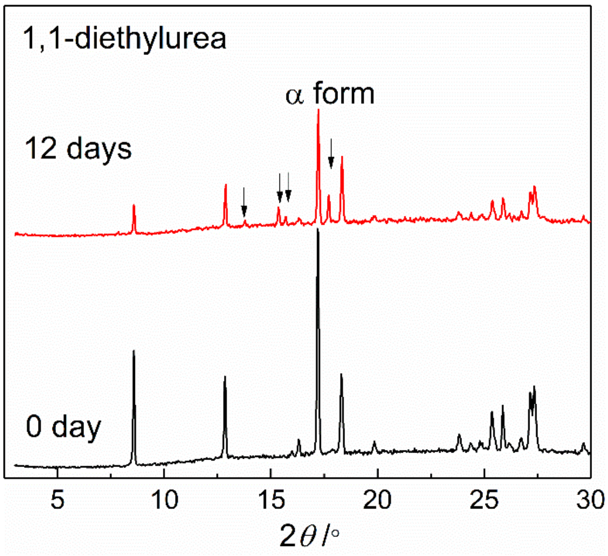

Figure VII.13 Powder X-ray diffraction patterns of the γ form of pyrazinamide obtained by spray drying in the presence of 1,1-diethylurea directly after spray drying and after 12 days

VII.2.2.7 1,3-Diethylurea

Spray drying experiments with pyrazinamide in the presence of 1,3-diethylurea were carried out at inlet temperatures of 353 K and 373 K. In co-spray drying experiments, the γ form of pyrazinamide and two polymorphs of 1,3-diethylurea (α and β form named by Della et al.[224]; DSC curves of 1,3-diethylurea showed a phase transition from form α to form β at about 348 K (see also Figure E.1 in Appendix E)) were obtained (Figure VII.14). The γ form prepared at 373 K did not transform at room temperature up to three weeks and sometimes up to more than two months. γ prepared at 353 K remains unchanged for more than 7 months. During storage, the β polymorph of 1,3-diethylurea transformed into the commercial one (α form) (shown in Figure VI.14a). Thus, the nature of the additive's polymorph appears not to be important for the enhancement of the persistence of form γ in the case of 1,3-diethylurea. The habit of the crystals is shown in Figure VII.15. The crystals are similar to those obtained in the presence of 1,3-dimethylurea.

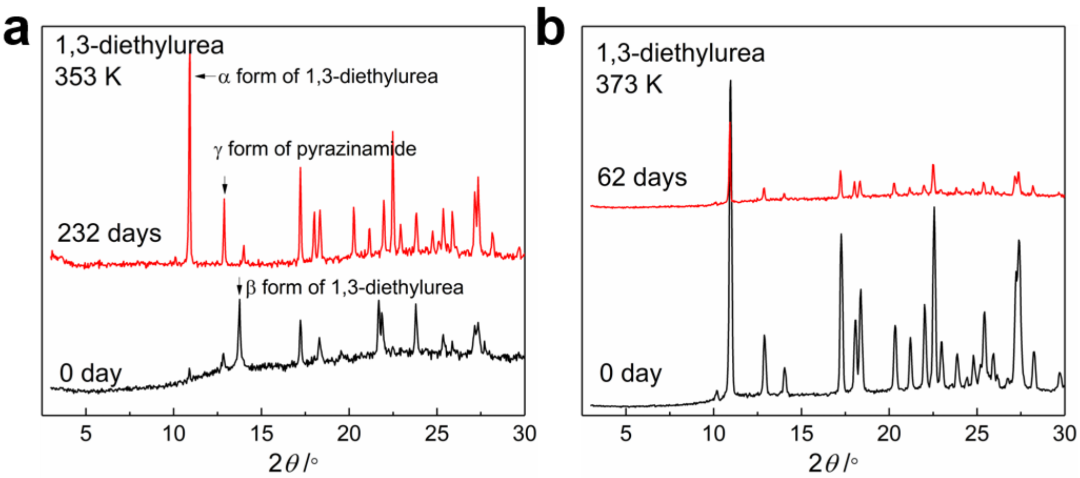

Figure VII.14 Powder X-ray diffraction patterns of the γ form of pyrazinamide obtained by spray drying in the presence of 1,3-diethylurea at an inlet temperature of (a) 353 K and (b) 373 K measured at different storage times

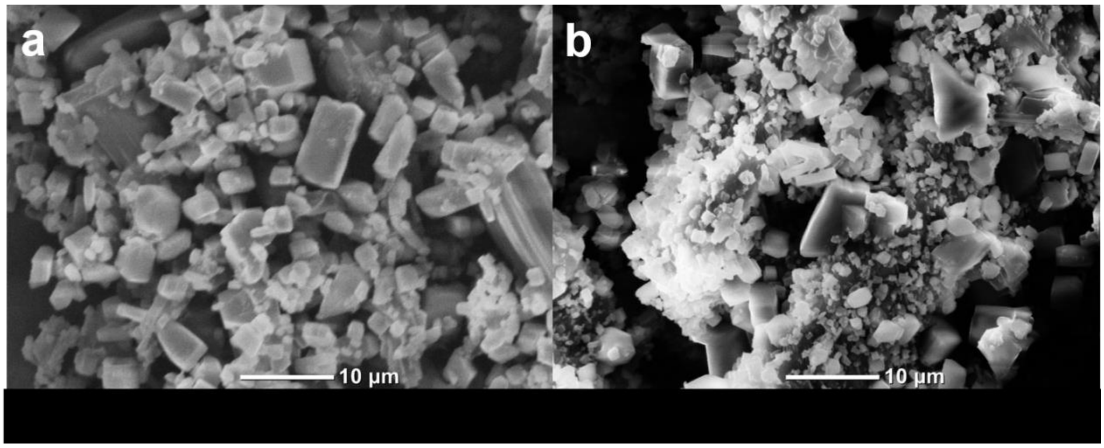

Figure VII.15 SEM micrograph of γ obtained in the presence of 1,3-diethylurea obtained by spray drying at (a) 353 K, (b) 373 K

VII.2.2.8 Tetramethylurea

Co-spray drying experiments of pyrazinamide in the presence of tetramethylurea were carried out at inlet temperature of 373 K. The PXRD pattern is presented in Figure VII.16. Since tetramethylurea is liquid at room temperature, the spray dried sample does not contain crystalline of tetramethylurea and contains only pyrazinamide. The PXRD shows that the spray dried sample contains amorphous material and pyrazinamide form γ; form α appeared within 2 weeks.

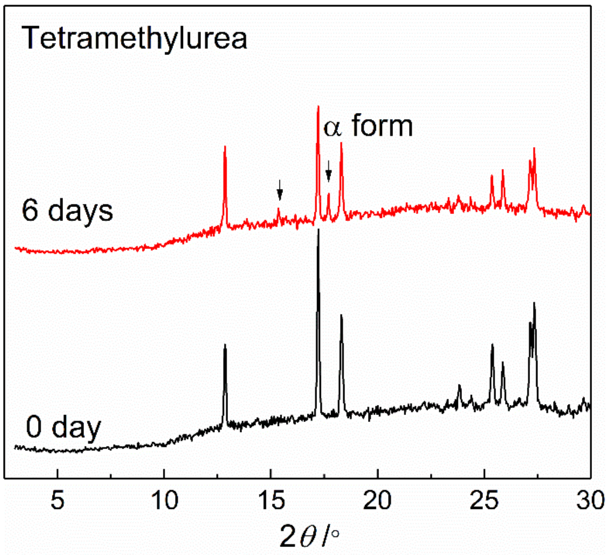

Figure VII.16 Powder X-ray diffraction patterns of the γ form of pyrazinamide obtained by spray drying in the presence of tetramethylurea measured directly after spray drying and after 6 days

VII.2.2.9 Overview of form γ persistence in co-spray dried samples

The γ form persistence in co-spray dried samples prepared at 373 K is summarized in Table VII.1. It is clear that form γ obtained by spray drying pyrazinamide in the presence of 1,3-dimethylurea is kept for a longer time compared to that obtained by co-spray drying with the other urea derivatives; however, some samples, like those obtained in the presence of trimethylurea and 1,3-diethylurea can remain 'pure' γ for more than two months.

Table VII.1 Persistence time of the γ form in co-spray dried samples prepared at 373 K

Sample	Transition time /days
pyrazinamide	7-21
pyrazinamide-urea	10-14
pyrazinamide-*N*-methylurea	5-30
pyrazinamide-1,1-dimethylurea	3-7
pyrazinamide-1,3-dimethylurea	>60
pyrazinamide-trimethylurea	>14
pyrazinamide-1,1-diethylurea	<14
pyrazinamide-1,3-diethylurea	>21
pyrazinamide-tetramethylurea	<14

VII.3 Estimating the temperature profile in the evaporating droplet

The results demonstrate that the spray drying conditions have an important influence on the persistence time of form γ in the final product. For spray drying experiments carried out with inlet temperatures of 353 K or 373 K, the outlet temperature is plotted as a function of time (Figure VII.17). The outlet temperature starts out high and decreases rapidly in the first two minutes; then it tends to remain constant. For the inlet temperature of 353 K, the outlet temperature stabilizes at 315 K. For an inlet temperature of 373 K, the stabilized outlet temperature is 325 K.

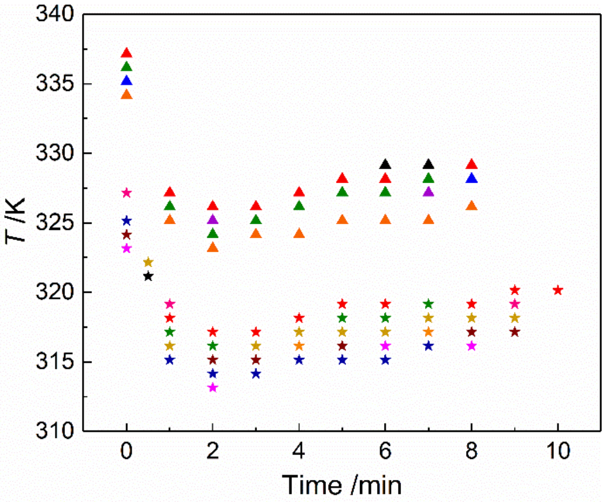

Figure VII.17 Outlet temperature of the spray dryer main chamber as a function of the operation time at inlet temperatures of 373 K (▲) and 353 K (★). Each color represents a single series of measurements

Using the inlet and outlet temperatures obtained in the experiments, the mean residence time (1-1.5 sec), which can be considered as the droplet drying time, and the particle size (1-25 μm) obtained from the operation manual[304], the droplet temperature as a function of the time was calculated using equations from the literature (see Appendix H)[305]. The resulting profiles are presented in Figure VII.18 for each inlet temperature. The size of the initial droplet is estimated to be 380 μm (diameter). Because the solvent is a mixture of water and acetone (50:50 v%) and the inlet temperature is above the boiling point of acetone, it is assumed that acetone evaporates first. Once acetone has left the droplet (50%), the volume of the droplet can be considered to be half of the original volume. The diameter of the droplet without acetone should then be 300 μm. The time acetone takes to evaporate (marked by the dashed line in Figure VII.18) is one third of the total droplet residence time in the spray chamber. Because the evaporation of acetone is fast, it can be assumed that crystallization occurs after acetone has evaporated. The droplet drying time at low inlet temperature is longer than at higher temperature when the particles have same size. It means the drying process is slower at lower inlet temperatures, which may facilitate the formation of solid particles with better powder characteristics (size, shape, size distribution).

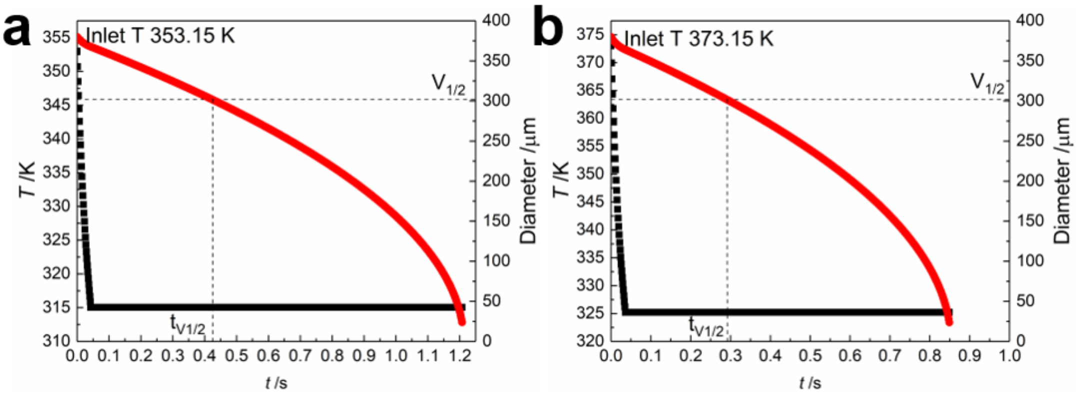

Figure VII.18 The temperature of a mean spray-dried droplet (black) and its diameter (red) as a function of its residence time in the spray chamber for the inlet temperature of (a) 353 K and (b) 373 K

VII.4 Eutectic mixtures of pyrazinamide with urea derivatives

The DSC curves with the eutectic temperatures of the mixtures of pyrazinamide with the respective urea derivatives are presented in Figures VII.19a to g. Each sample is a physical mixture of pyrazinamide with an additive. The melting points of pure pyrazinamide and pure urea derivatives, the onset temperatures of the eutectic peaks of the mixtures of pyrazinamide with the urea derivatives during heating and cooling together with the temperature difference are provided in Table VII.2. The eutectic temperatures and the crystallization temperatures of the mixtures with 1,3-dimethylurea and 1,3-diethylurea are very similar, so one would also expect similar behavior in the spray drying experiments. The eutectic temperature of the mixture with trimethylurea is close to room temperature, which implies that crystallization would happen at a very late stage in the spray drying experiment, if at all for trimethylurea.

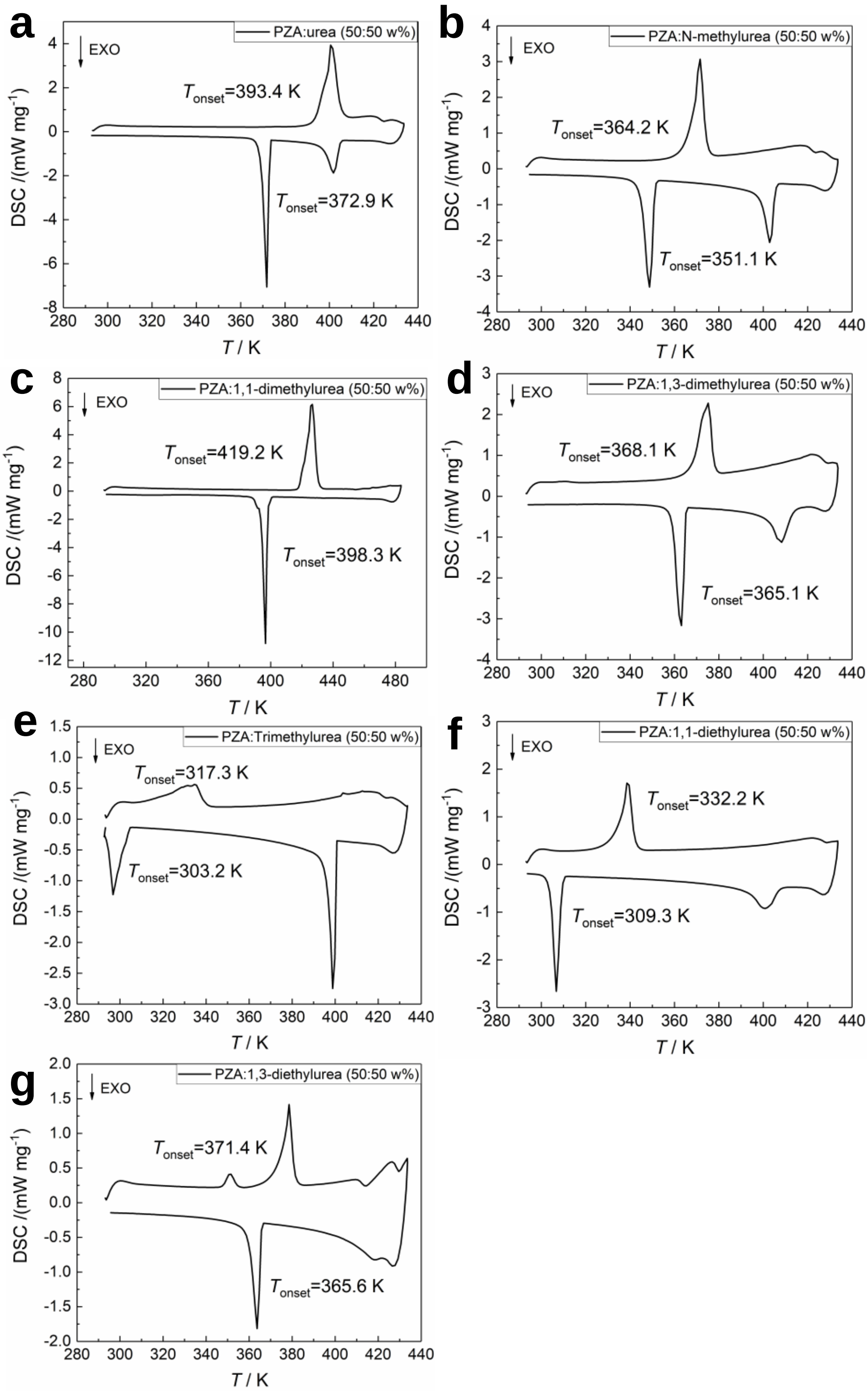

Figure VII.19 DSC curves of mixtures of pyrazinamide with the urea derivatives (a) urea, (b) *N*-methylurea, (c) 1,1-dimethylurea, (d) 1,3-dimethylurea, (e) trimethylurea, (f) 1,1-diethylurea, (g) 1,3-diethylurea

Table VII.2 Eutectic temperatures of the pyrazinamide mixtures with the urea derivatives (50:50 w%)

Mixture	Melting point of urea derivatives /K	Heating process T_{onset} /K	Cooling process T_{onset} /K	ΔT /K
pyrazinamide	457(1)[a]	-	-	-
pyrazinamide: urea	406.9[b]	393.4	372.9	20.5
pyrazinamide: *N*-methylurea	371.4[b]	364.2	351.1	13.1
pyrazinamide: 1,1-dimethylurea	455.0[b]	419.2	398.3	20.9
pyrazinamide: 1,3-dimethylurea	376.9[b]	368.1	365.1	3
pyrazinamide: trimethylurea	337.4[b]	317.3	303.2	14.1
pyrazinamide: 1,1-diethylurea	336.6[b]	332.2	309.3	22.9
pyrazinamide: 1,3-diethylurea	375.2[b]	371.4	365.6	5.8

[a] melting point of form α of pyrazinamide presented in Table IV.1 in Chapter IV.

[b] melting point of urea derivatives presented in Table VI.2 in Chapter VI.

VII.5 Solubility of urea derivatives

Because the evaporation of acetone in the spray drying process is fast, the solvent in the spray drying crystallizing mixture can be assumed to be water. The solubilities of urea, 1,1-dimethylurea, 1,3-dimethylurea, 1,1-diethylurea and 1,3-diethylurea in pure water were measured and the result is presented in Figure VII.20 and Table H.2 in Appendix H. The solubility of the different urea derivatives increases with increasing temperature; however, the solubilities of the urea derivatives show large differences. Compared to the other derivatives, the solubility of 1,3-diethylurea varies greatly with temperature. At 313 K, the solubility of urea derivatives is S(1,1-diethylurea) > S(1,3-dimethylurea) > S(1,3-diethylurea) > S(urea) > S(1,1-dimethylurea). Due to the high solubility of urea derivatives, the solubilities at higher temperature were estimated with the van't Hoff equation. The parameters are shown in Table H.2 in Appendix H. Comparing the solubility of pyrazinamide with that of the urea derivatives (See Figure VII.20 and chapter IV section IV.2.6), it is clear that pyrazinamide must crystallize before the urea derivatives during the spray-drying experiments.

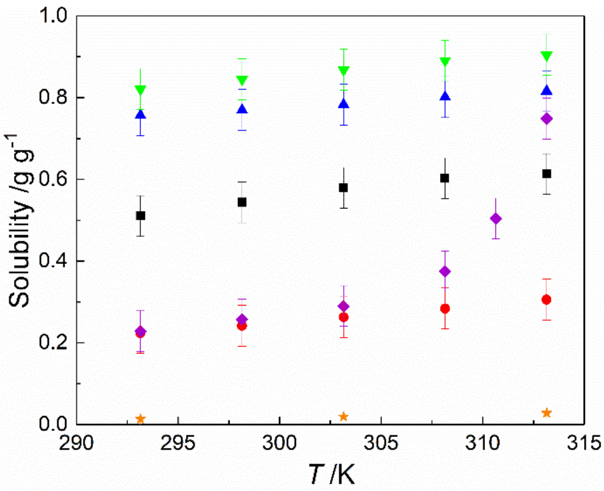

Figure VII.20 Solubilities of (■) urea, (●) 1,1- dimethylurea, (▲) 1,3-dimethylurea, (▼) 1,1-diethylurea, (◆) 1,3-diethylurea from 293.15 to 313.15 K in water and the solubility of (★) pyrazinamide form α in water (chapter IV section IV.2.6)

VII.6 Ternary phase diagrams

Ternary phase diagrams have been constructed to highlight the crystallization process. Assuming that the crystallization occurs after acetone has evaporated, the quaternary component system simplifies to a ternary component system. The pyrazinamide-urea-H_2O, pyrazinamide-1,1-dimethylurea-H_2O and pyrazinamide-1,1-diethylurea-H_2O phase diagrams at 313 K and 323 K, pyrazinamide-1,3-dimethylurea-H_2O phase diagram at 323 K have been constructed based on the solubility data of pure pyrazinamide and pure urea derivatives presented in Figure VII.20. The pyrazinamide-1,3-dimethylurea-H_2O and pyrazinamide-1,3-diethylurea-H_2O phase diagrams at 313 K have been constructed based on the solubility data of pure compound and mixtures in aqueous solution. Part of the solubility data is presented in Figure VII.21. The solubility of pyrazinamide increases in the presence of 1,3-dimethylurea and 1,3-diethylurea. It implies that crystallization of pyrazinamide in the presence of 1,3-dimethylurea or 1,3-diethylurea will occur at higher concentrations in the evaporation process. Due to the steep solubility curve of 1,3-diethylurea, the solubility at 323 K could not be obtained.

All ternary phase diagrams are provided in Figure VII.22. Due to the inability to measure the solubility of 1,3-diethylurea at 323 K, only the pyrazinamide-1,3-diethylurea-H_2O phase diagram at 313 K is presented in Figure VII.22e. Because the difference in solubility between pyrazinamide and the urea derivatives is very large, the dilute solution region is small. One clear difference of these ternary phase diagrams is the size of the S_P + L region, which is related to the solubility of the respective urea derivatives. The influence of the temperature on the ternary phase diagram is small, especially for the pyrazinamide-1,3-dimethylurea-H_2O phase diagram. For 1,3-diethylurea at 313 K, the ternary phase diagram is similar to that of pyrazinamide-1,3-dimethylurea-H_2O at 313 K. The solubility of 1,3-diethylurea at higher temperature must be much higher than its value at 313 K, which means that the S_P+ L region will be much larger than at 313 K. Because the solubility of 1,3-diethylurea is greatly affected by the temperature (Figure VII.20), a slight temperature change will cause a large change in solubility. Thus, during the spray drying process, in which the temperature in the droplet may fluctuate, the solubility of 1,3-diethylurea may sometimes reflect the solubility of 1,3-dimethylurea. This could explain why at an inlet temperature of 373 K, some of the samples obtained in the presence of 1,3-diethylurea could be maintained at ambient conditions for a long time.

In the ternary phase diagrams in Figure VII.22, the solute concentration used in the spray drying experiments is marked as a blue dot on each ternary phase diagram and it starts in the liquid region. During the evaporation process, the blue line crosses the solubility line of pyrazinamide, which will crystallize first, while the compounds 1,1-dimethylurea, urea, 1,3-diethylurea, 1,3-dimethylurea and 1,1-diethylurea will crystallize successively at a later stage. The persistence time shown in Table VII.1 indicates that the spray-dried samples in the presence of 1,3-dimethylurea and 1,3-diethylurea retain γ form for a long time at room temperature. Considering the DSC experiments, once the supersaturation of these two urea derivatives is reached, crystallization is probably very quick eliminating any further movement of the molecules. It can therefore be postulated that during droplet evaporation, a slow increase in viscosity provides a relatively controlled crystallization environment. Once most solvent has evaporated, rapid solidification of the urea derivatives results in partially amorphous material (see X-ray diffraction profiles in Fig VII.2-16) that severely limits the movement of uncrystallized pyrazinamide molecules and avoids uncontrolled formation of stacking faults or loose pyrazinamide aggregates that can quickly crystallize into a more stable polymorph. Thus, without mobility, crystallization into form α is avoided or at least extremely limited.

Additives with relatively low solubilities, like 1,1-dimethylurea, will crystallize fast themselves and therefore not significantly affect the crystallization of pyrazinamide. Additives with relatively high solubilities, like 1,1-diethylurea, will remain low viscosity liquids for most of the droplet evaporation allowing rapid crystallization of pyrazinamide during the entire spray drying process with more chance of stacking faults and α nucleation. Thus, we hypothesize that urea derivatives with the right properties in terms of solubility and eutectic temperature with pyrazinamide assist the control over the crystallization process in spray drying and lead to well-formed γ crystals with a long persistence time.

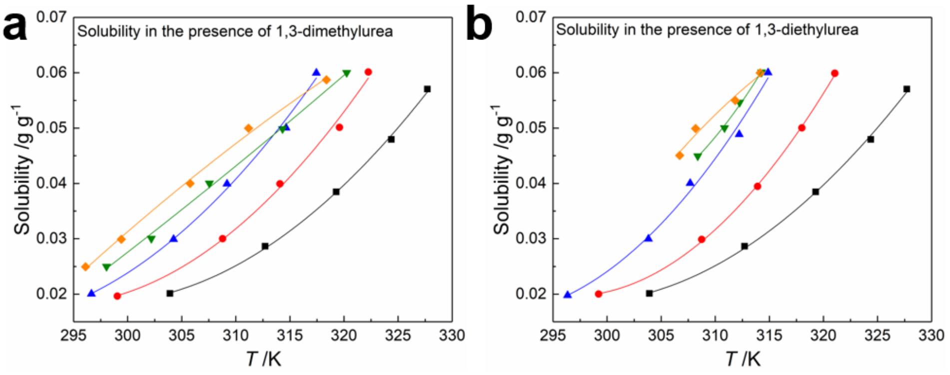

Figure VII. 21 Solubility of pyrazinamide in the presence of (a) 1,3-dimethylurea and (b) 1,3-diethylurea with (■) pure pyrazinamide, (●) pyrazinamide: urea derivatives 1:2 (w%), (▲) pyrazinamide: urea derivatives 1:4 (w%), (▼) pyrazinamide: urea derivatives 1:6 (w%), (◆) pyrazinamide: urea derivatives 1:8 (w%)

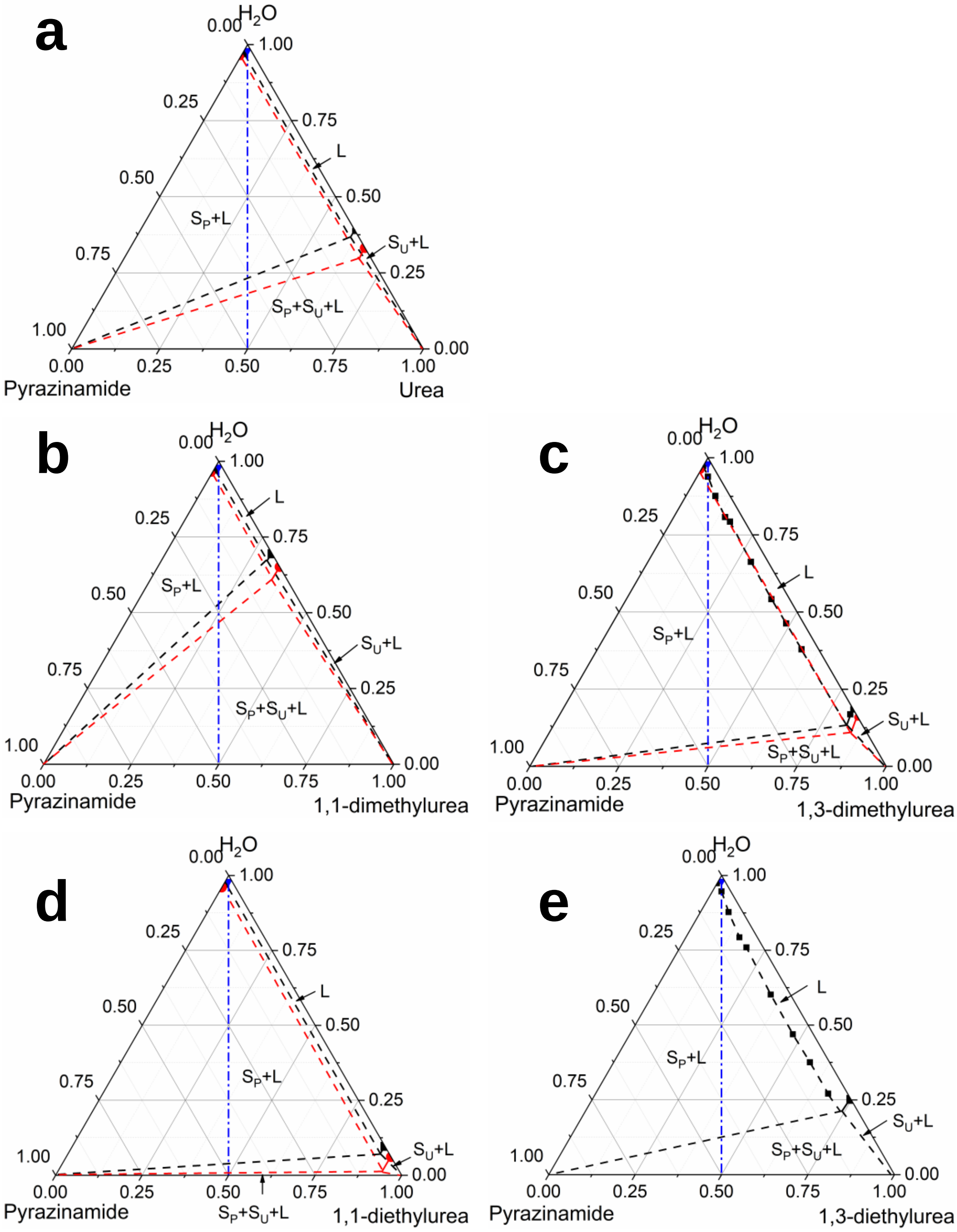

Figure VII.22 Ternary phase diagram of pyrazinamide-X-H_2O with (a) X = urea, (b) X =1,1- dimethylurea, (c) X =1,3- dimethylurea (d) X =1,1- diethylurea and (e)X = 1,3-diethylurea, (■) at 313 K, (●) at 323 K, the blue dashed line indicates the concentration evolution of the solutes during spray drying, S_P is solid phase of pyrazinamide, S_U is solid phase of urea derivatives and L is liquid phase

VII.7 Conclusion

In this chapter, the effect of the urea derivatives on the persistence of pyrazinamide's γ form prepared by spray drying was analyzed. It has been shown that the inlet temperature has an effect on the polymorphs and the habit of the resulting crystals. This may be related to the evaporation rate of the solvent in the droplets. The co-spray dried pyrazinamide samples exhibited a time persistence of γ at room temperature to varying degrees. Samples in the presence of 1,3-dimethylurea are the most persistent up to now of all urea derivatives. This result is consistent with previous findings by Baaklini.[4] In addition, some samples in the presence of trimethylurea and 1,3-diethylurea remained unchanged at room temperature for a number of months, even if most of the samples prepared with these urea derivatives converted more rapidly. The shape of the crystals obtained in the presence of the urea derivatives show better crystallinity than spray dried samples obtained with only pyrazinamide.

The DSC measurements of binary mixtures of pyrazinamide with 1,3-dimethylurea and with 1,3-diethylurea showed a rapid crystallization behavior at 365 K without much hysteresis. Considering that the spray dried droplets lose most of their water at temperatures around 315 or 325 K, it implies that pyrazinamide will have the time to crystallize from solution until the system suddenly solidifies due to lack of water. If the eutectic temperature would be too low, in the case of trimethylurea for example, then crystallization of pyrazinamide will not be slowed down until a very late stage.

The solubilities of some of the urea derivatives have been measured and they vary widely. Compared to solutions without urea derivatives, the solubility of pyrazinamide increases in their presence and it will therefore reduce the crystallization rate of pyrazinamide in the evaporating droplet.

Judging from the ternary phase diagrams and the eutectic data, it is clear that both the eutectic temperature and the solubility are important in defining the sweet spot for the crystallization and the persistence of form γ.

Chapter VIII: Conclusions and outlook

VIII.1 Conclusions

The objective of this work was to investigate the cause of the remarkable persistence of the metastable polymorph γ of pyrazinamide at room temperature obtained by spray drying in the presence of 1,3-dimethylurea.

The phase behavior between the known polymorphs of pyrazinamide were studied to determine the stable pressure and temperature domain of form γ. It has been empirically confirmed that the transition temperature between forms α and γ is about 392 K which is 20 K lower than the temperature reported in the literature. The resulting pressure-temperature phase diagram involving the polymorphs α and γ together with the liquid and the vapor phase demonstrates that form γ is stabilized by pressure and becomes stable relative to α at room temperature at a pressure of 260 MPa.

NMR results clearly demonstrated the interactions between pyrazinamide and the urea derivatives in solution. The strongest interactions between pyrazinamide and the urea derivatives are between the hydrogens of the amine groups and the carbonyl oxygens. Because both pyrazinamide and urea derivatives possess these groups, the chemical shift of the H5 proton of pyrazinamide and of the amine hydrogens in the urea derivatives change with concentration and in mixtures of these compounds.

Moreover, in the sublimation experiments, the induction time in the presence of a urea derivative is at least three times shorter than that in their absence and the complete sublimation time is significantly reduced as well. The relation between the induction time and the vapor pressure of urea derivatives shows that vapor pressure is one of the reasons that affect the sublimation crystallization but not the only one. Besides the acceleration of the crystallization rate, the changes in morphology of form γ in the presence of a urea derivative is clear. In crystals obtained in the presence of tetramethylurea, the mean size of face (10-2) becomes larger than its adjacent face (00-2). This change on face (10-2) happens in the presence of other urea derivatives. The influence of urea and of 1,3-dimethylurea on the crystal habit is similar. Face (100) is clearly affected by urea and 1,3-dimethylurea. The aspect ratio of this face is smaller than that in the absence of urea derivatives. Both the aspect ratio of face (100) and width-thickness ratio decrease in the presence of acetamide, which indicates that the growth of the (002), (100), and (10-2) faces is affected by acetamide. The carbonyl oxygen and/or the amide groups are exposed on the (10-2) and (100) faces and the changes in growth rate of these surfaces confirm the interactions demonstrated by the NMR results. The amine group is exposed on the (002) face. In the NMR results, the chemical shift of H5 in the presence of different concentrations of acetamide, 1,3-dimethylurea and tetramethylurea indicates that acetamide has the strongest effect on the chemical shift of H5, while tetramethylurea shows the weakest effect. The NMR result and the change in growth rate for this face caused by acetamide demonstrates the capability of acetamide to form strong double hydrogen bonds with pyrazinamide.

The results obtained by NMR and sublimation demonstrate that the interactions between pyrazinamide and the tested urea derivatives are similar and that 1,3-dimethylurea does not show any particular behavior towards pyrazinamide in this series of compounds.

Some samples obtained by spray drying in the presence of trimethylurea and 1,3-diethylurea exhibited a persistence time of γ form at room temperature similar to that of the samples prepared with 1,3-dimethylurea. It implies that the persistence induced by 1,3-dimethylurea on form γ is not limited to this compound.

The determination of the eutectic temperature of mixtures of pyrazinamide with urea derivatives and the ternary phase diagrams of pyrazinamide-urea derivatives-H_2O reveal the phase behavioral tendencies of the mixtures. Compared to other urea derivatives, the eutectic temperatures of the mixture of pyrazinamide and 1,3-dimethylurea and of the mixture of pyrazinamide and 1,3-diethylurea are similar, and their ternary phase diagrams at 313 K are similar. These similarities and persistence time of form γ co-spray dried samples indicate that the eutectic temperatures and the solubilities of the urea derivatives play important roles in determining the result in the spray drying process.

Thus, we postulate that the stabilizing effect of 1,3-dimethylurea on pyrazinamide should be due to the following. On the one hand, 1,3-dimethylurea works differently from insoluble additives that act as a template to induce crystallization and control the crystallizing polymorph. The solubility of 1,3-dimethylurea is much higher than the solubility of pyrazinamide, thus pyrazinamide will crystallize first during the spray drying process. The polymorph of pyrazinamide crystallizing in the absence or presence of additives in spray drying is most often form γ. On the other hand, the interactions between pyrazinamide and urea derivatives are similar. It implies that hydrogen bonding interactions between the two components in solution are not crucial for control over the crystallization process. In the spray drying process, the solvent disappears rapidly by evaporation. This causes the solution to become highly concentrated, increasing the viscosity, in particular, because of the high solubility of 1,3-dimethylurea. Once almost all the water is gone, the droplet will solidify, causing the 1,3-dimethylurea to crystallize as indicated by the eutectic obtained by DSC. Thus, the slow increase in viscosity and the sudden solidification of 1,3-dimethylurea by the end of the spray drying process affects the crystallization process of pyrazinamide and quite likely prevents stacking faults and α nuclei from forming (in large quantities). Additives with relatively low solubility will crystallize fast themselves and will have little effect on the nucleation or crystal growth of pyrazinamide. Additives with relatively high solubilities will not solidify at all or very late in the spray drying process allowing rapid crystallization of pyrazinamide during the entire spray drying process with more chance of stacking faults and α nucleation. Thus, it appears that the protective effect of 1,3-dimethylurea, and of 1,3-diethylurea to a lesser extent, purely depends on correctly tuned properties of in particular the solubility and the eutectic temperature with pyrazinamide which guides the pyrazinamide crystallization process in spray drying and leads to well-formed γ crystals with a long persistence time.

VIII.2 Outlook

1) It can be inferred from the experimental results that the spray drying process itself plays an important role in the persistence of form γ in the presence of 1,3-dimethylurea. However, there are many parameters that can affect the properties of the final product and some parameters such as the flow rate cannot be kept constant in the process. It would be of interest to optimize the spray drying parameters of the equipment, for instance the droplet size. It may be interesting to associate the spray dryer parameters with the persistence of samples. For example, the droplet size could change the final crystal size. In addition to PXRD and SEM, a particle size analyzer could be used to analyze the crystal size and its distribution. The relationship between the droplet size and the persistence of samples could be determined through the analysis of crystal size

and crystal size distribution.

2) The presence of a third component in the system (“additives”) can change the solution properties, such as viscosity, which will affect the crystallization kinetics and the powder properties, such as particle size. However, the crystallization process in spray drying is fast and process analysis techniques are lacking. Thus, if the spray drying parameters are known, simulation can be a solution to compare the crystallization process in the absence and the presence of third components. The FLUENT package of Computational Fluid Dynamics (CFD) software could be used to simulate the effect of temperature, humidity, and the flow field of gas in the spray column. This will provide information about crystallization time and droplet and particle size, solution viscosity. Comparison of the simulation results of the processes in the presence and in the absence of urea derivatives may than lead to improved control over the effect of the urea derivatives on the crystallization process during spray drying.

3) Besides the pyrazinamide samples obtained in the presence of 1,3-dimethylurea, some samples obtained with trimethylurea or 1,3-diethylurea are persistent under ambient conditions for a number of months. It implies that 1,3-dimethylurea is not the magical bullet and that other compounds show similar effects on the persistence of form γ. The intermolecular interactions between pyrazinamide and the urea derivatives are similar. The solubility of the urea derivatives on the other hand is important. Pyrazinamide γ crystals with a long persistence time may be obtained by optimizing the spray drying operation conditions with different urea derivatives, especially by controlling the solubility of the urea derivatives. Taking 1,3-diethylurea for example, the solubility of 1,3-diethylurea varies significantly with temperature compared to 1,3-dimethylurea, while their solubilities are quite similar at 313 K in water. It will be possible to find identical solubilities for 1,3-dimethylurea and 1,3-diethylurea by fine-tuning the temperature. Thus, co-spray dried pyrazinamide γ crystals obtained with 1,3-diethylurea possessing a long persistence time may be obtained by carefully adjusting the inlet temperature of the spray dryer. For urea, 1,1-dimethylurea, 1,1-diethylurea, their solubilities vary little with temperature in water like 1,3-dimethylurea and their solubilities are different from 1,3-dimethylurea below 313 K. It may be possible to use a solvent mixture to obtain a solubility similar to the one of 1,3-dimethylurea in spray drying.

4) In this work, the interactions between pyrazinamide and urea derivatives and the spray drying process have been studied. It appears that the direct molecular interactions

are not crucial to obtain persistent γ pyrazinamide crystals, but whether the interactions have an influence on the persistence-through the spray drying process is unknown. The solubility of the urea derivatives appears to be very important. It may therefore be interesting to find other molecules that cannot interact with pyrazinamide like the urea derivatives but with a solubility and glass forming ability close to that of 1,3-dimethylurea to study the importance of the interactions in the spray drying process.

Reference

[1] Hilfiker, R., *Polymorphism in the pharmaceutical industry*. ed.; Wiley Online Library: 2006; Vol. 2.

[2] Baaklini, G.; Dupray, V.; Coquerel, G., Inhibition of the spontaneous polymorphic transition of pyrazinamide γ form at room temperature by co-spray drying with 1, 3-dimethylurea. *International journal of pharmaceutics* **2015,** 479, (1), 163-170.

[3] Smets, M.; Baaklini, G.; Tijink, A.; Sweers, L.; Vossen, C.; Brandel, C.; Meekes, H.; Cuppen, H.; Coquerel, G., Inhibition of the Vapor-Mediated Phase Transition of the High Temperature Form of Pyrazinamide. *Crystal growth & design* **2018,** 18, (2), 1109-1116.

[4] Baaklini, G. Les Effets du Spray Drying sur le polymorphisme des composés pharmaceutiques et organiques. Rouen, 2015.

[5] Wunderlich, B., A classification of molecules, phases, and transitions as recognized by thermal analysis. *Thermochimica Acta* **1999,** 340, 37-52.

[6] Descamps, M., *Disordered pharmaceutical materials*. ed.; John Wiley & Sons: 2016.

[7] De Rosa, C.; Auriemma, F., *Crystals and crystallinity in polymers: diffraction analysis of ordered and disordered crystals*. ed.; John Wiley & Sons: 2013.

[8] Brandel, C. m.; Cartigny, Y.; Couvrat, N.; Eusébio, M. E. S.; Canotilho, J. o.; Petit, S.; Coquerel, G. r., Mechanisms of reversible phase transitions in molecular crystals: case of ciclopirox. *Chemistry of Materials* **2015,** 27, (18), 6360-6373.

[9] Hilfiker, R.; Von Raumer, M., *Polymorphism in the Pharmaceutical Industry: Solid Form and Drug Development*. ed.; John Wiley & Sons: 2019.

[10] Brittain, H. G., *Polymorphism in pharmaceutical solids*. ed.; CRC Press: 2016.

[11] Aitipamula, S.; Banerjee, R.; Bansal, A. K.; Biradha, K.; Cheney, M. L.; Choudhury, A. R.; Desiraju, G. R.; Dikundwar, A. G.; Dubey, R.; Duggirala, N., Polymorphs, salts, and cocrystals: what's in a name? *Crystal growth & design* **2012,** 12, (5), 2147-2152.

[12] Cruz-Cabeza, A. J., Acid–base crystalline complexes and the p K a rule. *CrystEngComm* **2012,** 14, (20), 6362-6365.

[13] Stahly, G. P., Diversity in single-and multiple-component crystals. The search for and prevalence of polymorphs and cocrystals. *Crystal growth & design* **2007,** 7, (6),

1007-1026.

[14]Romero, S.; Escalera, B.; Bustamante, P., Solubility behavior of polymorphs I and II of mefenamic acid in solvent mixtures. *International journal of pharmaceutics* **1999,** 178, (2), 193-202.

[15]Censi, R.; Di Martino, P., Polymorph impact on the bioavailability and stability of poorly soluble drugs. *Molecules* **2015,** 20, (10), 18759-18776.

[16]Babu, N. J.; Cherukuvada, S.; Thakuria, R.; Nangia, A., Conformational and synthon polymorphism in furosemide (Lasix). *Crystal Growth & Design* **2010,** 10, (4), 1979-1989.

[17]López-Mejías, V.; Kampf, J. W.; Matzger, A. J., Polymer-induced heteronucleation of tolfenamic acid: structural investigation of a pentamorph. *Journal of the American Chemical Society* **2009,** 131, (13), 4554-4555.

[18]Thun, J.; Seyfarth, L.; Butterhof, C.; Senker, J.; Dinnebier, R. E.; Breu, J., Wohler and Liebig Revisited: 176 Years of Polymorphism in Benzamide-and the Story Still Continues! *Crystal Growth and Design* **2009,** 9, (5), 2435-2441.

[19]Kelleher, J. M.; Lawrence, S. E.; Moynihan, H. A., Effect of the steric demand and hydrogen bonding capability of additives on the crystal polymorphism of sulfathiazole. *CrystEngComm* **2006,** 8, (4), 327-332.

[20]Blagden, N.; Davey, R.; Lieberman, H.; Williams, L.; Payne, R.; Roberts, R.; Rowe, R.; Docherty, R., Crystal chemistry and solvent effects in polymorphic systems Sulfathiazole. *Journal of the Chemical Society, Faraday Transactions* **1998,** 94, (8), 1035-1044.

[21]Babu, N. J.; Reddy, L. S.; Aitipamula, S.; Nangia, A., Polymorphs and polymorphic cocrystals of temozolomide. *Chemistry–An Asian Journal* **2008,** 3, (7), 1122-1133.

[22]Saifee, M.; Inamda, N.; Dhamecha, D.; Rathi, A., Drug polymorphism: a review. *International Journal of Health Research* **2009,** 2, (4).

[23]Dandekar, P.; Kuvadia, Z. B.; Doherty, M. F., Engineering crystal morphology. *Annual Review of Materials Research* **2013,** 43, 359-386.

[24]Berkovitch-Yellin, Z., Toward an ab initio derivation of crystal morphology. *Journal of the American Chemical Society* **1985,** 107, (26), 8239-8253.

[25]Dhanaraj, G.; Byrappa, K.; Prasad, V.; Dudley, M., *Springer handbook of crystal growth*. ed.; Springer Science & Business Media: 2010.

[26]Liu, X.-Y.; Bennema, P., Morphology of crystals: internal and external controlling factors. *Physical Review B* **1994,** 49, (2), 765.

[27] Tiwary, A.; Jindal, M., Crystal habit changes and dosage form performance. *Encyclopedia of Pharmaceutical Technology* **2006**, 73-74.

[28] Bravais, A., *Etudes cristallographiques*. ed.; Gauthier-Villars: 1866.

[29] Friedel, G., Etudes sur la loi de Bravais. *Bulletin de Minèralogie* **1907,** 30, (9), 326-455.

[30] Donnay, J. D. H.; Harker, D., A new law of crystal morphology extending the law of Bravais. *American Mineralogist: Journal of Earth and Planetary Materials* **1937,** 22, (5), 446-467.

[31] Docherty, R.; Clydesdale, G.; Roberts, K.; Bennema, P., Application of Bravais-Friedel-Donnay-Harker, attachment energy and Ising models to predicting and understanding the morphology of molecular crystals. *Journal of Physics D: Applied Physics* **1991,** 24, (2), 89.

[32] Hartman, P.; Perdok, W., On the relations between structure and morphology of crystals. I. *Acta Crystallographica* **1955,** 8, (1), 49-52.

[33] Hartman, P.; Perdok, W., On the relations between structure and morphology of crystals. II. *Acta Crystallographica* **1955,** 8, (9), 521-524.

[34] Hartman, P.; Perdok, W., On the relations between structure and morphology of crystals. III. *Acta Crystallographica* **1955,** 8, (9), 525-529.

[35] Hartman, P.; Chan, H.-K., Application of the periodic bond chain (PBC) theory and attachment energy consideration to derive the crystal morphology of hexamethylmelamine. *Pharmaceutical research* **1993,** 10, (7), 1052-1058.

[36] Hartman, P.; Bennema, P., The attachment energy as a habit controlling factor: I. Theoretical considerations. *Journal of Crystal Growth* **1980,** 49, (1), 145-156.

[37] Zhao, Q.; Liu, N.; Wang, B.; Wang, W., A study of solvent selectivity on the crystal morphology of FOX-7 via a modified attachment energy model. *RSC advances* **2016,** 6, (64), 59784-59793.

[38] Buerger, M., The genesis of twin crystals. *American Mineralogist: Journal of Earth and Planetary Materials* **1945,** 30, (7-8), 469-482.

[39] Klapper, H.; Hahn, T.; Chung, S., Optical, pyroelectric and X-ray topographic studies of twin domains and twin boundaries in KLiSO4. *Acta Crystallographica Section B: Structural Science* **1987,** 43, (2), 147-159.

[40] Schaskolsky, M.; Schubnikow, A., Über die künstliche Herstellung gesetzmässiger Kristallverwachsungen des Kalialauns. *Zeitschrift für Kristallographie-Crystalline Materials* **1933,** 85, (1-6), 1-16.

[41] Hartman, P., On the morphology of growth twins. *Zeitschrift für Kristallographie-Crystalline Materials* **1956,** 107, (1-6), 225-237.

[42] Ming, N.-B.; Sunagawa, I., Twin lamellae as possible self-perpetuating step sources. *Journal of crystal growth* **1988,** 87, (1), 13-17.

[43] Borovik-Romanov, A.; Grimmer, H., International Tables for Crystallography, Vol. D, edited by A. Authier. In ed.; Dordrecht: Kluwer Academic Publishers: 2003.

[44] Shekunov, B. Y.; York, P., Crystallization processes in pharmaceutical technology and drug delivery design. *Journal of crystal growth* **2000,** 211, (1-4), 122-136.

[45] Garside, J., Industrial crystallization from solution. *Chemical Engineering Science* **1985,** 40, (1), 3-26.

[46] Hartel, R. W., Advances in food crystallization. *Annual review of food science and technology* **2013,** 4, 277-292.

[47] Ulrich, J.; Stelzer, T., Crystallization. *Kirk-Othmer Encyclopedia of Chemical Technology* **2000**, 1-63.

[48] Kitamura, M., Strategy for control of crystallization of polymorphs. *CrystEngComm* **2009,** 11, (6), 949-964.

[49]Lerond, L.; Muhr, H.; Plasari, E.; Hassoun, M.; Valery, E.; Ludemann-Hombourger, O., Optimization of the cooling profile to improve the filterability of crystals isolated during an optical resolution by diastereomeric salt formation. *Powder technology* **2009,** 190, (1-2), 236-241.

[50] Rey, L.; May, J. C., *Freeze-Drying/Lyophilization Of Pharmaceutical & Biological Products, Revised and Expanded*. ed.; CRC Press: 2004.

[51]Jouyban, A., *Handbook of solubility data for pharmaceuticals*. ed.; Crc Press: 2009.

[52] Mersmann, A., *Crystallization technology handbook*. ed.; CRC press: 2001.

[53] Khoshkhoo, S.; Anwar, J., Crystallization of polymorphs: the effect of solvent. *Journal of Physics D: Applied Physics* **1993,** 26, (8B), B90.

[54] Di Martino, P.; Censi, R.; Malaj, L.; Capsoni, D.; Massarotti, V.; Martelli, S., Influence of solvent and crystallization method on the crystal habit of metronidazole. *Crystal Research and Technology: Journal of Experimental and Industrial Crystallography* **2007,** 42, (8), 800-806.

[55] Mohameed, H. A.; Abu-Jdayil, B.; Al Khateeb, M., Effect of cooling rate on unseeded batch crystallization of KCl. *Chemical Engineering and Processing: Process Intensification* **2002,** 41, (4), 297-302.

[56] Hermanto, M. W.; Yeoh, A.; Soh, B.; Chow, P. S.; Tan, R. B., Robust Crystallization

Process Development for the Metastable δ-form of Pyrazinamide. *Organic Process Research & Development* **2015,** 19, (12), 1987-1996.

[57] Nývlt, J., The Ostwald rule of stages. *Crystal Research and Technology* **1995,** 30, (4), 443-449.

[58] Beckmann, W., Seeding the desired polymorph: background, possibilities, limitations, and case studies. *Organic process research & development* **2000,** 4, (5), 372-383.

[59] Doki, N.; Yokota, M.; Kido, K.; Sasaki, S.; Kubota, N., Reliable and selective crystallization of the metastable α-form glycine by seeding. *Crystal growth & design* **2004,** 4, (1), 103-107.

[60] Kubota, N.; Doki, N.; Yokota, M.; Sato, A., Seeding policy in batch cooling crystallization. *Powder Technology* **2001,** 121, (1), 31-38.

[61] Kondepudi, D. K.; Bullock, K. L.; Digits, J. A.; Yarborough, P. D., Stirring rate as a critical parameter in chiral symmetry breaking crystallization. *Journal of the American Chemical Society* **1995,** 117, (1), 401-404.

[62] Zhang, K.; Xu, S.; Liu, S.; Tang, W.; Fu, X.; Gong, J., Novel Strategy to Control Polymorph Nucleation of Gamma Pyrazinamide by Preferred Intermolecular Interactions during Heterogeneous Nucleation. *Crystal Growth & Design* **2018,** 18, (9), 4874-4879.

[63] Masters, K., Spray drying handbook. *Spray drying handbook.* **1985**.

[64] SR, P., Improvement in drying and concentrating of liquid substances by atomizing. *US Patent* **1872**.

[65] Patel, R.; Patel, M.; Suthar, A., Spray drying technology: an overview. *Indian Journal of Science and Technology* **2009,** 2, (10), 44-47.

[66] Cal, K.; Sollohub, K., Spray drying technique. I: Hardware and process parameters. *Journal of pharmaceutical sciences* **2010,** 99, (2), 575-586.

[67] Messa, L. L.; Souza, C. F.; Faez, R., Spray-dried potassium nitrate-containing chitosan/montmorillonite microparticles as potential enhanced efficiency fertilizer. *Polymer Testing* **2020,** 81, 106196.

[68] Shishir, M. R. I.; Chen, W., Trends of spray drying: A critical review on drying of fruit and vegetable juices. *Trends in food science & technology* **2017,** 65, 49-67.

[69] Stunda-Zujeva, A.; Irbe, Z.; Berzina-Cimdina, L., Controlling the morphology of ceramic and composite powders obtained via spray drying–a review. *Ceramics International* **2017,** 43, (15), 11543-11551.

[70] Farshchi, A.; Hassanpour, A.; Bayly, A. E., The structure of spray-dried detergent powders. *Powder Technology* **2019,** 355, 738-754.

[71] Broadhead, J.; Edmond Rouan, S.; Rhodes, C., The spray drying of pharmaceuticals. *Drug development and industrial pharmacy* **1992,** 18, (11-12), 1169-1206.

[72] Goula, A. M.; Adamopoulos, K. G., Spray drying of tomato pulp: effect of feed concentration. *Drying technology* **2004,** 22, (10), 2309-2330.

[73] Gallo, L.; Llabot, J. M.; Allemandi, D.; Bucalá, V.; Piña, J., Influence of spray-drying operating conditions on Rhamnus purshiana (Cáscara sagrada) extract powder physical properties. *Powder Technology* **2011,** 208, (1), 205-214.

[74] Moran, A.; Buckton, G., Adjusting and understanding the properties and crystallisation behaviour of amorphous trehalose as a function of spray drying feed concentration. *International journal of pharmaceutics* **2007,** 343, (1-2), 12-17.

[75] Anandharamakrishnan, C., *Spray drying techniques for food ingredient encapsulation*. ed.; John Wiley & Sons: 2015.

[76] Mullin, J. W., *Crystallization*. ed.; Elsevier: 2001.

[77] Hubacher, M., Vaccum Sublimation. *Industrial & Engineering Chemistry Analytical Edition* **1943,** 15, (7), 448-450.

[78] Solomos, M. A.; Capacci-Daniel, C.; Rubinson, J. F.; Swift, J. A., Polymorph Selection via Sublimation onto Siloxane Templates. *Crystal Growth & Design* **2018,** 18, (11), 6965-6972.

[79] He, T.; Stolte, M.; Burschka, C.; Hansen, N. H.; Musiol, T.; Kälblein, D.; Pflaum, J.; Tao, X.; Brill, J.; Würthner, F., Single-crystal field-effect transistors of new Cl 2-NDI polymorph processed by sublimation in air. *Nature communications* **2015,** 6, (1), 1-9.

[80] Wagner, H. J.; Loutfy, R. O.; Hsiao, C.-K., Purification and characterization of phthalocyanines. *Journal of materials science* **1982,** 17, (10), 2781-2791.

[81] Karpinska, J.; Erxleben, A.; McArdle, P., Applications of low temperature gradient sublimation in vacuo: rapid production of high quality crystals. The first solvent-free crystals of ethinyl estradiol. *Crystal growth & design* **2013,** 13, (3), 1122-1130.

[82] Yu, Q.; Dang, L.; Black, S.; Wei, H., Crystallization of the polymorphs of succinic acid via sublimation at different temperatures in the presence or absence of water and isopropanol vapor. *Journal of Crystal Growth* **2012,** 340, (1), 209-215.

[83] Firsich, D. W. *Energetic materials separations and specific polymorph*

preparations via thermal gradient sublimation; Monsanto Research Corp., Miamisburg, OH (USA). Mound: 1983.

[84] Sharp, J. H.; Abkowitz, M., Dimeric structure of a copper phthalocyanine polymorph. *The Journal of Physical Chemistry* **1973,** 77, (4), 477-481.

[85] Kamali, N.; O'Malley, C.; Mahon, M. F.; Erxleben, A.; McArdle, P., Use of Sublimation Catalysis and Polycrystalline Powder Templates for Polymorph Control of Gas Phase Crystallization. *Crystal Growth & Design* **2018,** 18, (6), 3510-3516.

[86] Shen, S.; Xia, G.; Jiang, Z.; Shao, Q.; Shan, W.; Wang, H., Temperature Controlling Polymorphism and Polymorphic Interconversion in Sublimation Crystallization of 5-Methoxy-salicylaldhyde Azine. *Crystal Growth & Design* **2018,** 19, (1), 320-327.

[87] Mastai, Y., *Advanced Topics in Crystallization*. ed.; BoD–Books on Demand: 2015.

[88] Zhang, G. G.; Law, D.; Schmitt, E. A.; Qiu, Y., Phase transformation considerations during process development and manufacture of solid oral dosage forms. *Advanced drug delivery reviews* **2004,** 56, (3), 371-390.

[89] Mnyukh, Y., Fundamentals of Solid State Phase Transitions, Ferromagnetism and Ferroelectricity, 2001. In ed.; 1st Books.

[90] Krishnan, R. S.; Srinivasan, R.; Devanarayanan, S., *Thermal expansion of crystals: international series in the science of the solid state*. ed.; Elsevier: 2013.

[91] Fei, Y., Thermal expansion. *Mineral physics and crystallography: a handbook of physical constants* **1995,** 2, 29-44.

[92] Miller, W.; Smith, C.; Mackenzie, D.; Evans, K., Negative thermal expansion: a review. *Journal of materials science* **2009,** 44, (20), 5441-5451.

[93] Gatt, R.; Grima, J. N., Negative compressibility. *physica status solidi (RRL)–Rapid Research Letters* **2008,** 2, (5), 236-238.

[94] Song, R.-Q.; Cölfen, H., Additive controlled crystallization. *CrystEngComm* **2011,** 13, (5), 1249-1276.

[95] Caridi, A.; Kulkarni, S. A.; Di Profio, G.; Curcio, E.; Ter Horst, J. H., Template-induced nucleation of isonicotinamide polymorphs. *Crystal growth & design* **2014,** 14, (3), 1135-1141.

[96] Zhang, K.; Xu, S.; Gong, J.; Tang, W., Revealing the critical role of template functional group ordering in the template-directed crystallization of pyrazinamide. *CrystEngComm* **2019,** 21, (42), 6382-6389.

[97] Carter, P. W.; Ward, M. D., Topographically directed nucleation of organic crystals on molecular single-crystal substrates. *Journal of the American Chemical Society* **1993,**

115, (24), 11521-11535.

[98] Bonafede, S. J.; Ward, M. D., Selective nucleation and growth of an organic polymorph by ledge-directed epitaxy on a molecular crystal substrate. *Journal of the American Chemical Society* **1995,** 117, (30), 7853-7861.

[99] Wijethunga, T. K.; Baftizadeh, F.; Stojaković, J.; Myerson, A. S.; Trout, B. L., Experimental and mechanistic study of the heterogeneous nucleation and epitaxy of acetaminophen with biocompatible crystalline substrates. *Crystal Growth & Design* **2017,** 17, (7), 3783-3795.

[100] Chadwick, K.; Chen, J.; Myerson, A. S.; Trout, B. L., Toward the rational design of crystalline surfaces for heteroepitaxy: role of molecular functionality. *Crystal growth & design* **2012,** 12, (3), 1159-1166.

[101] Myerson, A. S.; Jang, S. M., A comparison of binding energy and metastable zone width for adipic acid with various additives. *Journal of crystal growth* **1995,** 156, (4), 459-466.

[102] Peng, J.; Dong, Y.; Wang, L.; Li, L.; Li, W.; Feng, H., Effect of impurities on the solubility, metastable zone width, and nucleation kinetics of borax decahydrate. *Industrial & Engineering Chemistry Research* **2014,** 53, (30), 12170-12178.

[103] Pons Siepermann, C. A.; Huang, S.; Myerson, A. S., Nucleation inhibition of benzoic acid through solution complexation. *Crystal Growth & Design* **2017,** 17, (5), 2646-2653.

[104] Pons Siepermann, C. A.; Myerson, A. S., Inhibition of nucleation using a dilute, weakly hydrogen-bonding molecular additive. *Crystal Growth & Design* **2018,** 18, (6), 3584-3595.

[105] Addadi, L.; Berkovitch-Yellin, Z.; Weissbuch, I.; van Mil, J.; Shimon, L. J.; Lahav, M.; Leiserowitz, L., Growth and dissolution of organic crystals with "Tailor-Made" inhibitors—implications in stereochemistry and materials science. *Angewandte Chemie International Edition in English* **1985,** 24, (6), 466-485.

[106] Han, G.; Chow, P. S.; Tan, R. B., Probing the mechanisms underlying electrolyte-assisted nucleation enhancement of DL-alanine. *Crystal growth & design* **2014,** 14, (3), 1406-1411.

[107] Han, G.; Thirunahari, S.; Chow, P. S.; Tan, R. B., Resolving the longstanding riddle of pH-dependent outcome of glycine polymorphic nucleation. *CrystEngComm* **2013,** 15, (6), 1218-1224.

[108] Dalvi, S. V.; Dave, R. N., Analysis of nucleation kinetics of poorly water-

soluble drugs in presence of ultrasound and hydroxypropyl methyl cellulose during antisolvent precipitation. *International journal of pharmaceutics* **2010,** 387, (1-2), 172-179.

[109] Kim, J.-W.; Park, J.-H.; Shim, H.-M.; Koo, K.-K., Effect of amphiphilic additives on nucleation of hexahydro-1, 3, 5-trinitro-1, 3, 5-triazine. *Crystal growth & design* **2013,** 13, (11), 4688-4694.

[110] Alonzo, D. E.; Raina, S.; Zhou, D.; Gao, Y.; Zhang, G. G.; Taylor, L. S., Characterizing the impact of hydroxypropylmethyl cellulose on the growth and nucleation kinetics of felodipine from supersaturated solutions. *Crystal growth & design* **2012,** 12, (3), 1538-1547.

[111] Ozaki, S.; Kushida, I.; Yamashita, T.; Hasebe, T.; Shirai, O.; Kano, K., Inhibition of crystal nucleation and growth by water-soluble polymers and its impact on the supersaturation profiles of amorphous drugs. *Journal of pharmaceutical sciences* **2013,** 102, (7), 2273-2281.

[112] Mukuta, T.; Lee, A. Y.; Kawakami, T.; Myerson, A. S., Influence of impurities on the solution-mediated phase transformation of an active pharmaceutical ingredient. *Crystal growth & design* **2005,** 5, (4), 1429-1436.

[113] Kamali, N.; Erxleben, A.; McArdle, P., Unexpected effects of catalytic amounts of additives on crystallization from the gas phase: Depression of the sublimation temperature and polymorph control. *Crystal Growth & Design* **2016,** 16, (5), 2492-2495.

[114] Dalmer, O.; Walter, E.; Firma, E., Merck in Darmstadt. Verfahren zur Herstellung von Abkömmlingen der Pyrazinmonocarbonsäure. **1936**.

[115] Malone, L.; Schurr, A.; Lindh, H.; McKenzie, D.; Kiser, J.; Williams, J., The effect of pyrazinamide (aldinamide) on experimental tuberculosis in mice. *American review of tuberculosis* **1952,** 65, (5), 511-518.

[116] Solotorovsky, M.; Gregory, F.; Ironson, E.; Bugie, E.; O'neill, R.; Pfister 3rd, K., Pyrazinoic acid amide-An agent active against experimental murine tuberculosis. *Proceedings of the Society for Experimental Biology and Medicine* **1952,** 79, (4), 563-565.

[117] Yeager, R. L.; Munroe, W.; Dessau, F. I., Pyrazinamide (aldinamide) in the treatment of pulmonary tuberculosis. *American review of tuberculosis* **1952,** 65, (5), 523-546.

[118] Mitchison, D., The action of antituberculosis drugs in short-course

chemotherapy. *Tubercle* **1985,** 66, (3), 219-225.

[119] Zhang, Y.; Mitchison, D., The curious characteristics of pyrazinamide: a review. *The international journal of tuberculosis and lung disease* **2003,** 7, (1), 6-21.

[120] Takaki, Y.; Sasada, Y.; Watanabé, T., The crystal structure of α-pyrazinamide. *Acta Crystallographica* **1960,** 13, (9), 693-702.

[121] Tamura, C.; Kuwano, H.; Sasada, Y., Crystallographic data of carboxylic acids and carboxyamides of picoline and pyrazine derivatives. *Acta Crystallographica* **1961,** 14, (6), 693-693.

[122] Rø, G.; Sørum, H., The crystal and molecular structure of β-pyrazinecarboxamide. *Acta Crystallographica Section B* **1972,** 28, (4), 991-998.

[123] Rø, G.; Sørum, H., The crystal and molecular structure of δ-pyrazinecarboxamide. *Acta Crystallographica Section B* **1972,** 28, (6), 1677-1684.

[124] Tiwari, R. K.; Deo, N.; Singh, T. P., *J. Sci. Res. Bhopal, India* **1980,** 2, 161.

[125] Nakata, K.; Takaki, Y., *Mem.Osaka Kyoiku Univ.Ser.* **1987,** 3, (36), 93.

[126] A.Nangia; A.Srinivasulu, *CSD Communication(Private Communication)* **2005**.

[127] Battilocchio, C.; Hawkins, J. M.; Ley, S. V., Mild and selective heterogeneous catalytic hydration of nitriles to amides by flowing through manganese dioxide. *Organic letters* **2014,** 16, (4), 1060-1063.

[128] Castro, R. A.; Maria, T. M.; Évora, A. O.; Feiteira, J. C.; Silva, M. R.; Beja, A. M.; Canotilho, J.; Eusébio, M. E. S., A new insight into pyrazinamide polymorphic forms and their thermodynamic relationships. *Crystal Growth & Design* **2009,** 10, (1), 274-282.

[129] Cherukuvada, S.; Thakuria, R.; Nangia, A., Pyrazinamide polymorphs: relative stability and vibrational spectroscopy. *Crystal Growth & Design* **2010,** 10, (9), 3931-3941.

[130] Rajalakshmi, G.; Hathwar, V. R.; Kumaradhas, P., Intermolecular interactions, charge-density distribution and the electrostatic properties of pyrazinamide anti-TB drug molecule: an experimental and theoretical charge-density study. *Acta Crystallographica Section B* **2014,** 70, (3), 568-579.

[131] Tiwari, R. K.; Patel, T. C.; Singh, T. P., *Indian J. Phys. Sect. A* **1982,** 56, 413.

[132] Jarzembska, K. N.; Hoser, A. A.; Kamiński, R.; Madsen, A. Ø.; Durka, K.; Woźniak, K., Combined experimental and computational studies of pyrazinamide and nicotinamide in the context of crystal engineering and thermodynamics. *Crystal Growth & Design* **2014,** 14, (7), 3453-3465.

[133] Choquesillo-Lazarte, D.; Nemec, V.; Cinčić, D., Halogen bonded cocrystals of active pharmaceutical ingredients: pyrazinamide, lidocaine and pentoxifylline in combination with haloperfluorinated compounds. *CrystEngComm* **2017,** 19, (35), 5293-5299.

[134] Wahlberg, N.; Ciochoń, P.; Petriĉek, V.; Madsen, A. Ø., Polymorph stability prediction: on the importance of accurate structures: a case study of pyrazinamide. *Crystal Growth & Design* **2013,** 14, (1), 381-388.

[135] Zhang, K.; Shen, H.; Xu, S.; Zhang, H.; Zhu, M.; Shi, P.; Fu, X.; Yang, Y.; Gong, J., Thermodynamic study of solubility for pyrazinamide in ten solvents from T=(283.15 to 323.15) K. *The Journal of Chemical Thermodynamics* **2017,** 112, 204-212.

[136] Tan, X.; Wang, K.; Li, S.; Yuan, H.; Yan, T.; Liu, J.; Yang, K.; Liu, B.; Zou, G.; Zou, B., Exploration of the pyrazinamide polymorphism at high pressure. *The Journal of Physical Chemistry B* **2012,** 116, (49), 14441-14450.

[137] Borba, A.; Albrecht, M.; Gómez-Zavaglia, A.; Suhm, M. A.; Fausto, R., Low temperature infrared spectroscopy study of pyrazinamide: from the isolated monomer to the stable low temperature crystalline phase. *The Journal of Physical Chemistry A* **2009,** 114, (1), 151-161.

[138] E. Castro, R. A.; Ribeiro, J. D.; Maria, T. M.; Ramos Silva, M.; Yuste-Vivas, C.; Canotilho, J.; Eusébio, M. E. S., Naproxen cocrystals with pyridinecarboxamide isomers. *Crystal Growth & Design* **2011,** 11, (12), 5396-5404.

[139] Blokhina, S. V.; Ol'khovich, M. V.; Sharapova, A. V.; Volkova, T. V.; Perlovich, G. L., Solution thermodynamics of pyrazinamide, isoniazid, and p-aminobenzoic acid in buffers and octanol. *The Journal of Chemical Thermodynamics* **2015,** 91, 396-403.

[140] Wheate, N. J.; Vora, V.; Anthony, N. G.; McInnes, F. J., Host–guest complexes of the antituberculosis drugs pyrazinamide and isoniazid with cucurbit [7] uril. *Journal of Inclusion Phenomena and Macrocyclic Chemistry* **2010,** 68, (3-4), 359-367.

[141] Blokhina, S.; Sharapova, A.; Ol'khovich, M.; Volkova, T.; Perlovich, G., Vapor pressures and thermodynamic sublimation of antitubercular drugs. *Journal of Thermal Analysis and Calorimetry* **2015,** 120, (1), 1053-1060.

[142] Luo, Y.-H.; Sun, B.-W., Pharmaceutical Co-crystals of pyrazinecarboxamide (PZA) with various carboxylic acids: crystallography, hirshfeld surfaces, and dissolution study. *Crystal Growth & Design* **2013,** 13, (5), 2098-2106.

[143] Lavor, E. P.; Freire, F. D.; Aragão, C. F. S.; Raffin, F. N., Application of thermal

analysis to the study of anti-tuberculosis drug compatibility. Part 1. *Journal of thermal analysis and calorimetry* **2012,** 108, (1), 207-212.

[144] Lourenço, C.; Melo, C. I.; Bogel-Łukasik, R.; Bogel-Łukasik, E., Solubility advantage of pyrazine-2-carboxamide: application of alternative solvents on the way to the future pharmaceutical development. *Journal of Chemical & Engineering Data* **2012,** 57, (5), 1525-1533.

[145] Pajula, K.; Taskinen, M.; Lehto, V.-P.; Ketolainen, J.; Korhonen, O., Predicting the formation and stability of amorphous small molecule binary mixtures from computationally determined Flory− Huggins interaction parameter and phase diagram. *Molecular pharmaceutics* **2010,** 7, (3), 795-804.

[146] Sharma, P.; Nandi, R.; Gangopadhyay, D.; Singh, A.; Singh, R. K., Temperature dependent polymorphism of pyrazinamide: An in situ Raman and DFT study. *Spectrochimica Acta Part A: Molecular and Biomolecular Spectroscopy* **2018,** 190, 177-180.

[147] Ribeiro da Silva, M. D.; Miranda, M. S.; Vaz, C. M.; Matos, M. A. R.; Acree Jr, W., Experimental thermochemical study of three monosubstituted pyrazines. *The Journal of Chemical Thermodynamics* **2005,** 37, (1), 49-53.

[148] Negoro, H., Solubility phenomena of pyridine-and pyrazinemonocarboxamides. I. *Heat of sublimation of picolinamide, nicotinamide, isonicotinamide, and pyrazinecarboxamide. Takamine Kenkyusho Nempo* **1959,** 11, 66-75.

[149] Negoro, H., Miki, T., Ueda, S., Solubility phenomena of pyridine- and pyrazinemonocarboxamides. I. Heat of sublimation of picolinamide, nicotinamide, isonicotinamide, and pyrazinecarboxamide. *Yakugaku Zasshi* **1960,** 80, 665-669.

[150] Abourahma, H.; Shah, D. D.; Melendez, J.; Johnson, E. J.; Holman, K. T., A Tale of Two Stoichiometrically Diverse Cocrystals. *Crystal Growth & Design* **2015,** 15, (7), 3101-3104.

[151] Kulla, H.; Greiser, S.; Benemann, S.; Rademann, K.; Emmerling, F., In situ investigation of a self-accelerated cocrystal formation by grinding pyrazinamide with oxalic acid. *Molecules* **2016,** 21, (7), 917.

[152] Adalder, T. K.; Sankolli, R.; Dastidar, P., Homo-or heterosynthon? A crystallographic study on a series of new cocrystals derived from pyrazinecarboxamide and various carboxylic acids equipped with additional hydrogen bonding sites. *Crystal Growth & Design* **2012,** 12, (5), 2533-2542.

[153] Wang, J.-R.; Ye, C.; Mei, X., Structural and physicochemical aspects of hydrochlorothiazide co-crystals. *CrystEngComm* **2014,** 16, (30), 6996-7003.

[154] Thakuria, R.; Cherukuvada, S.; Nangia, A., Crystal Structures of Pyrogallol, Its Hydrate, and Stable Multiple Z′ Cocrystals with N-Heterocycles Containing Metastable Conformers of Pyrogallol. *Crystal Growth & Design* **2012,** 12, (8), 3944-3953.

[155] Évora, A. O.; Castro, R. A.; Maria, T. M.; Rosado, M. T.; Ramos Silva, M.; Matos Beja, A.; Canotilho, J.; Eusébio, M. E. S., Pyrazinamide-diflunisal: a new dual-drug co-crystal. *Crystal Growth & Design* **2011,** 11, (11), 4780-4788.

[156] Cherukuvada, S.; Nangia, A., Fast dissolving eutectic compositions of two anti-tubercular drugs. *CrystEngComm* **2012,** 14, (7), 2579-2588.

[157] Kulla, H.; Greiser, S.; Benemann, S.; Rademann, K.; Emmerling, F., Knowing When To Stop Trapping Metastable Polymorphs in Mechanochemical Reactions. *Crystal Growth & Design* **2017,** 17, (3), 1190-1196.

[158] Eddleston, M. D.; Arhangelskis, M.; Fabian, L.; Tizzard, G. J.; Coles, S. J.; Jones, W., Investigation of an amide-pseudo amide hydrogen bonding motif within a series of theophylline: amide cocrystals. *Crystal Growth & Design* **2015,** 16, (1), 51-58.

[159] Rajbongshi, T.; Sarmah, K. K.; Sarkar, A.; Ganduri, R.; Cherukuvada, S.; Thakur, T. S.; Thakuria, R., Preparation of Pyrazinamide Eutectics versus Cocrystals Based on Supramolecular Synthon Variations. *Crystal Growth & Design* **2018,** 18, (11), 6640-6651.

[160] Liu, F.; Song, Y.; Liu, Y.-N.; Li, Y.-T.; Wu, Z.-Y.; Yan, C.-W., Drug-bridge-drug ternary cocrystallization strategy for antituberculosis drugs combination. *Crystal Growth & Design* **2018,** 18, (3), 1283-1286.

[161] Shirvan, S. A.; Haydari Dezfuli, S., Diaquabis (nitrato-κ2O, O′) bis (pyrazine-2-carboxamide-κN4) cadmium–pyrazine-2-carboxamide (1/2). *Acta Crystallographica Section E: Structure Reports Online* **2012,** 68, (7), m1008-m1009.

[162] Tabrizi, L.; Chiniforoshan, H.; Mcardle, P., Synthesis, structures, and electroluminescence properties of a 1D zinc (II) coordination polymer containing both dicyanamide and pyrazinamide ligands. *Journal of Coordination Chemistry* **2015,** 68, (11), 1936-1946.

[163] Aakery, C. B.; Desper, J.; Helfrich, B. A., Heteromeric intermolecular interactions as synthetic tools for the formation of binary co-crystals. **2004**.

[164] Jarzembska, K. N.; Hoser, A. A.; Varughese, S.; Kamiński, R.; Malinska, M.; Stachowicz, M.; Pedireddi, V. R.; Wozniak, K., Structural and energetic analysis of molecular assemblies in a series of nicotinamide and pyrazinamide cocrystals with dihydroxybenzoic acids. *Crystal Growth & Design* **2017,** 17, (9), 4918-4931.

[165] Ranjan, S.; Devarapalli, R.; Kundu, S.; Vangala, V. R.; Ghosh, A.; Reddy, C. M., Three new hydrochlorothiazide cocrystals: Structural analyses and solubility studies. *Journal of Molecular Structure* **2017,** 1133, 405-410.

[166] Sarmah, K. K.; Rajbongshi, T.; Bhowmick, S.; Thakuria, R., First-line antituberculosis drug, pyrazinamide, its pharmaceutically relevant cocrystals and a salt. *Acta Crystallographica Section B: Structural Science, Crystal Engineering and Materials* **2017,** 73, (5), 1007-1016.

[167] Rouelle, H., Sur l'urine humain, et sur celles se vache et de cheval, comparées ensemble. *J Méd* **1773**, 451-468.

[168] Wöhler, F., Ueber künstliche bildung des harnstoffs. *Annalen der Physik* **1828,** 87, (2), 253-256.

[169] Chandrasekhar, M.; Prasad, G. S.; Venkataramaiah, C.; Raju, C. N.; Seshaiah, K.; Rajendra, W., Synthesis, spectral characterization, docking studies and biological activity of urea, thiourea, sulfonamide and carbamate derivatives of imatinib intermediate. *Molecular diversity* **2019,** 23, (3), 723-738.

[170] Bremner, J., Recent research on problems in the use of urea as a nitrogen fertilizer. In *Nitrogen economy in tropical soils*, Springer: 1995; pp 321-329.

[171] Fournier, J.; Bruneau, C.; Dixneuf, P. H.; Lecolier, S., Ruthenium-catalyzed synthesis of symmetrical N, N'-dialkylureas directly from carbon dioxide and amines. *The Journal of Organic Chemistry* **1991,** 56, (14), 4456-4458.

[172] Yonova, P.; Stoilkova, G., Synthesis and biological activity of urea and thiourea derivatives from 2-aminoheterocyclic compounds. *Journal of Plant Growth Regulation* **2004,** 23, (4), 280-291.

[173] Briggs, H.; Gallup, W. D.; Darlow, A.; Stephens, D.; Kinney, C., Urea as an extender of protein when fed to cattle. *Journal of animal science* **1947,** 6, (4), 445-460.

[174] Helmer, L.; Bartley, E., Progress in the utilization of urea as a protein replacer for ruminants. A review. *Journal of Dairy Science* **1971,** 54, (1), 25-51.

[175] Briggs, M. H., *Urea as a protein supplement*. ed.; Elsevier: 2014.

[176] Conner, A. H., Urea-formaldehyde adhesive resins. *Polymeric materials encyclopedia* **1996,** 11, 8496-8501.

[177] Katla, R. V.; Syed, R.; Golla, M.; Shaik, A.; Chamarthi, R. N., Synthesis and biological evaluation of novel urea and thiourea derivatives of valacyclovir. *Journal of the Serbian Chemical Society* **2014,** 79, (3), 283-289.

[178] Abdel-Rahman, H. M.; Morsy, M. A., Novel benzothiazolyl urea and thiourea derivatives with potential cytotoxic and antimicrobial activities. *Journal of enzyme inhibition and medicinal chemistry* **2007,** 22, (1), 57-64.

[179] Domínguez, J. N.; León, C.; Rodrigues, J.; Gamboa de Domínguez, N.; Gut, J.; Rosenthal, P. J., Synthesis and evaluation of new antimalarial phenylurenyl chalcone derivatives. *Journal of Medicinal Chemistry* **2005,** 48, (10), 3654-3658.

[180] Mustafa, S.; Perveen, S.; Khan, A., Synthesis, enzyme inhibition and anticancer investigation of unsymmetrical 1, 3-disubstituted ureas. *Journal of the Serbian Chemical Society* **2014,** 79, (1), 1-10.

[181] Stafford, O., Acetamide as a Solvent. *Journal of the American Chemical Society* **1933,** 55, (10), 3987-3988.

[182] Jeffrey, G.; Ruble, J.; McMullan, R.; DeFrees, D.; Binkley, J.; Pople, J., Neutron diffraction at 23 K and ab initio molecular-orbital studies of the molecular structure of acetamide. *Acta Crystallographica Section B: Structural Crystallography and Crystal Chemistry* **1980,** 36, (10), 2292-2299.

[183] Hamilton, W. C., The crystal structure of orthorhombic acetamide. *Acta Crystallographica* **1965,** 18, (5), 866-870.

[184] Fabbiani, F. P.; Allan, D. R.; Marshall, W. G.; Parsons, S.; Pulham, C. R.; Smith, R. I., High-pressure recrystallisation—A route to new polymorphs and solvates of acetamide and parabanic acid. *Journal of crystal growth* **2005,** 275, (1-2), 185-192.

[185] Bridgman, P. In *Polymorphic Transitions up to 50,000 Kg/Cm□ of Several Organic Substances*, Proceedings of the American Academy of Arts and Sciences, 1938; JSTOR: 1938; pp 227-268.

[186] Dauber, P.; Hagler, A. T., Crystal packing, hydrogen bonding, and the effect of crystal forces on molecular conformation. *Accounts of Chemical Research* **1980,** 13, (4), 105-112.

[187] Kitaigorodsky, A., *Molecular crystals and molecules*. ed.; Elsevier: 2012; Vol. 29.

[188] Wyckoff, R. W., 35. A Powder Spectrometry Study of the Structure of Urea. *Zeitschrift für Kristallographie-Crystalline Materials* **1930,** 75, (1), 529-537.

[189] Hendricks, S. B., The crystal structure of urea and the molecular symmetry of

thiourea. *Journal of the American Chemical Society* **1928,** 50, (9), 2455-2464.

[190] Sklar, N.; Senko, M. E.; Post, B., Thermal effects in urea: the crystal structure at–140° C and at room temperature. *Acta Crystallographica* **1961,** 14, (7), 716-720.

[191] Olejniczak, A.; Ostrowska, K.; Katrusiak, A., H-bond breaking in high-pressure urea. *The Journal of Physical Chemistry C* **2009,** 113, (35), 15761-15767.

[192] Dziubek, K.; Citroni, M.; Fanetti, S.; Cairns, A. B.; Bini, R., High-pressure high-temperature structural properties of urea. *The Journal of Physical Chemistry C* **2017,** 121, (4), 2380-2387.

[193] Weber, H.; Marshall, W.; Dmitriev, V. In *High-pressure polymorphism in deuterated urea*, ACTA CRYSTALLOGRAPHICA A-FOUNDATION AND ADVANCES, 2002; INT UNION CRYSTALLOGRAPHY 2 ABBEY SQ, CHESTER, CH1 2HU, ENGLAND: 2002; pp C174-C174.

[194] Chemla, D. S., *Nonlinear optical properties of organic molecules and crystals*. ed.; Elsevier: 2012; Vol. 1.

[195] Ristic, R.; Shekunov, B. Y.; Sherwood, J., The growth and perfection of organic non-linear optical crystals: N-methyl urea (NMU) from methanol solution. I. Kinetics and growth anisotropy. *Journal of crystal growth* **1996,** 167, (3-4), 693-700.

[196] McEwan, A.; Ristic, R.; Shekunov, B. Y.; Sherwood, J., The growth and perfection of organic non-linear optical crystals: N-methyl urea (NMU) from methanol solution. II. Morphological instability. *Journal of crystal growth* **1996,** 167, (3-4), 701-708.

[197] Shepherd, E.; Sherwood, J.; Simpson, G., The growth and perfection of organic non-linear optical crystals: N-methyl urea (NMU) from methanol solution. III. The growth of large single crystals for optical examination. *Journal of crystal growth* **1996,** 167, (3-4), 709-715.

[198] Baaklini, G.; Gbabode, G.; Clevers, S.; Négrier, P.; Mondieig, D.; Coquerel, G., Trimorphism of N-methylurea: crystal structures, phase transitions and thermodynamic stabilities. *CrystEngComm* **2016,** 18, (25), 4772-4778.

[199] Harkema, S.; Ter Brake, J.; Meutstege, H., The crystal structure and thermal expansion of two modifications of N-methylurea–oxalic acid (2: 1). *Acta Crystallographica Section B: Structural crystallography and crystal chemistry* **1979,** 35, (9), 2087-2093.

[200] Jones, A. O.; Leech, C. K.; McIntyre, G. J.; Wilson, C. C.; Thomas, L. H., Engineering short, strong hydrogen bonds in urea di-carboxylic acid complexes.

CrystEngComm **2014,** 16, (35), 8177-8184.

[201] Lewandowski, K.; Murer, P.; Svec, F.; Fréchet, J. M., A combinatorial approach to recognition of chirality: Preparation of highly enantioselective aryl-dihydropyrimidine selectors for chiral HPLC. *Journal of combinatorial chemistry* **1999,** 1, (1), 105-112.

[202] Nardelli, M.; Coghi, L., Complexes of bivalent metals with organic molecules containing oxygen (formamide, acetamide, methylurea). *Ric. Sci* **1959,** 29, 134-138.

[203] Henschel, D.; Hamann, T.; Moers, O.; Blaschette, A.; Jones, P. G., Polysulfonylamine, CL [1]. Wasserstoffbrücken in kristallinen Oniumdimesylamiden: Ein robustes Achtring-Synthon in den Strukturen von Methyluronium-und 1, 1-Dimethyluronium-dimesylamid./Polysulfonylamines, CL [1]. Hydrogen Bonding in Crystalline Onium Dimesylamides: A Robust Eight-Membered Ring Synthon in the Structures of Methyluronium and 1, 1-Dimethyluronium Dimesylamide. *Zeitschrift für Naturforschung B* **2002,** 57, (1), 113-121.

[204] Wölper, C.; Rodríguez-Gimeno, A.; Iborra, K. C.; Jones, P. G.; Blaschette, A., Polysulfonylamine, CLXXXIX [1]. Weitere Beispiele für die O-Protonierung von Harnstoffen mit Di (organosulfonyl) aminen: Bildung und Kristallstrukturen von 1, 1-Dimethyluroniumdi (4-fluorbenzolsulfonyl) amid und Di (1-methylharnstoff)-hydrogen (I)-di (4-fluorbenzolsulfonyl) amid/Polysulfonylamines, CLXXXIX. Additional Examples of the O-Protonation of Ureas by Di (organosulfonyl) amines: Formation and Crystal Structures of 1, 1-Dimethyluronium Di (4-fluorobenzenesulfonyl) amide and Di (1-methylurea) hydrogen (I) Di (4-fluorobenzenesulfonyl) amide. *Zeitschrift für Naturforschung B* **2010,** 65, (11), 1363-1371.

[205] PATHIRANA, H. K.; Weiss, T.; Reibenspies, J.; Zingaro, R.; Meyers, E., Crystal structure of N, N-dimethylurea, $(CH_3)_2NOCNH_2$. *Zeitschrift für Kristallographie* **1994,** 209, (8).

[206] Anisimova, T. B.; Bokach, N. A.; Luzyanin, K. V.; Haukka, M.; Kukushkin, V. Y., Push-pull nitrile ligands exhibit specific hydration patterns. *Dalton Transactions* **2010,** 39, (44), 10790-10798.

[207] Jones, A. O.; Lemée-Cailleau, M.-H.; Martins, D. M.; McIntyre, G. J.; Oswald, I. D.; Pulham, C. R.; Spanswick, C. K.; Thomas, L. H.; Wilson, C. C., Temperature dependent solid-state proton migration in dimethylurea–oxalic acid complexes. *Physical Chemistry Chemical Physics* **2012,** 14, (38), 13273-13283.

[208] Kochergin, P.; Aleksandrova, E.; Persanova, L., Rational Chemical Schemes for the Synthesis of Medicinal Preparations of the Purine Series (A Review). *Pharmaceutical Chemistry Journal* **2001,** 35, (7), 388-392.

[209] Näther, C.; Döring, C.; Jess, I.; Jones, P. G.; Taouss, C., Thermodynamic and structural relationships between the two polymorphs of 1, 3-dimethylurea. *Acta Crystallographica Section B: Structural Science, Crystal Engineering and Materials* **2013,** 69, (1), 70-76.

[210] Tan, D.; Ng, Z. X.; Sim, Y.; Ganguly, R.; García, F., cis-Cyclodiphosph (v/v) azanes as highly stable and robust main group supramolecular building blocks. *CrystEngComm* **2018,** 20, (39), 5998-6004.

[211] Lam, C.-K.; Cheng, M.-F.; Li, C.-L.; Zhang, J.-P.; Chen, X.-M.; Li, W.-K.; Mak, T. C., Stabilization of D 5h and C 2v valence tautomers of the croconate dianion. *Chemical Communications* **2004**, (4), 448-449.

[212] Mitt, X., K. Wijaya, D. Henschel, O. Moers, A. Blaschette, PG Jones. *Z. Naturforsch. 52b* **1997,** 1219.

[213] Zhang, J.; Wu, T.; Chen, S.; Feng, P.; Bu, X., Versatile Structure-Directing Roles of Deep-Eutectic Solvents and Their Implication in the Generation of Porosity and Open Metal Sites for Gas Storage. *Angewandte Chemie International Edition* **2009,** 48, (19), 3486-3490.

[214] Ghassemzadeh, M.; Harms, K.; Dehnicke, K., N, N′-Dim ethylharnstoff als chelatisierende Lewis-Säure: Synthese und Kristallstrukturen von PPh_4 [Cl ($H_2Me_2N_2CO$)] und $(PPh_4)_2$ [Cl ($H_2Me_2N_2CO$)] Cl/NN′-Dimethylurea as a Chelating Lewis Acid: Synthesis and Crystal Structures of PPh_4 [Cl ($H_2Me_2N_2CO$)] and $(PPh_4)_2$ [Cl ($H_2Me_2N_2CO$)] Cl. *Zeitschrift für Naturforschung B* **1996,** 51, (10), 1423-1427.

[215] Babu, G. A.; Chandramohan, A.; Ramasamy, P.; Bhagavannarayana, G.; Varghese, B., Synthesis, structure, growth and physical properties of a novel organic NLO crystal: 1, 3-Dimethylurea dimethylammonium picrate. *Materials Research Bulletin* **2011,** 46, (3), 464-468.

[216] Hamann, T.; Henschel, D.; Lange, I.; Moers, O.; Blaschette, A.; Jones, P., Polysulfonylamines, CLVII. Molecular Co-crystals of Di (4-halobenzenesulfonyl) amines and Oxygen Bases: Lamellar Layers with Close CH… Hal, Cl… Cl or Br… Br Interlayer Contacts. *ZEITSCHRIFT FUR NATURFORSCHUNG B* **2002,** 57, (9), 1051-1065.

[217] Liu, T.; Luo, D.; Xu, D.; Zeng, H.; Lin, Z., Solvent induced structural variation

in magnesium carboxylate frameworks. *Inorganic Chemistry Communications* **2013,** 29, 110-113.

[218] Döring, C.; Taouss, C.; Jones, P. G., Trimethylurea. *Acta Crystallographica Section C: Crystal Structure Communications* **2012,** 68, (3), o108-o110.

[219] Wölper, C.; Rodríguez-Gimeno, A.; Iborra, K. C.; Dix, I.; Freytag, M.; Jones, P. G.; Blaschette, A., Polysulfonylamine, CXCII [1]. Polynäre Verbindungen aus Di (4-fluorbenzolsulfonyl) amin (FAH), 1, 1, 3-Trimethylharnstoff (TrMU) und Dimethylamin (Me_2NH): Bildung und Strukturen des Cokristalls FAH· TrMU (Z′= 1), des Salzes Me_2NH_2+· FA–(Z′= 6) und des Salz-Cokristalls FAH· TrMU· Me_2NH_2+· FA–(Z′= 1). Bemerkungen zur Oxophobie von C–F-Gruppen in Kristallstrukturen/Polysulfonylamines, CXCII. Polynary Compounds Based upon Di (4-fluorobenzenesulfonyl) amine (FAH), 1, 1, 3-Trimethylurea (TrMU) and Dimethylamine (Me_2NH): Formation and Structures of the Cocrystal FAH· TrMU (Z′= 1), the Salt Me_2 NH_2+· FA−(Z′= 6) and the Salt Cocrystal FAH· TrMU· Me_2NH_2+· FA−(Z′= 1). Comments on the Oxophobia of C–F Groups in Crystal Structures. *Zeitschrift für Naturforschung B* **2011,** 66, (11), 1161-1174.

[220] P.G.Jones, A. B., Cindy Doring, In *CSD Communication* ed.; 2016.

[221] P.G.Jones, A. B., M.Freytag, Cindy Doring,, In *CSD Communication* ed.; 2016.

[222] Smith, G.; Kennard, C. H., The crystal and molecular structure of the 1: 1 adduct hydrate of pyrazine-2, 3-dicarboxylic acid with 1, 1-diethylurea. *Australian Journal of Chemistry* **2000,** 53, (12), 999-1001.

[223] Smith, G.; Coyne, M. G.; White, J. M., Molecular cocrystals of aromatic carboxylic acids with 1, 1-diethylurea: synthesis and the crystal structures of a series of nitro-substituted analogues. *Australian Journal of Chemistry* **2000,** 53, (3), 203-208.

[224] Della Gatta, G.; Ferrq, D., Enthalpies of fusion and solid-to-solid transition, entropies of fusion for urea and twelve alkylureas. *Thermochimica Acta* **1987,** 122, (1), 143-152.

[225] Frampton, C. S.; Parkes, K. E., 1, 1, 3, 3-Tetramethylurea. *Acta Crystallographica Section C: Crystal Structure Communications* **1996,** 52, (12), 3246-3248.

[226] Hamann, T.; Wijaya, K.; Moers, O.; Blaschette, A.; Jones, P. G., Polysulfonylamine, CLIX [1]. Eine Vielfalt supramolekularer Synthone in zwei Molekülkomplexen von Di (4-halogenbenzolsulfonyl) aminen mit Sauerstoffbasen/Polysulfonylamines, CLIX [1]. A Variety of Supramolecular Synthons

in Two Molecular Complexes of Di (4-halobenzenesulfonyl) amines with Oxygen Bases. *Zeitschrift für Naturforschung B* **2002,** 57, (10), 1152-1164.

[227] Zerbe, E.-M.; Pinol, S. R.; Hamann, T.; Freytag, M.; Jones, P. G.; Blaschette, A., Polysulfonylamine, CLXXXVI [1]. Strukturvielfalt in sechs Cokristallen von Tetramethylharnstoff mit Di (4-X-benzolsulfonyl) aminen (X= F, Cl, Br, I, CH_3, NO_2)/Polysulfonylamines, CLXXXVI [1]. Structural Diversity in Six Tetramethylurea Di (4-X-benzenesulfonyl) amine Cocrystals (X= F, Cl, Br, I, CH_3, NO_2). *Zeitschrift für Naturforschung B* **2008,** 63, (11), 1276-1290.

[228] Zhang, J.; Bu, J. T.; Chen, S.; Wu, T.; Zheng, S.; Chen, Y.; Nieto, R. A.; Feng, P.; Bu, X., Urothermal synthesis of crystalline porous materials. *Angewandte Chemie* **2010,** 122, (47), 9060-9063.

[229] Igarashi, M.; Matsumoto, T.; Yagihashi, F.; Yamashita, H.; Ohhara, T.; Hanashima, T.; Nakao, A.; Moyoshi, T.; Sato, K.; Shimada, S., Non-aqueous selective synthesis of orthosilicic acid and its oligomers. *Nature communications* **2017,** 8, (1), 1-8.

[230] de Vries, E. J.; Nassimbeni, L. R.; Weber, E., Inclusion of amides by a fluorenyl diol host. *Journal of Inclusion Phenomena and Macrocyclic Chemistry* **2009,** 63, (3-4), 203-210.

[231] Servalli, M.; Trapp, N.; Solar, M.; Schlüter, A. D., Library of Single Crystal Structures of a D 3 h-Symmetric Hydrocarbon Cyclophane: A Comprehensive Packing Study of Anthraphane from 30 Solvents. *Crystal Growth & Design* **2017,** 17, (6), 3419-3432.

[232] Serezhkina, L.; Grigor'ev, M.; Shimin, N.; Klepov, V.; Serezhkin, V., First uranyl methacrylate complexes: Synthesis and structure. *Russian Journal of Inorganic Chemistry* **2015,** 60, (6), 672-683.

[233] Surov, A. O.; Solanko, K. A.; Bond, A. D.; Bauer-Brandl, A.; Perlovich, G. L., Crystal architecture and physicochemical properties of felodipine solvates. *CrystEngComm* **2013,** 15, (30), 6054-6061.

[234] Cullity, B. D., *Elements of X-ray Diffraction*. ed.; Addison-Wesley Publishing: 1956.

[235] Knipping, W.; von Laue, M., Interferenzerscheinungen bei Röntgenstrahlen. Sitzungsberichte der Bayerischen Akademie der Wissenschaften, Math. *Phys. Klasse* **1912**, 303-322.

[236] Connolly, J. R., Introduction to X-ray powder diffraction. *Diffraction Basics*

II: Intensities ", EPS400-001, epswww. unm. edu/xrd/xrdclass/06-Diffraction-Basics-II. ppt **2007**.

[237] Bunaciu, A. A.; UdriŞTioiu, E. G.; Aboul-Enein, H. Y., X-ray diffraction: instrumentation and applications. *Critical reviews in analytical chemistry* **2015,** 45, (4), 289-299.

[238] Rodriguez-Carvajal, J.; Roisnel, T.; Gonzales-Platas, J., FullProf suite (2005 version). *CEA-CNRS, CEN Saclay, France: Laboratoire Léon Brillouin* **2005**.

[239] Bruker, A., APEX3, SAINT-Plus, XPREP. In ed.; Bruker AXS Inc. Madison, WI, USA: 2016.

[240] Sheldrick, G. M., A short history of SHELX. *Acta Crystallographica Section A: Foundations of Crystallography* **2008,** 64, (1), 112-122.

[241] Farrugia, L., WinGX (Version 1.64. 05). *J. Appl. Crystallogr* **1999,** 32, 837-838.

[242] Höhne, G.; Hemminger, W. F.; Flammersheim, H.-J., *Differential scanning calorimetry*. ed.; Springer Science & Business Media: 2013.

[243] Menczel, J. D.; Prime, R. B., *Thermal analysis of polymers: fundamentals and applications*. ed.; John Wiley & Sons: 2009.

[244] Clas, S.-D.; Dalton, C. R.; Hancock, B. C., Differential scanning calorimetry: applications in drug development. *Pharmaceutical science & technology today* **1999,** 2, (8), 311-320.

[245] Turi, E., *Thermal characterization of polymeric materials*. ed.; Elsevier: 2012.

[246] Würflinger, A., Differential thermal analysis under high pressure IV: Low-temperature DTA of solid-solid and solid-liquid transitions of several hydrocarbons up to 3 kbar. *Berichte der Bunsengesellschaft für physikalische Chemie* **1975,** 79, (12), 1195-1201.

[247] Bloch, F., Nuclear induction. *Physical review* **1946,** 70, (7-8), 460.

[248] Purcell, E. M.; Torrey, H. C.; Pound, R. V., Resonance absorption by nuclear magnetic moments in a solid. *Physical review* **1946,** 69, (1-2), 37.

[249] Balci, M., *Basic 1H-and 13C-NMR spectroscopy*. ed.; Elsevier: 2005.

[250] Croasmun, W. R.; Carlson, R. M., *Two-dimensional NMR spectroscopy: Applications for chemists and biochemists*. ed.; John Wiley & Sons: 1994; Vol. 15.

[251] Kessler, H.; Gehrke, M.; Griesinger, C., Two-Dimensional NMR Spectroscopy: Background and Overview of the Experiments [New Analytical Methods (36)]. *Angewandte Chemie International Edition in English* **1988,** 27, (4), 490-536.

[252] Marion, D.; Wüthrich, K., Application of phase sensitive two-dimensional correlated spectroscopy (COSY) for measurements of 1 H-1 H spin-spin coupling constants in proteins. In *NMR in structural biology: A collection of papers by Kurt Wüthrich*, World Scientific: 1995; pp 114-121.

[253] Keeler, J., *Understanding NMR spectroscopy*. ed.; John Wiley & Sons: 2011.

[254] Claridge, T. D., *High-resolution NMR techniques in organic chemistry*. ed.; Elsevier: 2016; Vol. 27.

[255] Holzgrabe, U., *NMR spectroscopy in pharmaceutical analysis*. ed.; Elsevier: 2017.

[256] Larkin, P., *Infrared and Raman spectroscopy: principles and spectral interpretation*. ed.; Elsevier: 2017.

[257] Smith, B. C., *Fundamentals of Fourier transform infrared spectroscopy*. ed.; CRC press: 2011.

[258] Stoiber, R. E.; Morse, S. A., *Crystal identification with the polarizing microscope*. ed.; Springer Science & Business Media: 1994.

[259] Connors, K.; Higuchi, T., Phase solubility techniques. *Adv Anal Chem Instrum* **1965,** 4, (2).

[260] BIOVIA, D. S., Materials Studio 2019: Dassault Systèmes: San Diego, 2019.

[261] Sun, H.; Jin, Z.; Yang, C.; Akkermans, R. L.; Robertson, S. H.; Spenley, N. A.; Miller, S.; Todd, S. M., COMPASS II: extended coverage for polymer and drug-like molecule databases. *Journal of molecular modeling* **2016,** 22, (2), 47.

[262] Frisch, M.; Trucks, G.; Schlegel, H.; Scuseria, G.; Robb, M.; Cheeseman, J.; Scalmani, G.; Barone, V.; Mennucci, B.; Petersson, G., Gaussian 09 Revision Al, 2009, gaussian Inc. *Wallingford CT* **2016**.

[263] Roy, D.; Keith, T. A.; Millam, J. M., Current version: GaussView, Version 6. In ed.; Semichem Inc., Shawnee Mission, KS: 2016.

[264] Rietveld, I. B.; Barrio, M.; Veglio, N.; Espeau, P.; Tamarit, J. L.; Céolin, R., Temperature and composition-dependent properties of the two-component system D- and L-camphor at 'ordinary' pressure. *Thermochimica Acta* **2010,** 511, (1), 43-50.

[265] Cliffe, M. J.; Goodwin, A. L., PASCal: a principal axis strain calculator for thermal expansion and compressibility determination. *Journal of Applied Crystallography* **2012,** 45, (6), 1321-1329.

[266] Espeau, P.; Céolin, R., Thermodynamic studies of solids with non-negligible vapour pressure: T–v and p–T diagrams of the dimorphism of adamantane.

Thermochimica acta **2001,** 376, (2), 147-154.

[267] Lourenço, C.; Melo, C. I.; Bogel-Łukasik, R.; Bogel-Łukasik, E., Solubility Advantage of Pyrazine-2-carboxamide: Application of Alternative Solvents on the Way to the Future Pharmaceutical Development. *Journal of Chemical & Engineering Data* **2012,** 57, (5), 1525-1533.

[268] Borba, A.; Albrecht, M.; Gomez-Zavaglia, A.; Suhm, M. A.; Fausto, R., Low Temperature Infrared Spectroscopy Study of Pyrazinamide: From the Isolated Monomer to the Stable Low Temperature Crystalline Phase. *J. Phys. Chem. A* **2010,** 114, (1), 151-161.

[269] Toscani, S.; Céolin, R.; Ter Minassian, L.; Barrio, M.; Veglio, N.; Tamarit, J.-L.; Louër, D.; Rietveld, I. B., Stability hierarchy between Piracetam forms I, II, and III from experimental pressure–temperature diagrams and topological inferences. *International journal of pharmaceutics* **2016,** 497, (1-2), 96-105.

[270] Goodman, B. T.; Wilding, W. V.; Oscarson, J. L.; Rowley, R. L.; Goodman, B. T.; Wilding, W. V.; Oscarson, J. L.; Rowley, R. L., A Note on the Relationship between Organic Solid Density and Liquid Density at the Triple Point. *Journal of Chemical & Engineering Data* **2004,** 49, (6), págs. 1512-1514.

[271] Céolin, R.; Rietveld, I. B., The topological pressure-temperature phase diagram of ritonavir, an extraordinary case of crystalline dimorphism. *Annales Pharmaceutiques Françaises* **2015,** 73, (1), 22-30.

[272] Gavezzotti, A., *Molecular aggregation: structure analysis and molecular simulation of crystals and liquids.* ed.; OUP Oxford, 2007.

[273] Rietveld, I. B.; Barrio, M.; Tamarit, J. L.; Nicolaï, B.; Van de Streek, J.; Mahé, N.; Ceolin, R.; Do, B., Dimorphism of the prodrug l-tyrosine ethyl ester: Pressure–temperature state diagram and crystal structure of phase II. *Journal of pharmaceutical sciences* **2011,** 100, (11), 4774-4782.

[274] Barrio, M.; Maccaroni, E.; Rietveld, I. B.; Malpezzi, L.; Masciocchi, N.; Céolin, R.; Tamarit, J. l., Pressure–temperature state diagram for the phase relationships between benfluorex hydrochloride forms I and II: a case of enantiotropic behavior. *Journal of pharmaceutical sciences* **2012,** 101, (3), 1073-1078.

[275] Abraham, R. J.; Byrne, J. J.; Griffiths, L.; Perez, M., 1H chemical shifts in NMR: Part 23, the effect of dimethyl sulphoxide versus chloroform solvent on 1H chemical shifts. *Magnetic Resonance in Chemistry* **2006,** 44, (5), 491-509.

[276] Holzgrabe, U., Quantitative NMR spectroscopy in pharmaceutical

applications. *Progress in Nuclear Magnetic Resonance Spectroscopy* **2010,** 57, (2), 229-240.

[277] Gottlieb, H. E.; Kotlyar, V.; Nudelman, A., NMR chemical shifts of common laboratory solvents as trace impurities. *The Journal of organic chemistry* **1997,** 62, (21), 7512-7515.

[278] Laszlo, P., Solvent effects and nuclear magnetic resonance. *Progress in nuclear magnetic resonance spectroscopy* **1967,** 3, 231-402.

[279] Abraham, R., Solvent Effects in Nuclear Magnetic Resonance. *The Journal of Chemical Physics* **1961,** 34, (3), 1062-1064.

[280] Katsuyama, I.; Khalil, A. A.; Dunbar, C.; Zjawiony, J. K., Concentration-Dependent Variation of 1H-NMR Chemical Shifts of Aromatic Protons in Sampangine Derivatives. *Spectroscopy letters* **2003,** 36, (5-6), 477-485.

[281] Mitra, A.; Seaton, P. J.; Assarpour, R. A.; Williamson, T., Unprecedented concentration dependent chemical shift variation in1H-NMR studies: A caveat in the investigations of molecular recognition and structure elucidation. *Tetrahedron* **1998,** 54, (51), 15489-15498.

[282] Michaleas, S.; Antoniadou-Vyza, E., A new approach to quantitative NMR: Fluoroquinolones analysis by evaluating the chemical shift displacements. *Journal of pharmaceutical and biomedical analysis* **2006,** 42, (4), 405-410.

[283] Chiş, V.; Pirnau, A.; Jurca, T.; Vasilescu, M.; Simon, S.; Cozar, O.; David, L., Experimental and DFT study of pyrazinamide. *Chemical physics* **2005,** 316, (1-3), 153-163.

[284] Vishnyakov, A.; Widmalm, G.; Laaksonen, A., Carbohydrates exhibit a distinct preferential solvation pattern in binary aqueous solvent mixtures. *Angewandte Chemie* **2000,** 112, (1), 144-146.

[285] Bernet, B.; Vasella, A., ^{1}H-NMR Analysis of Intra-and Intermolecular H-Bonds of Alcohols in DMSO: Chemical Shift of Hydroxy Groups and Aspects of Conformational Analysis of Selected Monosaccharides, Inositols, and Ginkgolides. *Helvetica Chimica Acta* **2000,** 83, (5), 995-1021.

[286] Weinhold, M. W. J. M. F.; FARRAR, T., Solvent and concentration dependence of the hydroxyl chemical shift of methanol. *Molecular Physics* **1998,** 93, (1), 145-152.

[287] Cox, R.; Bothner-By, A., Proton nuclear magnetic resonance spectra of monosubstituted pyrazines. *The Journal of Physical Chemistry* **1968,** 72, (5), 1646-1649.

[288] Umemoto, K.; Ouchi, K., (^{15}N) acetamide in polar solvents: Hindered internal rotation and intermolecular interactions. *Organic Magnetic Resonance* **1981,** 15, (1), 13-17.

[289] Haushalter, K. A.; Lau, J.; Roberts, J. D., An NMR Investigation of the Effect of Hydrogen Bonding on the Rates of Rotation about the C− N Bonds in Urea and Thiourea. *Journal of the American Chemical Society* **1996,** 118, (37), 8891-8896.

[290] Denne, W.; Small, R., A refinement of the structure of rhombohedral acetamide. *Acta Crystallographica Section B: Structural Crystallography and Crystal Chemistry* **1971,** 27, (6), 1094-1098.

[291] Roszak, K.; Katrusiak, A., Giant anomalous strain between high-pressure phases and the mesomers of Urea. *The Journal of Physical Chemistry C* **2017,** 121, (1), 778-784.

[292] Huiszoon, C.; Tiemessen, G., Monomethylurea: a redetermination. *Acta Crystallographica Section B: Structural Crystallography and Crystal Chemistry* **1976,** 32, (5), 1604-1606.

[293] Song, G.; Bai, F.-y.; Xing, N.; Chen, C.; Shan, H.; Xing, Y.-h., Crystal engineering of multiple-component organic compound: Organic co-crystals of the functional groups of carboxyl and amino with persistent hydrogen bonding motifs. *Chemical Research in Chinese Universities* **2013,** 29, (3), 408-413.

[294] Acree Jr, W.; Chickos, J. S., Phase transition enthalpy measurements of organic and organometallic compounds. Sublimation, vaporization and fusion enthalpies from 1880 to 2015. Part 1. C1− C10. *Journal of Physical and Chemical Reference Data* **2016,** 45, (3), 033101.

[295] Štejfa, V.; Chun, S.; Pokorný, V.; Fulem, M.; Růžička, K., Thermodynamic study of acetamides. *Journal of Molecular Liquids* **2020,** 319, 114019.

[296] Bernhard, A. M.; Czekaj, I.; Elsener, M.; Wokaun, A.; Kröcher, O., Evaporation of urea at atmospheric pressure. *The Journal of Physical Chemistry A* **2011,** 115, (12), 2581-2589.

[297] Kozyro, A.; Kabo, G.; Krasulin, A.; Sevruk, V.; Simirsky, V.; Sheiman, M.; Frenkel, M., Thermodynamic properties of methylurea. *The Journal of Chemical Thermodynamics* **1993,** 25, (12), 1409-1417.

[298] Emel'yanenko, V. N.; Kabo, G. J.; Verevkin, S. P., Measurement and prediction of thermochemical properties: improved increments for the estimation of enthalpies of sublimation and standard enthalpies of formation of alkyl derivatives of urea. *Journal*

of Chemical & Engineering Data **2006,** 51, (1), 79-87.

[299] Zaitsau, D.; Kabo, G.; Kozyro, A.; Sevruk, V., The effect of the failure of isotropy of a gas in an effusion cell on the vapor pressure and enthalpy of sublimation for alkyl derivatives of carbamide. *Thermochimica acta* **2003,** 406, (1-2), 17-28.

[300] Piacente, V.; Ferro, D.; Della Gatta, G., Sublimation enthalpy of eleven alkyl derivatives of urea. *Thermochimica acta* **1990,** 158, (1), 79-85.

[301] Kneisl, P.; Zondlo, J. W., Vapor pressure, liquid density, and the latent heat of vaporization as functions of temperature for four dipolar aprotic solvents. *Journal of Chemical and Engineering Data* **1987,** 32, (1), 11-13.

[302] Gracin, S.; Rasmuson, Å. C., Polymorphism and crystallization of p-aminobenzoic acid. *Crystal growth & design* **2004,** 4, (5), 1013-1023.

[303] Li, K.; Gbabode, G.; Barrio, M.; Tamarit, J.-L.; Vergé-Depré, M.; Robert, B.; Rietveld, I. B., The phase relationship between the pyrazinamide polymorphs α and γ. *International Journal of Pharmaceutics* **2020**, 119230.

[304] Manual, O., Mini Spray Dryer B-290; Version G. In ed.; 2007.

[305] Rietveld, I. B.; Kobayashi, K.; Yamada, H.; Matsushige, K., Electrospray deposition, model, and experiment: toward general control of film morphology. *The Journal of Physical Chemistry B* **2006,** 110, (46), 23351-23364.

Appendices

Appendix A: Unit cell parameters of α, β, γ and δ form of pyrazinamide as a function of temperature

Table A.1 Unit cell parameters of α form of pyrazinamide as a function of temperature

T /K	a /Å	b /Å	c /Å	β /°	V /cm^3 g^{-1}
100	3.6190(2)	6.7437(4)	22.473(2)	92.455(4)	0.67011(6)
150	3.6404(2)	6.7380(4)	22.500(2)	92.248(4)	0.67441(6)
200	3.6646(2)	6.7304(4)	22.540(2)	92.086(4)	0.67942(6)
250	3.6919(2)	6.7171(3)	22.589(2)	91.912(5)	0.68467(6)
300	3.7198(2)	6.7123(4)	22.618(2)	91.819(4)	0.69026(7)
350	3.7511(2)	6.7078(6)	22.666(2)	91.745(3)	0.69711(8)
377.91	3.7700(2)	6.6996(5)	22.681(2)	91.678(4)	0.70027(7)
396.43	3.7811(2)	6.6981(5)	22.696(2)	91.661(4)	0.70264(8)
405.69	3.7872(2)	6.6962(5)	22.709(2)	91.648(4)	0.70400(8)
387.17	3.7757(2)	6.6977(6)	22.694(2)	91.676(4)	0.70153(8)
387.17	3.7742(3)	6.6986(10)	22.679(4)	91.608(7)	0.70090(15)
382.54	3.7727(2)	6.7018(5)	22.677(2)	91.632(4)	0.70090(8)
396.43	3.7798(3)	6.6981(6)	22.689(2)	91.628(5)	0.70219(10)
401.06	3.7852(3)	6.6993(7)	22.701(3)	91.635(6)	0.70369(11)

Table A.2 Unit cell parameters of β form of pyrazinamide as a function of temperature

T /K	a /Å	b /Å	c /Å	β /°	V /cm^3 g^{-1}
125	14.351(1)	3.6415(2)	10.6463(7)	101.278(5)	0.66724(7)
150	14.353(3)	3.6531(5)	10.6635(21)	101.332(15)	0.67042(21)
175	14.355(1)	3.6608(2)	10.6668(8)	101.434(5)	0.67190(8)
200	14.357(1)	3.6720(2)	10.6824(8)	101.543(5)	0.67480(8)
250	14.368(1)	3.6932(3)	10.7086(8)	101.777(6)	0.68029(9)
273	14.371(1)	3.7036(3)	10.7190(8)	101.867(6)	0.68279(8)
295	14.376(2)	3.7157(3)	10.7331(10)	102.006(6)	0.68580(10)
320	14.378(2)	3.7257(3)	10.7425(9)	102.091(6)	0.68815(9)

Table A.3 Unit cell parameters of γ form of pyrazinamide as a function of temperature

T /K	a /Å	b /Å	c /Å	β /°	V /cm^3 g^{-1}
100	7.1884(4)	3.6515(2)	10.6922(6)	106.580(4)	0.65789(6)
125	7.1933(5)	3.6582(3)	10.7066(9)	106.654(6)	0.66019(9)
150	7.1883(4)	3.6698(2)	10.7062(6)	106.626(4)	0.66189(6)
175	7.1931(5)	3.6767(3)	10.7174(9)	106.699(6)	0.66402(9)
200	7.1848(5)	3.6915(2)	10.7226(7)	106.656(5)	0.66638(7)
225	7.1934(6)	3.6990(3)	10.7363(10)	106.740(6)	0.66911(10)
250	7.1862(4)	3.7157(2)	10.7439(7)	106.716(4)	0.67201(7)
275	7.1955(5)	3.7232(3)	10.7582(9)	106.792(6)	0.67486(9)
297	7.1947(5)	3.7361(3)	10.7672(10)	106.804(6)	0.67765(9)
300	7.1872(5)	3.7373(2)	10.7626(8)	106.778(5)	0.67696(8)
325	7.1934(6)	3.7483(3)	10.7784(10)	106.870(6)	0.68022(9)
350	7.1913(6)	3.7638(3)	10.7873(10)	106.834(6)	0.68352(10)
373.28	7.1901(5)	3.7794(2)	10.7975(8)	106.903(5)	0.68664(8)
396.43	7.1970(6)	3.7918(3)	10.8127(9)	106.970(5)	0.69027(9)
419.58	7.2000(5)	3.8028(3)	10.8291(9)	107.014(5)	0.69345(9)
419.58	7.2061(5)	3.8035(3)	10.8320(9)	107.035(5)	0.69428(9)
424.21	7.2066(5)	3.8062(2)	10.8339(9)	107.059(5)	0.69485(9)
428.84	7.2022(5)	3.8076(3)	10.8340(9)	107.051(5)	0.69472(8)
433.47	7.2097(5)	3.8126(2)	10.8432(9)	107.111(5)	0.69673(8)
442.73	7.2082(5)	3.8149(3)	10.8428(10)	107.129(5)	0.69691(9)
461.25	7.2153(6)	3.8261(3)	10.8529(10)	107.201(5)	0.70002(9)

Table A.4 Unit cell parameters of δ form of pyrazinamide as a function of temperature

T /K	a /Å	b /Å	c /Å	α /°	β /°	γ /°	V /cm^3 g^{-1}
100	5.1262(3)	5.7101(3)	9.8561(8)	97.471(5)	98.183(4)	106.477(4)	0.65887(7)
150	5.1453(3)	5.7135(3)	9.8710(7)	97.409(5)	97.871(4)	106.444(4)	0.66370(7)
200	5.1668(3)	5.7163(3)	9.8855(8)	97.348(5)	97.525(4)	106.389(4)	0.66891(8)
250	5.1910(3)	5.7198(4)	9.9078(9)	97.244(6)	97.129(5)	106.314(4)	0.67534(8)
295	5.2156(3)	5.7229(4)	9.9260(9)	97.176(6)	96.753(4)	106.232(5)	0.68139(8)
300	5.2167(3)	5.7229(3)	9.9266(8)	97.192(6)	96.734(4)	106.238(4)	0.68156(8)
315	5.2254(3)	5.7231(4)	9.9339(9)	97.171(6)	96.601(4)	106.207(5)	0.68366(9)
325	5.2313(3)	5.7243(4)	9.9384(8)	97.112(6)	96.526(4)	106.177(5)	0.68527(8)
335	5.2384(3)	5.7253(4)	9.9397(8)	97.105(6)	96.424(5)	106.164(4)	0.68667(8)
350	5.2471(3)	5.7268(4)	9.9526(8)	97.070(6)	96.285(5)	106.136(5)	0.68934(8)
364.02	5.2585(3)	5.7270(4)	9.9638(9)	97.046(6)	96.092(8)	106.104(4)	0.69218(9)
368.65	5.2613(4)	5.7248(5)	9.9608(9)	96.942(5)	96.112(6)	106.131(6)	0.69214(10)

Table A.5 Unit cell parameters of single crystal of γ form of pyrazinamide as a function of temperature

T /K	a /Å	b /Å	c /Å	β /°
110	7.1797(17)	3.6530(9)	10.696(3)	106.630(10)
150	7.1916(2)	3.66860(10)	10.7088(3)	106.6140(10)
200	7.1927(2)	3.68970(10)	10.7275(2)	106.6580(10)
250	7.1950(2)	3.71510(10)	10.7527(4)	106.7080(10)
294	7.1962(3)	3.73780(10)	10.7692(4)	106.7550(10)
294	7.1925(3)	3.7394(2)	10.7695(5)	106.721(2)
308	7.1981(3)	3.7422(2)	10.7748(4)	106.764(2)
320	7.2001(3)	3.7454(2)	10.7900(5)	106.767(2)
355	7.2027(4)	3.7497(2)	10.7844(5)	106.774(2)
375	7.1950(3)	3.7483(2)	10.7747(4)	106.794(2)
395	7.1908(4)	3.7510(2)	10.7724(5)	106.783(2)
415	7.2030(3)	3.7625(2)	10.7940(5)	106.804(2)
435	7.1987(3)	3.76460(10)	10.7946(4)	106.804(2)
450	7.2004(4)	3.7710(2)	10.8003(6)	106.791(2)

Appendix B: Unit cell parameters of α, β, γ and δ form of pyrazinamide as a function of pressure

Table B.1 Unit cell parameters of α form of pyrazinamide as a function of pressure

p /MPa	a /Å	b /Å	c /Å	β /°	V /cm^3 g^{-1}
17(5)	3.7128(3)	6.7125(5)	22.610(3)	91.85(1)	0.6887(1)
16(5)	3.7120(2)	6.7109(5)	22.604(3)	91.85(1)	0.6882(1)
19(5)	3.7114(2)	6.7107(4)	22.601(3)	91.85(1)	0.6880(1)
22(5)	3.7103(2)	6.7108(4)	22.597(2)	91.86(1)	0.6877(1)
26(5)	3.7091(2)	6.7108(5)	22.595(3)	91.86(1)	0.6874(1)
31(5)	3.7079(2)	6.7107(5)	22.593(3)	91.86(1)	0.6871(1)
36(5)	3.7062(2)	6.7109(5)	22.592(3)	91.89(1)	0.6868(1)
41(5)	3.7050(3)	6.7109(5)	22.589(3)	91.88(2)	0.6865(1)
47(5)	3.7032(3)	6.7110(3)	22.587(2)	91.89(2)	0.6861(1)
60(5)	3.7007(3)	6.7096(6)	22.583(3)	91.87(2)	0.6854(2)
70(5)	3.6979(3)	6.7093(6)	22.580(3)	91.88(2)	0.6847(2)
80(5)	3.6953(3)	6.7091(6)	22.576(3)	91.88(2)	0.6841(2)
93(5)	3.6921(3)	6.7094(6)	22.571(3)	91.89(2)	0.6834(2)
108(5)	3.6889(4)	6.7100(6)	22.563(3)	91.89(2)	0.6826(2)
124(5)	3.6841(4)	6.7102(6)	22.556(3)	91.86(2)	0.6815(2)
139(5)	3.6798(3)	6.7092(6)	22.552(3)	91.87(2)	0.6805(2)
155(5)	3.6759(3)	6.7091(6)	22.545(3)	91.89(2)	0.6796(2)
174(5)	3.6722(4)	6.7085(7)	22.541(3)	91.90(2)	0.6787(2)
193(5)	3.6688(4)	6.7081(7)	22.535(3)	91.92(2)	0.6779(2)
222(5)	3.6616(4)	6.7073(8)	22.529(4)	91.97(2)	0.6763(2)
255(5)	3.6552(4)	6.7087(7)	22.517(4)	92.02(2)	0.6748(2)
286(5)	3.6499(4)	6.7088(8)	22.506(4)	92.04(2)	0.6735(2)
318(5)	3.6440(4)	6.7074(8)	22.498(4)	92.07(2)	0.6720(2)
341(5)	3.6400(4)	6.7072(8)	22.490(4)	92.09(2)	0.6710(2)
363(5)	3.6332(5)	6.7119(8)	22.466(4)	92.05(2)	0.6696(2)
386(5)	3.6296(5)	6.7112(8)	22.460(4)	92.07(2)	0.6686(2)
407(5)	3.6257(5)	6.7110(8)	22.455(4)	92.10(2)	0.6677(2)

p /MPa	a /Å	b /Å	c /Å	β /°	V /cm^3 g^{-1}
428(5)	3.6222(5)	6.7108(8)	22.448(4)	92.14(2)	0.6668(2)
451(5)	3.6182(5)	6.7108(8)	22.439(4)	92.17(2)	0.6658(2)
471(5)	3.6146(5)	6.7105(8)	22.437(4)	92.21(2)	0.6650(2)
492(5)	3.6115(5)	6.7104(9)	22.430(4)	92.25(3)	0.6642(2)
512(5)	3.6081(5)	6.7104(9)	22.425(5)	92.28(3)	0.6635(2)
533(5)	3.6049(5)	6.7099(9)	22.422(5)	92.31(3)	0.6627(2)
554(5)	3.6016(5)	6.7094(9)	22.416(5)	92.34(3)	0.6618(2)
573(5)	3.5986(5)	6.7095(9)	22.407(5)	92.34(2)	0.6610(2)
594(5)	3.5955(5)	6.7089(9)	22.403(4)	92.36(3)	0.6603(2)
613(5)	3.5923(5)	6.7086(9)	22.396(5)	92.35(3)	0.6595(2)
633(5)	3.5894(6)	6.7084(9)	22.390(5)	92.36(3)	0.6588(2)
654(5)	3.5867(6)	6.7077(10)	22.385(5)	92.36(3)	0.6580(2)
673(5)	3.5835(5)	6.7065(10)	22.384(5)	92.36(3)	0.6573(2)
691(5)	3.5811(6)	6.7061(10)	22.380(5)	92.37(3)	0.6567(2)
708(5)	3.5788(6)	6.7053(10)	22.375(5)	92.38(3)	0.6561(2)
728(5)	3.5756(5)	6.7047(10)	22.370(5)	92.39(3)	0.6553(2)
747(5)	3.5706(6)	6.7073(10)	22.351(5)	92.56(3)	0.6540(3)
764(5)	3.5681(7)	6.7066(10)	22.348(5)	92.56(3)	0.6533(2)
782(5)	3.5659(6)	6.7061(10)	22.340(5)	92.56(3)	0.6527(3)
799(5)	3.5640(8)	6.7055(10)	22.336(5)	92.58(3)	0.6521(3)
817(5)	3.5618(8)	6.7051(11)	22.326(6)	92.58(4)	0.6514(3)
835(5)	3.5591(8)	6.7042(11)	22.321(5)	92.61(4)	0.6506(3)
852(5)	3.5563(9)	6.7037(12)	22.313(6)	92.64(4)	0.6498(3)
871(5)	3.5532(8)	6.7043(12)	22.304(6)	92.69(4)	0.6490(3)
887(5)	3.5509(9)	6.7041(12)	22.295(6)	92.71(4)	0.6483(3)
903(5)	3.5495(10)	6.7032(12)	22.291(6)	92.73(4)	0.6479(3)
939(5)	3.5464(11)	6.7010(12)	22.281(6)	92.75(4)	0.6468(3)
979(5)	3.5387(11)	6.6986(12)	22.267(6)	92.82(4)	0.6447(3)
1018(5)	3.5359(12)	6.6960(13)	22.256(6)	92.84(4)	0.6436(3)
1059(5)	3.5333(14)	6.6932(13)	22.251(6)	92.88(5)	0.6427(3)
1135(5)	3.5273(16)	6.6882(14)	22.232(7)	92.95(6)	0.6406(4)
1209(5)	3.5227(17)	6.6837(15)	22.207(8)	92.92(7)	0.6386(4)
1317(5)	3.5067(17)	6.6751(16)	22.187(8)	92.75(8)	0.6344(4)

p /MPa	a /Å	b /Å	c /Å	β /°	V /cm^3 g^{-1}
1420(5)	3.4981(18)	6.6698(16)	22.161(8)	92.62(8)	0.6316(5)
1514(5)	3.4921(20)	6.6656(17)	22.136(8)	92.66(9)	0.6294(5)
1603(5)	3.4870(21)	6.6614(17)	22.109(9)	92.65(10)	0.6274(5)
1688(5)	3.4813(25)	6.6551(18)	22.093(9)	92.59(11)	0.6253(6)
1776(5)	3.4777(26)	6.6507(18)	22.062(9)	92.51(12)	0.6234(6)
1864(5)	3.4697(26)	6.6419(19)	22.051(9)	92.52(12)	0.6208(6)
1950(5)	3.4662(27)	6.6362(19)	22.038(10)	92.53(14)	0.6193(6)
2065(5)	3.4609(26)	6.6220(20)	22.037(9)	92.59(15)	0.6170(6)

Table B.2 Unit cell parameters of β form of pyrazinamide as a function of pressure

p /MPa	a /Å	b /Å	c /Å	β /°	V /cm^3 g^{-1}
24(9)	14.360(3)	3.710(1)	10.723(1)	101.93(1)	0.6835(2)
84(9)	14.356(4)	3.709(1)	10.723(2)	101.95(2)	0.6830(2)
85(12)	14.375(6)	3.706(1)	10.720(3)	101.94(3)	0.6832(3)
144(9)	14.373(5)	3.699(1)	10.722(3)	101.91(3)	0.6822(3)
147(9)	14.370(5)	3.694(1)	10.724(3)	101.96(3)	0.6810(3)
206(10)	14.358(5)	3.686(1)	10.719(3)	101.94(3)	0.6787(4)
208(10)	14.347(6)	3.677(2)	10.703(3)	101.73(4)	0.6760(4)
271(10)	14.326(7)	3.666(2)	10.708(6)	101.70(6)	0.6734(6)
334(13)	14.329(9)	3.648(2)	10.676(13)	101.36(10)	0.6690(10)
397(16)	14.379(6)	3.600(3)	10.658(6)	101.52(9)	0.6611(7)
398(16)	14.379(6)	3.600(3)	10.658(6)	101.52(9)	0.6611(7)
399(15)	14.373(6)	3.599(2)	10.652(5)	101.49(8)	0.6603(6)
403(22)	14.318(9)	3.631(2)	10.661(7)	101.41(5)	0.6644(7)
464(18)	14.351(11)	3.596(2)	10.635(12)	101.35(19)	0.6580(10)
468(15)	14.336(7)	3.589(2)	10.631(7)	101.48(12)	0.6555(7)
530(16)	14.298(10)	3.618(1)	10.648(12)	101.31(9)	0.6606(9)
597(28)	14.321(10)	3.586(2)	10.588(15)	101.47(14)	0.6517(11)
598(21)	14.282(9)	3.605(2)	10.637(15)	101.22(10)	0.6569(11)
665(20)	14.340(10)	3.590(2)	10.558(16)	101.57(16)	0.6511(12)
670(22)	14.280(8)	3.590(2)	10.617(16)	101.12(9)	0.6532(11)
733(17)	14.331(8)	3.584(2)	10.554(16)	101.54(13)	0.6494(11)
802(28)	14.275(7)	3.579(2)	10.589(10)	101.06(9)	0.6492(8)
803(17)	14.303(13)	3.582(2)	10.574(19)	101.22(24)	0.6499(14)
877(28)	14.262(8)	3.568(2)	10.570(10)	100.95(10)	0.6459(8)
943(38)	14.240(11)	3.560(3)	10.564(17)	100.81(21)	0.6432(13)
1016(19)	14.242(21)	3.557(2)	10.548(18)	100.83(44)	0.6419(18)
1019(60)	14.239(10)	3.554(2)	10.553(22)	100.84(16)	0.6415(15)
1234(38)	14.236(21)	3.531(3)	10.541(37)	100.71(43)	0.6366(26)
1312(24)	14.221(12)	3.552(3)	10.523(23)	100.51(21)	0.6391(16)
1622(27)	14.223(13)	3.521(4)	10.504(24)	100.88(23)	0.6317(17)

Table B.3 Unit cell parameters of γ form of pyrazinamide as a function of pressure

p /MPa	a /Å	b /Å	c /Å	β /°	V /cm^3 g^{-1}
209(6)	7.186(1)	3.6998(3)	10.7220(6)	106.65(1)	0.6680(1)
223(7)	7.185(1)	3.6986(3)	10.7203(6)	106.64(1)	0.6676(1)
403(8)	7.174(2)	3.6689(5)	10.6949(8)	106.65(2)	0.6596(2)
516(9)	7.178(2)	3.6461(6)	10.6780(9)	106.66(2)	0.6548(2)
604(9)	7.180(2)	3.6294(6)	10.6662(9)	106.62(2)	0.6514(2)
684(9)	7.175(1)	3.6168(5)	10.6580(8)	106.68(2)	0.6480(2)
812(8)	7.162(1)	3.5978(5)	10.6439(8)	106.72(1)	0.6424(2)
924(8)	7.154(1)	3.5839(4)	10.6306(8)	106.72(2)	0.6385(2)
1027(9)	7.150(1)	3.5710(4)	10.6171(9)	106.72(2)	0.6350(2)
1124(9)	7.143(2)	3.5600(4)	10.6049(9)	106.70(2)	0.6318(2)
1271(9)	7.141(2)	3.5437(5)	10.5850(10)	106.65(2)	0.6277(2)
1434(10)	7.142(2)	3.5263(5)	10.5640(10)	106.56(2)	0.6238(2)
1620(11)	7.151(2)	3.5048(7)	10.5440(12)	106.56(2)	0.6195(3)
1849(11)	7.153(2)	3.4797(8)	10.5213(12)	106.55(2)	0.6140(3)

Table B.4 Unit cell parameters of δ form of pyrazinamide as a function of pressure

p /MPa	a /Å	b /Å	c /Å	α /°	β /°	γ /°	V /cm^3 g^{-1}
13(3)	5.2132(6)	5.7186(4)	9.930(2)	97.18(2)	96.68(2)	106.25(2)	0.6809(2)
16(3)	5.2119(5)	5.7181(4)	9.928(2)	97.15(2)	96.71(2)	106.25(2)	0.6805(2)
17(3)	5.2112(5)	5.7184(4)	9.928(2)	97.18(2)	96.71(1)	106.25(1)	0.6805(2)
17(3)	5.2111(5)	5.7184(4)	9.928(2)	97.18(2)	96.71(1)	106.25(1)	0.6804(2)
18(3)	5.2124(5)	5.7185(4)	9.928(2)	97.16(2)	96.71(1)	106.25(1)	0.6806(2)
22(3)	5.2110(5)	5.7182(4)	9.928(2)	97.17(2)	96.72(1)	106.25(1)	0.6804(2)
29(3)	5.2102(5)	5.7178(4)	9.928(2)	97.17(2)	96.72(1)	106.25(1)	0.6802(2)
16(3)	5.2117(6)	5.7172(5)	9.923(2)	97.16(2)	96.73(2)	106.25(2)	0.6801(2)
15(3)	5.2113(7)	5.7163(5)	9.921(2)	97.16(2)	96.71(2)	106.25(2)	0.6798(2)
16(3)	5.2114(7)	5.7152(5)	9.919(2)	97.17(2)	96.71(2)	106.25(2)	0.6795(2)
22(3)	5.2096(8)	5.7143(6)	9.917(3)	97.15(2)	96.72(2)	106.26(2)	0.6790(2)
29(4)	5.2090(8)	5.7134(6)	9.913(3)	97.15(2)	96.73(2)	106.27(2)	0.6785(3)
32(3)	5.2077(9)	5.7119(6)	9.908(3)	97.15(2)	96.74(2)	106.27(2)	0.6778(3)
50(3)	5.2045	5.7093(6)	9.898(3)	97.12(2)	96.83(3)	106.28(2)	0.6763(3)
79(3)	5.1972	5.7071(7)	9.876(4)	97.10(2)	97.01(3)	106.32(2)	0.6730(3)
117(2)	5.1860	5.7028(7)	9.865(4)	97.07(2)	97.17(3)	106.39(2)	0.6698(4)
164(2)	5.1776	5.6960(7)	9.835(4)	97.09(2)	97.40(3)	106.31(2)	0.6656(3)
218(2)	5.1668	5.6899(7)	9.817(4)	97.06(2)	97.57(3)	106.34(2)	0.6619(3)
274(2)	5.1562	5.6839(7)	9.796(3)	97.04(3)	97.74(3)	106.36(2)	0.6581(3)
327(3)	5.1473	5.6781(7)	9.781(3)	97.02(3)	97.90(2)	106.38(2)	0.6548(3)
382(3)	5.1383	5.6722(7)	9.762(3)	97.02(3)	98.04(2)	106.39(2)	0.6514(3)
440(3)	5.1278	5.6675(7)	9.751(3)	97.03(2)	98.18(2)	106.44(2)	0.6483(3)
500(4)	5.1196	5.6622(7)	9.737(3)	97.02(3)	98.30(2)	106.45(2)	0.6454(3)
631(4)	5.1045	5.6499(8)	9.706(3)	97.01(3)	98.53(2)	106.38(3)	0.6398(3)
785(5)	5.0887	5.6402(9)	9.675(3)	97.06(3)	98.76(2)	106.38(3)	0.6341(3)
1079(5)	5.0623	5.6213(9)	9.616(4)	97.10(3)	99.19(2)	106.39(3)	0.6237(4)
1079(5)	5.0624	5.6213(9)	9.616(4)	97.10(3)	99.18(2)	106.39(3)	0.6238(4)
1216(5)	5.0498	5.6127(10)	9.593(4)	97.16(4)	99.37(2)	106.37(4)	0.6192(4)
1369(4)	5.0347	5.6035(11)	9.576(4)	97.25(4)	99.54(2)	106.31(4)	0.6149(4)
1511(6)	5.0215	5.5952(11)	9.559(4)	97.24(3)	99.72(2)	106.29(4)	0.6109(5)
1647(5)	5.0064	5.5878(11)	9.545(5)	97.25(3)	99.87(2)	106.28(4)	0.6070(5)

Appendix C: Data of α and γ form of pyrazinamide measured for P-T phase diagram

Table C.1 The melting point and enthalpy of fusion of γ form as a function of the sample mass (obtained by the DSC 214, Netzsch)[a]

NO.	Mass of sample /mg	V/mass /cm^3 g^{-1}	Melting point /K	Enthalpy of fusion /J g^{-1}
1	15.09	2.98	462.05	240.60
2	11.63	3.87	462.32	240.10
3	10.27	4.38	462.08	237.30
4	8.58	5.24	462.21	239.30
5	8.50	5.29	461.98	238.10
6	7.19	6.26	461.94	237.20
7	5.88	7.65	462.08	234.80
8	5.44	8.27	461.86	233.20
9	4.74	9.49	461.85	235.00
10	4.72	9.53	462.04	231.80
11	4.11	10.95	462.04	233.80
12	3.87	11.63	461.94	235.00
13	3.42	13.16	461.95	232.30
14	3.20	14.06	462.03	235.30
15	3.17	14.20	461.98	231.50
16	2.43	18.52	462.06	230.00
17	1.99	22.61	462.15	230.90
18	1.93	23.32	462.05	228.90
19	1.04	43.27	461.93	229.60
20	0.93	48.39	462.01	226.60
21	0.58	77.59	461.96	224.50
22	0.45	100.00	462.03	217.00
23	0.39	115.38	462.15	221.10
24	0.17	264.71	461.95	211.60
25	0.08	562.50	461.93	173.10

NO.	Mass of sample /mg	V/mass /cm^3 g^{-1}	Melting point /K	Enthalpy of fusion /J g^{-1}
26	0.06	750.00	461.90	130.30
27	0.03	1500.00	461.85	39.45
28	0.01	4500.00	449[b]	

[a] The volume of the DSC pan is 45 μL.

[b] The end of the sublimation peak. No solid was left once the temperature of fusion was reached.

Table C.2 Transition temperature and enthalpy of α to γ form at different heating rate

NO.	Heating rate /K min^{-1}	Transition temperature /K	Transition enthalpy /J g^{-1}
		DSC 214 (Netzsch)	
1	0.05	407.73	12.15
2	0.05	407.73	13.59
3	0.1	410.88	13.05
4	0.1	409.15	14.20
5	0.2	413.30	12.35
6	0.2	410.64	12.62
7	0.2	411.34	12.62
8	0.5	413.33	12.31
9	0.5	414.53	15.21
10	1	419.02	11.66
11	2	418.12	12.47
12	2	418.57	12.96
13	5	421.67	13.16
14	5	422.46	12.47
15	5	422.08	13.12
16	5	421.41	13.95
17	5	421.83	12.84
18	10	424.73	13.51
19	10	424.44	13.09
20	10	423.29	13.48
21	10	424.91	13.59
22	10	425.03	13.52

NO.	Heating rate /K min^{-1}	Transition temperature /K	Transition enthalpy /J g^{-1}
23	10	424.82	13.50
24	10	424.26	13.33
25	10	425.03	14.70
26	10	424.50	14.14
27	10	424.82	13.10
28	10	424.40	13.75
29	20	427.26	12.83
30	20	427.52	13.56
31	20	427.17	13.94
32	30	429.37	14.91
33	40	430.82	13.08
34	40	430.28	14.16
35	40	431.05	13.02
36	50	431.64	12.73
37	50	431.85	12.88
38	50	431.85	13.74
39	60	432.70	13.58
40	60	432.76	13.80
41	70	433.24	13.19
42	80	434.99	12.84
43	100	436.05	13.22
44	120	436.91	12.36
45	140	436.71	-[a]
46	140	436.81	-[a]
47	160	438.77	-[a]
48	160	439.44	-[a]
49	180	438.70	-[a]
50	180	438.36	-[a]
51	200	439.20	-[a]
		TA Q100	
52	10	423.08	13.05
53	10	423.30	13.28

NO.	Heating rate /K min^{-1}	Transition temperature /K	Transition enthalpy /J g^{-1}
54	10	423.42	12.96
55	10	423.44	13.22
56	10	423.53	13.36
57	10	423.61	13.48
58	10	423.73	12.71
59	10	423.78	13.08
60	10	423.82	13.27
61	10	423.85	13.18
62	10	423.92	13.08
63	10	423.98	13.47
64	10	423.98	12.88
65	10	424.00	13.66
66	10	424.01	13.3
67	10	424.01	13.04
68	10	424.03	13.33
69	10	424.04	13.50
70	10	424.05	12.98
71	10	424.15	13.05
72	10	424.15	13.13
73	10	424.26	13.33
74	10	424.28	13.42
75	10	424.29	13.03
76	10	424.29	12.97
77	10	424.30	12.80
78	10	424.34	13.49
79	10	424.43	12.86
80	10	424.48	12.79
81	10	424.53	13.21
82	10	424.72	13.34
83	10	424.82	13.20
84	10	424.86	12.94
85	10	424.88	13.12

NO.	Heating rate /K min^{-1}	Transition temperature /K	Transition enthalpy /J g^{-1}
86	10	424.90	13.12
87	10	424.95	12.70
88	10	425.00	13.13
89	10	425.01	12.61
90	10	425.48	12.23

[a] Enthalpy data not accurate enough due to high scanning rate

Table C.3 The melting temperature and pressure obtained by HP-DTA

NO.	The melting point / K	The pressure / MPa
1	463.55	9.89
2	467.15	17.74
3	468.55	21.87
4	470.35	28.76
5	465.95	29.04
6	473.15	40.13
7	470.55	43.8
8	473.15	46.33
9	475.75	48.32
10	475.15	49.03
11	473.75	57.86
12	476.55	59.18
13	475.65	59.83
14	477.75	65.15
15	481.55	68.52
16	479.95	71.27
17	481.15	73.88
18	482.55	80.05
19	483.15	83.74
20	486.55	88.82

Table C.4 The transition temperature and pressure of α to γ form obtained by HP-DTA

The transition temperature /K	The pressure /MPa
414.55	6.81
415.15	12.93
411.15	23.26
407.55	36.82

Table C.5 The vapor pressure of α and γ form at different temperatures

α form		γ form	
T /K	*p* /Pa	*T* /K	*p* /Pa
293.15	0.001207(60)	323.15	0.0564(20)
295.15	0.001657(190)	333.15	0.167(9)
301.15	0.0036(1)	343.15	0.484(32)
313.15	0.01804(5)	363.16	2.88(6)
323.15	0.04922(92)	383.15	11.9(1.3)
333.15	0.1621(34)		
343.15	0.428(10)		
363.15	2.59(1)		
373.15	5.68(49)		
383.15	10.32(65)		

TableC.6 The solubility of α and γ form at different temperatures in water

This work		Literature[a]		Literature[b]	
T /K	x /mmol mol^{-1}	T /K	x /mmol mol^{-1}	T /K	x /mmol mol^{-1}
		Form α			
283.15	1.302(18)	284.85	1.194	278.15	1.048
293.15	1.967(5)	290.35	1.610	283.15	1.312
303.15	2.844(42)	297.25	2.239	288.15	1.684
313.15	4.259(3)	300.75	2.480	293.15	1.941
		305.45	3.115	298.15	2.396
		310.55	3.785	303.15	2.839
		322.85	6.755	308.15	3.622
		344.05	17.538	313.15	4.211
				318.15	5.210
				323.15	6.000
		Form γ			
283.15	1.506(18)	283.15	1.402		
293.15	2.147(17)	290.85	1.939		
303.15	3.037(19)	300.65	3.130		
313.15	4.495(83)	308.65	3.892		
		310.15	4.661		
		313.15	5.079		
		316.15	5.437		

[a] Hermanto, M. W.; Yeoh, A.; Soh, B.; Chow, P. S.; Tan, R. B., Robust Crystallization Process Development for the Metastable δ-form of Pyrazinamide. *Organic Process Research & Development* **2015**, 19, (12), 1987-1996

[b] Zhang, K.; Shen, H.; Xu, S.; Zhang, H.; Zhu, M.; Shi, P.; Fu, X.; Yang, Y.; Gong, J., Thermodynamic study of solubility for pyrazinamide in ten solvents from T=(283.15 to 323.15) K. *The Journal of Chemical Thermodynamics* **2017**, 112, 204-212.

The standard uncertainty of temperature is u (T) = 0.1 K. The relative standard uncertainty of the solubility is u_r (x) = 0.039.

Appendix D: DSC results measured by using δ form

Table D.1 DSC results measured by using δ form at different heating rate

NO.	Heating rate /K min^{-1}	Transition temperature /K	Transition enthalpy /J g^{-1}
		Transition of δ to γ	
1	2	400.09	14.69
2	2	402.24	14.59
3	4	401.76	16.68
4	4	402.63	12.81
5	4	405.84	14.47
6	5	402.61	16.33
7	5	402.15	15.70
8	6	406.36	15.01
9	6	405.95	15.71
10	8	406.23	16.17
11	8	404.89	16.58
12	10	405.65	16.58
13	10	406.21	16.38
14	10	405.98	16.44
15	10	407.11	16.51
16	10	406.20	15.68
17	10	406.97	16.92
18	10	404.26	17.57
19	10	404.96	17.92
20	10	404.99	17.37
21	10	406.07	16.88
22	10	404.94	17.06
23	10	405.37	17.10
24	10	406.40	16.93
25	10	405.49	18.36
26	10	405.03	18.10

NO.	Heating rate /K min^{-1}	Transition temperature /K	Transition enthalpy /J g^{-1}
27	10	405.54	17.70
28	10	407.97	17.03
		Transition of δ to α	
29	0.5	386.33	5.46
30	1	386.72	6.02

Appendix E: Calculation results

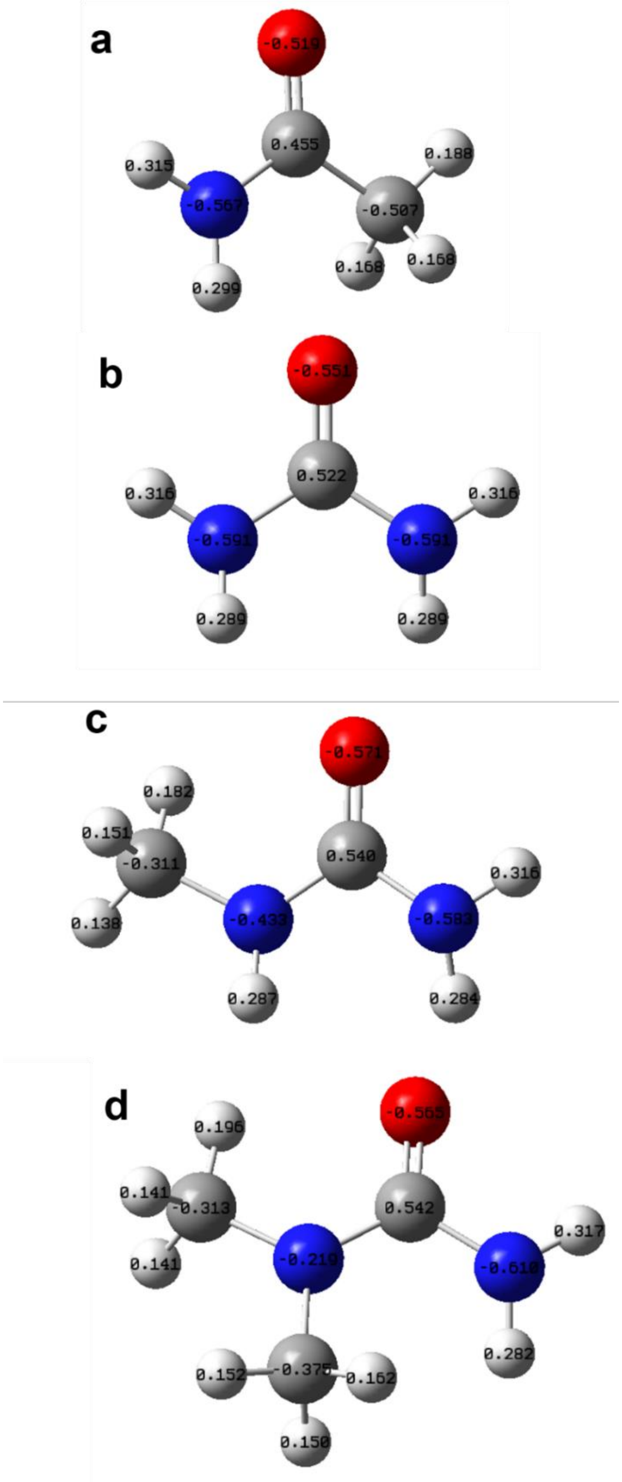

Figure E1-1 Atomic charge distribution of (a) acetamide, (b) urea, (c) *N*-methylurea, (d) 1,1-dimethylurea

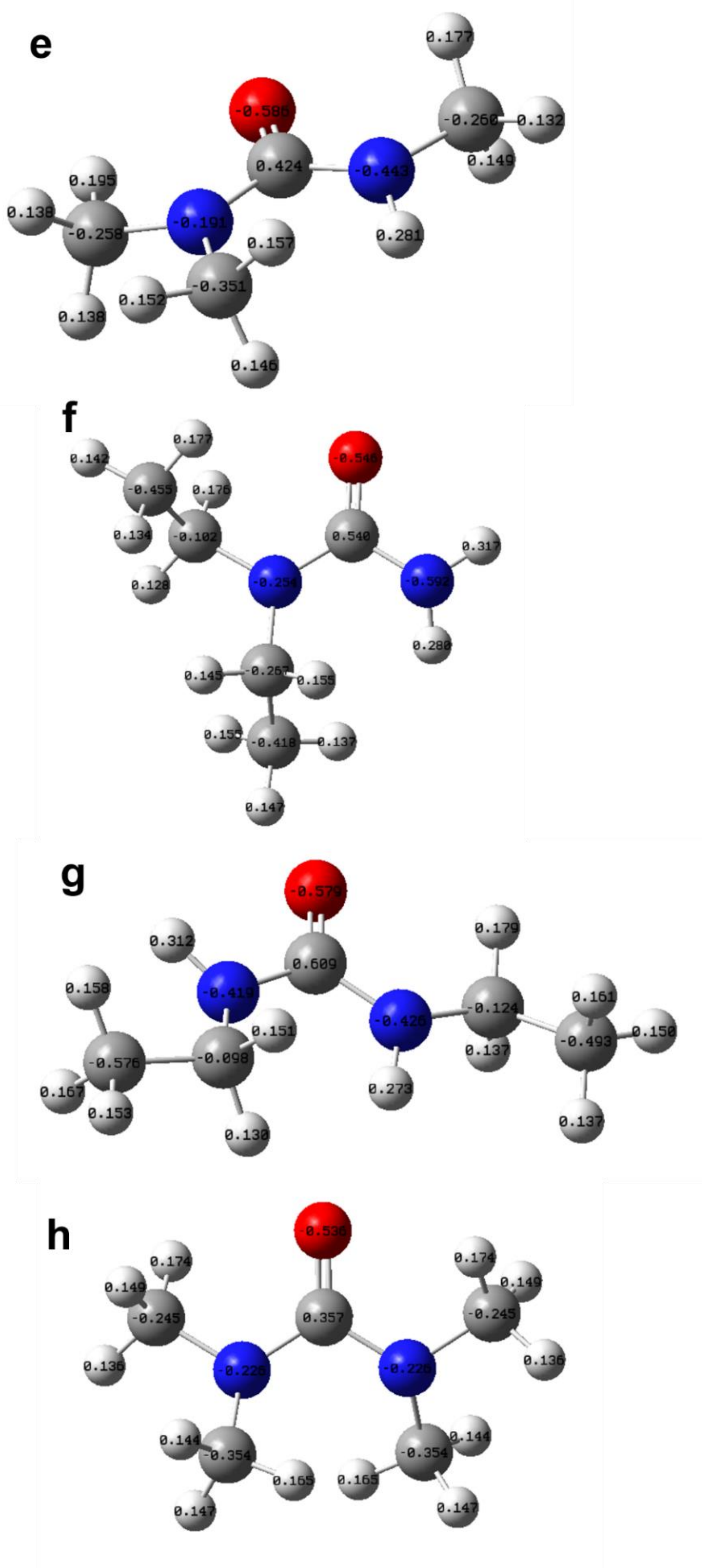

Figure E.1-2 Atomic charge distribution of (e) trimethylurea, (f) 1,1-diethylurea, (g) 1,3-diethylurea and (h) tetramethylurea

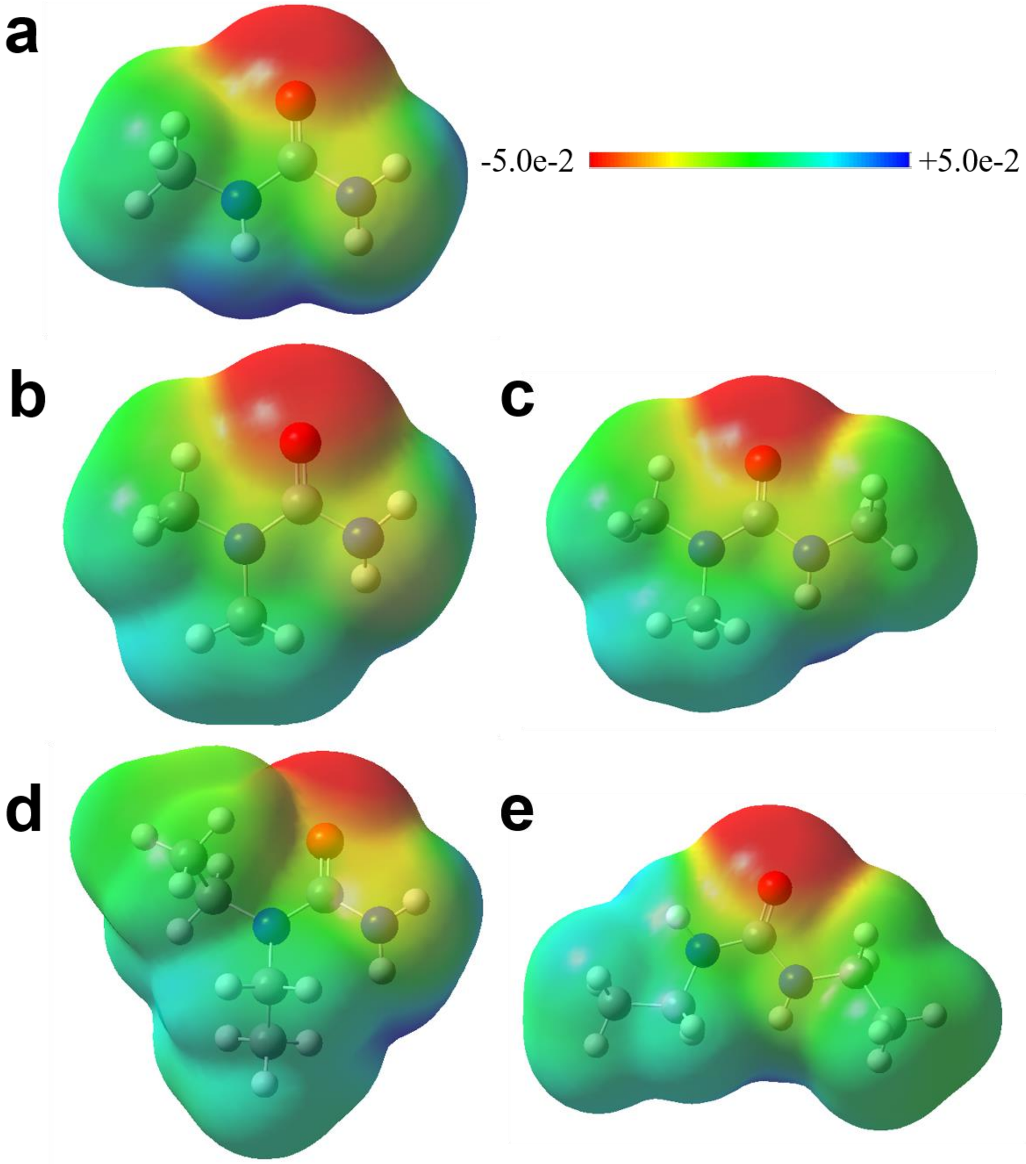

Figure E.2 Electron density distribution maps of (a) *N*-methylurea, (b) 1,1-dimethylurea, (c) trimethylurea, (d) 1,1-diethylurea and (e) 1,3-diethylurea

Appendix F: DSC curves with the melting points of the urea derivatives

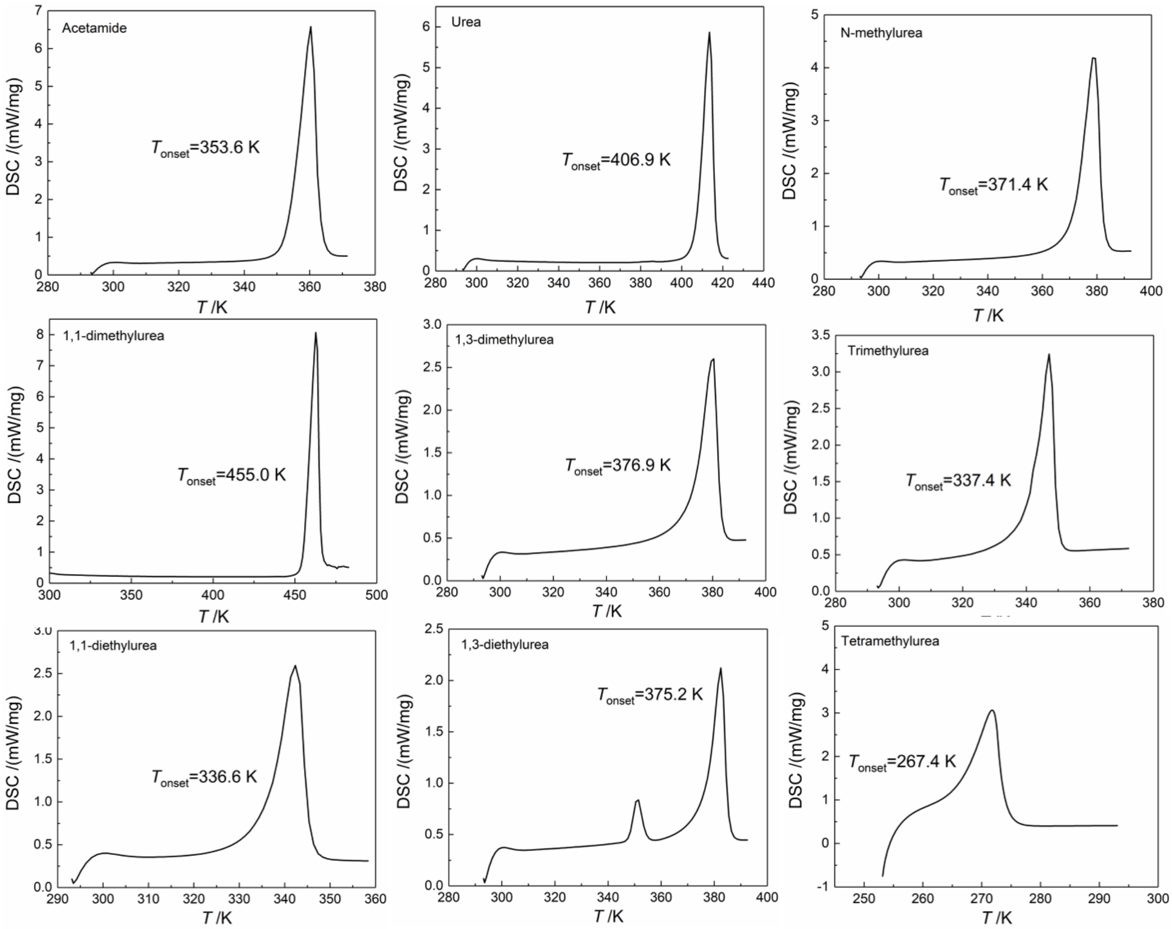

Figure F.1 DSC curves with the melting points of the urea derivatives used in this thesis

Appendix G: Vapor pressure of additives as a function of temperature in the literature

Table G.1 Vapor pressure of liquid acetamide in the literature[a]

T /K	p /Pa
324.07	45[b]
324.08	44.97[b]
324.09	45.05[b]
328.62	62.83[b]
328.62	62.8[b]
328.62	62.87[b]
333.22	87.32[b]
333.22	87.32[b]
333.23	87.31[b]
337.74	119.27[b]
337.74	119.33[b]
337.75	119.28[b]
342.09	159.47[b]
342.09	159.57[b]
342.09	159.61[b]
346.71	215.28[b]
346.71	215.33[b]
346.71	215.39[b]
351.22	285.98[b]
351.22	285.95[b]
351.22	286.01
355.59	373.3
355.59	373.36
355.59	373.59
360.09	487.28
360.09	487.29
360.09	487.27

T /K	p /Pa
364.47	626.64
364.47	626.73

[a] Štejfa, V.; Chun, S.; Pokorný, V.; Fulem, M.; Růžička, K., Thermodynamic study of acetamides. *Journal of Molecular Liquids* **2020**, 319, 114019.

[b] Supercooled liquid

Table G.2 Vapor pressure of solid urea in the literature[a]

T /K	p /Pa
353.15	0.46
363.15	0.71
373.15	1.82
383.15	3.65
390.15	8.43
393.15	10.87
393.15	9.42
396.15	11.49
399.15	17.44
402.15	16.39
403.15	19.79

[a] Bernhard, A. M.; Czekaj, I.; Elsener, M.; Wokaun, A.; Kröcher, O., Evaporation of urea at atmospheric pressure. *The Journal of Physical Chemistry A* **2011**, 115, (12), 2581-2589.

Table G.3 Vapor pressure of liquid *N*-methylurea in the literature[a]

T /K	p /Pa
377.2	23.45
381.51	33.06
385.62	44.3
389.72	58.79
393.5	76.44
397.6	99.55
401.85	131.3
406	167.8
410.3	212.5

[a] Kozyro, A.; Kabo, G.; Krasulin, A.; Sevruk, V.; Simirsky, V.; Sheiman, M.; Frenkel, M., Thermodynamic properties of methylurea. *The Journal of Chemical Thermodynamics* **1993**, 25, (12), 1409-1417.

Table G.4 Vapor pressure of solid 1,1-dimethylurea in the literature[a]

T /K	p /Pa
346.3	3.14
356.1	7.53
362.2	12.56
365.2	16.62
368.1	20.55
371.2	27.35
374.2	27.35
377.2	43.28
380.2	54.27
383.3	67.39
386.3	86.51
389.3	105.95
392.2	130.09
395.2	159.23
398.3	197.68

[a] Emel'yanenko, V. N.; Kabo, G. J.; Verevkin, S. P., Measurement and prediction of thermochemical properties: improved increments for the estimation of enthalpies of sublimation and standard enthalpies of formation of alkyl derivatives of urea. *Journal of Chemical & Engineering Data* **2006**,

51, (1), 79-87.

Table G.5 Vapor pressure of solid 1,3-dimethylurea in the literature[a]

T /K	p /Pa
317.14	0.2418
321.16	0.3689
325.22	0.5514
329.31	0.8489
332.97	1.188
336.41	1.652
340.05	2.282
343.12	3.017
346.35	4.407
349.95	5.558
353.24	7.502
356.27	8.856
360.91	13.27
364.8	19.66
364.83	19.89
366.08	20.79
369.05	26.77
372.66	33.64
377.61	48.13

[a] Zaitsau, D.; Kabo, G.; Kozyro, A.; Sevruk, V., The effect of the failure of isotropy of a gas in an effusion cell on the vapor pressure and enthalpy of sublimation for alkyl derivatives of carbamide. *Thermochimica acta* **2003,** 406, (1-2), 17-28.

Table G.6 Vapor pressure of solid 1,1-diethylurea in the literature[a]

T /K	p /Pa
305.11	0.2261
309.81	0.4104
314.23	0.7069
322.22	1.762
326.32	2.719
330.04	3.93
334.26	6.098
337.81	8.737
338.09	9.031
340.53	11.73
343.68	16.27
347.1	21.79

[a] Zaitsau, D.; Kabo, G.; Kozyro, A.; Sevruk, V., The effect of the failure of isotropy of a gas in an effusion cell on the vapor pressure and enthalpy of sublimation for alkyl derivatives of carbamide. *Thermochimica acta* **2003,** 406, (1-2), 17-28.

Table G.7 Vapor pressure of solid 1,3-diethylurea in the literature[a]

T /K	p /Pa
323.42	0.2699
328.41	0.4558
333.51	0.8021
338.26	1.286
343.22	2.05
347.77	3.036
353.33	5.031
358.98	8.315
362.86	11.13
368.16	17.39
368.19	17.6
372.84	24.69
378.52	38.87
383.3	54.85

T /K	p /Pa
384.73	66.3
384.73	68.21

[a] Zaitsau, D.; Kabo, G.; Kozyro, A.; Sevruk, V., The effect of the failure of isotropy of a gas in an effusion cell on the vapor pressure and enthalpy of sublimation for alkyl derivatives of carbamide. *Thermochimica acta* **2003,** 406, (1-2), 17-28.

Table G.8 Vapor pressure of liquid tetramethylurea in the literature[a]

T /K	p /Pa
318.92	507
330.21	1024
362.22	5165
378.69	10325
397.36	20717
409.51	31239
413.37	41362
425.73	51682
432.1	62151
437.68	72692
442.54	83029
446.88	93229
448.65	97469
450.7	102737

[a] Piacente, V.; Ferro, D.; Della Gatta, G., Sublimation enthalpy of eleven alkyl derivatives of urea. *Thermochimica acta* **1990**, 158, (1), 79-85.

Appendix H: The evaporation rate of a droplet

The evaporation rate of a droplet is be expressed as[a,b]:

$$\frac{\partial d}{\partial t}=\frac{4DM}{R\rho d}\left(\frac{p_C}{T_C}-\frac{p_d}{T_d}\right)f \tag{H.1}$$

The temperature decrease of the droplet can be described as[a]:

$$\frac{\partial T_d}{\partial t} = \frac{1}{d}\left[\frac{3H}{C_P M}\frac{\partial d}{\partial t} + \frac{12h_{air}}{C_p \rho}(T_C - T_d)\right] \tag{H.2}$$

[a] Rietveld, I. B.; Kobayashi, K.; Yamada, H.; Matsushige, K., Electrospray deposition, model, and experiment: toward general control of film morphology. *The Journal of Physical Chemistry B* **2006**, 110, (46), 23351-23364.

[b] Hinds, W. C., Aerosol technology: properties, behavior, and measurement of airborne particles. ed.; John Wiley & Sons: 1999.

The meaning and the value of the symbols are listed in Table H.1:

Table H.1 The meaning and the value of the symbols in eqs. H.1 and H.2

Symbols	Meaning	Value
d	the diameter of the droplet	380 μm (beginning)
t	the evaporation time	-
D	the diffusion of a solvent molecule in air	1.20×10^{-5} m^2 s^{-1}
M	the molar weight of a solvent molecule	0.0581 kg mol^{-1}
ρ	the density of the solution in the droplet	1000 kg m^{-3}
R	gas constant	8.314 J mol^{-1} K^{-1}
p_C	the vapor pressure of the solvent in the spray chamber	10^(4.42-1312.25/(T_C-32.45))*100000 Pa
T_C	the temperature in the spray chamber	Outlet temperature
p_d	the vapor pressure of the droplet	0.1*p_C
T_d	the temperature of the droplet	Inlet temperature (beginning)
f	coefficient	≈ 1
H	The heat of evaporation of the solvent	29000 J mol^{-1}
C_p	The heat capacity of the droplet	75.5 J mol^{-1} K^{-1}
h_{air}	The heat transfer coefficient of air	0.0251 J m^{-2} s^{-1} K^{-1}

Table H.2 The solubility of urea derivatives

Name	Solubility /g g^{-1}					
	293 K	298 K	303 K	308 K	311 K	313 K
Urea	0.5102	0.5439	0.5786	0.6021	-	0.6128
1,1-Dimethylurea	0.2235	0.2416	0.2626	0.2840	-	0.3057
1,3-Dimethylurea	0.7565	0.7696	0.7830	0.8010	-	0.8158
1,1-Diethylurea	0.8206	0.8446	0.8679	0.8904	-	0.9041
1,3-Diethylurea	0.2284	0.2572	0.2897	0.3749	0.5040	0.7488

Table H.3 The van't Hoff equation parameters

Name	van't Hoff equation		
	$\Delta_{d(i)}H$ / J mol^{-1}	$\Delta_{d(i)}S$ / J mol^{-1} K^{-1}	R^2
Urea	11476(1312)	24(4)	0.954
1,1-Dimethylurea	15264(186)	28(1)	0.999
1,3-Dimethylurea	7839(371)	19(2)	0.991
1,1-Diethylurea	13830(571)	40(2)	0.994
1,3-Diethylurea	187436(73109)	589(164)	0.863

Abstract

A previous study has demonstrated that the γ polymorph of pyrazinamide, which is metastable at room temperature, has a significantly increased persistence when obtained by spray drying in the presence of 1,3-dimethylurea. In this thesis the reasons behind this effect have been investigated. The thesis consists of three parts. The first part explores the preparation methods of the four known polymorphs of pyrazinamide and their physical properties among which the thermal expansion and their compression behavior. The pressure-temperature phase diagram involving forms α and γ has been constructed and the transition temperature from α to γ has been determined to be 392 K, that is, around 20 K below the value commonly found in the literature. At room temperature, form γ becomes more stable than α above 260 MPa. The second part of the thesis focuses on the interactions between pyrazinamide and a number of urea derivatives, such as acetamide, urea, 1,3-dimethylurea, and tetramethylurea. Nuclear magnetic resonance has been used to investigate the interactions between pyrazinamide molecules themselves and between pyrazinamide and the urea derivatives in solution. The hydrogen atoms in the amine group of pyrazinamide interacts with the carbonyl oxygen of the urea derivatives and vice versa. Furthermore, sublimation crystallization and the morphology of the γ crystals obtained in the absence and the presence of the urea derivatives have been analyzed through a statistical study (more than 500 single crystals investigated). The crystallization rate accelerates dramatically in the presence of the urea derivatives (for example: the induction time of form γ in the presence of 1,3-dimethylurea is only one seventh of that in the absence of urea derivatives). The morphology of the γ crystals is different depending on the urea derivative present in the vapor. This is related to the individual vapor pressures of the urea derivatives and on the specific interactions between pyrazinamide and the urea derivative in question. Both solution NMR results and sublimation results indicate that the interactions between pyrazinamide and the urea derivatives are similar in solution and in the vapor phase. Therefore, it can be inferred that in spray drying the interactions between pyrazinamide and the urea derivatives must be similar too and it appears therefore that the interactions as such are not a direct cause of the long persistence time of the γ crystals. In the last part of the thesis, the pyrazinamide and urea derivatives co-spray dried samples have been studied. In addition to 1,3-dimethylurea, some γ crystals obtained in the presence of 1,3-diethylurea exhibit a long persistence time. Eutectic temperatures, solubilities, and ternary phase diagrams show similarities between 1,3-dimethylurea and 1,3-diethylurea, implying that these properties affect the conditions inside the spray dried droplet and lead to form γ with a long persistence time.

Keywords: pyrazinamide, polymorphism, additives, phase diagram, intermolecular interactions, sublimation, spray drying

Résumé

Une étude précédente a montré que la forme γ de la pyrazinamide, laquelle est métastable à la température ambiante, a une forte persistance dans le temps quand elle est obtenue par voie du spray dry en présence de la 1, 3-diméthylurée. Ainsi l'objectif de cette thèse est de chercher à expliquer ce phénomène de persistance dans le temps pour cette forme de la pyrazinamide. Le sujet de thèse est divisé en trois parties : Une première partie qui va exploiter les différentes méthodes de préparation des quatre formes connues de la pyrazinamide ainsi que leurs propriétés physiques en particulier leur comportement thermique. Le diagramme de phase entre la pression et la temperature pour les phases α et γ a été construit et que leur température de transition se trouve être à 392 K, 20 K de moins que la valeur existante dans la littérature. A la température ambiante, la forme γ est plus stable que la forme α au-dessus d'une pression de 260 MPa. La deuxième partie de la thèse traite les relations entre la pyrazinamide et un certain nombre des dérivés de l'urée comme l'acétamide urée, la 1, 3-diméthylrée et la tétraméthylurée. La technique de la Résonance Magnétique Nucléaire (RMN) a été utilisée pour visualiser les interactions entre molécules de la pyrazinamide d'une part et d'autre part entre la pyrazinamide et les dérivés de l'urée en solution. Les hydrogènes du groupement amine de la pyrazinamide interagissent avec le groupement carbonylé des dérivés de l'urée et vice versa. En plus la cristallisation par voie de sublimation et la morphologie des cristaux γ obtenus en présence et en absence de dérivés de l'urée ont été analysées à travers une étude statistique (plus de 500 monocristaux). Le taux de cristallisation augmente considérablement en absence de dérivés de l'urée (par exemple : le temps d'induction de la forme γ en présence de la 1, 3-diméthylurée est seulement 1/7 de ce temps en absence de dérivés de l'urée). La morphologie des cristaux γ varie en fonction du dérivé de l'urée présent dans la vapeur. Ceci est lié à la pression de vapeur du dérivé de l'urée et de l'interaction spécifique entre la pyrazinamide et le dérivé en question. Les résultats obtenus par la RMN et la sublimation montrent que les interactions en solution comme en vapeur entre la pyrazinamide et les dérivés de l'urée sont pratiquement similaires. Par conclusion, les interactions entre la pyrazinamide et les dérivés de l'urée sont aussi pareilles en spray dry et ne sont pas donc directement à l'origine de la persistance dans le temps des cristaux γ. Pour la troisième et dernière partie de ce manuscrit, l'étude porte sur des échantillons du co-spray dry entre la pyrazinamide et les dérivés de l'urée. En plus de la 1, 3-diméthylurée, une partie des cristaux γ obtenus en présence de la 1,3-diéthylurée montre une longue persistance dans le temps. Les températures à l'eutectique, les solubilités et les diagrammes de phases ternaires montrent une similitude entre la 1, 3-diméthylurée et la 1, 3-diéthylurée, indiquant que leurs propriétés affectent les conditions du spray dry et conduisent aux cristaux γ avec une longue persistance dans le temps.

Mots clés : pyrazinamide, polymorphisme, additifs, diagramme de phase, interactions intermoléculaires, sublimation, spray dry